Reactions of novel self-assembled iron(II) phosphine complexes

Kirk, Andrew

Award date:
2008

Awarding institution:
University of Bath

Reactions of novel self-assembled iron(II) phosphine complexes

Andrew Stuart Kirk

A thesis submitted for the degree of Doctor of Philosophy

University of Bath

Department of Chemistry

May 2008

Acknowledgements

I would like to thank my supervisors Dr. Andrew Burrows and Dr. Michael Whittlesey for all their help and ideas over the course of my Ph.D. studies. I would also like to thank members of the Burrows and Whittlesey research groups past and present, in particular Dr. Chris Richardson for his help and chemistry advice. My gratitude extends to Deborah Dodds, Jimmy White, Laura Fisher, and Araminta Ledger, who all contributed to my work in their undergraduate projects. Thanks also to Dr. Mary Mahon and Dr. Gabriele Kociok-Köhn for collecting X-ray data and solving the crystal structures, to Dr. John Lowe for his help with all things NMR, and to Dr. Frank Marken for his electrochemistry expertise and guidance.

I would like to thank all my friends and colleagues for making my Ph.D. more fun than work, including Mike Bonné, Kevin Cassar, Hamid Chouja, Gillian Eade, Alberto Fattori, Cathy Frankis, Rob French, Haniti Hamid, Nathan Hollingsworth, Mathi Kandiah, Stuart Macdonald, Graeme Nawn, Chris Richardson, Anna Stevenson, Claire Thompson, Lorena Tomas Laudo, Mariya Zhelyazkova and many, many others. Special thanks go to Cathy, Graeme and Nathan for giving me somewhere to sleep in Bath for so long, and of course to Claire for all the fun and good times we've had.

Most of all I'd like to thank all my family for their support over the course of my Ph.D. studies, especially my Mum, Dad, Sister and my Grandparents Ken and Eva. Without them this achievement would not have been possible.

Contents

Chapter 3 – Self-assembly and coordination chemistry of a new iron(II) phosphine complex

Abstract

This thesis describes the synthesis and coordination chemistry of self-assembled multidentate iron(II) phosphine complexes.

Chapter 1 introduces the background to phosphine ligands, their properties, interactions with transition metals and applications. The chapter then discusses macrocyclic and medium ring P,N-containing ligands, as well as some water soluble phosphines. The chapter also introduces the novel self-assembled macrocyclic phosphine complex $[FeL^1(H_2O)_2]SO_4$ (**1**) and its tetradentate cyclic phosphine ligand L^1.

Chapter 2 describes the synthesis of $[FeL^1(H_2O)_2]SO_4$ (**1**) and its coordination chemistry with a variety of ligands, including halides, pseudo-halides, and CO. ^{57}Fe labelled versions of complex **1** and the related dicarbonyl complex $[FeL^1(H_2O)_2]SO_4$ (**9**) were synthesised as models for the hydrogenase protein Hmd in a Nuclear Resonance Vibrational Spectroscopy study. Reactions were also undertaken to functionalise the hydroxymethyl groups in order to alter the properties of the complexes. The reaction of **1** with acetic anhydride afforded complex $[Fe(L^2)(\kappa^2\text{-}O_2SO_2)]$ (**13**), possessing the acylated ligand L^2 and a coordinated sulfate ligand. The coordination chemistry of **13** was explored with a variety of neutral and anionic ligands, including halides, pseudo-halides, carbonate, and CO. Electrochemical cyclic voltammetric investigations of L^1 and L^2 complexes were also explored.

Chapter 3 reports the investigations carried out to explore the effect of altering the reagents of the self-assembly reaction. The self-assembly reaction to synthesise complex **1** was also attempted with copper(II), nickel(II), copper(II) and zinc(II) salts, as well as in the absence of a metal template, which all did not lead to the formation of any isolable species. The syntheses of the novel iron(II) complexes $[Fe(L^3)_2(SO_4)]$ (**23**) and *cis*-$[Fe(L^3)_2Cl_2]$ (**24a**) containing the new bidentate phosphine ligand L^3 are also reported, as well as the coordination chemistry of **24a** with a variety of ligands. The reaction of **24a** with $NaBH_4$ gave the *trans* hydride-chloride complex *trans*-$[Fe(L^3)_2(H)Cl]$ (**29**). Electrochemical investigations of the L^3 complexes were also carried out.

Chapter 4 provides the experimental details for the reactions described in chapters 2 and 3.

Abbreviations

δ	chemical shift (NMR)
ν	frequency (IR and NMR)
$\{^1H\}$	proton decoupled (NMR)
Å	angstrom
br	broad (NMR)
cod	1,5-cyclooctadiene
CV	cyclic voltammetry/cyclic voltammogram
d	doublet (NMR)
dppe	bis(diphenylphosphino)ethane
EDTA	ethylenediaminetetraacetic acid
ES-MS	electrospray mass spectrometry
Et	ethyl group
EtOH	ethanol
Fc^+/Fc	ferrocenium/ferrocene
HMPB	1,2-bis(bis(hydroxymethyl)phosphino)benzene
HMPE	1,2-bis(bis(hydroxymethyl)phosphino)ethane
HMQC	Heteronuclear Multiple Quantum Coherence (NMR)
IR	infra-red
J	nuclear spin-spin coupling constant (NMR)
L	generic ligand
M	metal
Me	methyl group
m	multiplet (NMR)
NMR	nuclear magnetic resonance
NRVS	nuclear resonance vibrational spectroscopy
Ph	phenyl group
PTA	1,3,5-triaza-7-phosphaadamantane
R	alkyl or aryl group
s	singlet (NMR)
SCE	saturated calomel electrode
t	triplet (NMR)
THMP	tris(hydroxymethyl)phosphine
THPS	tetrakis(hydroxymethyl)phosphonium sulfate
TPPMS	(3-sulfonatophenyl)diphenylphosphine
TPPTS	tris(3-sulfonatopheny)phosphine

Chapter 1 – Introduction

1.1 Phosphorus-based compounds in chemistry

The interest in phosphorus-based compounds of the type PR_3 (where R is an alkyl or aryl group) has existed ever since the first synthesis of trimethylphosphine from methyl chloride and impure calcium phosphide at 180-300 °C by Thenard in 1847.[1] Many later studied this area of chemistry, including Michaelis who in 1885 discovered the first synthesis of triphenylphosphine,[2] but it was not until Chatt and Mann's study of the coordination chemistry of tertiary phosphines to palladium halides[3] in the 1930s that interest in transition metal phosphine chemistry really took off.[4] This has ultimately given birth to a number of new and exciting applications, most notably the use of phosphines as ligands in transition metal-catalysed reactions. The ability of phosphines to assist the control and selectivity of these catalytic transformations is in no small part responsible for much of this interest. Varying the R groups on the phosphine can dramatically change the steric and electronic properties of the ligand, and this in turn can alter the ability of the compound to act as a useful ligand in catalysis.

Phosphines are useful in organometallic and inorganic chemistry largely because the phosphorus possesses a lone pair that enables the phosphine to create new bonds to the phosphorus, such as coordination to transition metals *via* donation of the lone pair into a vacant metal bonding orbital. The major difference between phosphorus(III) compounds and their analogous nitrogen-based relatives is that despite both having pyramidal geometry, amines undergo rapid pyramidal inversion at room temperature. This inversion is much slower in phosphines, effectively giving them fixed pyramidal structures.[5] This leads to large differences between the properties of phosphines and amines within coordination chemistry.

In this chapter, Sections 1.2 to 1.4 discuss some fundamental aspects of the coordination chemistry of phosphine-based ligands to transition metals including steric and electronic effects. Sections 1.5 and 1.6 introduce the concept of macrocyclic chemistry including phosphorus-containing macrocycles, and smaller P,N-containing heterocyclic ligands. Section 1.7 covers the area of water-soluble phosphines, their coordination chemistry and applications, while Section 1.8 discusses the discovery of a novel water-soluble iron(II) phosphine complex and its potential applications, which forms the basis of this thesis.

1.2 Transition metal – phosphine interactions in organometallic chemistry

It has long been known that varying the nature of the R groups on the phosphine (PR_3) can lead to large changes in its ability to coordinate to metals, as well as differences in chemical and physical properties. Traditionally, the two main ways of measuring these differences are in terms of the electronic and steric effects of changing the R substituents. **Figure 1.1** shows a representation of the differences between steric and and electronic effects.

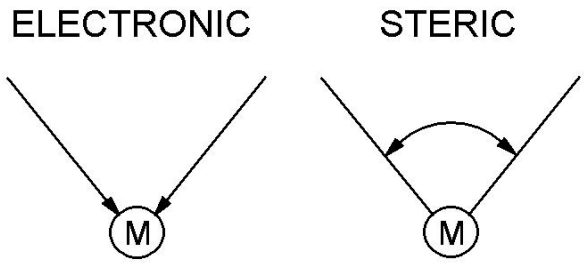

Figure 1.1 – Schematic representation of electronic and steric effects.

Steric effects in terms of tertiary phosphine ligands are loosely defined as the effective size of the phosphine and its R substituents. Tolman in his seminal papers in the 1970s[6, 7] first proposed a parameter called the cone angle θ, which has perhaps been the most widely used method of determining the relative size of phosphines since its introduction.

Electronic effects are associated with the nature of the chemical bonding itself. It is well established that the nature of the bonding of phosphines to transition metals contains both a σ and a π element, and studies of electronic effects are usually concerned with how the differences in the bond character influence the coordination ability of the phosphine and the chemistry of the complexes it forms.

It is important to note, however, that these steric and electronic properties cannot be regarded as completely separate factors, as they are often intrinsically intertwined and that altering the sterics of a particular ligand will often have an effect on the electronics and *vice versa*. For example, by placing a bulkier R group on a phosphine its steric properties are altered by definition, but this could have an additional effect on the lone pair of the phosphorus and thus also alter the electronic properties.

1.3 The steric properties of phosphine ligands

Sterics play an important part in determining how a phosphine ligand binds to a transition metal and the subsequent reactivity of that complex. Tolman was among the first researchers to realise the importance of sterics with respect to phosphine ligands.[6] During a study of the relative ability for a series of tertiary phosphine ligands to compete for coordination on a Ni(0) centre, it became clear to Tolman that the results could not be accounted for solely by the electronic properties of the ligands. Instead, he noticed that the results correlated well with the relative sizes of the phosphines, in general with the least bulky showing the greatest coordinating ability to the metal. This led him to come up with a new parameter to determine the relative size of the phosphines, which he called the ligand cone angle θ.[7] The cone angle θ for symmetric ligands (where all three R substituents are the same) is defined by Tolman as "the apex angle of a cylindrical cone, centred 2.28 Å from the centre of the P atom, which just touches the van der Waals radii of the outermost atom of the model" (**Figure 1.2a**). The value 2.28 Å is used as it is the average bond length for a Ni-P bond in Tolman's study, which is a typical value for an M-P bond.

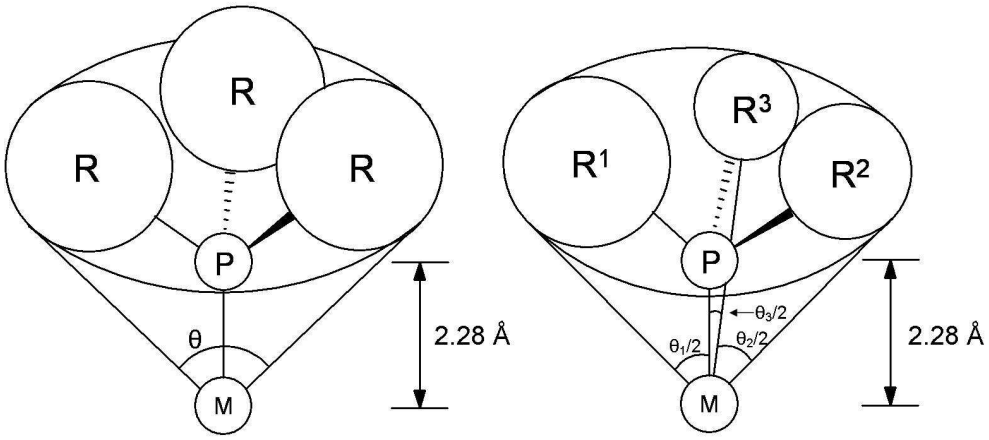

Figure 1.2 – Tolman cone angle for PR_3 ligands (above left – 1.2a) and half cone angles for $PR^1R^2R^3$ ligands (above right – 1.2b).

In the case where the phosphine ligand is asymmetrical (*i.e.* all three R substituents are not the same), the effective cone angle θ can be defined by taking the sum of all the half angles of the three different substituents, as shown in **Equation 1.1**. A diagrammatic representation is shown in **Figure 1.2b**.

$$\theta = \frac{2}{3}\sum_{i=1}^{3}\theta_i / 2$$

Equation 1.1 – Tolman cone angle equation.

In essence, this asymmetrical cone angle parameter can be described as 'twice the mean average of the sum of the three half cone angles'. This equation therefore assumes that each individual R group contributes to the cone angle in an asymmetrical ligand $PR^1R^2R^3$, the exact same amount that it would in the symmetrical ligand PR^1_3. This may not be completely accurate in reality, but is a good enough approximation for most purposes. **Tables 1.1** and **1.2** show some examples of symmetric phosphines and phosphites, as well as some unsymmetrical phosphine ligands.

Ligand	Cone Angle θ
$P(OEt)_3$	109°
PMe_3	118°
$P(OPh)_3$	128°
PEt_3, $P(n\text{-}Pr)_3$, $P(n\text{-}Bu)_3$	132°
PPh_3	145°
$P(t\text{-}Bu)_3$	185°
$P(mesityl)_3$	212°

Table 1.1 – Tolman Cone Angles for a range of symmetric phosphorus-based ligands.[7]

Ligand	Cone Angle θ
$P(OEt)_2Ph$	116°
PMe_2Ph	122°
$PHPh_2$	128°
$P(OEt)Ph_2$	133°
$PMePh_2$, PEt_2Ph	136°
$PEtPh_2$	140°
$PPh(t\text{-}Bu)_2$	170°

Table 1.2 – Tolman Cone Angles for a range of unsymmetrical phosphorus-based ligands.[7]

For cone angles greater than 180°, it is more convenient to calculate them by employing trigonometry as shown by **Equation 1.2**. **Figure 1.3** illustrates how this can be achieved.

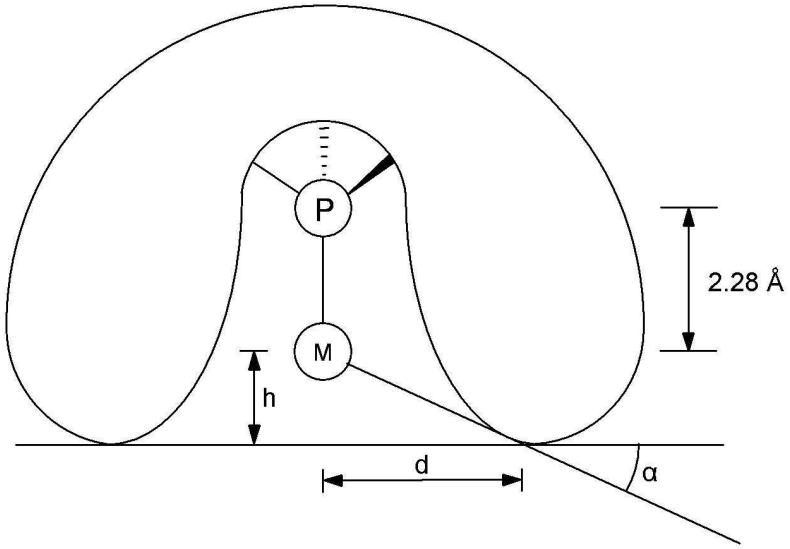

Figure 1.3 – Method of calculating cone angles greater than 180°.[7]

$$TAN\alpha = h/d$$
$$\theta = 180 + 2\alpha$$

Equation 1.2 – Trigonometric equation for the calculation of θ greater than 180°.[7]

It is important to consider that all cone angles in general are derived from the ligand models and are not determined from the molecules themselves. This has a number of implications:

a) Phosphine ligands do not necessarily possess 'cone-shaped' symmetry as assumed by the model and method of measurement. The models assume free rotation of the R groups where possible, which might not (necessarily) be the case in reality.
b) The model assumes the minimum cone angle possible – it is difficult to determine how likely this is in reality due to the potential strain caused by placing the R groups as close together as possible.
c) Bond lengths and angles in the model are fixed, which does not allow for any flexibility or fluxional motion as in the real molecule.
d) The electronic effects of the ligand are not considered, nor are the steric and electronic effects of other ligands coordinated to the metal.

Various people have introduced a number of refinements and modifications to address some of these shortcomings, including determining the cone angles from single-crystal X-ray crystallographic data,[8] ligand profile plots,[9] molecular mechanics calculations,[10,11] and using other parameters such as the solid angle.[12]

A more accurate technique introduced by Brown and Lee[11] uses molecular mechanics calculations to determine the steric bulk of ligands. This method involves computationally measuring the ligand repulsive energies (E_R values) in energy-minimised structures. They found a very good correlation between their E_R values and Tolman's cone angle, which highlights the importance of Tolman's work more than forty years later.

More recently, the steric effects of more complicated phosphorus-based ligands such as diphosphines and other polydentate phosphine ligands have received considerable attention.[13] This is largely due to the fact they have played an increasingly important role as ligands for catalytic applications. Measuring the steric size of a bidentate ligand can be carried out in a similar manner to that of a monodentate ligand, *i.e.* by calculating the Tolman cone angle for each half of a diphosphine ligand using **Equation 1.1**. The value for the $\theta_i/2$ for the backbone fragment of the ligand should be measured by taking the angle between the M-P bond and an imaginary line bisecting the P-M-P angle (**Figure 1.4**).[14]

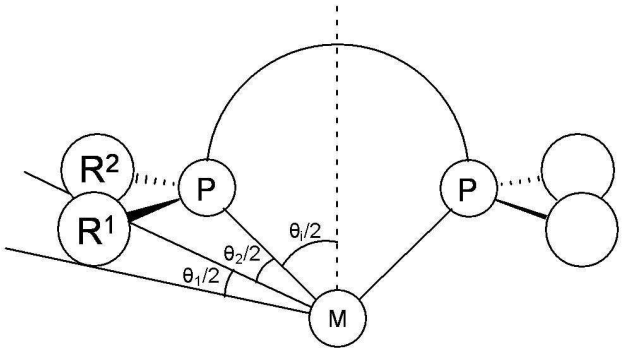

Figure 1.4 – Tolman half cone angles for diphosphines.

However, it is difficult to define such a parameter that is dependant on the behaviour and characteristics of the ligand backbone. The angles are usually determined from the X-ray crystal structure of a metal diphosphine complex, which may or may not differ significantly from the angles of the complex in solution due to changes in conformation and flexibility. Therefore all parameters based on crystallographically-determined angles are essentially properties of the X-ray crystal structure in question, and not simply the ligand itself.

The P-M-P angle (bite angle) of a bidentate ligand is another important way of classifying diphosphine ligands, and this angle in particular can vary between different ligands, but also from metal to metal. This is largely because the bite angle of any

metal-ligand complex is a compromise between the metal's preferred bite angle and the one preferred by the ligand.[15] The preferred bite angle of a ligand generally depends on constraints imposed by the ligand backbone, as well as steric factors determined by the substituents on the phosphorus donor (including the backbone). Metal preferred bite angles, however, are largely determined by electronic effects. If a particular ligand/metal combination fails to find a conformation in which both the metal and ligand are satisfied, this can lead to changes in the geometry of the complex, or even lead to another coordination mode such as the bridging mode. This is when each donor atom of a bidentate ligand is coordinated to a different metal centre. Ligands with unusually large or small bite angles have long been used to synthesise complexes that would otherwise be unstable with ligands possessing classic bite angles. **Figure 1.5** shows some examples of average crystallographically determined bite angles of a range of diphosphine ligands.

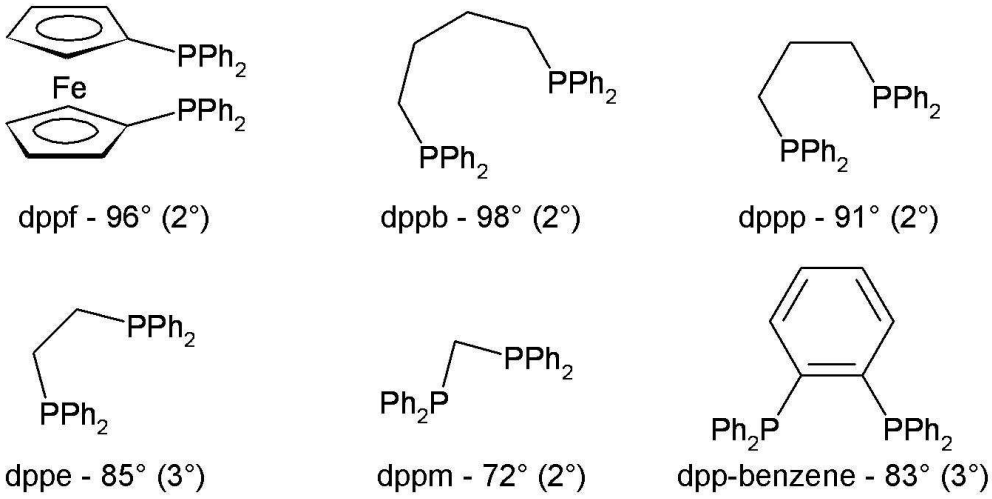

Figure 1.5 – Selected bite angles of diphosphines as determined by X-ray crystallography (standard deviation in brackets).[15]

Dierkes and van Leeuwen[15] found in a study of a range of bidentate phosphine ligands, that the bite angles had a pronounced effect on both selectivity and rate of metal catalysed reactions.

1.4 The electronic properties of phosphine ligands

Before attempting to explain how electronic effects influence the behaviour of phosphine ligands in terms of their coordination chemistry and reactivity, it is necessary to discuss the nature of the M-P bond, and its context within coordination chemistry. The traditionally accepted description of the M-P bond within a transition metal phosphine complex can be broken down into two main components. The first is the σ-

donation of electron density from the lone pair of the phosphine to a symmetric empty bonding orbital on the transition metal. The other is the π-acceptor (or π-back bonding) component, which is when electrons from a filled orbital on the transition metal donate back into an empty orbital on the phosphorus (See **Figure 1.6**).

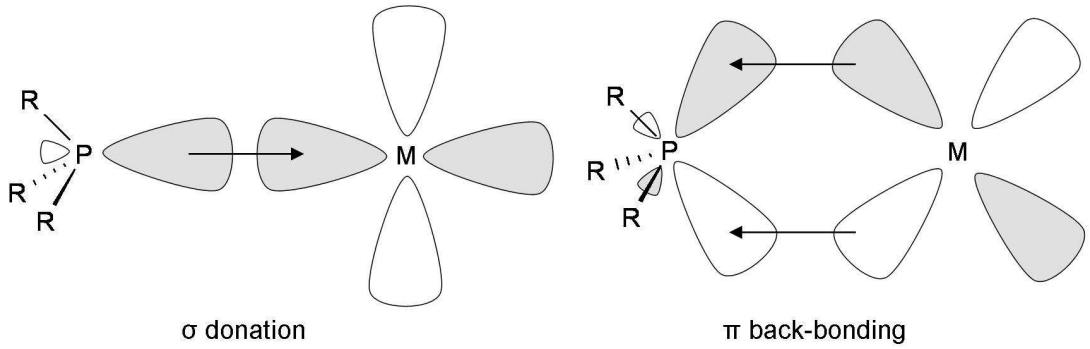

Figure 1.6 - representation of the traditionally accepted σ and π components of the M-P bond. The phosphorus π-acceptor orbital is a σ* orbital, only part of which is shown.

In the case of an octahedral complex, the metal *d* orbitals involved in σ bonding with the six ligands are the e_g orbitals. This leaves the t_{2g} orbitals non-bonding and directed in-between the six M-P bonds. The main part of the M-P bond is the σ bond formed from a metal *d* orbital and an sp^3 orbital on the phosphorus. This essentially means that phosphorus ligands act as both Lewis bases (σ-electron donors) and Lewis acids (π-electron acceptors). This helps phosphine ligands to stabilise metals both in high and low oxidation states, which is a very useful property in organometallic catalysis. This 'synergetic' σ + π approach was originally successfully applied as a description of metal carbonyl bonding, and which was then applied to metal-phosphorus bonding as a result of this success. Despite this, however, the electronic factors in metal-phosphorus interactions remain contentious.[16] All studies generally agree that the M-P bond contains a σ component, but it is the π-back bonding component which has received most attention. The traditional Dewar-Chatt-Duncanson model[17, 18] describes the π-back bonding component as the drift of the electrons from filled transition metal *d* orbitals to the empty 3*d* orbitals on the phosphorus. However, some have suggested that the π-donation of electrons from the metal occurs into either the phosphorus *p* orbitals[19] or the P-R σ* antibonding orbitals.[20] Calculations carried out by Pacchioni and Bagus[21] have also suggested that the *d* orbitals of the phosphorus are too diffuse and high in energy to effectively participate solely in the π-back bonding of electron density, and instead the electron density is being donated into a combination of the P-R σ* antibonding orbitals and phosphorus *d* orbitals. Computational models have been compared with X-ray crystal structural data of various metal-phosphine complexes in order to determine the accuracy and viability of such calculations. In the study by

Orpen and Connelly,[20] twenty four sets of transition metal-phosphine and -phosphite complexes, whose X-ray crystal structures were known for multiple oxidation states, were studied for variations in their geometry. They found that the M-P bond lengths tended to increase upon oxidation of the metal, consistent with there being an important element of π-back bonding present. Other authors have even suggested that some phosphine ligands are pure σ-donors[22-25] and others even π-donors.[22, 23]

It is now generally accepted that the nature (or even existence) of this π-back bonding depends greatly on the nature of the R substituents on the phosphorus atom. When highly electronegative substituents are present, such as in PF_3, the P-X bond is highly polarised and therefore the P-X σ* orbital is low in energy and mainly centred around the P atom, favouring back bonding.[26, 27] Where various experimental and theoretical studies have shown that ligands such as PF_3, PCl_3, $P(OR)_3$ all clearly accept π electron density from transition metals, the amount of π back bonding towards alkyl- and aryl-substituted phosphorus ligands is much harder to quantify, with different methods leading to different conclusions.

Apart from using computational and crystallographic methods to determine the σ-donor and π-acceptor properties of phosphorus ligands, other experimental techniques, and therefore other parameters are often employed. One of the most commonly used spectroscopic techniques is to use infrared spectroscopy to measure the CO stretching frequency of a range of transition metal carbonyl complexes in which steric factors do not play a major role. Tolman, in addition to his studies on the role of steric factors of phosphorus ligands, also carried out investigations into their electronic factors using this technique.[6] This method is based on the strong π-acceptor properties of the carbonyl ligand, which is able to accept electron density into an antibonding orbital of the CO bond. The stretching frequency of the carbonyl bond is dependent on the electron density at the transition metal centre, and this in turn depends on the σ-donor and π-acceptor properties of the other ligands coordinated to the metal. Strong π-acceptor and weak σ-donor ligands draw electron density away from the metal, reducing the amount of π back bonding to the carbonyl and therefore increasing the stretching frequency of the carbonyl group. Conversely, weak π-acceptor and strong σ-donor ligands effectively increase the electron density at the metal centre, increasing the amount of π back bonding to the CO and decreasing the CO stretching frequency. Tolman's study was based on complexes in CH_2Cl_2 solution, where L is any monodentate phosphorus-based ligand (mainly phosphines and phosphites), either symmetric or asymmetric. As a result of his study, Tolman introduced the measured

electronic parameter ν_{CO} (A_1) as a measure of the σ-donor and π-acceptor properties of a PR_3 ligand. ν_{CO} (A_1) is defined in **Equation 1.3**.

$$\nu_{CO}(A_1) = 2056.1 + \sum_{i=1}^{i=3} \chi_i cm^{-1}$$

Equation 1.3 – equation relating Tolman electronic parameters ν and χ_i.

The value 2056.1 cm^{-1} is the ν_{CO} (A_1) value for P(*t*-Bu)$_3$, the ligand with the lowest ν_{CO} (A_1) value used in Tolman's study. χ_i is the substituent modification parameter, which is set at zero for P(*t*-Bu)$_3$. **Table 1.3** contains selected values for both ν_{CO} (A_1) for selected ligands and χ_i for their corresponding substituents.

Ligand	χ_i / cm^{-1}	$\Sigma\chi_i$ / cm^{-1}	ν_{CO} (A_1) / cm^{-1}
P(*t*-Bu)$_3$	0.0	0.0	2056.1
PEt_3	1.8	5.4	2061.7
PMe_3	2.6	7.8	2064.1
PPh_3	4.3	12.9	2068.9
$P(OEt)_3$	6.8	20.4	2076.3
$P(OMe)_3$	7.7	23.1	2079.5
$P(OPh)_3$	9.7	29.1	2085.3
PCl_3	14.8	44.4	2097.0
PF_3	18.2	54.6	2110.8

Table 1.3 – Examples of Tolman's χ_i and ν_{CO} (A_1) values of PR_3 ligands for $[Ni(CO)_3(PR_3)]$.[6]

The examples in **Table 1.3** clearly show how the electronic parameters are affected by increasing the electronegativity of the substituents on the phosphorus ligand. Increased electronegativity of the substituents as the table is descended leads to increased ν_{CO} (A_1) as a result of the decrease in σ-donor character and an increase in π-acceptor character.

Although Tolman's electronic parameters are a useful way of comparing the electronic character of a series of ligands, they are a measure of the combined effect of both the σ-donor and π-acceptor character, and do not separate the two characteristics. Partially as a result of this and partially independently, others have made attempts to devise other parameters that can separately characterise the σ and π elements of a ligand.

As the phosphorus donates a pair of electrons to the metal in a transition metal phosphine complex, it can be regarded as a Lewis base, and therefore a measure of the basicity of phosphorus ligands is a good approximation of its σ-donor capabilities. The standard measure of phosphine basicity, however, is its pK_a(H_2O), which is a measure of Brönsted basicity and is not always the same as Lewis basicity.[28] pK_a values are the most widely quoted in the literature and a selection are shown in **Table 1.4** below.

Ligand	**pK_a**
P(*t*-Bu)$_3$	11.40
PCy$_3$	9.65
PEt$_3$	8.69
PMe$_3$	8.65
PPhMe$_2$	6.49
P(4-MeC$_6$H$_4$)$_3$	3.84
PPh$_3$	2.73
P(4-ClC$_6$H$_4$)$_3$	1.03

Table 1.4 – Examples of pK_a values for selected phosphine ligands.[28]

The values in the above table clearly show the correlation of the electron donating ability of the R substituents on the phosphorus with the pK_a of the ligand. The problem with this approach is that the sterics of these ligands vary quite a lot and this is not taken into consideration, which inevitably has an effect on the electronic parameters and therefore the pK_a. Increasing the steric bulk of the substituents on the phosphorus increases the R-P-R bond angle, which in turn increases the *p* character of the lone pair due to the increasing *s* character of the bonding orbital. Goel and Allman[29] carried out a study in which the pK_a values of a series of *para*-substituted phenyl phosphines with similar steric properties were compared to triphenylphosphine in order to compare a series of ligands possessing different electronic properties whilst ruling out the role of sterics in the analysis. They found, as expected, that increasing the electron donating ability of the *para* substituent on the aryl groups increased the basicity, and therefore increased the pK_a of the ligand without altering the sterics.

Other methods of measuring the σ-donor capabilities of phosphorus based ligands have been proposed, including gas phase proton affinity,[30] the heat of protonation of PR_3 complexes,[31] and $^1J_{P\text{-}Se}$ NMR coupling constants in Se=PR_3 complexes.[32]

Puddephatt *et al.*[33] have used the ionisation potentials of a range of phosphorus ligands as a measure of basicity, *i.e.* the availability of the lone pair. They found that the ionisation energies of the phosphorus lone pair in the gas phase followed the sequence PMe_3 > $PPhMe_2$ > PPh_2Me > PPh_3. This shows a good correlation between phosphorus lone pair ionisation potential and basicity within a series of closely related phosphines. However, this technique is not ideal for comparing the relative basicities of substantially different phosphines such as PCy_3 and PF_3. Also, as the ionisation energies are measured in the gas phase, this is not always useful as most chemists are interested in basicities of phosphine ligands in solution. The basicities of phosphines in solution differ greatly mainly because they are dominated by solvation effects, especially in ionising solvents.

1.5 Macrocycles and macrocyclic ligands

A macrocycle is a large cyclic molecule and, in the eyes of a coordination chemist, a macrocyclic ligand can be defined as "a cyclic molecule consisting of an organic framework into which heteroatoms capable of coordinating to metals have been incorporated."[34] More specifically, a macrocyclic ligand should contain at least three or more potential donor atoms in a ring of at least nine atoms.[35] Macrocycles are commonly found in nature in the form of porphyrins, corrins, and chlorins, but it was not until 1936 that the first synthesis of a macrocycle (1,4,8,11-tetraazacyclotetradecane) was reported.[36] The popularity of macrocyclic chemistry began to increase in the 1960s, thanks in part to the efforts of Busch[37] and Curtis,[38] who discovered the synthesis of nickel(II) diimine Schiff base coordination compounds from the reaction of nickel(II) diamines and aliphatic ketones. These initial studies were primarily aimed at mimicking porphyrins and other naturally occurring macrocycles such as corrins, chlorins, and corphins.

Another area of development for macrocyclic chemistry began in the late 1960s focused on using macrocycles such as oxygen-based crown ethers (Pedersen),[39] mixed oxygen nitrogen bicyclic cryptands (Lehn),[40] and cavitands (Cram)[41] to model biological processes such as ion transport. Traditionally macrocycles have been studied both for their use as models for naturally occurring macrocyclic systems such as porphyrins, as well as their use in supramolecular chemistry and as receptors for molecular recognition and complexation. To highlight the importance of macrocyclic chemistry, the 1987 Nobel Prize in Chemistry was awarded to Cram, Lehn and Pedersen "for their development and use of molecules with structure-specific interactions of high selectivity" based on their development of macrocycles in this area.

Today many different kinds of macrocycles have been discovered and studied, including simple polyaza-macrocycles, heteroatom-based macrocycles such as polythia-, polyphospha-, and polyarsa-macrocycles, as well as a wide range of mixed-donor macrocycles.

1.5.1 The macrocyclic effect

It is well known that complexes containing polydentate ligands are more stable than those complexes containing the equivalent number of similar monodentate ligands. This is known as the *chelate effect*.[42] It is therefore obvious to ask whether macrocyclic ligands give rise to more stable complexes than their related linear open-chain relatives. This is in fact the case and has become known as the *macrocyclic effect*. The *macrocyclic effect* was first reported by Cabbiness and Margerum[43] in 1969 by comparing the stability constants of the copper(II) complexes of a tetraamino macrocyclic ligand and a similar tetraamino acyclic ligand. They determined that the macrocyclic copper(II) complex was approximately ten thousand times more stable than its acyclic analogue, despite having a similar sequence of chelate rings. This large increase in stability cannot be simply attributed to the chelate effect in terms of entropy, and exists despite the restricted geometry that the macrocycle imposes on the metal. They also noticed that the rate of coordination for the macrocyclic ligand was much slower than that of the related open-chain ligand, which is in general the case for most macrocyclic ligand systems. Macrocyclic complexes are almost invariably more stable than those of their open-chain counterparts, though the difference decreases and eventually becomes insignificant when the macrocyclic rings are large and very flexible.[35] Many applications of macrocyclic ligands rely on the macrocyclic effect and the increased stability of the complexes which they form.

The origins of the macrocyclic effect have been the subject of much discussion. It is tempting to imagine both the macrocyclic and chelate effects in terms of possessing a common entropic origin. It is now clear, however, that this is not the case and it is not possible to describe the macrocyclic effect simply in terms of a single origin.[35] Studies by Paoletti and co-workers[44-49] have shown that the macrocyclic effect has both entropic and enthalpic contributions. Experimentally determined values of ΔH and $T\Delta S$ for the formation of nickel(II) high-spin and low-spin complexes of the 1,4,8,11-tetraazacyclotetradecane macrocycle (cyclam) and its open-chained analogue increased (*i.e.* more negative ΔH and more positive $T\Delta S$) upon going from the complex of the open chain ligand to the cyclam complex.

1.5.2 Phosphorus-containing macrocycles

The first phosphorus-containing macrocycles were prepared in 1897 by Stokes,[50] when he discovered cyclophosphazenes $(X_2P=N)_n$ ($n \geq 5$). It is surprising then, that intensive study of phosphorus macrocycles did not commence until the mid 1970s, despite the development of crown ethers by Pedersen[39] several years earlier in 1967. This is even after knowing the benefits and complexing ability of macrocyclic ligands. A lack of progress in this area can potentially be attributed to experimental difficulties, such as complex multi-step procedures, unstable and air sensitive products, and low yielding reactions. One of the main driving forces for interest in the field was to create more efficient macrocycles by introducing tri-coordinated phosphorus atoms into the ring, or phosphoryl and thiophosphoryl groups possessing high complex forming ability.[51] Macrocycles containing tri-coordinated phosphorus groups usually bind very easily to transition metals, whereas alkali metals can be captured with phosphine oxide or sulfide groups. Like most phosphine ligands, macrocyclic phosphines are also extremely useful in stabilising transition metals in their lowest oxidation states. Other potential uses include molecular recognition, complexation of salts and anions, as well as homogeneous and phase-transfer catalysis. Thiophosphoryl macrocycles have even been known to assist the transport of transition metal ions such as Fe^{3+}, Cu^{2+}, Co^{2+}, and Ni^{2+} through liquid membranes.[52]

There are, in general, two separate methods of preparing phosphorus-containing macrocycles; those utilising classical methods of macrocycle synthesis, and those taking into account specific properties of the phosphorus groups. It must be noted that there are many different kinds of phosphorus macrocycle containing different linking groups such as C-P-C, N-P-N, and O-P-O within the macrocyclic ring, but this review will concentrate on C-P-C linking groups. The three main strategies for the synthesis of phosphorus containing macrocycles are:

i) Cyclocondensations
ii) Ring-opening reactions
iii) Template-assisted reactions

Cyclocondensations are reactions where the condensation of two functionalised species leads to the formation of a macrocycle. For example, a [1+1] cyclocondensation is the formation of a macrocycle from one molecule of each reactant, whereas a [2+2] cyclocondensation combines two molecules of each. One method of forming C-P-C macrocycles by cyclocondensation is to react the lithium salts

of diphosphines with an appropriate dihalogenated species using high dilution conditions. Kyba *et al.* used this method from 1977 to 1985 to great effect to prepare a series of tri-donor nine-membered rings and tetra-donor fourteen-membered rings. **Scheme 1.1** shows the formation of a tri-phosphorus (**4**) and a tetra-phosphorus macrocycle (**5**) from the dilithium salt of the *ortho*-bis(phenylphosphino)benzene (**1**) and the relevant tertiary phosphine dichlorides (**2** and **3**).[53]

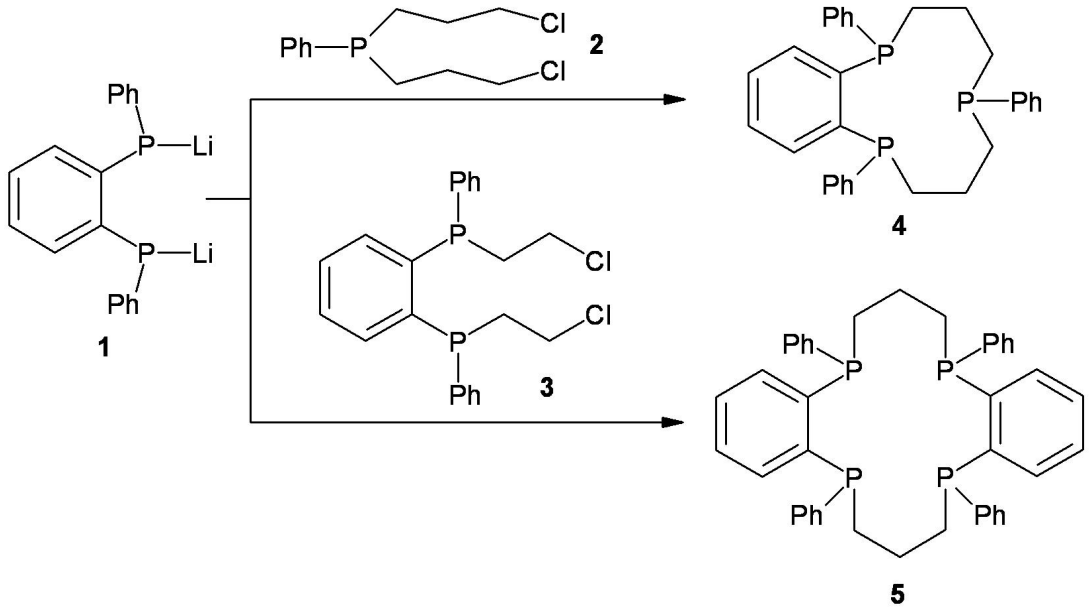

Scheme 1.1 – Formation of tri- and tetra-phosphorus macrocycles.[53]

Replacing the phenyl-phosphine based dilithium salt **1** with the dilithium salt of dithiocatechol allowed the formation of mixed P, S donor macrocyclic ligands.[53] Other P-containing mixed-donor macrocycles have also been prepared with arsenic,[54-58] nitrogen,[55, 57-61] and oxygen.[55, 58, 59, 61]

Macrocycles **4** and **5** exist as a number of geometrical isomers. Species **4** exists as three isomers (two *meso* and one *dl* pair), whereas **5** exists as five isomers, three *meso* and two *dl* pairs. Both **4** and **5** have been shown to be capable of coordinating to transition metals. The tridentate macrocycle **4** binds to transition metals using all three P-donor atoms in a *fac*-tridentate manner, whereas **5** is large enough to ligate to the metal in either a *cis*- or *trans*-tetradentate fashion to afford an octahedral complex (**Figure 1.7**).

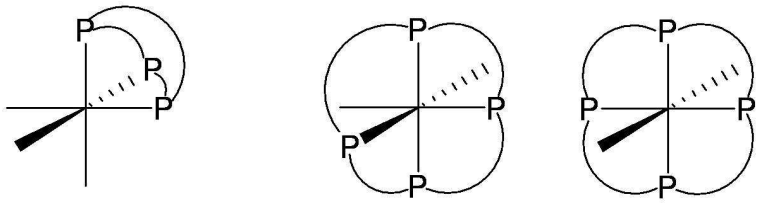

fac-complex of **4** *cis*-complex of **5** *trans*-complex of **5**

Figure 1.7 – Ligation modes of macrocycles 4 and 5 in octahedral complexes.[53]

Ring-opening reactions are another useful method of preparing phosphorus-containing macrocycles. In almost all cases, macrocycles containing C-P-C linkages prepared by this method lead to nine-membered rings. These are generally synthesised from phosphorus-containing five-membered rings such as phospholes. The first attempts to synthesise macrocycles *via* this method were carried out by Wittig in 1964. He took neat spirophosphoranes (*e.g.* **6**) and heated them up to their melting point, which induces the opening of the two five-membered rings, leading to the formation of a C-C bond to give the phosphorus(III) macrocycle **7**.[62] The lone pair of the phosphorus can also undergo addition reactions such as methylation with methyl iodide, to give the cationic macrocycle **8**. The reaction is shown below in **Scheme 1.2**.

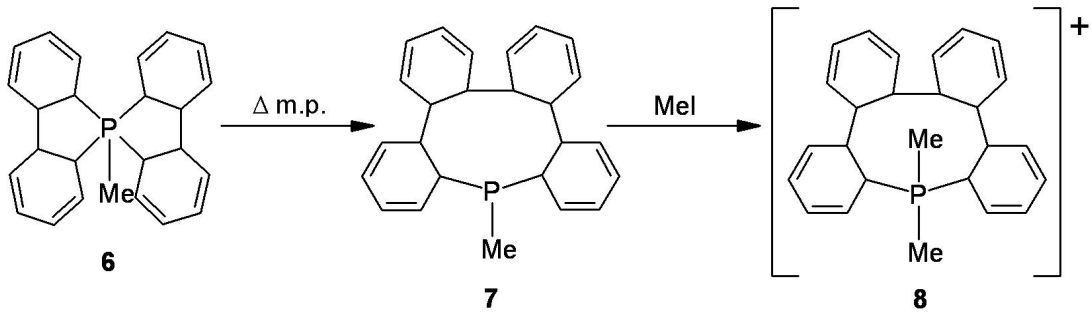

Scheme 1.2 – Ring-opening of a spirophosphorane 6 to form the macrocycle 7 and subsequent methylation to form 8.[62]

The ionic macrocycle **8** can also be prepared directly from **6** by heating it with methyl iodide in a one-pot reaction. Many other substituted variants of **7** and **8** have been prepared by using spirophosphoranes containing different alkyl and aryl substituents at a variety of positions on the aromatic rings, as well as the phosphorus itself.

Using a template (such as a transition metal) to assist the formation of a macrocycle can be a very useful method, and has been part of the field of macrocyclic chemistry since its inception. In many cases it is possible to successfully replace traditional multi-step macrocycle syntheses with template-assisted reactions offering less steps and higher yields. Two different roles exist for the metal in the template process, either

kinetic or thermodynamic in nature.[63] In the kinetic role, the ligands are already coordinated to the metal and arranged in a manner that allows one final condensation to complete the macrocyclic complex. The thermodynamic role is when the formation of the macrocycle would not happen at all without the presence of the metal ion. The cyclisation process can either take place on the phosphorus itself or on a substituent of the phosphorus atom. The first example of template-assisted macrocycle synthesis containing a phosphorus atom was prepared by Marty and Schwartzenbach[64] in 1970. Their method involved reacting the tetradentate mercaptophosphine nickel complex **9** with dibromoxylene **10** to form the {P_2S_2} macrocyclic Ni complex **11** (**Scheme 1.3**).

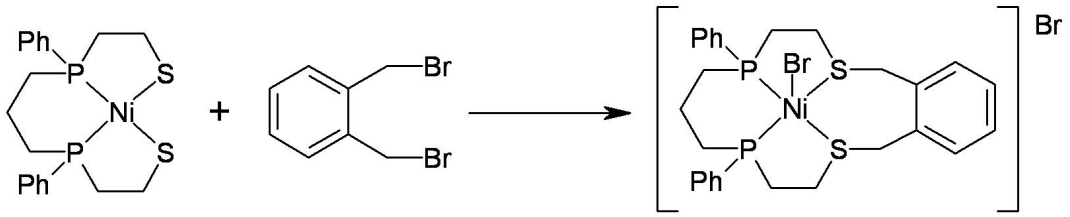

9 **10** **11**

Scheme 1.3 – Template-assisted synthesis of the P_2S_2 macrocyclic ligand complex 11.

This is an example of a kinetic template synthesis with the cyclisation process taking place at the sulphur atoms, and not at the phosphorus atoms themselves.

An advantage of using a template synthesis is that it forms the metal complex directly, without the need for further complexation reactions. However, this is fine if the metal used in the templating process is the desired metal in the final complex, but if the free macrocycle itself is wanted, then it is necessary to remove the metal *via* a decomplexation reaction. In some cases the demetallation has been shown to occur automatically, but this is rare and in most examples it is necessary to devise a method for removing the metal. In many instances, it has proven very difficult to separate the macrocycle from the metal template largely due the macrocyclic effect.

An example where the researchers[65] managed to successfully remove the metal from a phosphorus-containing macrocyclic complex formed by template-assisted assembly is shown below in **Scheme 1.4**.

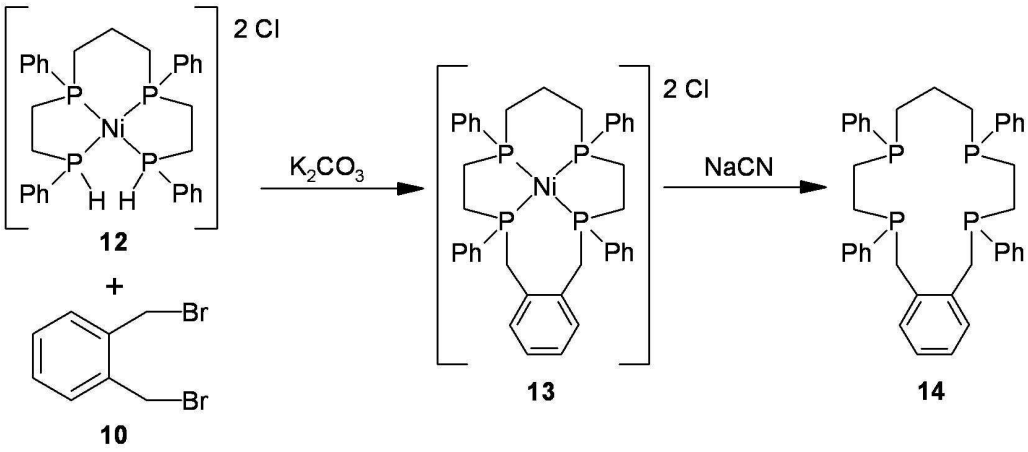

Scheme 1.4 – Template synthesis of a tetradentate P_4 macrocyclic Ni complex and subsequent demetallation.

This process involves the cyclocondensation reaction of the aryl dibromide **10** with a nickel(II) disecondary phosphine complex **12**. In the presence of potassium carbonate as a base, the reaction gives the fifteen-membered macrocyclic nickel(II) tetradentate phosphine complex **13**. This is also the first example of a template-assisted reaction where the cyclisation process occurs at the phosphine centre itself. The chloride anions can then be exchanged with other anions such as BF_4^- and NCS^- *via* metathesis reactions. The free macrocycle **14** can be liberated from the metal by treating the complex with an aqueous solution of sodium cyanide, thus complexing the nickel to give nickel cyanides and releasing the free ligand.

Another more recent example of the template synthesis and liberation of a tetradentate macrocyclic phosphine has been demonstrated by Lebbe *et al.* (**Scheme 1.5**).[66]

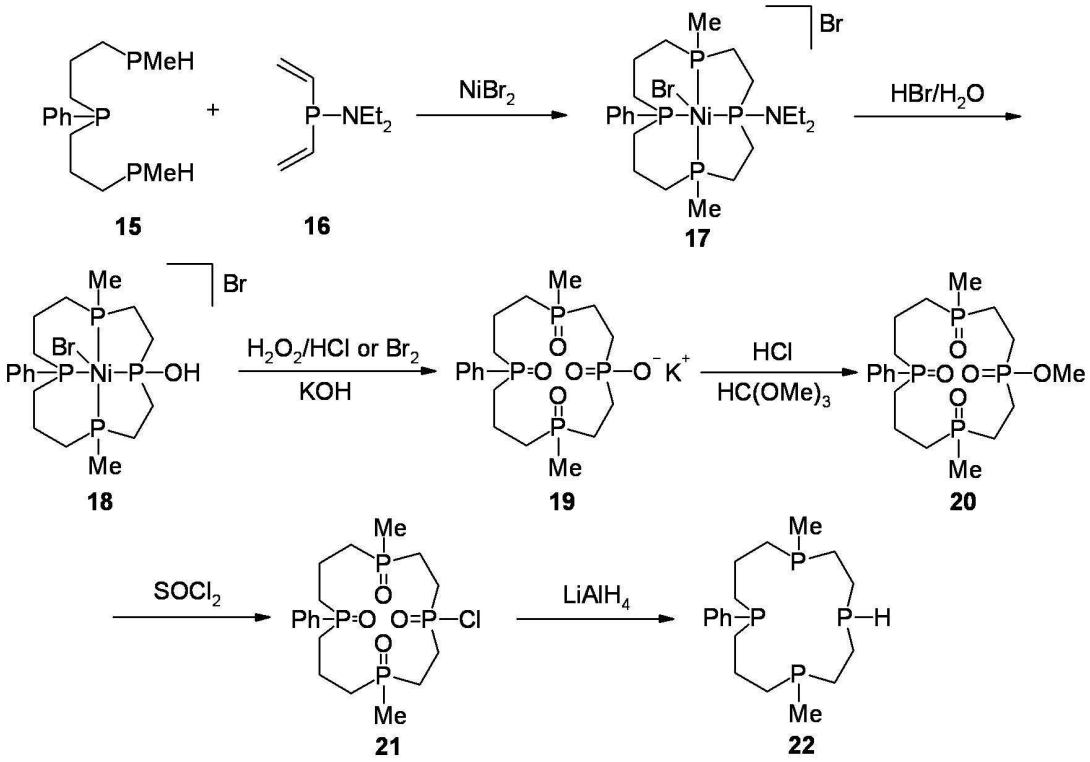

Scheme 1.5 – Template synthesis and oxidative demetallation of a Ni P_4 macrocyclic complex, followed by reduction to give the free macrocycle.

The tridentate phosphine ligand H(Me)P$(CH_2)_3$P(Ph)$(CH_2)_3$P(Me)H **15** was reacted with the divinylaminophosphine $(CH_2{=}CH_2)_2PNEt_2$ **16** in the presence of $NiBr_2$ to form the nickel(II) tetradentate aminophosphine macrocyclic complex **17**. This was then reacted with an aqueous solution of HBr to replace the NEt_2 with an OH group to give **18**.

To obtain the free ligand, Lebbe *et al.* treated **18** with a strong oxidising agent such as aqueous solutions of H_2O_2/HCl or Br_2. This completely oxidised the four phosphine donors to phosphine oxide groups to give the free ligand oxide and precipitated the nickel from solution as $Ni(OH)_2$. Upon subsequent addition of a base such as potassium hydroxide, the hydroxy group is deprotonated to give the phosphonate oxide derivative **19**, which was converted to the methyl ester **20** by acidification with HCl and reaction with $HC(OMe)_3$. Excess thionyl chloride was reacted with **20** to form the phosphinic acid chloride **21**. This then reacted cleanly with $LiAlH_4$ in good yield to give the reduced macrocyclic phosphine ligand **22**. NMR spectroscopy showed four different diastereoisomers, two symmetrical and two unsymmetrical.

Tridentate {P_3} ligands have also attracted a lot of recent attention due to their potential applications in coordination chemistry and homogeneous catalysis. There are three main methods of preparing these triphosphamacrocycles *via* a template synthesis; the 1+1+1, 2+1, and 3+0 approaches.[67] The 1+1+1 method involves all three chelate rings

of the macrocycle forming successively at the metal centre from three appropriately-functionalised monodentate phosphines. In the 2+1 closure, only two chelate rings are formed as one is already present in the pre-bound bidentate phosphine. The 3+0 approach uses a coordinated tridentate phosphine ligand requiring only one ring-closing step to give the final macrocycle. Though this approach seems to be the simplest on offer, no literature examples exist to this date for the 3+0 method.[67] A good example of the 1+1+1 method by Norman *et al.*[68] is based on the preparation of a triphosphacyclododecane using a molybdenum tricarbonyl complex as a template. However, they failed to release the free macrocycle from the metal due to its high stability, though Edwards and co-workers[69] managed to achieve the stereoselective liberation of this macrocycle at a later date by the reaction of the molybdenum and chromium macrocyclic complexes with base.

Edwards *et al.*[67, 70-74] have developed a technique of synthesising a variety of tridentate phosphino macrocycles using Fe(II) half-sandwich complexes as a template in a 2+1 method. In one example, the trimethylsilylcyclopentadienyl iron(II) complex **23** was reacted with a diphosphine, which displaces two acetonitrile ligands and coordinates to the iron centre. Trivinylphosphine is then added, which displaces the remaining CH_3CN ligand to give **25**. Upon the addition of a base such as triethylamine, a two-step metathesis coupling of the terminal unsaturated alkenyl groups occurs to complete the ten-membered macrocycle **27**. The third alkenyl group is then reduced with hydrogen in the presence of a palladium catalyst to give **28**. The two P-H bonds are then reacted with EtBr in the presence of a base to give the fully ethylated complex **29** (**Scheme 1.6**). A top down view of **29** is also shown.

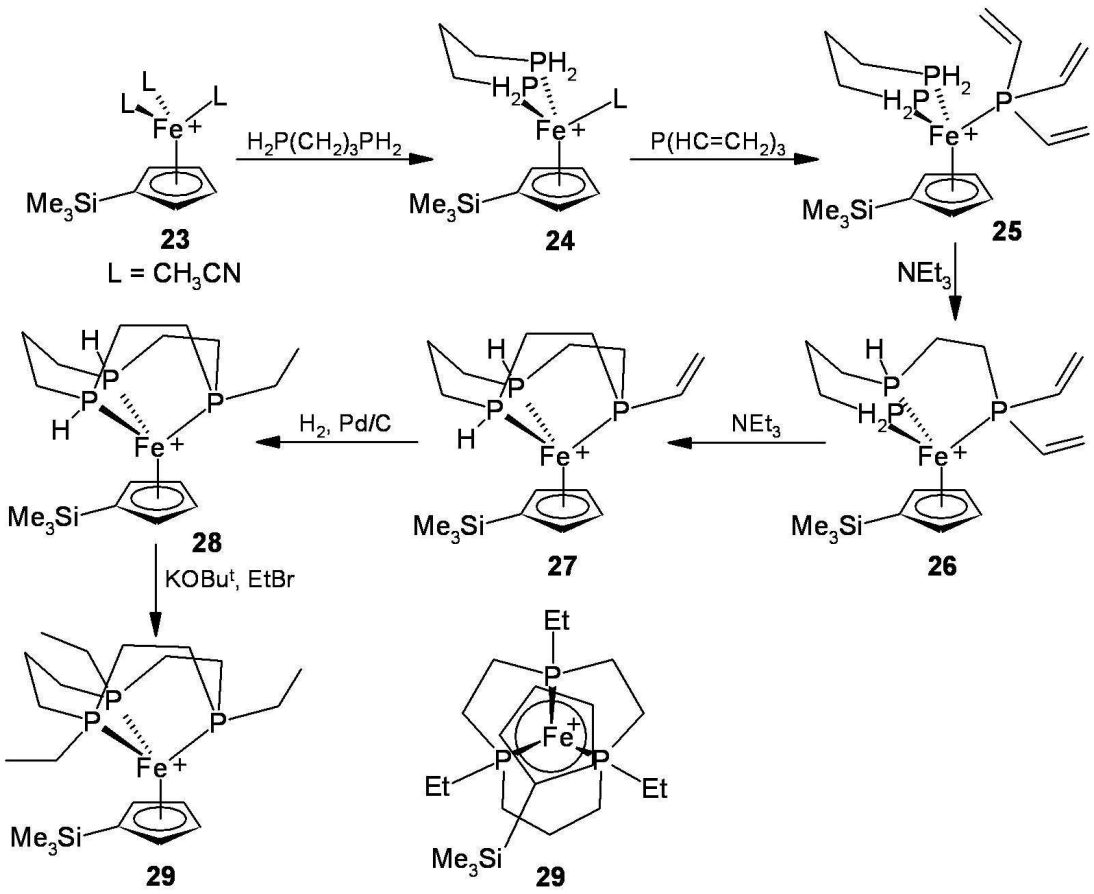

Scheme 1.6 – Synthesis of a symmetric ten-membered P_3 macrocyclic Fe(II) complex.[67]

Edwards *et al.*[67, 70-74] also used this same method to produce a range of symmetric and asymmetric tri-phosphorus 9- to 12- membered rings containing a range of secondary and tertiary alkyl and aryl phosphine groups. Repeated attempts to liberate these triphosphorus macrocycles with conventional agents such as CN^- were not successful. The d^6 octahedral Fe(II) template appears to be very kinetically inert and resitant to disruption. One nine-membered ring was successfully liberated as its trioxide by exhaustive oxidation,[72] but none of the free uncoordinated ligands were obtained. The iron centre was found to undergo reversible one electron oxidation in most of these complexes, but attempts to scavenge the Fe(III) ions from the oxidised complexes with various complexing agents (such as CN^-, OH^-, $EDTA^{4-}$) were unsuccessful.

1.6 Medium-ring heterocyclic diphosphines

Another interesting class of phosphine ligands is the medium-ring diphosphines. These are generally defined as compounds in which two phosphorus atoms are incorporated into a ring of between seven and twelve atoms.[75] These medium-sized rings are usually quite strained and show strong tendancies to undergo transannular reactions. Currently the state of understanding of these compounds and their

coordination chemistry is quite limited, but it has been proposed that compounds in this category will show novel properties and reactions.[75]

Eight-membered rings containing at least two donor atoms are unique in coordination chemistry, as they occupy a niche between large polydentate macrocycles with the ability to readily coordinate one or more metal centres and small heterocycles which posses limited chelating ability.[76] They are not themselves technically classed as macrocycles, as they do not meet the criteria of the minimum number of nine atoms and three donors. As incorporating donor atoms such as phosphorus into these cyclic and polycyclic molecules gives rise to rigid steric constraints on the metal, eight membered rings should have major implications for coordination chemistry and catalysis.[77]

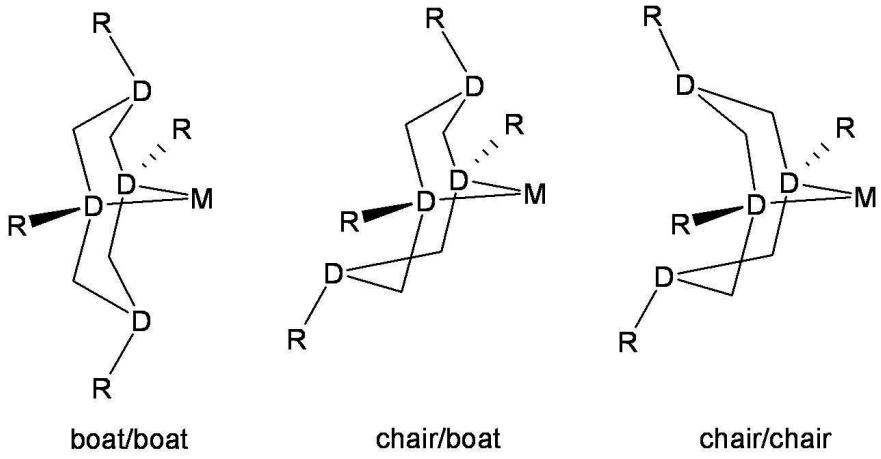

Figure 1.8 – Potential coordination modes and conformations of bidentate eight-membered rings.

Figure 1.8 (above) shows three potential coordination modes and conformations of polydentate eight-membered ring systems. Another interesting prospect for tetradentate eight-membered ring systems is the potential to chelate to two different metals in an *exo*-ditopic manner.[78] In order for the cyclic ligand to obtain this binding mode the heterocycle must be in the *chair/chair* conformation (**Figure 1.9**).

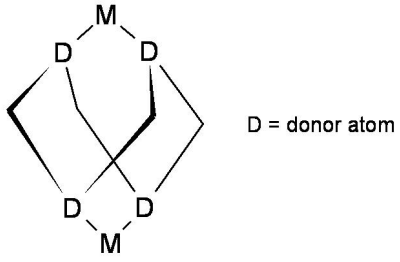

Figure 1.9 – *chair*/*chair* conformation of a tetradentate eight-membered heterocycle coordinating to two metals in an *exo*-ditopic manner.

An important class of eight-membered bidentate phosphines are the 1,5-diaza-3,7-diphosphacyclooctanes, first synthesised by Märkl and co-workers in 1980.[79] These were prepared by reacting two equivalents of an alkyl or aryl bis(hydroxymethyl) phosphine with two equivalents of a primary amine in a modified version of the Mannich reaction (**Scheme 1.7**). This Mannich-type synthesis of phosphines is a very important and convenient method of constructing heterocyclic bis(phosphines) and other heterocyclic phosphine ligands for transition metal coordination chemistry.[80]

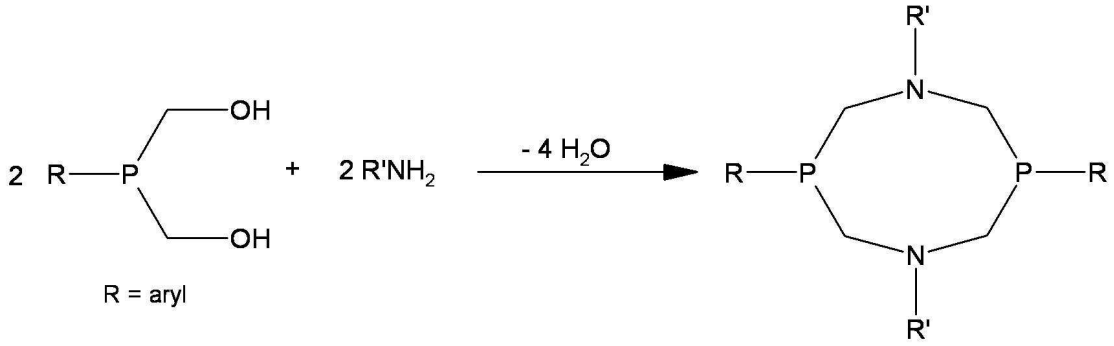

Scheme 1.7 – General synthesis of 1,5-diaza-3,7-diphosphacyclooctanes.

X-ray crystallographic studies by Wong *et al.*[81] on $[CH_2P(Ph)CH_2N(2\text{-pyridyl})]_2$ (**30**) (*i.e.* where R = Ph, R' = *o*-pyridyl) showed that the free ligand adopts a *crown* configuration in the solid state. The lone pairs of the phosphorus were also found to be *syn* to each other, which is perfect for chelation to metals. Coordination studies of this ligand with $Mo(CO)_4(\eta^2\text{-norbornadiene})$ gave the octahedral mononuclear complex as expected. The X-ray structure, however, showed that while the ligand does indeed chelate to the metal in a bidentate manner, the ligand actually adopts a *chair/boat* conformation by inversion of one half of the ligand (**31**) (**Figure 1.10**).

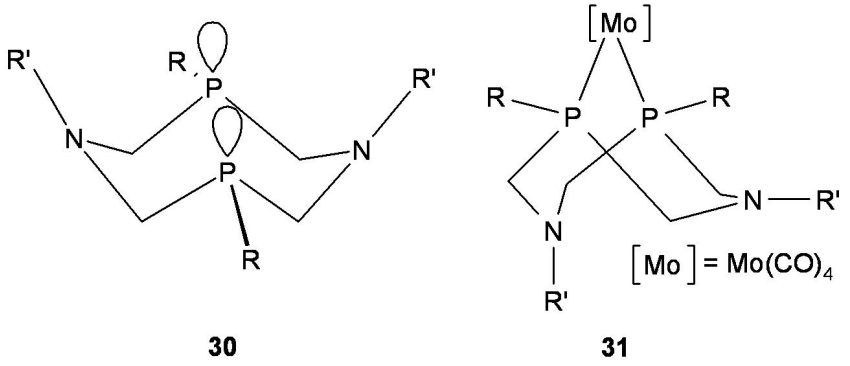

Figure 1.10 – Uncoordinated *crown* conformation of (30) and coordinated *chair/boat* conformation of its $Mo(CO)_4$ complex (31).

Attempts by the authors to create heterobimetallic complexes *via* coordination of a second metal (such as Zn^{2+}, Co^{2+}, Ni^{2+}) to the ring nitrogen atoms proved unsuccessful.

Further research in this area has been carried out over the past decade using 1,5-diaza-3,7-diphosphacyclooctanes functionalised with chiral,[82] unsaturated,[83] ferrocenyl,[84] ferrocenylmethyl,[85] *o*-oxyphenyl,[86, 87] and amino acid[88, 89] substituents at the heteroatoms. The general method of synthesis involves the Mannich-type preparation of hydroxymethyl phosphines from primary phosphines and formaldehyde, followed by the reaction with primary amines. These ligands have been used in coordination chemistry to prepare a range of asymmetric,[82] polymetallic,[85] water-soluble,[85-89] and chelate[82, 83, 85, 86, 88, 90-94] complexes of transition metals.

Karasik, Hey-Hawkins and co-workers discovered that the type of amine used in the synthesis of these ligands is crucial in determining the final product.[85, 89] Depending on the amine used in the reaction with a range of aryl phosphines, they obtained either the linear bis(arylaminomethyl)phosphines **32**, the six-membered 1,3-diaza-5-phosphacyclohexanes **33** and **34**, or the 1,5-diaza-3,7-diphosphacyclooctanes **35** (**Scheme 1.8**).

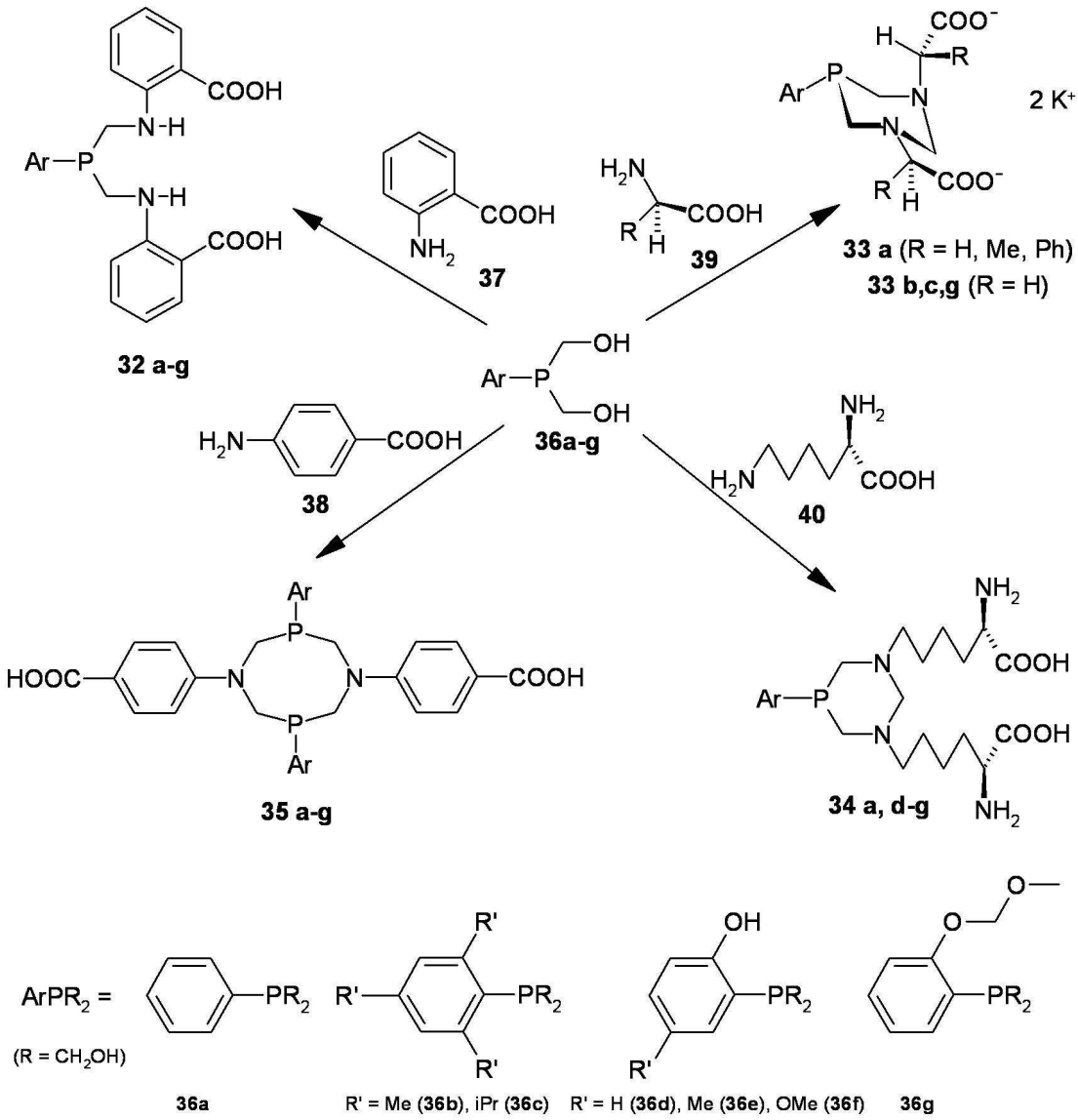

Scheme 1.8 – Reactions of bis(hydroxymethyl)arylphosphines with primary amines.

Interestingly, using different phosphines in the reaction whilst keeping the amine constant does not lead to the formation of a different type of product. When 2-aminobenzoic acid (**37**) is used as the amine, the linear bis(2-carboxyphenylaminomethyl)phosphines (**32a-g**) are generated as the products, even if the stoichiometry is altered to favour the cyclic 2+2 products. Interestingly however, when the 4-aminobenzoic acid (**38**) is instead used as the amine, both the linear bis(4-carboxyphenylaminomethyl)phosphines (analogous to **32a-g**) and the eight-membered heterocyclic 1,5-diaza-3,7-diphosphacyclooctanes are formed as products (**35a-g**), depending on the stoichiometry employed in the reaction. In contrast to the aromatic amines already mentioned, when the aliphatic amines glycine, D- or L-phenylglycine, L-alanine (all derivatives of **39**), or L-lysine (**40**) were used in the reaction instead, the six-membered 1,3-diaza-5-phosphacyclohexanes (**33a, b, c, g** and **34a, d-g**) are formed. This presumably occurs from the reaction of two equivalents of amine with

one equivalent of bis(hydroxymethyl)phosphine to initially give the linear bis(aminophosphines), followed by the condensation of a molecule of formaldehyde (which is present because the reactions to form the bis(hydroxymethyl)phosphines (**36a-g**) from the analogous primary phosphines and formaldehyde is done *in situ* and the products are not isolated) with the two NH groups to complete the six-membered ring. It is remarkable that these three different classes of ligand can be formed simply by altering the substituents on the amine, whereas using different substituted phosphines does not alter the final product.

The coordination chemistry of 1,5-diaza-3,7-diphosphacyclooctanes has also been studied.[82, 85, 91, 93, 95] When a series of 1,5-diaza-3,7-diphosphacyclooctane ligands were reacted with $PtCl_2$(cod), both binuclear (**41**) and chelate (**42**, **43**) complexes were isolated (**Scheme 1.9**).[95]

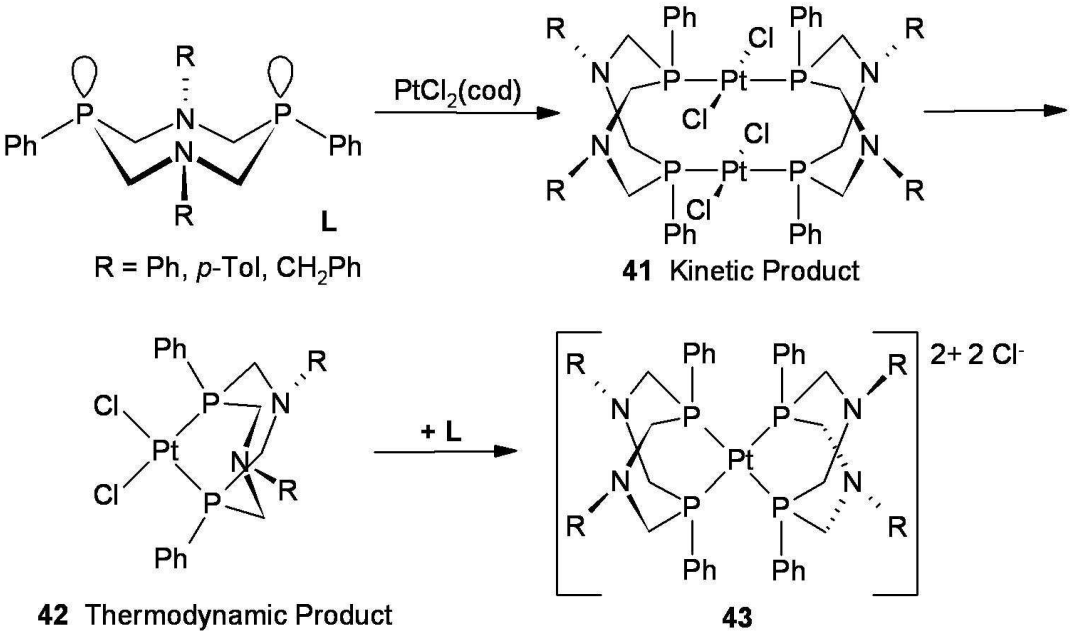

Scheme 1.9 – Coordination of 1,5-diaza-3,7-diphosphacyclooctanes with $PtCl_2$(cod).

The authors suggest that the binuclear complex **41** is a kinetic product, which converts to the chelate complex **42** (the thermodynamic product) over time in solution. The dicationic bischelate product **43** can also formed by increasing the amount of ligand present in the reaction to two equivalents, which can convert back to **41** over time. Palladium analogues have also been synthesised. The X-ray structures of the chelate complexes show that the ligand exists in a *chair*/*boat* conformation, while the free ligands occupy the *crown* configuration. This *chair*/*boat* conformation is typical for all eight-membered 1,5-donors found in the literature, as previously mentioned. This

conformation is favoured most likely due to the minimisation of ring strain which occurs as a result of the ligand chelating to the metal.

The six-membered 1,3-diaza-5-phosphacyclohexane ligands are also good ligands for transition metals, and behave as monodentate phosphine ligands as would be expected. *cis*-Bis(1,3-diaza-5-phosphacyclohexane) platinum and palladium complexes (**44**) have been synthesised, as well as monodentate carbonyl complexes of molybdenum and tungsten (**45** and **46**) (**Figure 1.11**).

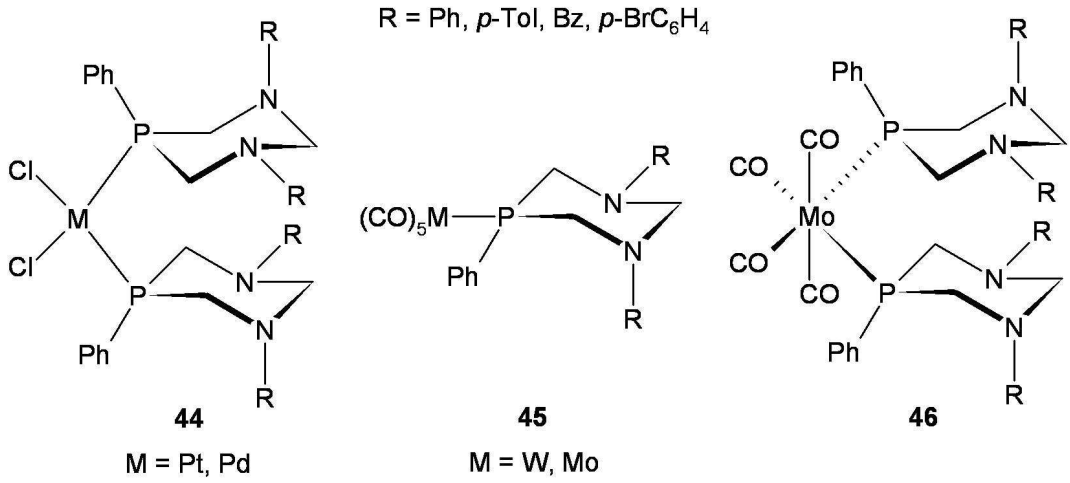

Figure 1.11 – Complexes of 1,3-diaza-5-phosphacyclohexane ligands.

When primary diamines (**48a-c**) are used in the ligand synthesis instead of monoamines, the entirely unexpected formation of macrocyclic aminomethylphosphines (**49a-e**) is achieved (**Scheme 1.10**).[96, 97]

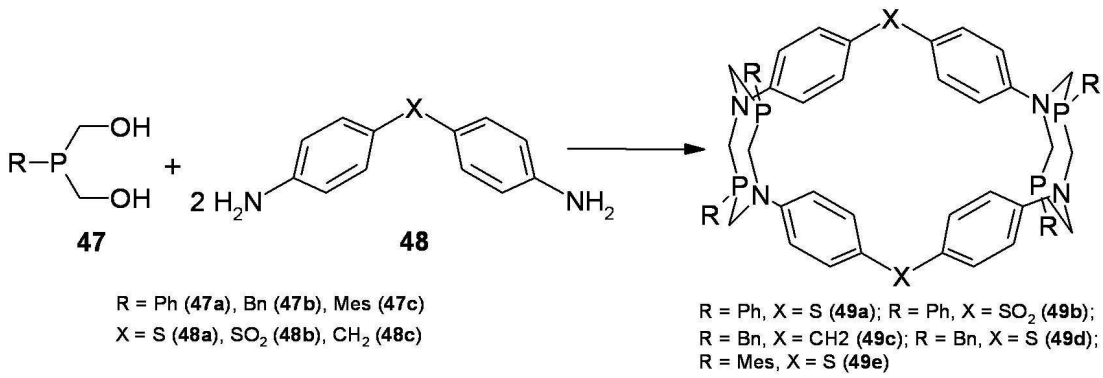

Scheme 1.10 – Formation of aminomethylphosphino macrocycles (49a-e).

In a similar manner to the reaction using 4-aminobenzoic acid, the 1,5-diaza-3,7-diphosphacyclooctane motif is formed from two equivalents each of phosphine and

amine. However, in this instance the two remaining primary amino groups on the alternate ends of the aromatic diamines condense with two further equivalents of phosphine to form a second 1,5-diaza-3,7-diphosphacyclooctane moiety. The resulting macrocyclic product is formed in approximately 50% yield, which is very high for a one-pot synthesis of a highly organised structure from six components,[98] especially without the use of high-dilution techniques. The macrocycle itself contains a large, hollow, basket-like intramolecular cavity, potentially useful for the construction of organised coordination compounds containing a catalytic site (such as a transition metal).

Other phosphorus- and nitrogen- containing heterocyclic ligands have also been prepared from diphosphines. Karasik *et al.*[93] have prepared a series of six-membered 1,3-diphospha-5-azacyclohexanes (**51a-d**) from the diphosphine $PhP(CH_2OH)_2CH_2$ (**50**) (**Scheme 1.11**).

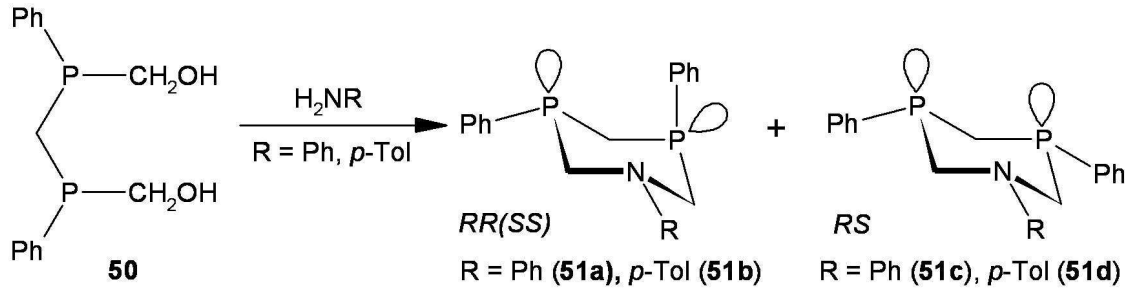

Scheme 1.11 – Preparation of 1,3-diphospha-5-azacyclohexanes (51a-d).

The condensation of one equivalent of the hydroxymethylphenyl diphosphine with one equivalent of primary amine leads to the formation of two stereoisomers of the six-membered P_2N heterocycle. In the *RR(SS)* isomer (**51a,b**), the lone pairs on the phosphorus atoms are orthogonal in all conformations, whereas the chair conformation of the *RS* isomer (**51c,d**) should give parallel phosphorus lone pairs when the phenyl groups are in the equatorial positions. The *RS* stereoisomer (**51a,b**) was isolated by fractional crystallisation and its coordination chemistry was explored with the Group 10 metals platinum and palladium (**Scheme 1.12**).

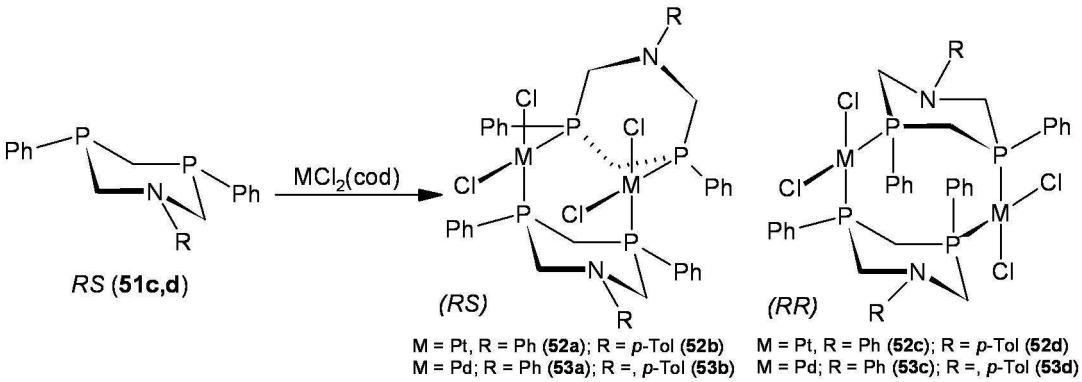

Scheme 1.12 – Coordination chemistry of *RS* 1,3-diphospha-5-azacyclohexane ligands (51c,d).

With both platinum and palladium, the resulting complexes are all dinuclear, and no chelate complexes are observed. This is due to the fact that the six-membered ring is too rigid to bend to a position where both phosphorus lone pairs could face towards the same metal centre. This is in contrast to the more flexible 1,5-diaza-3,7-diphosphacyclooctanes, which are commonly known to chelate to one metal. Their flexibility allows for the ligand to bend around in order to allow the second phosphorus lone pair to coordinate to the metal, after the first has already done so.

In order to make an analogue of these heterocyclic {P_2N} ligands capable of chelating to one metal centre, Karasik and co-workers[92, 99] targeted a more flexible version based on the eight-membered 1,5-diaza-3,7-diphosphacyclooctanes. Their strategy was similar to the synthesis of 1,3-diphospha-5-azacyclohexanes: to react a hydroxymethylaryl diphosphine with one equivalent of primary amine to form the ring. In order to make an eight-membered ring, two more carbon atoms are needed, and this is achieved by using a diphosphine with a propylene spacer group between the two phosphorus atoms. **Scheme 1.13** below shows the reaction of bis(hydroxymethylarylphosphino)propanes (**54a,b**) with the primary amines 5-aminoisophthalic acid and benzylamine.

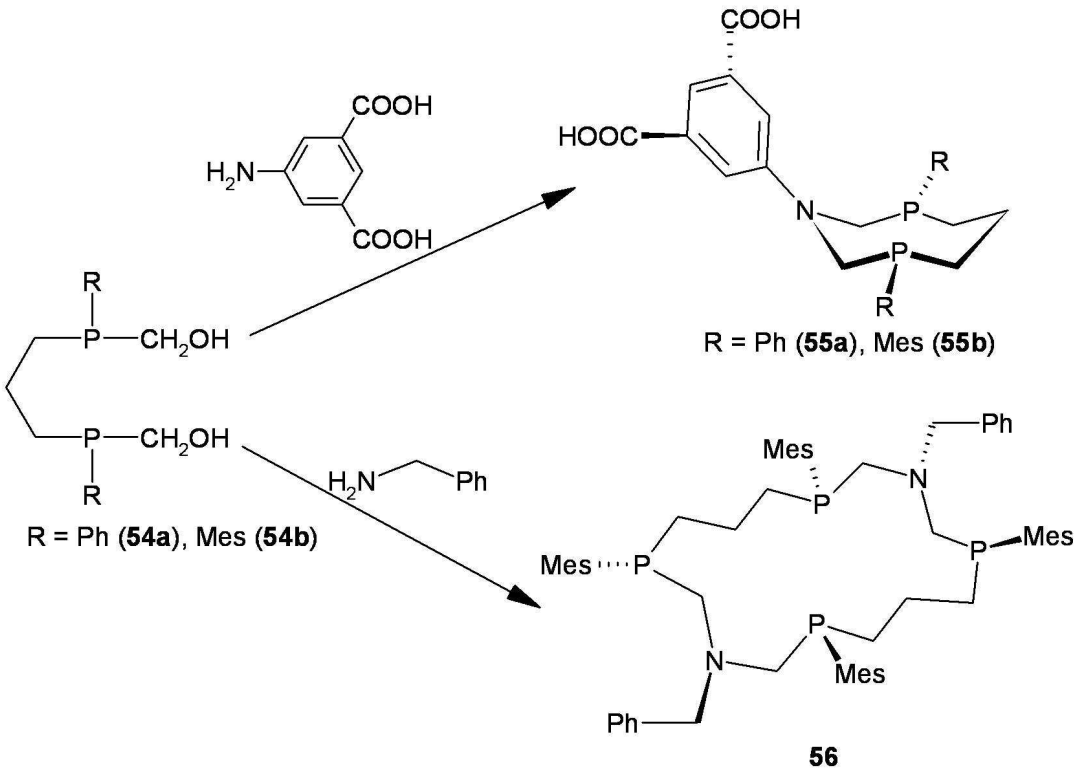

Scheme 1.13 – Assembly of ligands (55a,b) and (56) from bis(arylhydroxymethyl)phosphino propanes.

When both the phenyl and the mesityl-substituted diphosphines **54a** and **54b** respectively are reacted with 5-aminoisophthalic acid and formaldehyde, the desired 1-aza-3,7-diphosphacyclooctane ligands (**55a,b**) are formed. The molecular structures and NMR spectra of these ligands show that they adopt the familiar *crown* conformation both in the solid state and in solution. In contrast to this, when 5-aminoisophthalic acid is replaced with benzylamine, an entirely unexpected product is formed. Instead of 2+1 cycloaddition being observed in the case with 5-aminoisophthalic acid, a 4+2 cycloaddition occurs to give the sixteen-membered P_4N_2 macrocycle (**56**) in 51% yield. This reaction is a rare example of a high-yielding self-assembly of a large phosphine containing macrocycle without employing the use of metal-templating or high-dilution techniques. The product is isolated as only the *RSSR* isomer, despite using a mixture of the *(RS)*- and *(RR/SS)*- diastereoisomers of 1,3-bis(mesitylhydroxymethylphosphino)propane. The coordination chemistry of this sixteen-membered tetraphosphine macrocycle has yet to be explored, but the 1-aza-3,7-diphosphacyclooctane ligands exhibit coordination chemistry very similar to that of the 1,5-diaza-3,7-diphosphacyclooctanes in that they tend to chelate to Group 10 metals such as Pt to give the *cis*-bidentate complexes upon reaction with $[PtCl_2(cod)]$.[92]

Katti and co-workers[88, 100] have also investigated the reactions of a number of hydroxymethyl phosphines with primary amines, with the intent of linking together

biologically useful molecules such as amino acids, peptides and proteins under mild conditions. This potentially shows huge scope for applications in the biomedical sciences, such as the immobilisation of phosphines on peptides to give interesting peptide- or protein-metal conjugates, and subsequent coordination of a metal centre. Altering metal-binding sites within peptides and proteins has even been shown to enhance structural integrity, stabilise conformations that are biologically active, and overall help to assist new enzymatic activity.[101]

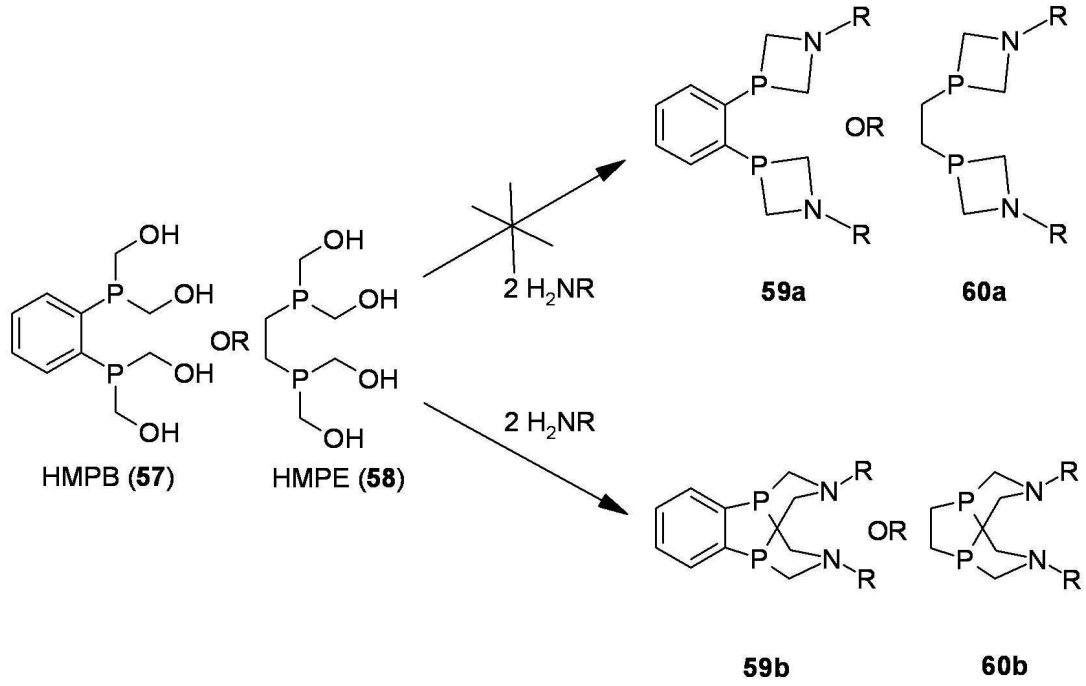

Scheme 1.14 – Reactions of HMPB (57) and HMPE (58) with primary amines.

The hydroxymethyl phosphines 1,2-bis(bis(hydroxymethyl)phosphino)benzene (**57**) (HMPB) and 1,2-bis(bis(hydroxymethyl)phosphino)ethane (**58**) (HMPE) were reacted with a range of amino acids and model peptides in ethanol. Two possible structures were initially proposed for the products of the reactions, one in which each primary amino moiety reacts with both hydroxymethyl groups on each phosphorus to create two four-membered rings (**59a** and **60a**). The second possibility is where a CH_2OH group from each adjacent phosphorus atom reacts with the NH_2 terminus of the amine to afford two seven-membered heterocyclic rings (**59b** and **60b**). X-ray structural analysis confirmed that the second of the two possible structures to be correct (**Scheme 1.14**). These results show that the water-soluble phosphines HMPB (**57**) and HMPE (**58**), when reacted with primary amines, kinetically favour monomeric products, and do not tend to undergo cross-linking to form polymers. This is important in context to using HMPB (**57**) and HMPE (**58**) to modify peptides and proteins to produce P-CH_2-N linkages, without creating cross-linked polymers.

1.7 Water-soluble phosphine ligands

Phosphine ligands able to impart water solubility upon a transition metal complex have received much attention, most notably in the fields of homogeneous catalysis[102] and biomedicine.[103] The abundant nature of water and its non-toxic nature make it an ideal green solvent for many industrial processes. Water-soluble phosphines have been prepared by the addition of sulfonate,[104] ammonium,[105] carboxylate,[106] carbohydrate,[107] phosphonium and phosphonate,[108] and hydroxymethyl[109] groups to the parent phosphine.

The most widely used water-soluble phosphines are the sulfonated arylphosphines, such as (3-sulfonatophenyl)diphenylphosphine (TPPMS) (**61**) and tris(3-sulfonatopheny)phosphine (TPPTS) (**62**) (**Figure 1.12**).

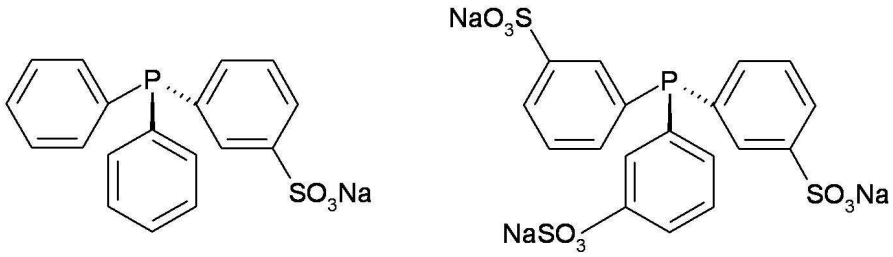

TPPMS (**61**) TPPTS (**62**)

Figure 1.12 – The sulfonated phosphine ligands TPPMS (61) and TPPTS (62).

TPPMS (**61**) was first synthesised by Ahrland, Chatt and co-workers[104] in 1958. It is commonly used as a ligand in the selective hydrogenation of aldehydes by hydrogen transfer using $[RuCl_2(TPPMS)_2]$ as the catalyst, giving the unsaturated alcohol in high yield (**Scheme 1.15**).[110]

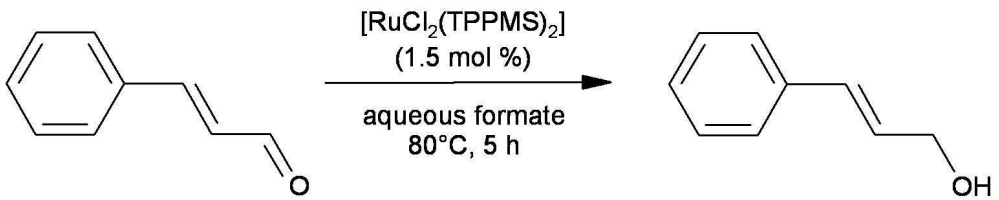

cinnamaldehyde (**63**) **64**, 98% yield

Scheme 1.15 – Selective hydrogenation of cinnamaldehyde (63) using a Ru TPPMS catalyst.

The use of TPPTS (**62**) as ligand in organometallic chemistry and biphasic homogeneous catalysis has also been widely studied. It is most famously employed in

the Ruhrchemie/Rhône-Poulenc oxo process, based on a rhodium catalyst (**Scheme 1.16**). This process has been commercially used for the hydroformylation of alkenes since 1984.[111]

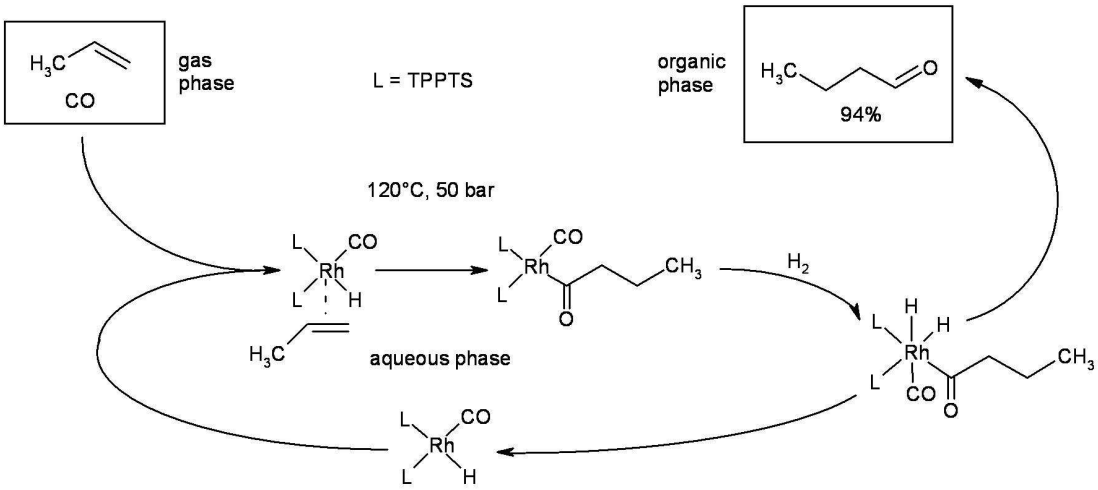

Scheme 1.16 – The Ruhrchemie/Rhône-Poulenc oxo process.

One drawback of sulfonated phosphines is that their syntheses from arylphosphines and oleum are often cumbersome and hard to accurately reproduce, due to the formation of phosphine oxides during the reaction. Some authors have also found that the sulfonate groups are non-innocent and can alter other properties of the ligand and its complexes. For example, Tyler and co-workers discovered that the sulfonate groups affected the ability of their iron complexes to bind small molecules such as dinitrogen.[112] However, methods of synthesising sulfonated arylphosphines cleanly with almost no oxide formation have also been proposed.[113, 114]

1.7.1 PTA-based phosphine ligands

1,3,5-triaza-7-phosphaadamantane (PTA) (**66**) is a cage-like monodentate phosphine ligand based on adamantane, first prepared by Daigle *et al.* in 1974.[115] It has received much attention in the field of coordination chemistry and organometallic catalysis, largely due to its air stability and solubility in water. Its water solubility is a result of hydrogen bonding of the nitrogen atoms to water.[116] It can be synthesised by reaction of 1,3,5,7-tetraazaadamantane with tris(hydroxymethyl)phosphine (THMP) (**65**) (route (a) in **Scheme 1.17**).[115] Alternatively, it can be made by reacting THMP (**65**) with a solution of ammonia and formaldehyde (route (b) in **Scheme 1.17**).[115]

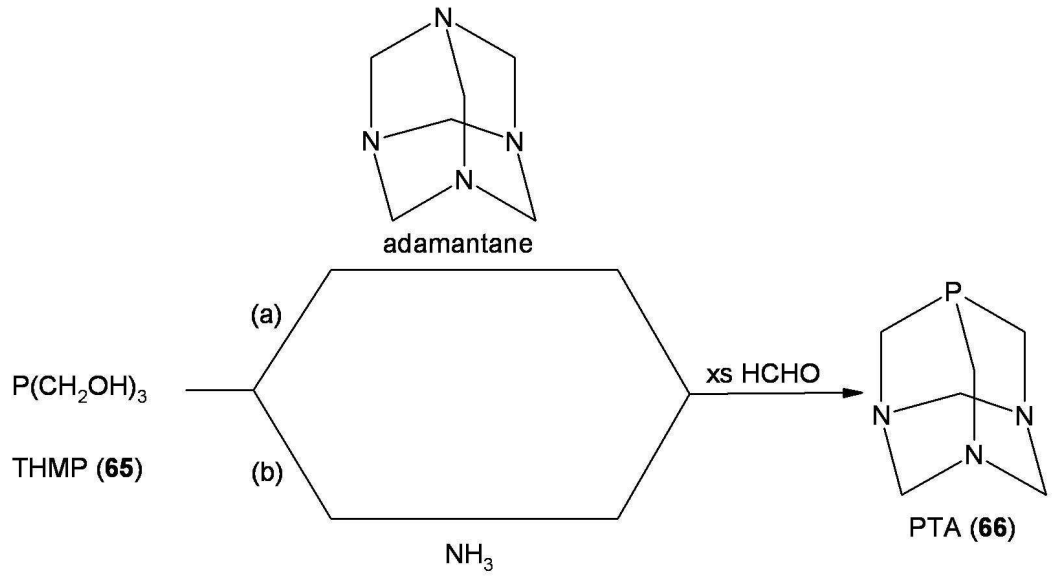

Scheme 1.17 – Syntheses of 1,3,5-triaza-7-phosphaadamantane (PTA) (66) from tris(hydroxymethyl)phosphine (THMP) (65).

PTA (**66**) has excellent donating ability (similar to PMe_3) and has a relatively small cone angle of 102°.[117] Additionally, it is thermally stable up to 260°C.[118] In acidic media **66** is protonated to give $[PTA(H)]^+$, which shows greater solubility. For these reasons, PTA complexes of rhodium and ruthenium have been the subject of much research, including both monophasic[119, 120] and biphasic[121-123] hydrogenation of alkenes and aldehydes. Tang *et al.*[124] have even shown that PTA itself is effective as an organocatalyst in the Morita-Baylis-Hillman reactions of certain activated alkenes with electrophiles such as aldehydes and imines.

Additionally, **66** can also be readily modified to give other similar P-CH_2-N heterocycles. Most modifications to date have focused on reactions of the 'lower rim' of the ligand, the triazacyclohexane ring. Examples include ring-expanded variants of PTA (**67**, **68**),[125, 126] the sulfone derivative $PTASO_2$ (**69**),[127, 128] the diacetyl DAPTA (**70**),[117, 129] and a ring-opened version (RO-PTA) (**71**) (**Figure 1.13**).[130-132] Only one example of a modification of the 'upper rim' of PTA has been reported to date, the bidentate phosphine PTA-PPh_2 (**72**) (**Figure 1.13**).[133]

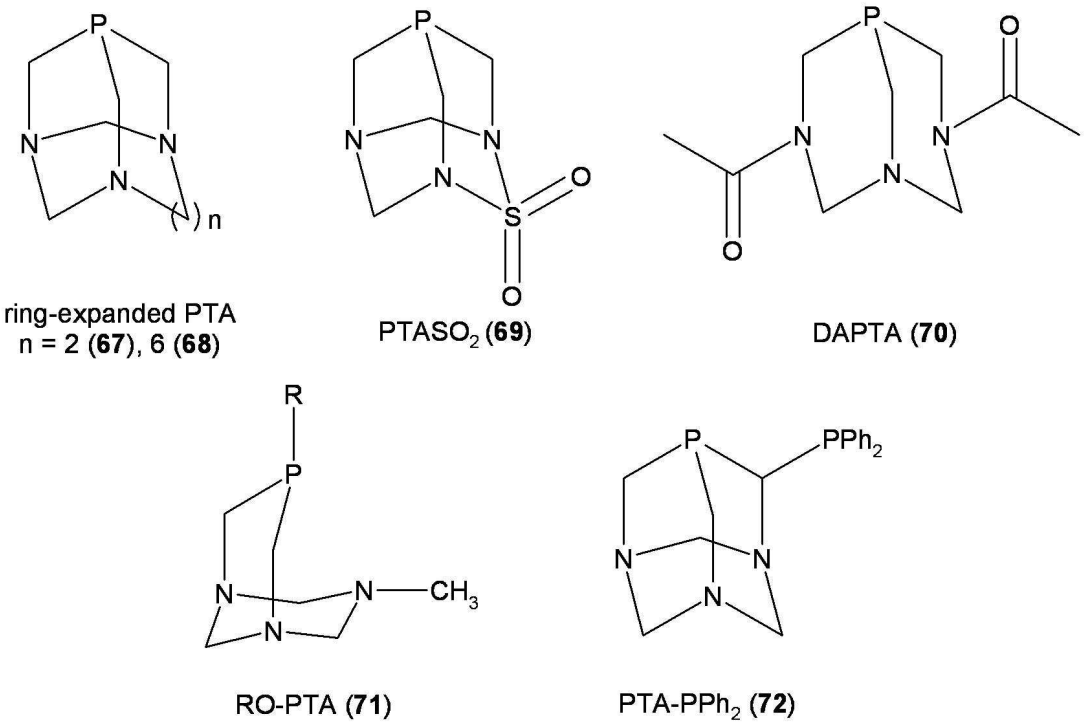

Figure 1.13 – Derivatives of PTA.

Majoral and co-workers[125, 126] have shown that diamines possessing differently sized spacer groups between the nitrogen atoms (such as $H_2N(CH_2)_nNH_2$ (n = 2, 6)) can be used instead of formaldehyde to prepare the ring-expanded PTA derivatives in a modified version of the reaction in **Scheme 1.17**. A similar method is employed when preparing the 2-thia-1,3,5-triaza-7-phosphaadamantane 2,2-dioxide ($PTASO_2$) (**69**), where sulfamide ($H_2NSO_2NH_2$) is employed in the reaction, using an excess of formaldehyde.[127, 128] Interestingly, however, replacing the CH_2 group with an SO_2 moiety renders $PTASO_2$ (**69**) almost completely insoluble in water, making it useless as a water-solubilising ligand in organometallic catalysis. The reaction of PTA (**66**) with acetic anhydride acetylates two of the nitrogen groups and removes one of the CH_2 spacers to afford the bicyclic ligand 3,7-diacetyl-1,3,7-triaza-5-phosphabicyclo[3.3.1]nonane (DAPTA) (**70**), first reported by Siele in 1977.[129] Unexpectedly, the water solubility of DAPTA (**70**) was found to be 7.4 M,[117] making it one of the most water-soluble phosphine ligands ever reported. This makes DAPTA (**70**) of much interest in the field of water-soluble catalysis, and recently it has been used as a ligand for water-soluble models of the active site of the Fe-only hydrogenase enzyme.[134, 135] The open-cage version of PTA (RO-PTA (**71**)) has also been synthesised by cleavage of one of the C-P bonds of the phosphonium chloride salt of PTA (**73**) by reaction with sodium amide in liquid ammonia (**Scheme 1.18**).[130-132] The product **71** is isolated by sublimation of the crude product. The resulting compound

acts as a P, N bidentate ligand, and complexes of gold and molybdenum have been isolated and characterised.[130-132]

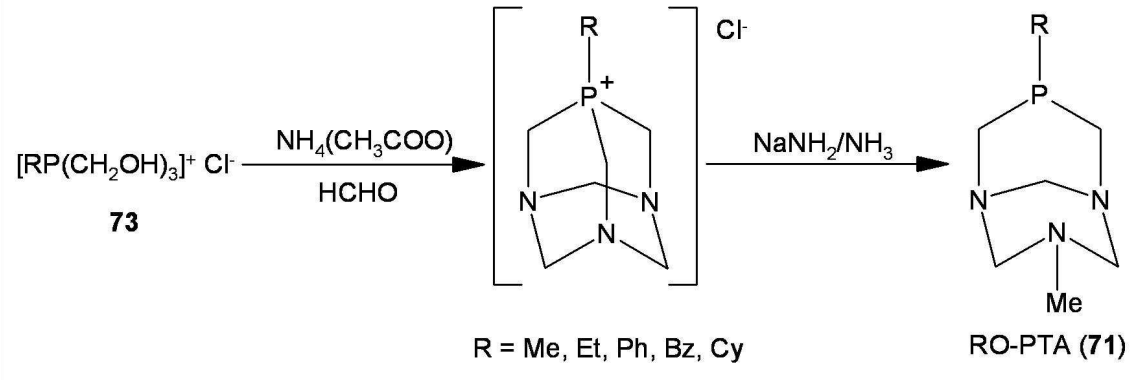

Scheme 1.18 – Synthesis of RO-PTA (71).

The only P, P bidentate derivative of PTA is the diphenylphosphine-modified PTA-PPh_2 (**72**).[133] It is synthesised by the selective lithiation of one of the CH_2 groups of the 'upper rim' of PTA, followed by reaction of the lithium salt (PTA-Li) (**74**) with chlorodiphenylphosphine (**Scheme 1.19**). Coordination complexes of PTA-PPh_2 (**72**) with both molybdenum and tungsten have been reported, and in both cases the ligand acts as a bidentate phosphine donor, creating a four-membered chelate ring between the ligand and metal.[133]

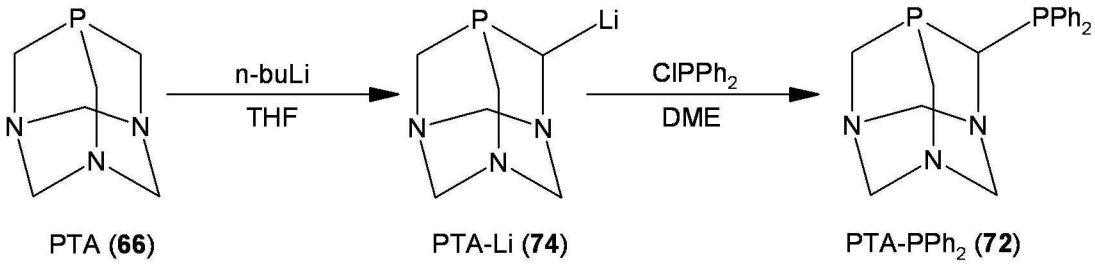

Scheme 1.19 – Synthesis of PTA-PPh_2 (72).

1.7.2 Hydroxyalkylphosphine Ligands

Another alternative to using sulfonated aryl phosphines as water-solubilising ligands is to use hydroxyalkyl phosphines. The most simple hydroxyalkyl phosphine is tris(hydroxymethyl)phosphine (THMP) (**65**), which is moderately air stable and unusually for trialkylphosphines is a crystalline solid at room temperature (mp = 58 °C).[136] It can be synthesised by reacting PH_3 gas with formaldehyde in the presence of catalytic amounts of $K_2[PtCl_4]$ in aqueous solution, which is efficient but requires the handling of extremely toxic gaseous PH_3 in large amounts (Reaction 1, **Scheme**

1.20).[137] An alternative method of synthesising THMP (**65**) without the use of PH_3 is to react the commercially available $[P(CH_2OH)_4]Cl$ (THPC) (**73**) with base (Reaction 2, **Scheme 1.20**).[138]

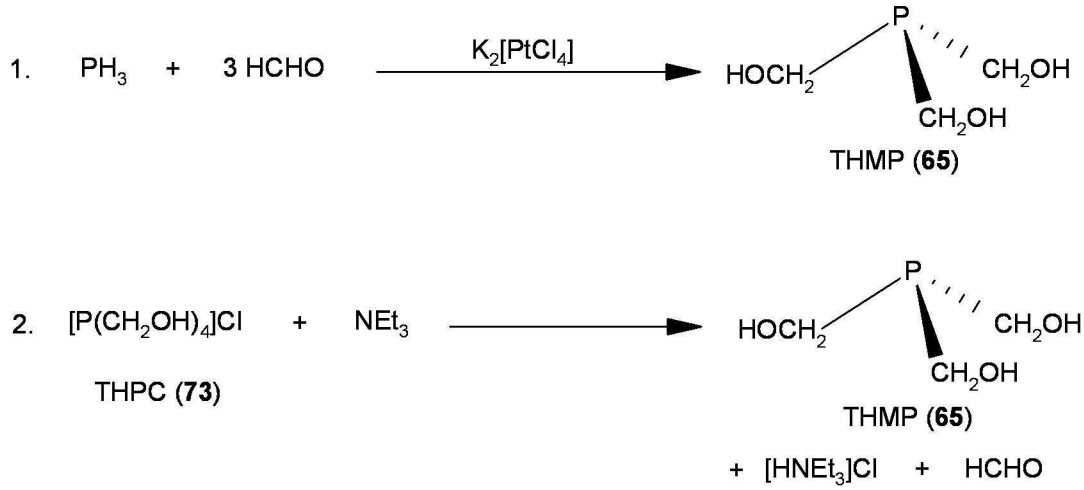

Scheme 1.20 – Syntheses of tris(hydroxy)methyl phosphine (THMP) (65).

In coordination chemistry THMP (**65**) acts as a monodentate ligand much like the similar trialkylphosphines. The *cis*-dihalo platinum(II) and palladium(II) complexes of the formula $[MX_2\{P(CH_2OH)_3\}_2]$ can simply and reliably be prepared from the corresponding $[MX_2(cod)]$ salts.[136] These same dichloro complexes have also previously been reported by Chatt *et al*.[109] using the appropriate $[MCl_4]^{2-}$ salt (Pt or Pd), though this route has been reported by Ellis *et al.*[136] to give impure products and poor yields. Some ruthenium complexes of **65** have also been synthesised which have been shown to catalyse the hydrogenation of sorbic acid.[139] The sorbic acid is reduced in the presence of $[Ru(Cp^*)(Cl)(CO)\{P(CH_2OH)_3\}]$, with a TOF of 2.6 h^{-1} giving a 40% yield of 3-hexenoic acid (80% *cis*) in 15h. These results are better than the equivalent TPPTS based catalyst, though they are not exceptional.[102] Other THMP complexes of iridium and rhodium have also been shown to catalyse the hydrogenation of cinnamaldehyde and the hydroformylation of 1-pentene respectively.[140] Higham *et al.* have also synthesised ruthenium and rhodium complexes of a range of monodentate hydroxymethyl phosphines including THMP, bis(hydroxymethyl)phenylphosphine, and tris(hydroxypropyl)phosphine.[141, 142]

Using hydroxymethyl groups to impart solubility upon phosphines is an idea that has also been extended to diphosphines, such as HMPB (**57**) and HMPE (**58**), first reported by Katti and co-workers in 1996.[143] They investigated the coordination chemistry of these ligands with palladium and platinum for potential use in organometallic

catalysis,[144] as well as ^{198}Au,[145] and Re (**75-78**) for potential use as water-soluble complexes for radiopharmaceuticals in nuclear medicine (**Scheme 1.21**).[143, 146]

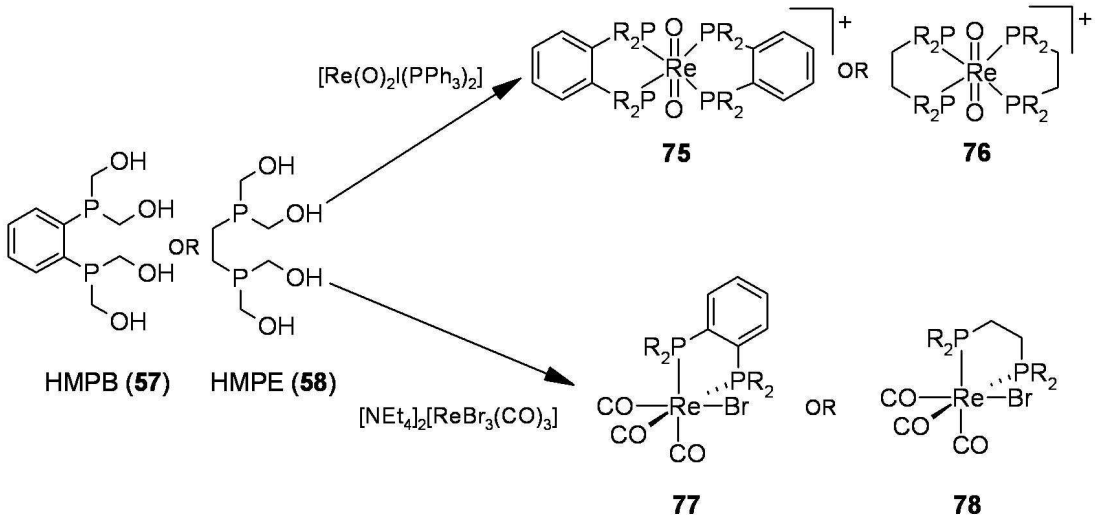

Scheme 1.21 – Synthesis of rhenium HMPB and HMPE complexes.

Hydroxyalkyldiphosphines with longer-chain hydroxyalkyl groups were first produced by Tyler and co-workers.[147] Ligands based on HMPE containing $(CH_2)_xOH$ groups where x = 3, 4, 5 where prepared and their coordination chemistry investigated with Ni(II), Ru(III), and Rh(I). More recently, they have synthesised a range of water-soluble iron(II) complexes (**79a-e** and **80a-e**) based on these longer-chained hydroxyalkyl ligands and their related ester variants for potential use as dinitrogen and dihydrogen binding agents (**Scheme 1.22**).[112, 148, 149]

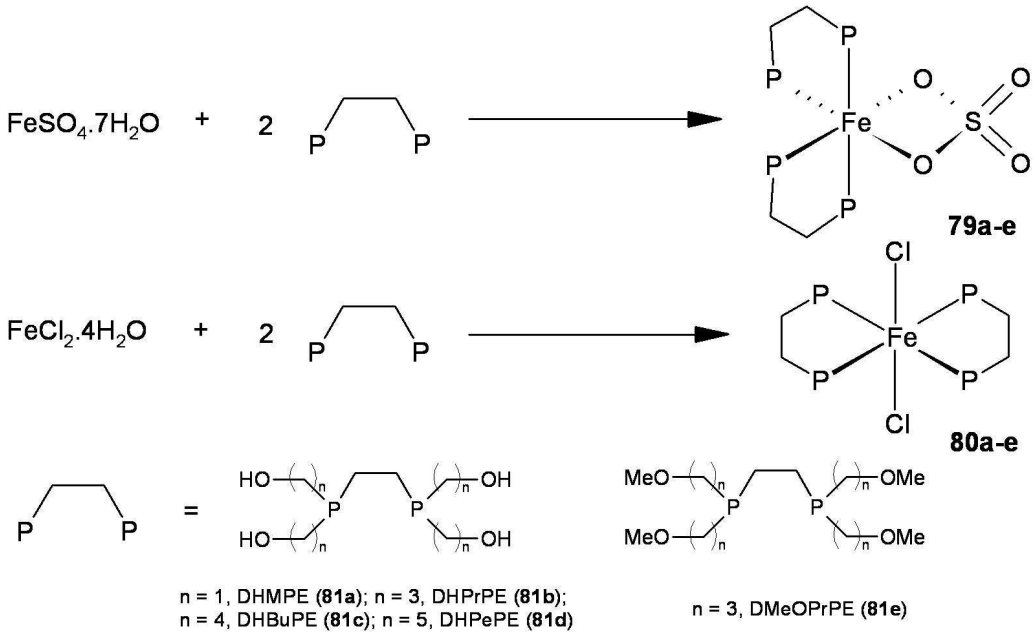

Scheme 1.22 – Synthesis of water-soluble long-chained hydroxyalkyl and methyl ester bisphosphine iron(II) complexes (79a-e and 80a-e).

Iron(II) chloride and iron(II) sulfate salts were reacted with two equivalents of diphosphine in either methanol or ethanol to give the *cis*-Fe(II) bis(diphosphine) sulfates **79a-e** and the *trans*-Fe(II) bis(diphosphine) dichlorides **80a-e** respectively. The *trans*-dichlorides **80a-e** have been shown to be capable of binding small molecules such as dinitrogen, carbon monoxide and acetonitrile in the presence of sodium tetraphenylborate in alcoholic solvents (**Scheme 1.23**).[112] However, the dinitrogen complexes (**81c,e**) only forms under 50 psi of dinitrogen gas.

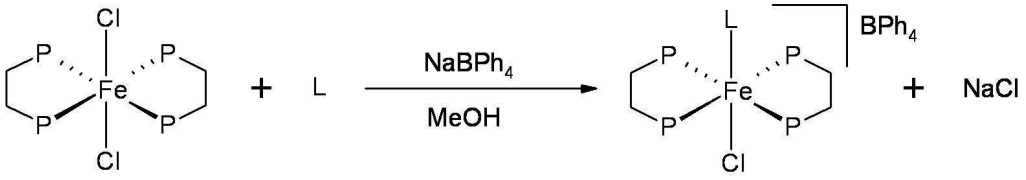

80a-e L = N_2 (**81a-e**), CO (**82a-e**), MeCN (**83a-e**)

Scheme 1.23 – Coordination chemistry of small molecules with *trans*-[FeL_2Cl_2] complexes 80a-e in alcoholic solvents.

In aqueous solutions however, the *trans*-dichloride complexes **80a-e** first react with the solvent to form complexes of the general formula *trans*-[$FeL_2(H_2O)(Cl)]^+$ (where L is a water-soluble chelating diphosphine ligand). Subsequent exposure to dinitrogen or dihydrogen affords the complexes *trans*-[$FeL_2(N_2)(Cl)]^+$ and [$FeL_2(H_2)(Cl)]^+$ (Reaction 1, **Scheme 1.24**).

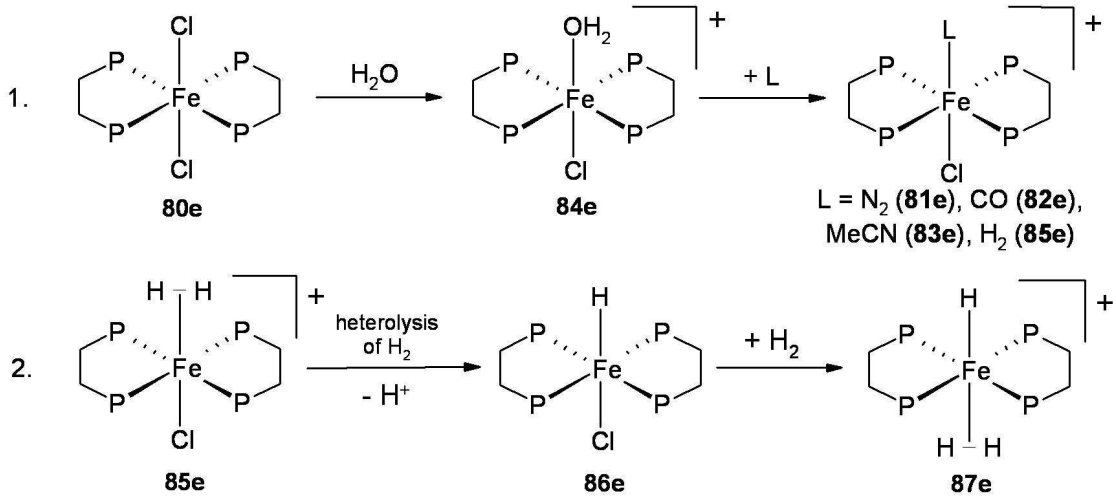

Scheme 1.24 – Coordination chemistry of N_2 and H_2 with *trans*-[FeL_2Cl_2] complexes in aqueous solution.

In the case of the dihydrogen complex **85e**, the coordinated H_2 molecule undergoes heterolysis and loses a proton to ultimately give the *trans*-[$FeL_2(H)(H_2)]^+$ product **87e**

(Reaction 2, **Scheme 1.24**).[148, 149] Spectroscopic studies show that following the loss of the first chloride and replacement with dihydrogen, heterolysis of the H_2 occurs to initially form *trans*-[$FeL_2(H)(Cl)$] (**86e**). The second chloride is then replaced by a second molecule of H_2 to give the *trans*-[$FeL_2(H)(H_2)]^+$ product (**87e**). When exposed to an atmosphere of dinitrogen, the H_2 molecule is substituted by N_2 to give the *trans*-[$FeL_2(H)(N_2)]^+$ product. Water soluble complexes with coordinated H_2 and N_2 ligands are quite rare in the literature, and ultimately show promise as water-soluble gas scrubbers to separate dinitrogen and dihydrogen from natural gas streams. Solubility of the complexes in polar solvents is especially important for gas scrubbing applications due to the need to minimise the solubility of the natural gas in the carrier solvent to maximise the separation.

1.8 A novel self-assembled iron(II) hydroxymethylphosphine complex

The phosphonium salt tetrakis(hydroxymethyl)phosphonium sulfate $[P(CH_2OH)_4]SO_4$ (THPS) is used as a biocide in oil wells. It was noticed by oil well engineers that THPS aids the dissolution of iron sulfide particulates and deposits which are a result of anaerobic microbial activity and indigenous H_2S. It is necessary to remove these deposits as they can lead to blockage and restrictions with the pipework and upset the oil/water separation, both of which are undesirable and lead to damage. It was also discovered that the dissolution of the FeS particulates is accompanied by a red colouration of the water in the well. Recently, researchers at Albright and Wilson (now part of Rhodia plc) undertook studies to explain how THPS helps to dissolve iron sulfide deposits and also to determine the origin of the red colouration observed which was believed to be due to a water-soluble iron complex.

The reactions of THPS and its related phosphine THMP were performed with a variety of Fe(II) and Fe(III) salts (*e.g.* FeS, $FeCl_2$, $FeCl_3$, $FeSO_4$, $[Fe(NH_4)_2(SO_4)_2]$) in order to simulate the oil well conditions within the laboratory.[150] The development of coordination chemistry of water-soluble phosphines with relatively cheap metals such as iron is also an attractive prospect due to the financial and environmental benefits they offer. They found that only the ferrous ammonium sulfate afforded a red colouration of the aqueous solution when reacted with THPS and THMP. Other hydroxyalkylphosphonium salts formed no red complexes at all. Crucially however, it was discoved that the presence of ammonium cations (naturally present in oil well waters and also as a result of the addition of ammonium bisulfite as an oxygen scavenger), an iron(II) salt, and THPS or THMP are all of paramount importance to the formation of the red complex. Following optimisation of the reaction conditions, it was

discovered that two equivalents of THPS (*i.e.* four equivalents of phosphonium ions) added to ferrous ammonium sulfate (Mohr's salt) in aqueous solution at room temperature, followed by the slow addition of a base (*i.e.* NaOH) whilst maintaining the pH between 4.5 and 5 leads to a deep red solution. Deep red crystals suitable for single crystal X-ray diffraction analysis were isolated when the solution was left at 5°C for two weeks.

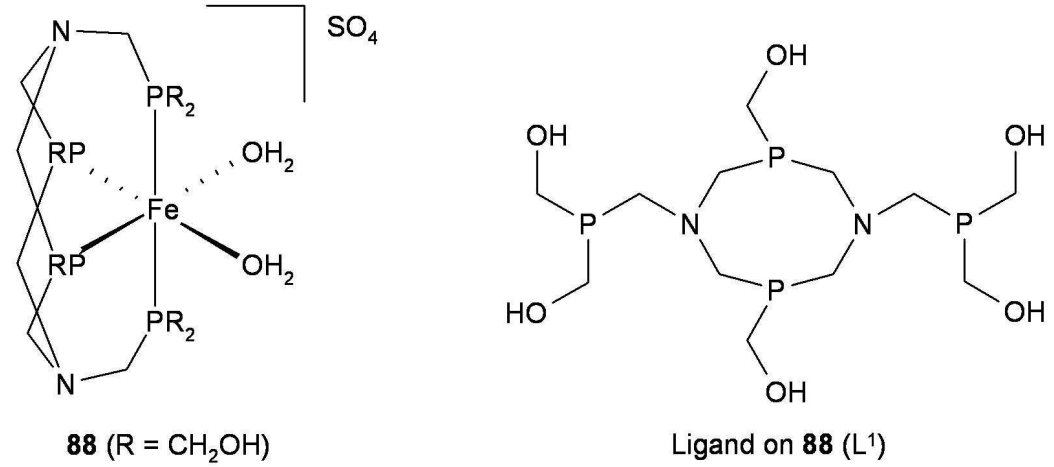

88 (R = CH_2OH) Ligand on **88** (L^1)

Figure 1.14 – Structure of the Fe(II) phosphine complex 88 and its self assembled ligand L^1.

The molecular structure of **88** shows that the red complex is a dicationic pseudo octahedral Fe(II) complex with an interesting self-assembled 1,5-diaza-3,7-diphosphacyclooctane based hydroxymethyl ligand (L^1) (**Figure 1.14**). The ligand acts as a chelating bidentate ligand with the two ring-phosphorus atoms coordinating to the metal in a *cis* equatorial fashion. The two nitrogen atoms of the cyclic ring possess pendant $CH_2P(CH_2OH)_2$ groups which each coordinate to the metal via the *trans* axial sites. The two remaining equatorial sites are occupied by two water molecules. It is not known the exact mechanism by which the complex is formed but is believed to involve a Mannich-like condensation of a $[P(CH_2OH)_4]^+$ moiety with two ammonium ions, the whole process being templated by the metal to form the eight-membered ring and its pendant arms.

1.9 Concluding Remarks

Phosphorus-based ligands represent an extremely important class of ligand in the fields of organometallic and transition metal coordination chemistry, due to the wide range of steric and electronic properties that can be altered by changing the substituents on phosphorus. The study of phosphine ligands in particular has received

much attention due to their ability to stabilise metals in their lowest oxidation states by accepting π electron density from the metal as well as potential applications as ligands in transition metal catalysis. $^{31}P\{^{1}H\}$ NMR spectroscopy as a characterisation technique is also useful and convenient for monitoring reactions and identifying products containing phosphorus nuclei.

The incorporation of multiple phosphine donor atoms into macrocyclic rings has important implications in coordination chemistry, offering greater stability in terms of both chelating ability and the additional stability offered by the macrocyclic effect. Phosphorus donors incorporated into smaller heterocyclic rings show much promise within the field of coordination chemistry and have been shown to be useful ligands in coordinating to a wide range of transition metals.

There is increasing interest in performing chemistry in aqueous media for applications in biomedicine, biphasic catalysis, and natural gas scrubbing. Chemistry in water is also more financially and environmentally friendly as it does not generate large amounts of expensive organic solvent waste or consume large amounts of energy needed to produce them. Water-solublising phosphine ligands such as sulfonated phosphines, PTA based ligands, and hydroxyalkylphosphines in particular are receiving much attention in this field.

Chapter 2 of this thesis investigates the coordination chemistry of the water-soluble Fe(II) cyclic hydroxymethylphosphine complex **88** with a range of neutral and ionic ligands, and examines the reactivity of the pendant hydroxymethyl groups on the coordinated ligand L^1 to give other functionalised derivative complexes.

Chapter 3 extends the self-assembly process by altering the substrates involved in the formation of **88**, and determines whether related complexes can be formed and isolated using this method. The formation of an iron(II) complex containing a new bicyclic bidentate phosphine ligand is described, and its coordination chemistry with a range of ligands investigated.

Chapter 4 is the experimental section and describes experimental techniques and procedures used in the synthesis and investigation of the compounds described in Chapters 2 & 3.

1.10 References

1. P. Thenard, *C.R. Hebd. Seances Acad. Sci., Ser. C*, 1847, **25**, 892.
2. A. Michaelis and H. V. Soden, *Annalen*, 1885, **229**, 295.
3. J. Chatt and F. G. Mann, *J. Chem. Soc.*, 1938, 1949.
4. C. A. McAuliffe, in *"Comprehensive Coordination Chemistry"*, Eds. G. Wilkinson, R. D. Gillard and J. A. McCleverty, Pergamon Press, 1987, vol. 2, p. 990.
5. J. H. Downing and M. B. Smith, in *"Comprehensive Coordination Chemistry II"*, eds. J. A. McCleverty and T. J. Meyer, Elsevier Pergamon, 2004, vol. 1, p. 253.
6. C. A. Tolman, *J. Am. Chem. Soc.*, 1970, **92**, 2956.
7. C. A. Tolman, *Chem. Rev.*, 1977, **77**, 313.
8. E. C. Alyea, S. A. Dias, G. Ferguson and R. J. Restivo, *Inorg. Chem.*, 1977, **16**, 2329.
9. G. Ferguson, P. J. Roberts, E. C. Alyea and M. Khan, *Inorg. Chem.*, 1978, **17**, 2965.
10. T. L. Brown, *Inorg. Chem.*, 1992, **31**, 1286.
11. T. L. Brown and K. J. Lee, *Coord. Chem. Rev.*, 1993, **128**, 89.
12. D. White, B. C. Taverner, P. G. L. Leach and N. J. Coville, *J. Comput. Chem.*, 1993, **14**, 1042.
13. P. W. N. M. van Leeuwen, P. J. C. Kamer, J. N. H. Reek and P. Dierkes, *Chem. Rev.*, 2000, **100**, 2741.
14. C. A. Tolman, W. C. Seidel and L. W. Gosser, *J. Am. Chem. Soc.*, 1973, **96**, 53.
15. P. Dierkes and P. W. N. M. van Leeuwen, *J. Chem. Soc., Dalton Trans.*, 1999, 1519.
16. M. S. Davies, M. J. Aroney, I. E. Buys, T. W. Hambley and J. L. Calvert, *Inorg. Chem.*, 1995, **34**, 330.
17. M. J. S. Dewar, *Bull. Soc. Chim. Fr.*, 1951, **18**, C71.
18. J. Chatt and L. A. Duncanson, *J. Chem. Soc.*, 1953, 1939.
19. S.-X. Xiao, W. C. Trogler, D. E. Ellis and Z. Berkovitch-Yellin, *J. Am. Chem. Soc.*, 1983, **105**, 7033.
20. A. G. Orpen and N. G. Connelly, *Organometallics*, 1990, **9**, 1206.
21. G. Pacchioni and P. S. Bagus, *Inorg. Chem.*, 1992, **31**, 4391.
22. M. N. Golovin, M. M. Rahman, J. E. Belmonte and W. P. Giering, *Organometallics*, 1985, **4**, 1981.
23. M. M. Rahman, H.-Y. Liu, A. Prock and W. P. Giering, *Organometallics*, 1987, **6**, 650.
24. R. J. Angelici and M. D. Malone, *Inorg. Chem.*, 1967, **6**, 1731.

25. M. M. Rahman, H.-Y. Liu, K. Eriks, A. Prock and W. P. Giering, *Organometallics*, 1989, **8**, 1.
26. T. Leyssens, D. Peeters, A. G. Orpen and J. N. Harvey, *New J. Chem.*, 2005, **29**, 1424.
27. T. Leyssens, D. Peeters, A. G. Orpen and J. N. Harvey, *Organometallics*, 2007, **26**, 2637.
28. C. A. McAuliffe, in *"Comprehensive Coordination Chemsitry"*, Eds. G. Wilkinson, R. D. Gillard and J. A. McCleverty, Pergamon Press, 1987, vol. 2, p. 1030.
29. R. G. Goel and T. Allman, *Can. J. Chem.*, 1982, **60**, 716.
30. P. B. Dias, M. E. M. d. Piedade and J. A. M. Simoes, *Coord. Chem. Rev.*, 1994, **135-136**, 737.
31. R. J. Angelici, *Acc. Chem. Res.*, 1995, **28**, 51.
32. J. G. Verkade and J. A. Mosbo, in *"Phosphorus-31 NMR Spectroscopy in Stereochemical Analysis"*, Eds. J. G. Verkade and L. D. Quin, VCH, 1987, p. 425.
33. R. J. Puddephat, G. M. Bancroft and T. Chan, *Inorg. Chim. Acta.*, 1983, **73**, 83.
34. K. Bowman-James, in *"Encyclopedia of Inorganic Chemistry"*, Ed. R. B. King, Wiley, New York, 2005.
35. E. C. Constable, *Coordination Chemistry of Macrocyclic Compounds*, Oxford University Press, 1999.
36. J. V. Alphen, *Recl. Trav. Chim. Pays-Bas*, 1936, **55**, 835.
37. M. C. Thompson and D. H. Busch, *J. Am. Chem. Soc.*, 1962, **84**, 1762.
38. N. F. Curtis, *J. Chem. Soc.*, 1960, 4409.
39. C. J. Pedersen, *J. Am. Chem. Soc.*, 1967, **89**, 7017.
40. B. Dietrich, J.-M. Lehn and J.-P. Sauvage, *Tetrahedron Lett.*, 1969, 2889.
41. J. Almy, D. C. Garwood and D. J. Cram, *J. Am. Chem. Soc.*, 1973, **95**, 2961.
42. A. E. Martell, in *"Advances in Chemistry"*, Oxford University Press, 1967, vol. 62, p. 272.
43. D. K. Cabbiness and D. W. Margerum, *J. Am. Chem. Soc.*, 1969, **91**, 6540.
44. L. Fabbrizzi, P. Paoletti and A. B. P. Lever, *Inorg. Chem.*, 1976, **15**, 1502.
45. A. Anichini, L. Fabbrizzi, P. Paoletti and R. M. Clay, *Inorg. Chim. Acta.*, 1977, **24**, L21.
46. A. Anichini, L. Fabbrizzi, P. Paoletti and R. M. Clay, *J. Chem. Soc., Dalton Trans.*, 1978, 577.
47. R. M. Clay, M. Micheloni, P. Paoletti and W. V. Steele, *J. Am. Chem. Soc.*, 1979, **101**, 4119.

48. E. Gallori, E. Martini, M. Micheloni and P. Paoletti, *Inorg. Chim. Acta.*, 1980, **40**, X66.
49. M. Micheloni and P. Paoletti, *Inorg. Chim. Acta.*, 1980, **43**, 109.
50. H. N. Stokes, *Am. Chem. J.*, 1897, **19**, 782.
51. A.-M. Caminade and J. P. Majoral, *Chem. Rev.*, 1994, **94**, 1183.
52. R. M. Izatt, K. Pawlak, J. S. Bradshaw and R. L. Bruening, *Chem. Rev.*, 1991, **91**, 1721.
53. E. P. Kyba, C. W. Hudson, M. J. McPhaul and A. M. John, *J. Am. Chem. Soc.*, 1977, **99**, 8053.
54. E. P. Kyba and S. S. P. Chou, *J. Chem. Soc., Chem. Commun.*, 1980, 449.
55. E. P. Kyba and S. S. P. Chou, *J. Am. Chem. Soc.*, 1980, **102**, 7012.
56. E. P. Kyba and S. S. P. Chou, *J. Org. Chem.*, 1981, **46**, 860.
57. E. P. Kyba and S.-Z. Liu, *Inorg. Chem.*, 1985, **24**, 1613.
58. E. P. Kyba, C. N. Clubb, S. B. Larson, V. J. Schueler and R. E. Davis, *J. Am. Chem. Soc.*, 1985, **107**, 2141.
59. E. P. Kyba, A. M. John, B. Brown, C. W. Hudson, M. J. McPhaul, A. Harding, K. Larsen, S. Niedzwiecki and R. E. Davis, *J. Am. Chem. Soc.*, 1980, **102**, 189.
60. M. A. Fox, K. A. Campbell and E. P. Kyba, *Inorg. Chem.*, 1981, **20**.
61. E. P. Kyba, R. E. Davis, C. W. Hudson, A. M. John, S. B. Brown, M. J. McPhaul, L.-K. Liu and A. C. Glover, *J. Am. Chem. Soc.*, 1981, **103**, 3868.
62. G. Wittig and A. Maercker, *Chem. Ber.*, 1964, **97**, 747.
63. M. C. Thompson and D. H. Busch, *J. Am. Chem. Soc.*, 1964, **86**, 3651.
64. W. Marty and G. Schwarzenbach, *Chimia*, 1970, **24**, 431.
65. T. A. DelDonno and W. J. Rosen, *J. Am. Chem. Soc.*, 1977, **99**, 8051.
66. T. Lebbe, P. Machnitzki, O. Stelzer and W. S. Sheldrick, *Tetrahedron*, 2000, **56**, 157.
67. A. R. Battle, P. G. Edwards, R. Haigh, D. E. Hibbs, D. Li, S. M. Liddiard and P. D. Newman, *Organometallics*, 2007, **26**, 377.
68. B. N. Diel, R. C. Haltiwanger and A. D. Norman, *J. Am. Chem. Soc.*, 1982, **104**, 4700.
69. P. G. Edwards, J. S. Fleming and S. S. Liyanage, *Inorg. Chem.*, 1996, **35**, 4563.
70. T. Albers and P. G. Edwards, *Chem. Commun.*, 2007, 858.
71. P. G. Edwards and M. L. Whatton, *Dalton Trans.*, 2006, 442.
72. P. G. Edwards, R. Haigh, D. Li and P. D. Newman, *J. Am. Chem. Soc.*, 2006, **128**, 3818.
73. P. G. Edwards, P. D. Newman and D. E. Hibbs, *Angew. Chem., Int. Ed.*, 2000, **39**, 2722.

74. P. G. Edwards, P. D. Newman and K. M. A. Malik, *Angew. Chem., Int. Ed.*, 2000, **39**, 2922.
75. R. W. Alder and D. Read, *Coord. Chem. Rev.*, 1998, **176**, 113.
76. L. D. Quinn, in *"The Heterocyclic Chemistry of Phosphorus"*, J. Wiley, New York, 1981.
77. E. H. Wong, *Comments Inorg. Chem.*, 1996, **18**, 283.
78. X. Delaigue, J. M. Harrowfield, M. W. Hosseini, A. D. Cian, J. Fischer and N. Kyritsakas, *J. Chem. Soc., Chem. Commun.*, 1994, 1579.
79. G. Märkl, G. Y. Jin and C. Schoerner, *Tetrahedron Lett.*, 1980, **21**, 1409.
80. B. A. Arbuzov and G. N. Nikonov, *Adv. Heterocycl. Chem.*, 1994, **61**, 59.
81. J. C. Kane, E. H. Wong, G. P. A. Yap and A. L. Rheingold, *Polyhedron*, 1999, **18**, 1183.
82. A. A. Karasik, R. N. Naumov, O. G. Sinyashin, G. P. Belov, H. V. Novikova, P. Lönnecke and E. Hey-Hawkins, *Dalton Trans.*, 2003, 2209.
83. F. Z. Baimukhametov, V. F. Zheltukhin, G. N. Nikonov and A. S. Balueva, *Zh. Obshch. Khim*, 2002, **72**, 1754.
84. A. A. Karasik, Y. S. Spiridonova, D. G. Yakhvarov, O. G. Sinyashin, P. Lönnecke, R. Sommer and E. Hey-Hawkins, *Mendeleev Commun.*, 2005, **15**, 89.
85. A. A. Karasik, R. N. Naumov, R. Sommer, O. G. Sinyashin and E. Hey-Hawkins, *Polyhedron*, 2002, **21**, 2251.
86. A. A. Karasik, I. O. Georgiev, E. I. Musina, O. G. Sinyashin and J. Heinicke, *Polyhedron*, 2001, **20**, 3321.
87. J. Heinicke, M. He, A. A. Karasik, I. O. Georgiev, O. G. Sinyashin and P. G. Jones, *Heteroat. Chem.*, 2005, **16**, 379.
88. D. E. Berning, K. V. Katti, C. L. Barnes and W. A. Volkert, *J. Am. Chem. Soc.*, 1999, **121**, 1658.
89. A. A. Karasik, O. G. Sinyashin, J. Heinicke and E. Hey-Hawkins, *Phosphorus, Sulfur, Silicon Relat. Elem.*, 2002, **177**, 1469.
90. A. A. Karasik, A. V. Krashilina, A. T. Gubaidullin, I. A. Litvinov, V. K. Cherkasov, O. G. Sinyashin and G. A. Abakumov, *Russ. Chem. Bull.*, 2000, **49**, 1782.
91. A. A. Karasik, R. N. Naumov, A. S. Balueva, Y. S. Spiridonova, O. N. Golodkov, H. V. Novikova, G. P. Belov, S. A. Katsyuba, E. E. Vandyukova, P. Lönnecke, E. Hey-Hawkins and O. G. Sinyashin, *Heteroat. Chem.*, 2006, **17**, 499.
92. A. A. Karasik, R. N. Naumov, Y. S. Spiridonova, O. G. Sinyashin, P. Lönnecke and E. Hey-Hawkins, *Z. Anorg. Allg. Chem.*, 2007, **633**, 205.
93. S. V. Bobrov, A. A. Karasik and O. G. Sinyashin, *Phosphorus, Sulfur, Silicon Relat. Elem.*, 1999, **144-146**, 289.

94. E. V. Novikova, A. A. Karasik, E. Hey-Hawkins and G. P. Belov, *Russ. J. Coord. Chem.*, 2005, **31**, 260.
95. A. A. Karasik, S. V. Bobrov, G. N. Nikonov, A. P. Pisarevskii, I. A. Litvinov, A. S. Dokuchaev, Y. T. Struchkov and K. M. Enikeev, *Russ. J. Coord. Chem.*, 1995, **21**, 574.
96. A. S. Balueva, R. M. Kuznetsov, S. N. Ignat'eva, A. A. Karasik, A. T. Gubaidullin, I. A. Litvinov, O. G. Sinyashin, P. Lönnecke and E. Hey-Hawkins, *Dalton Trans.*, 2004, 442.
97. D. V. Kulikov, A. A. Karasik, A. S. Balueva, O. N. Kataeva, I. A. Litvinov, E. Hey-Hawkins and O. G. Sinyashin, *Mendeleev Commun.*, 2007, **17**, 195.
98. I. Bauer, O. Rademacher, M. Gruner and W. D. Habicher, *Chem. Eur. J.*, 2000, **6**, 3043.
99. R. N. Naumov, A. A. Karasik, O. G. Sinyashin, P. Lönnecke and E. Hey-Hawkins, *Dalton Trans.*, 2004, 357.
100. K. V. Katti, R. Kannan, K. K. Katti, N. Pillarsetty and C. L. Barnes, *Phosphorus, Sulfur Silicon Relat. Elem.*, 2002, **177**, 1587.
101. B. L. Iverson, S. A. Iverson, V. A. Roberts, E. D. Getzoff, J. A. Tainer, S. J. Benkovic and R. A. Lerner, *Science*, 1990, **249**, 659.
102. N. Pinault and D. W. Bruce, *Coord. Chem. Rev.*, 2003, **241**, 1.
103. K. V. Katti, H. Gali, C. J. Smith and D. E. Berning, *Acc. Chem. Res.*, 1999, **32**, 9.
104. S. Ahrland, J. Chatt, N. R. Davies and A. A. Williams, *J. Chem. Soc.*, 1958, 276.
105. R. T. Smith, R. K. Ungar, L. J. Sanderson and M. C. Baird, *Organometallics*, 1983, **2**, 1138.
106. V. Ravindar, H. Schumann, H. Hemling and J. Blum, *Inorg. Chim. Acta.*, 1995, **240**, 145.
107. T. N. Mitchell and K. Heesche-Wagner, *J. Organomet. Chem.*, 1992, **436**, 43.
108. E. Renaud, R. B. Russell, S. J. Forestier, M. C. Brown and J. Baird, *J. Organomet. Chem.*, 1991, **419**, 403.
109. J. Chatt, G. J. Leigh and R. M. Slade, *J. Chem. Soc., Dalton Trans.*, 1973, 2023.
110. F. Joo and A. Bényei, *J. Organomet. Chem.*, 1989, **363**, C19.
111. C. W. Kohlpaintner, R. W. Fischer and B. Cornils, *Appl. Catal., A*, 2001, **221**, 219.
112. W. K. Miller, J. D. Gilbertson, C. Leiva-Paredes, P. R. Bernatis, T. J. R. Weakley, D. K. Lyon and D. R. Tyler, *Inorg. Chem.*, 2002, **41**, 5453.
113. T. Thorpe, S. M. Brown, J. Crosby, S. Fitzjohn, J. P. Muxworthy and J. M. J. Williams, *Tetrahedron Lett.*, 2000, **41**, 4503.

114. H. Gulyás, A. Szöllösy, B. E. Hanson and J. Bakos, *Tetrahedron Lett.*, 2002, **43**, 2543.
115. D. J. Daigle, A. B. Pepperman, Jr. and S. L. Vail, *J. Heterocycl. Chem.*, 1974, **17**, 407.
116. D. J. Daigle, *Inorg. Synth.*, 1998, **32**, 40.
117. D. J. Darensbourg, C. G. Ortiz and J. W. Kamplain, *Organometallics*, 2004, **23**, 1747.
118. A. D. Phillips, L. Gonsalvi, A. Romerosa, F. Vizza and M. Peruzzini, *Coord. Chem. Rev.*, 2004, **248**, 955.
119. D. J. Darensbourg, F. Joó, L. Nádasdi and A. Bényei, *J. Organomet. Chem.*, 1996, **512**, 45.
120. P. Smolenski and F. P. Pruchnik, *Appl. Organomet. Chem.*, 1999, **13**, 829.
121. D. J. Darensbourg, F. Joó, M. Kannisto, A. Kathó, J. H. Reibenspies and D. J. Daigle, *Inorg. Chem.*, 1994, **33**, 200.
122. D. J. Darensbourg, F. Joó, M. Kannisto, A. Kathó and J. H. Reibenspies, *Organometallics*, 1992, **11**, 1990.
123. D. J. Darensbourg, N. W. Stafford, F. Joó and J. H. Reibenspies, *J. Organomet. Chem.*, 1995, **488**, 99.
124. X. Tang, B. Zhang, Z. He, R. Gao and Z. He, *Adv. Synth. Catal.*, 2007, **349**, 2007.
125. J. Navech, R. Kraemer and J. P. Majoral, *Tetrahedron Lett.*, 1980, **21**, 1449.
126. M. Benhammou, R. Kraemer, H. Germa, J. P. Majoral and J. Navech, *Phosphorus, Sulfur Silicon Relat. Elem.*, 1982, **14**, 105.
127. J. R. Delerno, R. J. Majeste and L. M. Trefonas, *J. Heterocycl. Chem.*, 1976, **13**, 757.
128. D. J. Daigle, A. B. Pepperman, Jr. and G. Boudreaux, *J. Heterocycl. Chem.*, 1974, **11**, 1085.
129. V. I. Siele, *J. Heterocycl. Chem.*, 1977, **14**, 337.
130. B. Assman, K. Angermaier and H. Schmidbaur, *J. Chem. Soc., Chem. Commun.*, 1994, 941.
131. B. Assman, K. Angermaier, M. Paul, J. Riede and H. Schmidbaur, *Chem. Ber.*, 1995, **128**, 891.
132. E. Fluck and H. J. Weissgraeber, *Chem.-Ztg.*, 1977, **101**, 304.
133. G. W. Wong, J. L. Harkreader, C. A. Mebi and B. J. Frost, *Inorg. Chem.*, 2006, **45**, 6748.
134. Z. Wang, J. Liu, C. He, S. Jiang, B. Åkermark and L. Sun, *Inorg. Chim. Acta.*, 2007, **360**, 2411.

135. Y. Na, M. Wang, K. Jin, R. Zhang and L. Sun, *J. Organomet. Chem.*, 2006, **691**, 5045.
136. J. W. Ellis, K. N. Harrison, P. A. T. Hoye, A. G. Orpen, P. G. Pringle and M. B. Smith, *Inorg. Chem.*, 1992, **31**, 3026.
137. M. Reuter, L. Orthner, *Ger. Pat.*, 1 035 135, 1958.
138. K. A. Petrov, V. A. Parshina and M. B. Luzanova, *Zh. Obshch. Khim*, 1962, **32**, 553.
139. B. Drießen-Hölscher and J. Heinen, *J. Organomet. Chem.*, 1998, **570**, 141.
140. A. Fukuoka, W. Kosugi, F. Morishita, M. Hirano, L. McCaffrey, W. Henderson and S. Komiya, *Chem. Commun.*, 1999, 489.
141. L. J. Higham, M. K. Whittlesey and P. T. Wood, *Dalton Trans.*, 2004, 4202.
142. L. Higham, A. K. Powell, M. K. Whittlesey, S. Wocadlo and P. T. Wood, *Chem. Commun.*, 1998, 1107.
143. V. S. Reddy, D. E. Berning, K. V. Katti, C. L. Barnes, W. A. Volkert and A. R. Ketring, *Inorg. Chem.*, 1996, **35**, 1753.
144. V. S. Reddy, K. V. Katti and C. L. Barnes, *J. Chem. Soc., Dalton Trans.*, 1996, 1301.
145. D. E. Berning, K. V. Katti, W. A. Volkert, C. J. Higginbotham and A. R. Ketring, *J. Nucl. Med.*, 1998, **25**, 577.
146. R. Schibli, K. V. Katti, W. A. Volkert and C. L. Barnes, *Inorg. Chem.*, 2001, **40**, 2358.
147. G. T. Baxley, W. K. Miller, D. K. Lyon, B. E. Miller, G. F. Nieckarz, T. J. R. Weakley and D. R. Tyler, *Inorg. Chem.*, 1996, **35**, 6688.
148. J. D. Gilbertson, N. K. Szymczak and D. R. Tyler, *Inorg. Chem.*, 2004, **43**, 3341.
149. J. D. Gilbertson, N. K. Szymczak, J. L. Crossland, W. K. Miller, D. K. Lyon, B. M. Foxman, J. Davis and D. R. Tyler, *Inorg. Chem.*, 2007, **46**, 1205.
150. J. C. Jeffery, B. Odell, N. Stevens and R. E. Talbot, *Chem. Commun.*, 2000, 101.

Chapter 2 – Coordination chemistry and derivatisation reactions of a novel water-soluble iron(II) phosphine complex

2.1 Introduction: A novel water-soluble iron(II) macrocyclic phosphine complex

There is increasing interest in performing chemistry in aqueous media for applications in biomedicine, biphasic catalysis, and natural gas scrubbing. Chemistry in water is also more financially and environmentally friendly as it does not generate large amounts of expensive organic solvent waste, or even consume large amounts of energy needed to produce the solvents themselves. Water-solubilising phosphine ligands such as hydroxyalkylphosphines in particular are receiving attention in this field, mainly due to their catalytic potential and also due to the convenient nature of the $^{31}P\{^{1}H\}$ NMR spectroscopic handle that the ^{31}P nucleus provides. The simplest hydroxyalkylphosphine is tris(hydroxymethyl)phosphine $P(CH_2OH)_3$ (THMP), and this has been used to create water-soluble complexes of metals from groups 7 to 11.[1-16] These include complexes of platinum, palladium and nickel,[1-5] gold,[6, 7] rhenium,[8] ruthenium,[9, 10, 13, 15, 16] iridium and rhodium,[12] and copper.[14]

The development of coordination chemistry of water-soluble phosphines with relatively cheap metals such as iron is also an attractive prospect, mainly due to the financial and environmental benefits that the metals themselves offer. The discovery of the water-soluble iron(II) hydroxymethylphosphine complex **1**, containing the self-assembled tetradentate cyclic ligand L^1 (**Figure 2.1**), is interesting due to the novel templated synthesis in which it is formed.

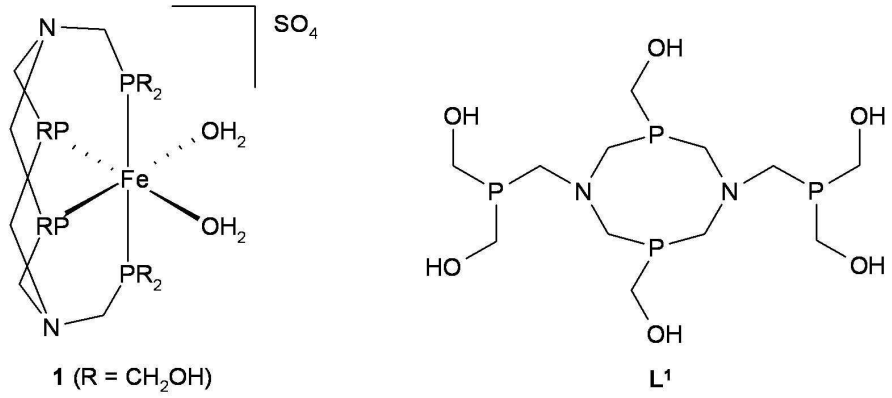

Figure 2.1 – Structure of the Fe(II) phosphine complex 1 and its self-assembled ligand L^1.

Due to the conformation that ligand $\mathbf{L^1}$ imposes on complex **1**, two equatorial *cis* sites are occupied by solvent water molecules, which should be readily replaced by other ligands. This *cis* conformation is ubiquitous in catalysis, as two adjacent sites are often required for the binding of a substrate (such as an alkene) to the metal before its subsequent transformation and separation from the metal centre. Therefore **1** shows promise as a potential catalyst precursor.

Despite the obvious potential of complex **1** as a water-soluble catalyst of Fe(II), and as a natural gas scrubbing agent by reversibly binding small molecules such as N_2, no extensive studies have been carried out on this system in the literature. Because of the interest in water-soluble transition metal complexes and the lack of studies carried out with this system, it was decided to study the coordination chemistry of **1**. It was also decided to investigate the reactivity of the ligand itself and to determine the possibility of decomplexing the ligand from the metal and isolating it.

2.2 Synthesis of $[Fe(L^1)(H_2O)_2]SO_4$ (1)

Complex **1** was synthesised according to a literature procedure.[17] The synthesis can be carried out using two equivalents of tris(hydroxymethyl)phosphine (THPS) with one of iron(II) ammonium sulfate as in the literature method (reaction 1, **Scheme 2.1**), or using the separate iron(II) and ammonium sulfates (reaction 2, **Scheme 2.1**). The two methods work in the same way, and once the reagents have been dissolved there is essentially no difference between them, as both solutions will contain a mixture of $[P(CH_2OH)_4]^+$, $[Fe(H_2O)_6]^{2+}$, NH_4^+, and SO_4^{2-} ions in the same stoichiometry (4:1:2:4 ratio respectively).

The THPS was added as a 50% aqueous solution. Aqueous sodium hydroxide solution (1 M) was then added dropwise to the reaction mixture, taking care to keep the pH of the solution below 5. The slow addition of base converts the THPS into THMP and formaldehyde, which initiates the reaction. This gave a deep red solution of **1**. The reaction was complete when the pH stabilised at approximately 5, at which point most of the THPS had been used up.

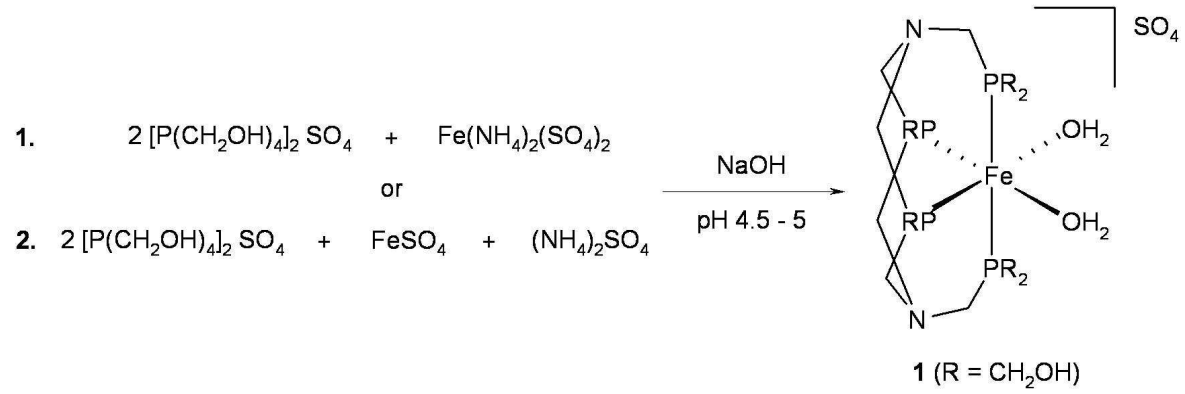

Scheme 2.1 – Formation of $[Fe(L^1)(H_2O)_2]SO_4$ (1).

The deep red solution was then left at 5°C for *ca.* one week yielding a deep red microcrystalline solid in approximately 10% yield. When a two-fold excess of THPS was used, the yield (based on Fe^{2+} ions) increased to approximately 20% of solid. This is most likely due to the decreased solubility of the final product in the more viscous reaction solution.

The $^{31}P\{^1H\}$ NMR spectrum of the isolated low-spin d^6 product **1** in D_2O (**Figure 2.2**) showed the expected characteristic triplet resonances at δ 20.1 and -1.5 due to the two pairs of chemically inequivalent phosphines (axial and equatorial).

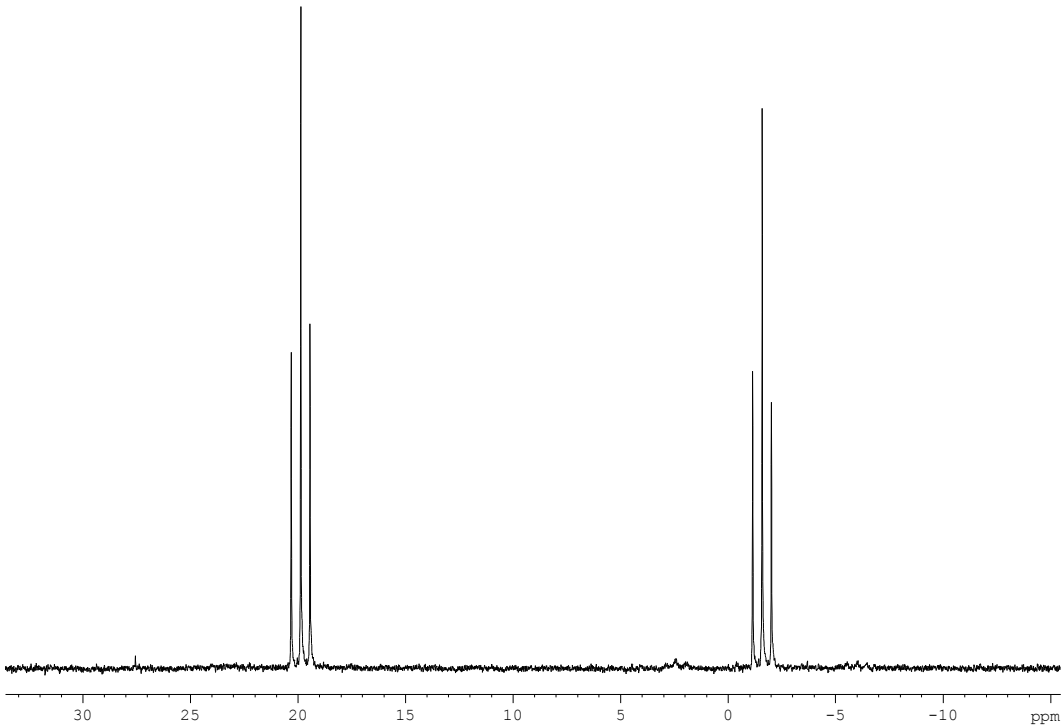

Figure 2.2 – $^{31}P\{^1H\}$ NMR spectrum of $[Fe(L^1)(H_2O)_2]SO_4$ (1) in D_2O at 122 MHz.

The ^{1}H NMR spectrum of **1** is more complex, but can be assigned (**Figure 2.3**). There are four groups of chemically inequivalent CH_2 protons in an 8:8:4:4 ratio; eight CH_2 protons on the four axial pendant CH_2OH arms (♦), four on the two equatorial pendant arms (●), four on the two CH_2 bridges between the axial phosphorus atoms and the nitrogens (■), and eight on the four CH_2 groups in the eight-membered ring (▲). It may be expected that the *exo*- and *endo*-protons in the eight-membered ring are chemically inequivalent due to the imposed rigidity of the complexed ligand, as found in other similar complexed cyclic ligands.[18] This is indeed the case and the protons on the CH_2 groups within the eight-membered (▲) ring give rise to an AB system at δ 4.45. The two groups of pendant $C\underline{H_2}OH$ protons give rise to broad singlets at δ 3.52 (●) and 3.00 (♦) due to their ability to rotate freely about the P-C bond. However, the CH_2 protons linking the pendant phosphines to the eight-membered ring (■) must be structurally rigid due to their inclusion into a six-membered ring formed as a result of the chelation of the ligand to the metal. Despite this rigidity, these protons give rise to a sharp singlet at δ 4.23 due to their chemical equivalence.

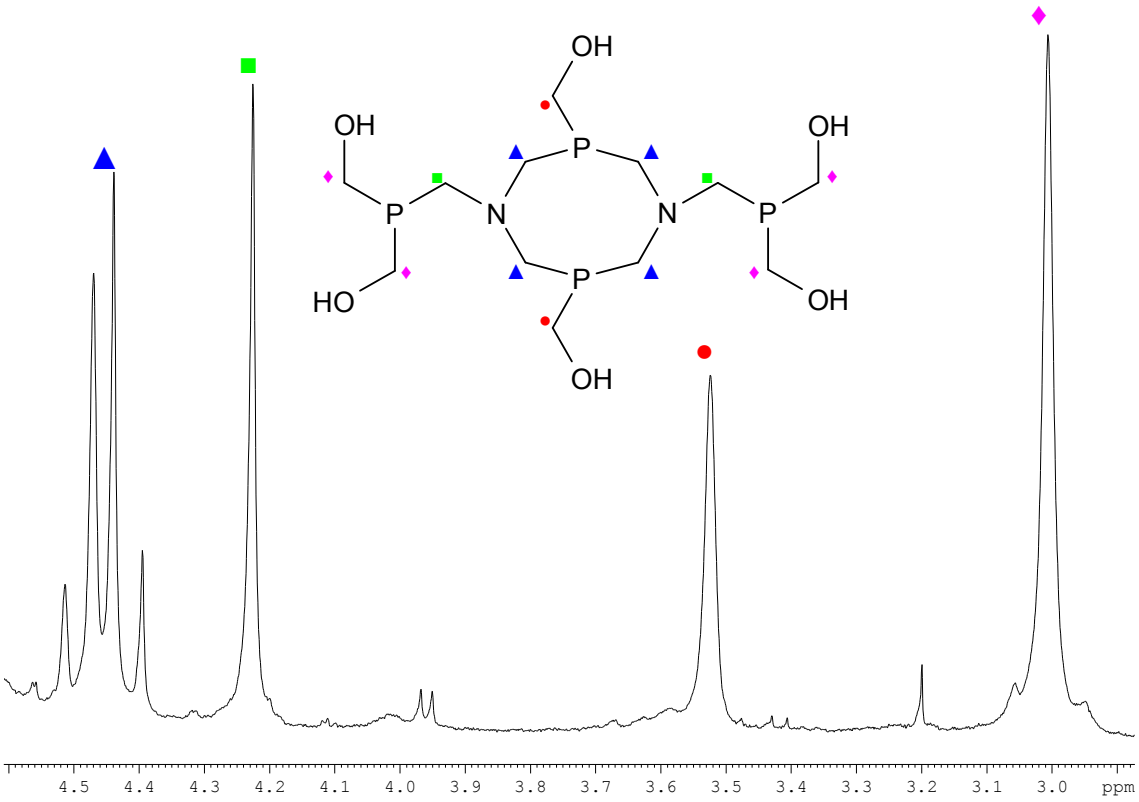

Figure 2.3 – ^{1}H NMR Spectrum of $[Fe(L^{1})(H_2O)_2]SO_4$ (1) in D_2O at 300 MHz.

^{31}P – ^{1}H HMQC spectroscopy indicated that the triplet resonance at δ 20.1 in the $^{31}P\{^{1}H\}$ NMR spectrum correlates to the AB resonance at δ 4.45 in the ^{1}H NMR spectrum assigned as the methylene protons in the eight-membered ring. This suggests that the resonance at δ 20.1 in the $^{31}P\{^{1}H\}$ NMR spectrum is the equatorial phosphine resonance, due to the close proximity of these nuclei to the methylene

groups in the eight-membered ring. The ^{31}P – ^{1}H HMQC also showed that the triplet resonance at δ 20.1 in the $^{31}P\{^{1}H\}$ NMR spectrum correlates to the peak at δ 4.23 in the ^{1}H NMR spectrum assigned as the methylene protons linking the pendant phosphines to the eight-membered ring. This helps to confirm that the resonance at δ -1.5 in the $^{31}P\{^{1}H\}$ NMR spectrum is the axial phosphine due to the close proximity to the linking methylene groups. No $^{2}J_{P\text{-}H}$ coupling of any of the pendant methylene protons to the phosphines was observed.

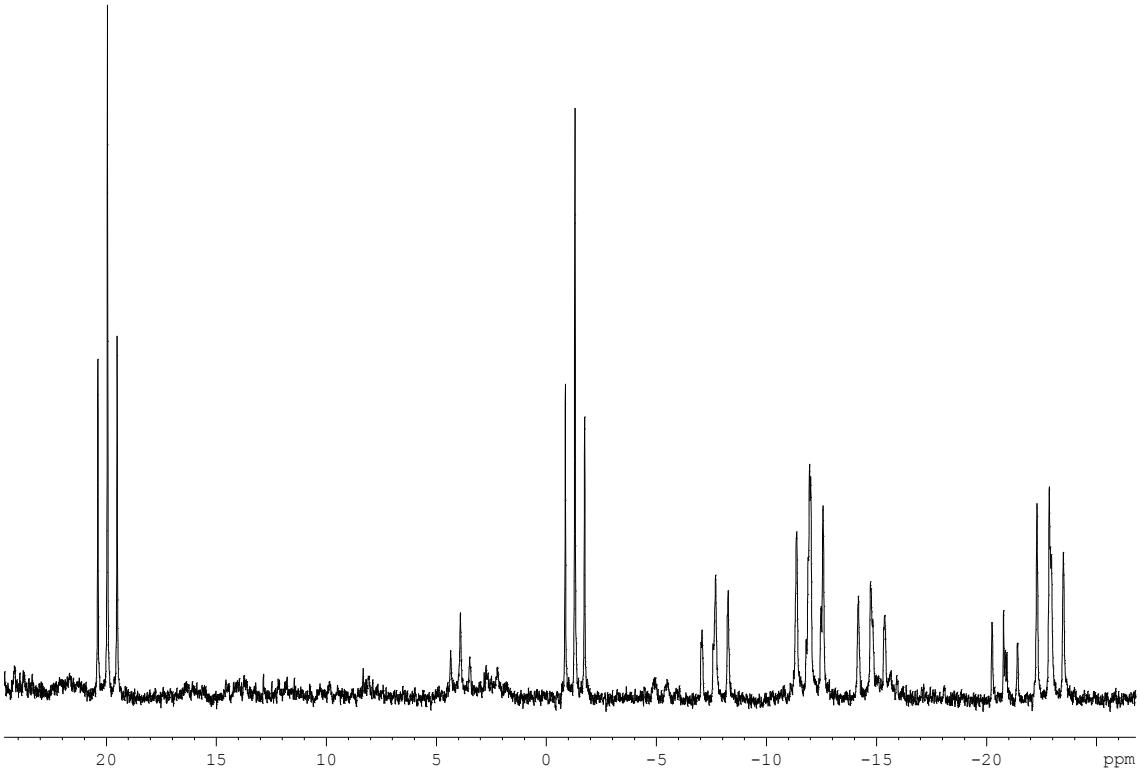

Figure 2.4 – $^{31}P\{^{1}H\}$ NMR spectrum of the self-assembly reaction solution before isolation of $[Fe(L^{1})(H_2O)_2]SO_4$ (1) in D_2O at 122 MHz.

The $^{31}P\{^{1}H\}$ NMR spectrum of the crude reaction mixture (**Figure 2.4**) showed a large number of peaks present suggesting that there are at least four species present in solution. Jeffery *et al.*[17] observed the formation of a second pair of triplets at -12.0 and -22.8 ppm with the related reduction in intensity of the resonances associated with **1** when excess base was added. This can be associated with the conversion of **1** to a new complex, tentatively assigned by Jeffery *et al.*[17] as either the neutral hydroxy complex **2a**, or the oxy-bridged species **2b**, which forms due to the base induced deprotonation of the H_2O molecules coordinated to Fe in **1** (**Scheme 2.2**).

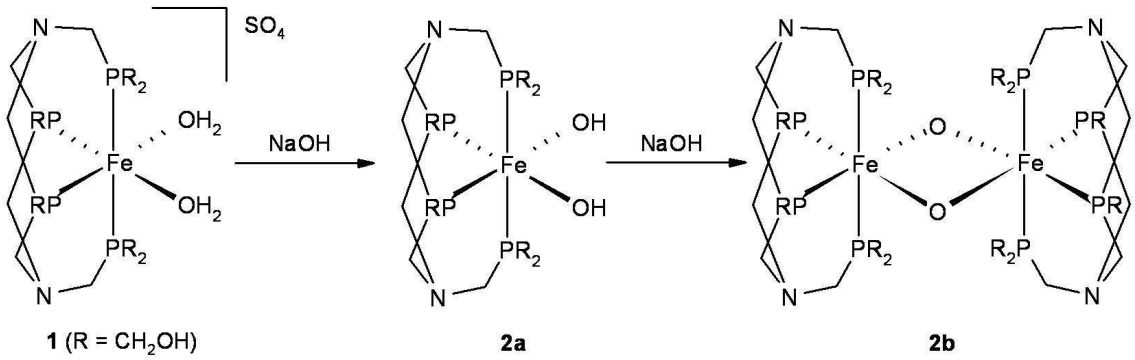

Scheme 2.2 – Suggested reaction of 1 with base.

The triplet-like resonances at δ -12.0 and -22.8 (**Figure 2.4**) were observed as well as others at δ -5.7, -14.9, and -20.8, though these resonances all appeared to be second-order and more like doublets of doublets than triplets, in which case they would not correlate exactly with the structures of **2a** or **2b**. These other species did not crystallise from solution and were therefore not possible to characterise them unambiguously.

The addition of two equivalents of a sodium hydroxide solution to an aqueous solution of **1** gave rise to two triplet resonances at δ 22.8 and 8.6 in the $^{31}P\{^{1}H\}$ NMR spectrum. Other peaks were also visible, which are potentially intermediates and side-products showing multiple species in solution. When triethylamine was used instead of sodium hydroxide, a very similar spectrum was observed. Alternatively, when Na_4EDTA was used as the base, the spectrum was much cleaner. $^{31}P\{^{1}H\}$ NMR spectroscopy showed the same triplet resonances at δ 22.8 and 8.6, as well as a broad peak at *ca.* δ 21 and a related broad triplet at δ 3.8 which were also observed in the reaction with NaOH.

Kinetic studies were undertaken to determine the relationship of these resonances (**Figure 2.5**). The kinetic studies show that when one equivalent of $EDTA^{4-}$ was added (essentially four equivalents of base due to the four carboxylate groups) the broad peak and broad triplet at *ca.* δ 21 and 3.8, respectively, formed very quickly. These peaks slowly converted over time into the two much sharper triplet resonances at δ 22.8 and 8.6. If a larger excess of Na_4EDTA was added the reaction proceeded faster. It is unlikely that either of these two species are complexes of EDTA, as both are clearly observed in the similar reaction with NaOH or NEt_3 as the base. The kinetic studies were carried out using $EDTA^{4-}$ instead of NaOH or NEt_3 due to the simplicity of the spectra, with many other unidentifiable peaks observed with these latter two bases, presumably as a result of side reactions and/or decomposition.

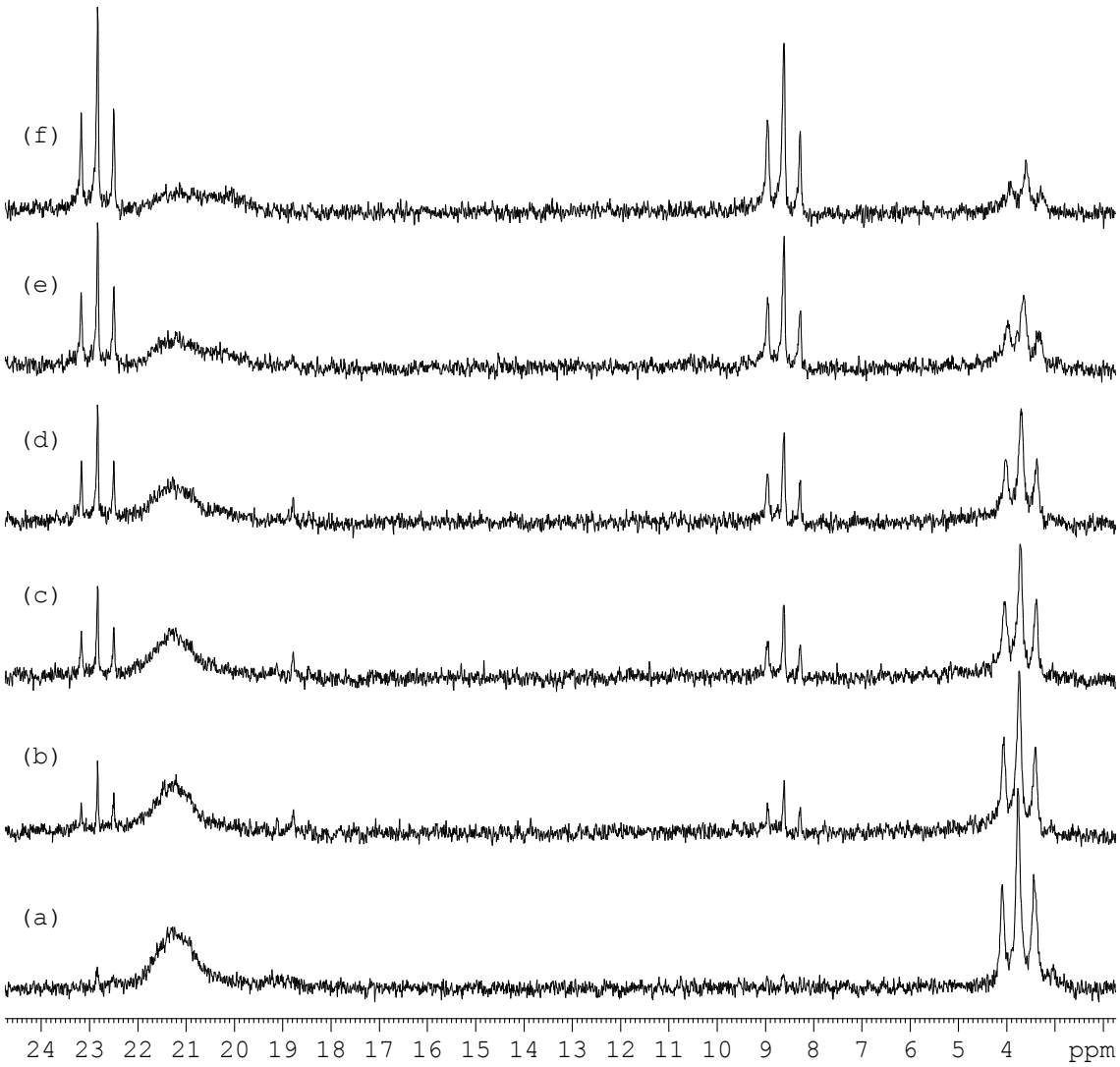

Figure 2.5 – Kinetic studies of the reaction of $[Fe(L^1)(H_2O)_2]SO_4$ (1) with 1 equiv. Na_4EDTA in D_2O at 162 MHz using $^{31}P\{^1H\}$ NMR spectroscopy after: (a) 5 mins, (b) 1 hr, (c) 2 hrs, (d) 3 hrs, (e) 6 hrs, and (f) 12 hrs.

The structural identity of the two species formed in the study cannot be easily unambiguously identified. Single crystals could not be grown despite numerous attempts and a pure sample of neither species could be isolated. One possible interpretation is that the two triplets at δ 22.8 and 8.6 represent the neutral bis(hydroxy) complex $[Fe(L^1)(OH)_2]$ **2a**, with the broad resonances potentially belonging to the intermediate mono(hydroxy), mono(aqua) cation $[Fe(L^1)(OH)(H_2O)]^+$. However, the $^{31}P\{^1H\}$ NMR spectrum of the $[Fe(L^1)(OH)(H_2O)]^+$ cation would be expected to consist of two doublets of triplets and a doublet of doublets, rather than the two observed broad triplets. If the hydroxyl ligand was exchanging with the H_2O solvent molecules, the observed broad resonance pattern maybe expected. A similar resonance pattern is observed in the reaction of **1** with sodium chloride in section 2.3, the broad peaks likely being a result of the coordinated aqua groups exchanging with chloride anions. Interestingly, when pyridine was used as the base, not only was the reaction fairly

clean, but the intermediate broad peaks at *ca.* δ 21 and 3.8 were not observed in the $^{31}P\{^{1}H\}$ NMR spectrum. Instead, only the starting material and triplet resonances at δ 22.8 and 8.6 were observed. This suggests that the first step in the reaction is now the rate determining step as the second step is faster when pyridine is used as the base, whereas the opposite is true with the other bases.

2.3 Coordination chemistry of $[Fe(L^1)(H_2O)_2]SO_4$ (1) with halides

A good starting point into the investigation of the coordination chemistry of **1** is to explore the reactivity with halide salts. When two equivalents of NaCl were added to an aqueous solution of **1**, a colour change from deep red to purple was observed. $^{31}P\{^{1}H\}$ NMR spectroscopy showed a decrease in the resonances of **1** accompanied by the appearance of a very broad resonance at *ca*. δ 22, as well as a corresponding triplet at δ 0.4 (**Figure 2.6**), which appears similar to the intermediate species in the reaction of **1** with EDTA. These broad peaks appear to be the result of the dichloride complex $[Fe(L^1)Cl_2]$ (**3**), though the broadness may be due to exchange with the solvent water molecules or sulfate anion.

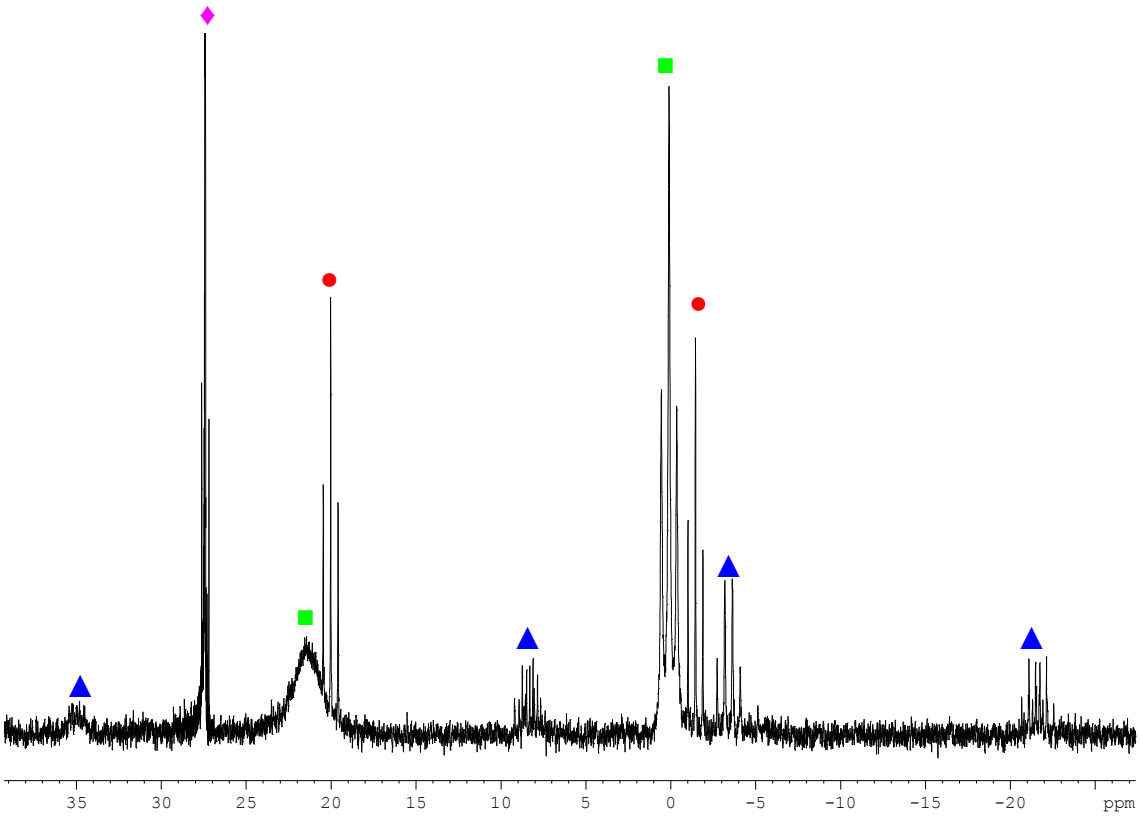

Figure 2.6 – $^{31}P\{^{1}H\}$ NMR spectrum of the reaction of 1 with NaCl in D_2O at 122 MHz. The symbol ▲ is complex 4, ■ is complex 3 (exchanging with solvent), ● is unreacted 1, ♦ is excess THPS.

The other four resonances observed (apart from unreacted starting materials) were three doublets of doublets of triplets at δ 35.0, 8.4 and -21.6 and an overlapping doublet of doublets of doublets at δ -3.3. This coupling pattern combined with the four different phosphine environments is a result of the presence of excess THPS in the reaction solution, leading to the formation of the related phosphine THMP (which is in equilibrium with THPS), one of which coordinates to the iron centre. The two axial phosphines are therefore magnetically equivalent, with the three equatorial phosphines all being inequivalent. **Figure 2.7** shows three possibilities for the structure of complex **4**.

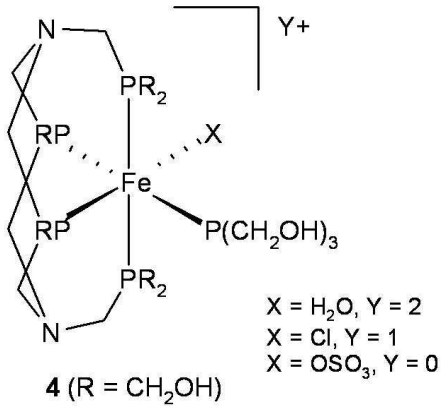

Figure 2.7 – Possible structures of complex 4.

Attempts to crystallise and isolate **3** from aqueous solution resulted in the reprecipitation of complex **1**. This is consistent with **1** existing in equilibrium with **3**, with the equilibrium shifting to the left due to the precipitation of the less soluble **1** in preference to **3** (**Scheme 2.3**).

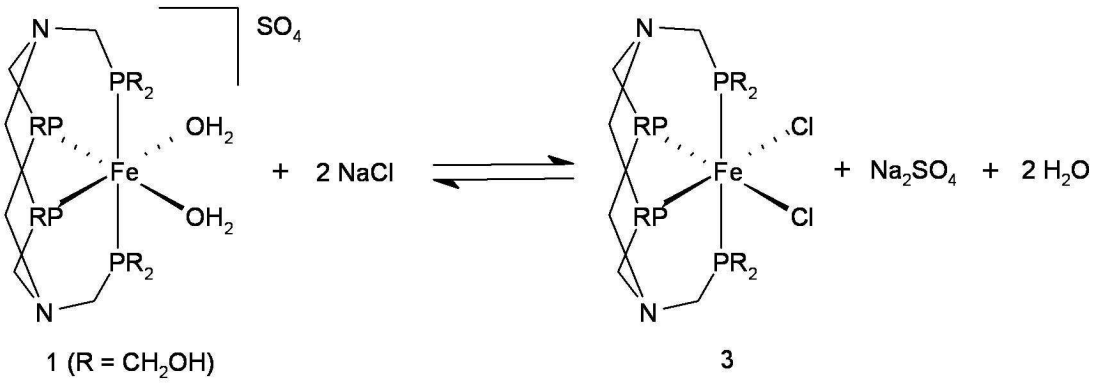

Scheme 2.3 – Equilibrium between $[Fe(L^1)(H_2O)_2]SO_4$ (1) and $[Fe(L^1)Cl_2]$ (3) in H_2O.

The reaction of **1** with $BaCl_2$ in order to replace the sulfate counter ion with chloride anions was also attempted. Reacting an aqueous solution of **1** with $BaCl_2$ gave an

insoluble white precipitate of $BaSO_4$, which was removed by filtration. The $^{31}P\{^1H\}$ NMR spectrum of the reaction solution showed the familiar broad resonance at *ca*. δ 22, as well as a corresponding triplet at δ 0.4 as in the reaction with NaCl, though this still could not be isolated and led to the reprecipitation of **1** as before. As the isolation of the dichloride complex **3** could not be achieved in aqueous solution, reactions with the pseudo-halide thiocyanate and azide anions were carried out in water (see **Section 2.5**). These reactions were preformed as a comparison to the chemistry with halides and in order to see if the corresponding bis(pseudo-halide) complexes could be isolated from aqueous solution.

When the reaction of **1** with tetramethylammonium chloride as the chloride source was carried out in methanol in the presence of excess THPS using excess (20 equivalents), $^{31}P\{^1H\}$ NMR spectroscopy in d_4-methanol (**Figure 2.8**) showed the major complex formed possessed four phosphine environments, similar to the resonance pattern observed for complex **4**. Though it was not possible to completely unambiguously characterise this complex (as in the similar reaction in water), the $^{31}P\{^1H\}$ NMR resonances of the product are consistent with the proposed structures of **4** (**Figure 2.7**).

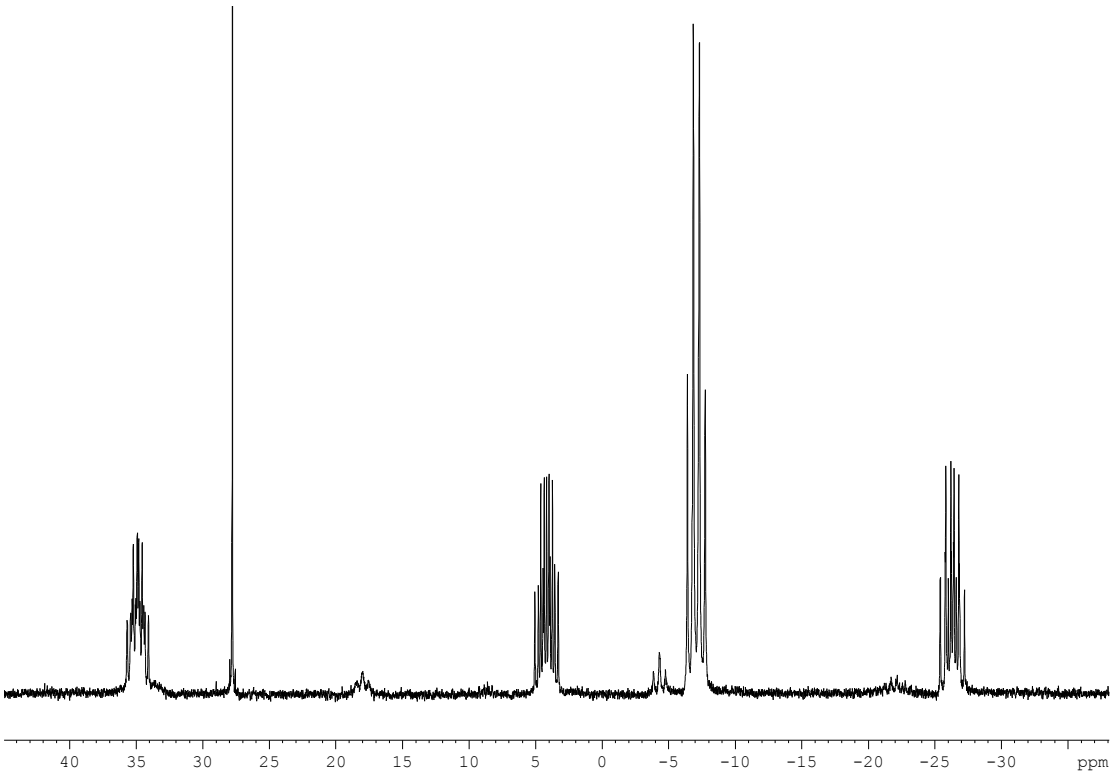

Figure 2.8 – $^{31}P\{^1H\}$ NMR spectrum of the reaction of 1 with Me_4NCl in the presence of excess THPS in d_4-methanol at 122 MHz.

When the reaction was repeated without the presence of THPS, $^{31}P\{^{1}H\}$ NMR spectroscopy in d_4-methanol showed that two sharp triplets are formed at δ 15.5 and -6.6. This corresponds to the formation of the dichloro complex $[Fe(L^1)Cl_2]$ **3**, though only in 85% yield despite using 20 equivalents of Me_4NCl in the reaction, with the remaining 15% being $[Fe(L^1)(H_2O)_2]SO_4$ **1**.

In order to isolate complex **3**, the reaction of **1** with chloride was attempted in acetone. When a suspension of **1** was heated at reflux for several hours with excess sodium chloride in dry acetone a purple solution was obtained. The reaction is slow due to the low solubility of both **1** and NaCl in acetone. As the sodium sulfate by-product is insoluble in acetone it precipitates out of solution, thus shifting the equilibrium between the starting material (**1**) and product (**3**) further to the right. Slow evaporation of the acetone solution of **3** led to the formation of purple crystals. The $^{31}P\{^{1}H\}$ NMR spectrum of **3** (in d_6-acetone) gave rise to the familiar pattern of two sharp triplet resonances at δ 14.8 and δ -7.9 ($^{2}J_{PP}$ = 56 Hz). These resonances appeared at lower frequency than the parent diaqua complex **1**, which is partly due to the change in solvent. This is also because of the increased shielding from the iron centre as a result of the increased donation of electron density from the substitution of the neutral coordinated H_2O molecules with anionic chloride ligands. $^{31}P\{^{1}H\}$ NMR spectroscopy of crystalline **3** dissolved in D_2O shows the reformation of the triplet resonances associated with **1**, which in this case is the $[Fe(L^1)(D_2O)_2]^{2+}$ cation, but in water is the diaqua cation of complex **1**.

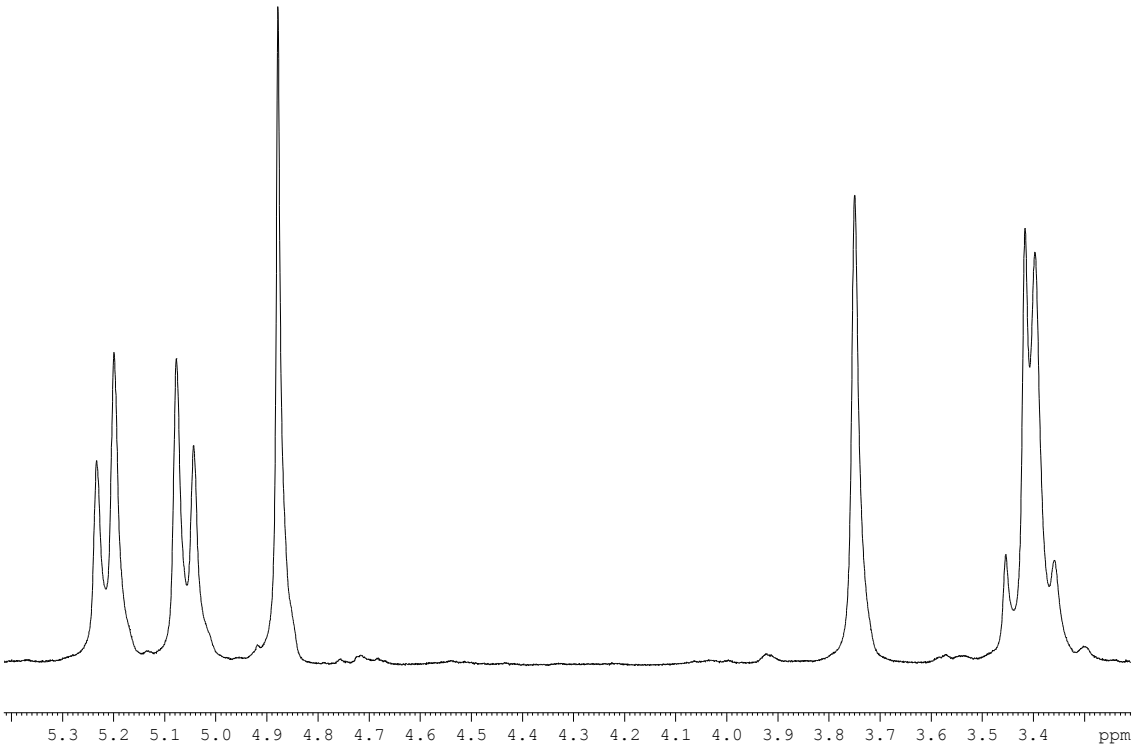

Figure 2.9 – ^{1}H NMR spectrum of $[Fe(L^1)Cl_2]$ 3 in d_6-acetone at 300 MHz.

^{1}H NMR spectroscopy of **3** (**Figure 2.9**) revealed a similar spectrum to that of **1**, which is similar for all complexes of general formula [Fe(L^1)X_2], although differences in chemical shift and separation between the AB resonances were observable. The resonance at δ 3.41 now showed signs of being an AB system, whereas in the ^{1}H NMR spectrum of **1** the corresponding peak was clearly a singlet at room temperature. This resonance corresponds to the CH_2 protons on the CH_2OH groups of the axial phosphine pendant arms. In complex **1**, these groups can freely rotate about the P-C bond, making both CH_2 protons equivalent, leading to a singlet. It is possible that in complex **3**, the large chloride ligands prevent rotation through steric bulk or hydrogen bonding, which would make the axial P$C\underline{H_2}$OH protons inequivalent, and lead to an AB system.

The reaction with KBr to form the dibromo complex [Fe(L^1)Br_2] **5** was carried out, using excess KBr in acetone. The ^{31}P{^{1}H} NMR spectrum of **5** dissolved in d_6-acetone showed two triplet resonances at δ 15.6 and -12.2 ($^2J_{P\text{-}P}$ = 56 Hz). The ^{1}H NMR spectrum of **5** is similar to the spectrum of **3**.

2.4 X-ray structures of [Fe(L^1)Cl_2]·H_2O (**3**·H_2O) and [Fe(L^1)Br_2]·H_2O (**5**·H_2O)

Purple crystals of **3** suitable for single crystal X-ray analysis were isolated by slow evaporation of an acetone solution in air. The solved crystal structure revealed the crystals were of the monohydrate, represented in **Figure 2.10**. Selected bond lengths and angles are given in **Table 2.1**. The structure confirmed that the substitution of both *cis*-aqua ligands for two chloride groups has taken place, as indicated by the NMR data. The ligand L^1 has remained intact and is coordinated in a tetradentate manner. This gives a distorted octahedral geometry similar to complex **1**, with the oriented Fe-P bonds in the equatorial plane ranging from 80.190(15)° to 94.863(15)°. This distortion is in part enforced by the chelating equatorial phosphine donors, which have a crystallographic bite angle of 80.190(15)°. This angle is lower than the ideal 90° angle for an octahedral complex, which then causes further distortion within the molecule. The Fe-P bond lengths (between 2.16 and 2.26 Å) and Fe-Cl bond lengths (ca. 2.40 Å) in **3** are consistent with related iron(II) phosphine structures, such as [Fe(P{$CH_2CH_2CH_2PMe_2$}$_3$)Cl_2]).[19] The Fe-P bond lengths of the axial phosphorus donors are longer than those of the equatorial phosphine groups. This observation is expected due to the greater *trans* influence of phosphines compared to the chloride anions.[20] The C-P-C bond angles for the axial and equatorial phosphine atoms vary between 98.90(7)° and 102.65(7)°, which are low compared to the ideal angle of 109.5° for an sp^3 hybridised atom. This is because the bonding of the phosphines to the Fe(II)

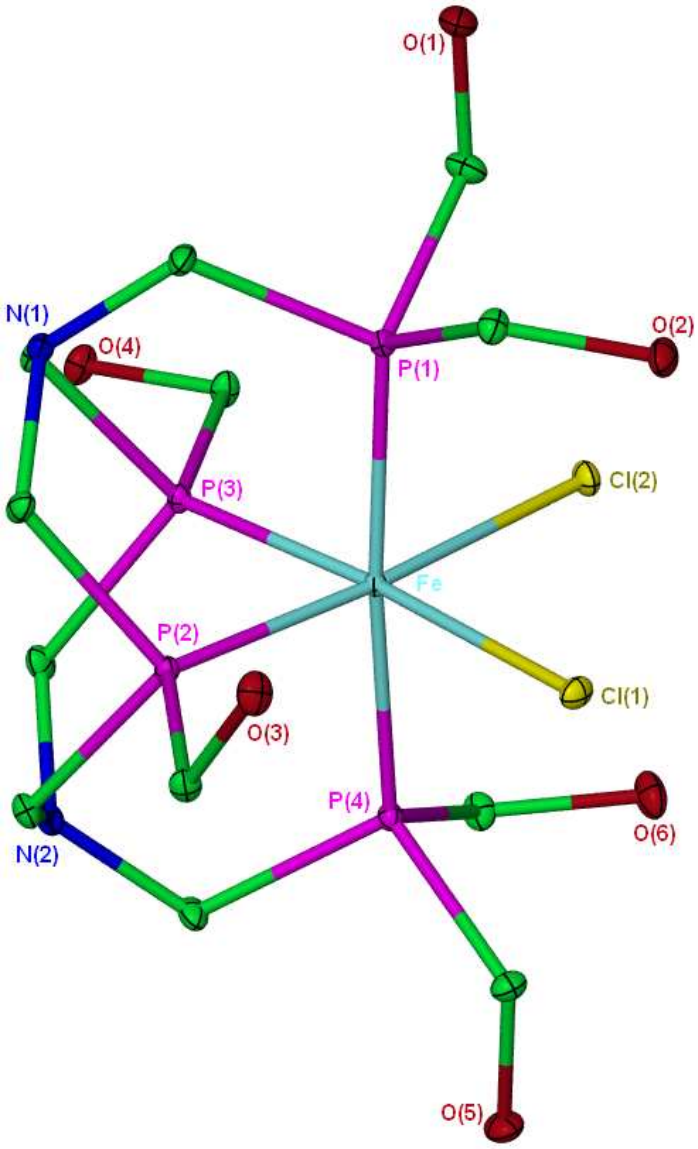

Figure 2.10 –Molecular structure of $[Fe(L^1)Cl_2]\cdot H_2O$ ($3\cdot H_2O$). Thermal ellipsoids are at the 30% probability level. The included water molecule and hydrogen atoms have been omitted for clarity.

Bond Lengths

Fe(1)-P(1)	2.2553(4)	Fe(1)-P(4)	2.2541(4)
Fe(1)-P(2)	2.1836(4)	Fe(1)-Cl(1)	2.4006(4)
Fe(1)-P(3)	2.1639(4)	Fe(1)-Cl(2)	2.4001(4)

Bond Angles

P(4)-Fe-P(1)	174.612(17)	Cl(2)-Fe-Cl(1)	90.374(15)
P(3)-Fe-Cl(1)	174.945(17)	P(3)-Fe-P(2)	80.190(15)
P(2)-Fe-Cl(2)	174.760(17)		

Table 2.1 – Selected bond lengths (Å) and angles (°) for complex $3\cdot H_2O$.

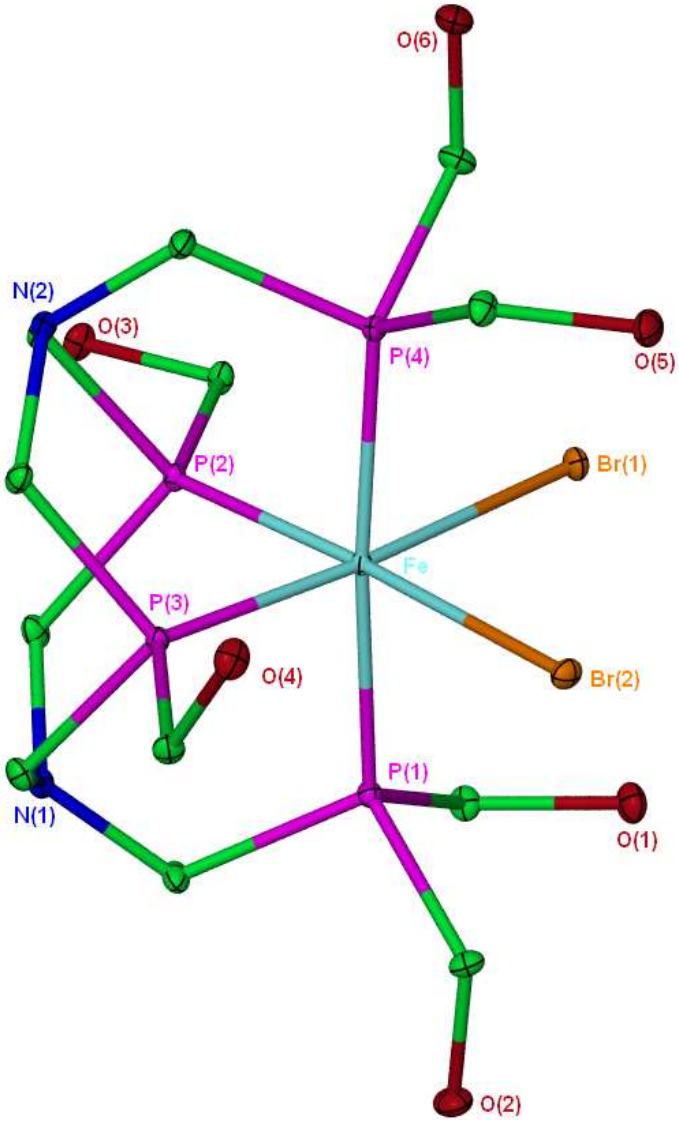

Figure 2.11 - Molecular structure of $[Fe(L^1)Br_2]\cdot H_2O$ ($5\cdot H_2O$). Thermal ellipsoids are at the 30% probability level. The included water molecule and hydrogen atoms have been omitted for clarity.

Bond Lengths

Fe(1)-P(1)	2.2679(5)	Fe(1)-P(4)	2.2701(5)
Fe(1)-P(2)	2.1646(5)	Fe(1)-Br(1)	2.5378(3)
Fe(1)-P(3)	2.1873(5)	Fe(1)-Br(2)	2.5405(3)

Bond Angles

P(4)-Fe-P(1)	175.263(18)	Br(2)-Fe-Br(1)	90.697(9)
P(3)-Fe-Br(1)	173.612(16)	P(3)-Fe-P(2)	80.149(17)
P(2)-Fe-Br(2)	175.810(16)		

Table 2.2 – Selected bond lengths (Å) and angles (°) for complex $5\cdot H_2O$.

centre creates strain within the ligand, as a result of the preference of the Fe(II) metal for the octahedral geometry. Crystals of **5** suitable for single crystal X-ray diffraction analysis were also isolated by slow evaporation of an acetone solution, and proved to be of the mono-hydrate. As with **3**, the structure is consistent with the NMR data, and shows that both *cis*-aqua ligands have been substituted by bromide ligands (**Figure 2.11**). Selected bond lengths and angles are given in **Table 2.2**. The molecular structure of **5** is very similar overall to that of **3**, showing a distorted octahedral geometry, with the *cis* bond angles in the equatorial plane varying from 80.149(17)° to 95.680(14)°. The crystallographic bite angle of the equatorial phosphine donors of the L^1 ligand is 80.149(17)°, which is the same as the bite angle of the L^1 ligand on **3** within experimental error. The Fe-Br bond lengths are 2.5378(3) and 2.5405(3) Å, which are significantly longer than the similar Fe-Cl bond lengths in the structure of **3** (2.4006(4) and 2.4001(4) Å), as would be expected for the larger bromide atoms.

2.5 Coordination chemistry of $[Fe(L^1)(H_2O)_2]SO_4$ (1) with pseudo-halides

In contrast to the reaction with halides, the reaction of **1** with two equivalents of potassium thiocyanate in aqueous solution gave an orange precipitate of $[Fe(L^1)(NCS)_2]$ (**6**) in high yield (**Scheme 2.4**).

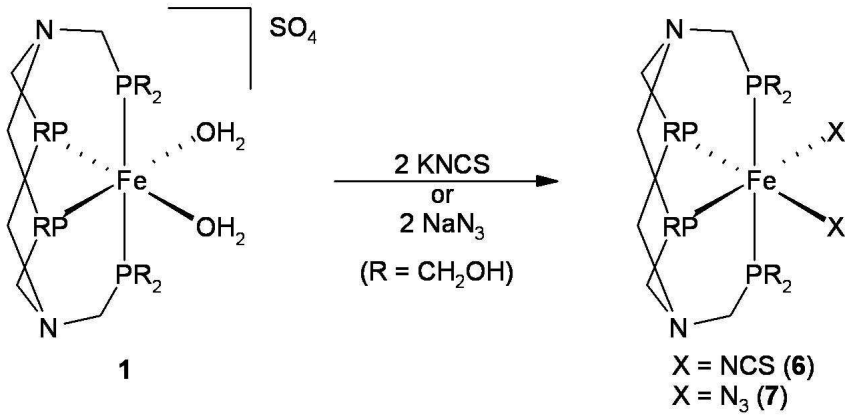

Scheme 2.4 – Synthesis of isothiocyanato and azido complexes 6 and 7.

The $^{31}P\{^1H\}$ NMR spectrum of **6** in D_2O, in which it is sparingly soluble, showed two second order resonances at δ 13.7 and δ 9.5. These resonances resemble triplets, but appear more complex than those for complex **1**. Interestingly, the appearance of the resonances is dependant on the magnetic field strength of the spectrometer. At higher field strength, less second order character is observed, as was shown by running the $^{31}P\{^1H\}$ NMR spectrum at 81, 122, and 162 MHz, respectively. This effect is due to the fact that resonances begin to coalesce when the value of the coupling constant

approaches the value of the peak separation (Hz), which is itself dependant on the spectrometer field strength. Simulations of the $^{31}P\{^{1}H\}$ NMR spectra at all three spectrometer frequencies were carried out and compared to the corresponding experimental spectra (**Figure 2.12**). At all three frequencies the experimental and simulated spectra match each other closely.

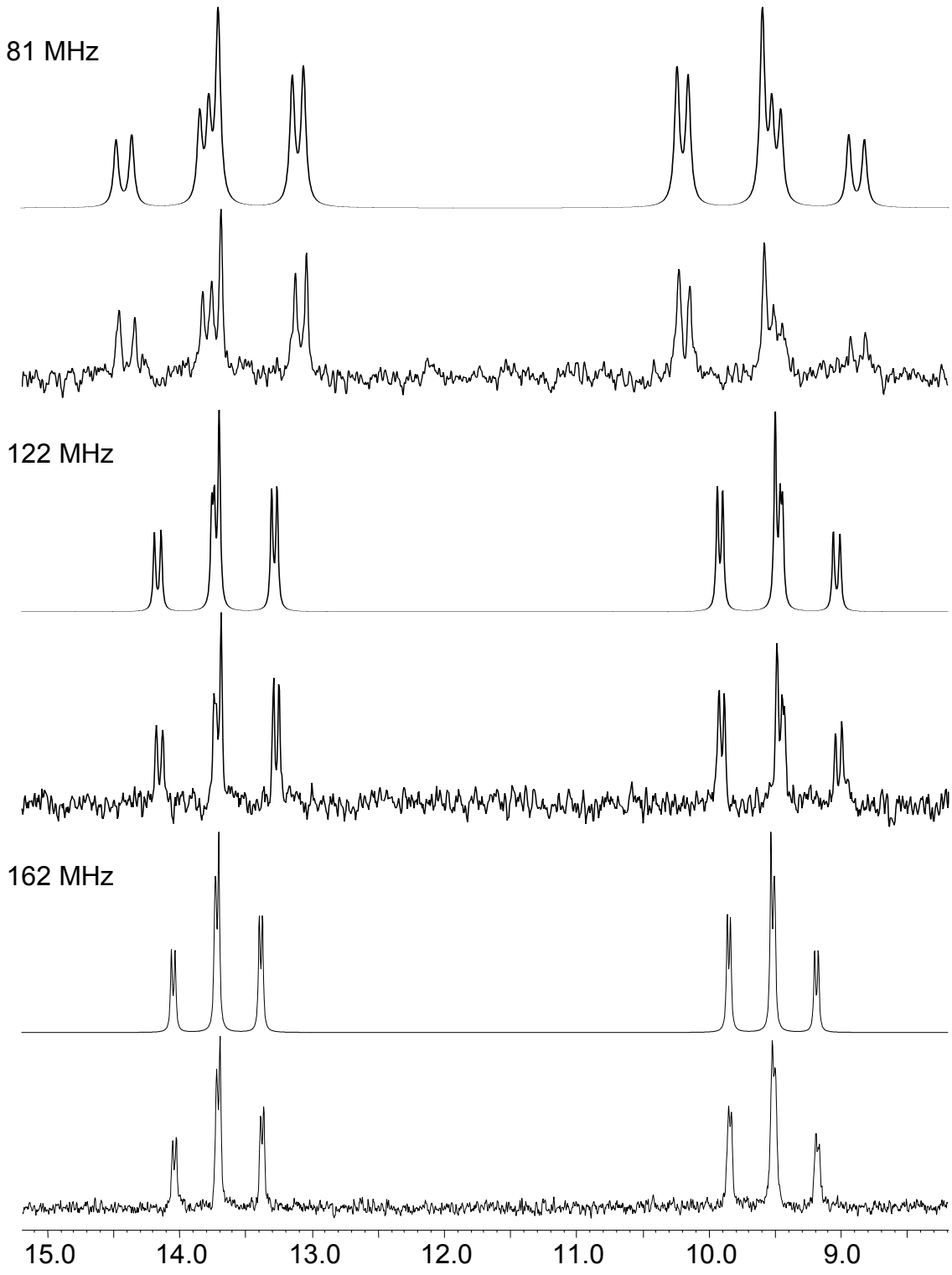

Figure 2.12 – Simulated (upper) and experimental (lower) $^{31}P\{^{1}H\}$ NMR spectra of $[Fe(L^{1})(NCS)_2]$ (6) in D_2O at different field strengths.

When the $^{31}P\{^{1}H\}$ NMR spectrum was run in acetone at 122 MHz there was a larger separation between the two resonances, which gave rise to a much reduced second order spectrum (**Figure 2.13**).

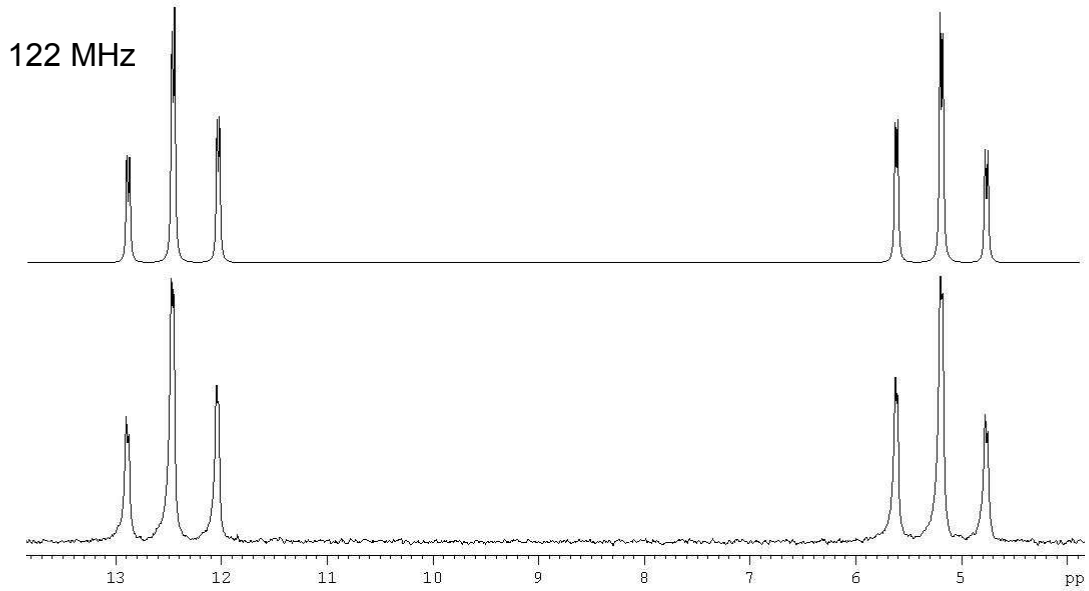

Figure 2.13 – Simulated (upper) and experimental (lower) $^{31}P\{^{1}H\}$ NMR spectra of $[Fe(L^1)(NCS)_2]$ (6) in d_6-acetone at 122 MHz.

When the reaction was carried out with the addition of only one equivalent of thiocyanate, the $^{31}P\{^{1}H\}$ NMR spectrum showed a 1:1 mixture of the starting material **1** and the product **6**. This suggests that the first substitution of a water ligand for a thiocyanate anion to form $[Fe(L^1)(H_2O)(NCS)]^+$ is the rate determining step, and the second substitution to form **6** is faster. The IR spectrum of **6** shows two absorption peaks at 2109 and 2098 cm^{-1} for ν(NCS), which are due to the symmetric and asymmetric stretches of the *cis* equatorially coordinated thiocyanate ligands. The small frequency separation of the two absorptions has also been observed in the case of $[Fe(pp_3)(NCS)_2]$ (pp_3 = tris(2-diphenylphosphinoethyl)phosphine).[21, 22]

The reaction of **1** with sodium azide to give the $[Fe(L^1)(N_3)_2]$ complex (**7**) required an excess of N_3^- anions to drive the reaction to completion (**Scheme 2.4**). The $^{31}P\{^{1}H\}$ NMR spectrum of **7** showed the expected pair of triplets (δ 16.9 and δ 12.4, $^{2}J_{P\text{-}P}$ = 54 Hz), consistent with two azido ligands occupying the *cis* sites following the substitution of both H_2O ligands. When two equivalents of sodium azide are used, other products are observed in the $^{31}P\{^{1}H\}$ NMR spectrum (**Figure 2.14**). A ^{31}P-^{31}P COSY experiment shows that the triplet-like peak at δ 11.3 couples to two second order resonances at δ 18.3 and 14.4, which appear to be doublets of triplets. Therefore, the resonance at δ

11.3 is actually a second-order doublet of doublets, which would be expected for an ABX_2 spin system, such as the $[Fe(L^1)(N_3)(H_2O)]^+$ complex. Unlike **6**, complex **7** did not precipitate from aqueous solution during the reaction, but can be precipitated by the addition of acetone. In contrast to the reaction of **1** with chloride in aqueous solution, precipitation of the product **7** did not lead to reversion back to **1**.

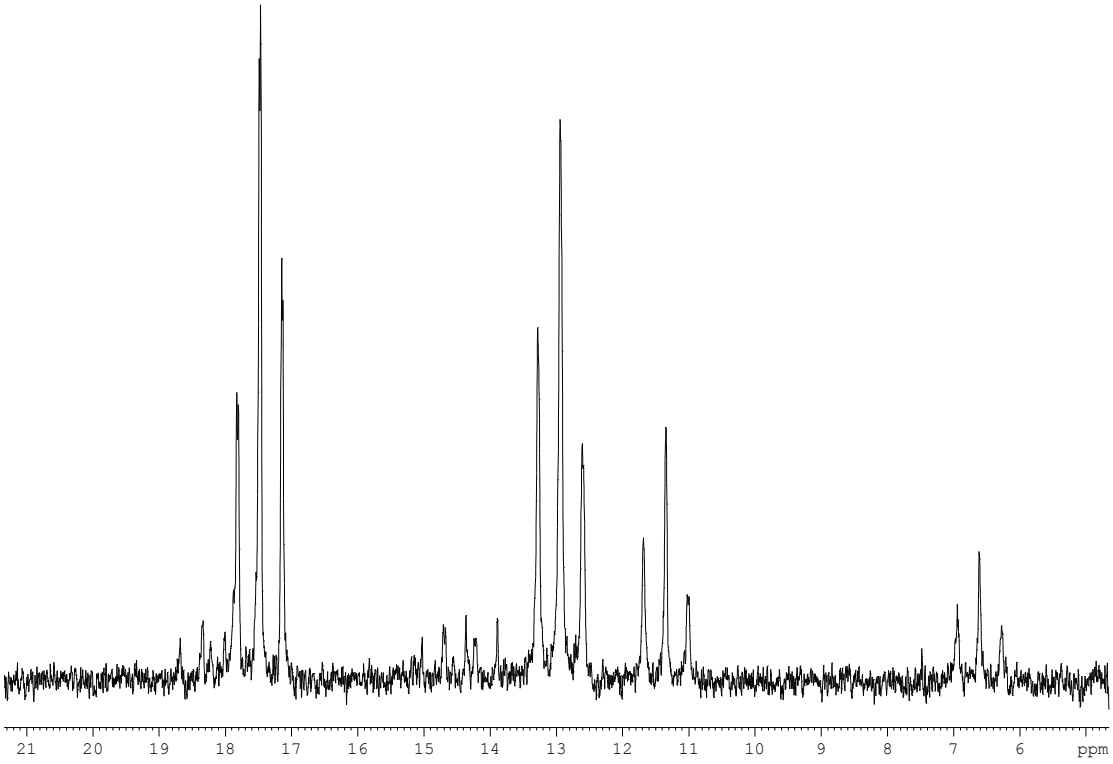

Figure 2.14 – $^{31}P\{^1H\}$ NMR spectrum of the reaction of 1 with two equivalents of NaN_3 in D_2O at 122 MHz.

In comparison with the thiocyanate chemistry, the $^{31}P\{^1H\}$ NMR spectrum of the product of the reaction of one equivalent of azide with **1** showed that the main species (as well as small amounts of **1** and **7**) was now the asymmetric complex represented by the doublet of doublets at δ 11.3 and two doublets of triplets at δ 18.3 and 14.4, which has been proposed to be of the asymmetric cation $[Fe(L^1)(N_3)(H_2O)]^+$. This suggests that the second substitution of a water ligand for an azide anion to give $[Fe(L^1)(N_3)_2]$ (**7**) is the rate determining step, in complete contrast of the reaction of complex **1** with thiocyanate.

The IR spectrum of **7** showed only one azide absorption at 2056 cm^{-1}. As the two coordinated azide anions are *cis* to one another, two absorptions would be expected as a result of the symmetric and asymmetric stretching modes of the ligands. Only one peak is observed presumably due to both stretching modes being very close in energy.

Similar observations have been made by Field *et al.* for related *cis* bis(azido) iron(II) phosphine complexes[23].

2.6 X-ray structures of $[Fe(L^1)(NCS)_2]\cdot 2H_2O$ ($6\cdot 2H_2O$) and $[Fe(L^1)(N_3)_2]\cdot 0.812H_2O$ ($7\cdot 0.812H_2O$)

Unequivocal characterisation of **6** was provided by X-ray crystallography. Orange crystals of **6** were grown upon slow evaporation of an acetone solution. The analysis confirms the substitution of both H_2O molecules for thiocyanate anions has occured, as indicated by the NMR data. The structure is of the dihydrate and shows that the thiocyanato groups on **6** are bound *via* the harder nitrogen atoms of the NCS^- ligand, rather than the softer sulfur donors (**Figure 2.15**). This is expected due to the better match between the relatively hard iron(II) centre and the nitrogen donors. The Fe-N-C bond angles in **6** are almost linear (173.5(3) and 175.5(3)°), reflecting the *sp* hybridisation of the orbitals on the N atom of the thiocyanate ligand. These values are within the range reported for iron-thiocyanate complexes, though greater than the mean values reported in the Cambridge Structural Database for compounds of this type (164.4(9.6)°). Other main bond lengths and angles are largely similar to those in the structures of **3** and **5** (**Table 2.3**).

Red crystals of **7** were grown by adding diethyl ether to a water/acetone solution. As expected from the NMR data, the structure confirms the substitution of both aqua groups for azide ligands has occurred (**Figure 2.16**). The structure of $\mathbf{7}\cdot 0.812H_2O$ has two molecules of the iron complex in the asymmetric unit, the main difference between them being the Fe-N-N bond angles. For the molecule containing Fe(1), the angles are 144.32(8) and 145.30(18)°, whereas in the molecule containing Fe(2) the angles are more diverse at 138.9(2) and 152.4(2)° (**Tables 2.4a** and **2.4b**). These angles are all above the mean average values for iron azide complexes found in the Cambridge Structural Database (125.8(9.5)°),[24, 25] and are all higher than the 120° angle that would be expected for the sp^2 hybridised terminal nitrogen atom on the azide group. The two molecules of complex **7** are interconnected into a three-dimensional structure through a combination of O-H···O and O-H···N hydrogen bonds, with the latter involving the azido groups as acceptors.

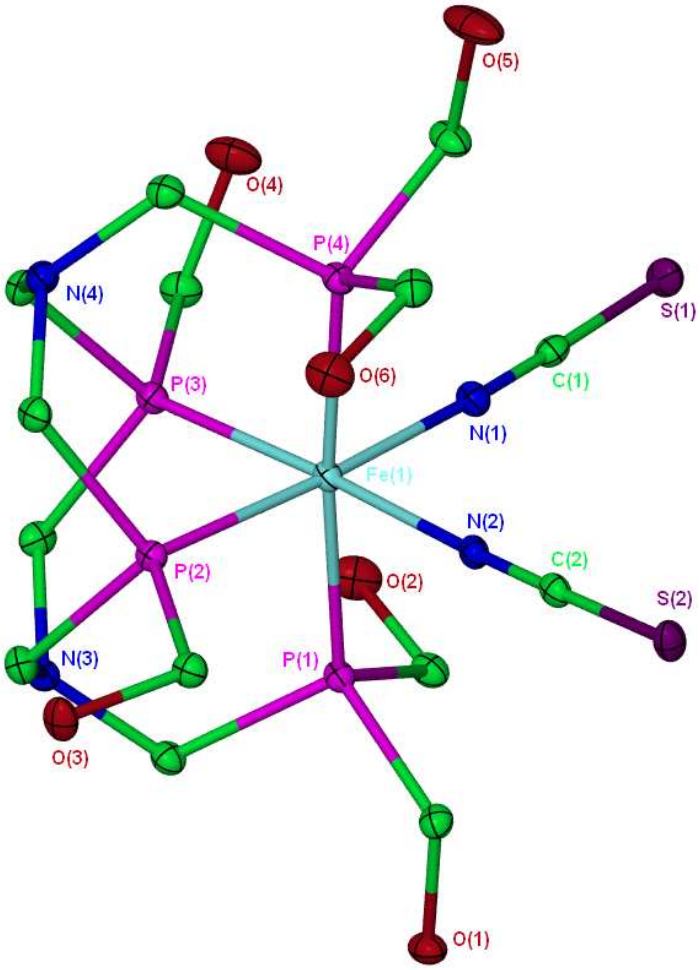

Figure 2.15 - Molecular structure of $[Fe(L^1)(NCS)_2]\cdot 2H_2O$ ($6\cdot 2H_2O$). Thermal ellipsoids are at the 30% probability level. The included water molecules and hydrogen atoms have been omitted for clarity.

Bond Lengths

Fe(1)-P(1)	2.2320(10)	Fe(1)-N(2)	1.952(3)
Fe(1)-P(2)	2.1840(10)	N(1)-C(1)	1.160(4)
Fe(1)-P(3)	2.1907(11)	S(1)-C(1)	1.660(4)
Fe(1)-P(4)	2.2469(10)	N(2)-C(2)	1.162(5)
Fe(1)-N(1)	1.960(3)	S(2)-C(2)	1.656(4)

Bond Angles

P(1)-Fe(1)-P(4)	174.32(4)	Fe(1)-N(1)-C(1)	175.5(3)
N(1)-Fe(1)-P(2)	175.02(10)	Fe(1)-N(2)-C(2)	173.5(3)
N(2)-Fe(1)-P(3)	175.67(9)	N(1)-C(1)-S(1)	178.1(3)
N(2)-Fe(1)-N(1)	90.30(13)	N(2)-C(2)-S(2)	178.3(4)
P(3)-Fe(1)-P(2)	80.99(10)		

Table 2.3 – Selected bond lengths (Å) and angles (°) for complex $6\cdot 2H_2O$.

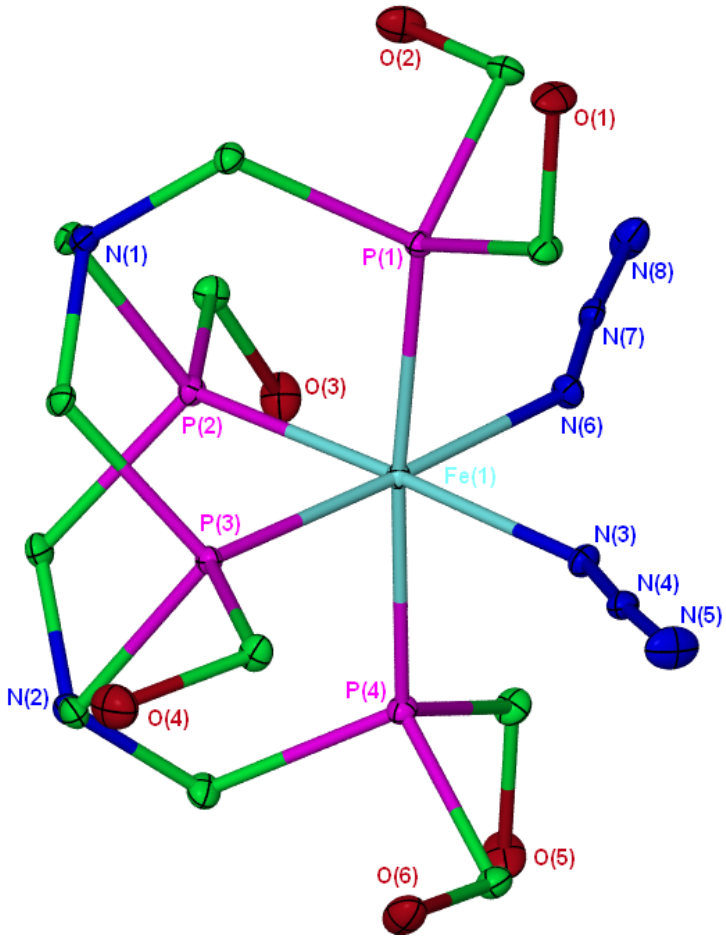

Figure 2.16 - Molecular structure of $[Fe(L^1)(N_3)_2]\cdot 0.812H_2O$ (7·0.812H_2O) showing molecule 1 of 2 independent molecules in the asymmetric unit. Thermal ellipsoids are at the 30% probability level. The included water molecules and hydrogen atoms have been omitted for clarity.

Bond Lengths (molecule 1)

Fe(1)-P(1)	2.2313(7)	Fe(1)-N(6)	2.028(2)
Fe(1)-P(2)	2.1846(7)	N(3)-N(4)	1.169(3)
Fe(1)-P(3)	2.1753(7)	N(4)-N(5)	1.182(3)
Fe(1)-P(4)	2.2453(7)	N(6)-N(7)	1.173(3)
Fe(1)-N(3)	2.029(2)	N(7)-N(8)	1.185(3)

Bond Angles (molecule 1)

P(1)-Fe(1)-P(4)	174.71(3)	N(4)-N(3)-Fe(1)	144.32(18)
N(3)-Fe(1)-P(2)	177.61(6)	N(7)-N(6)-Fe(1)	145.30(18)
N(6)-Fe(1)-P(3)	177.68(6)	N(3)-N(4)-N(5)	176.1(3)
N(6)-Fe(1)-N(3)	85.48(8)	N(6)-N(7)-N(8)	174.4(3)
P(3)-Fe(1)-P(2)	80.92(2)		

Table 2.4a – Selected bond lengths (Å) and angles (°) for complex 7·0.812H_2O (molecule 1).

Bond Lengths (molecule 2)

Fe(2)-P(5)	2.2611(7)	Fe(2)-N(14)	2.032(2)
Fe(2)-P(6)	2.1783(7)	N(11)-N(12)	1.180(3)
Fe(2)-P(7)	2.1847(7)	N(12)-N(13)	1.180(3)
Fe(2)-P(8)	2.2324(7)	N(14)-N(15)	1.161(3)
Fe(2)-N(11)	2.052(2)	N(15)-N(16)	1.185(3)

Bond Angles (molecule 2)

P(5)-Fe(2)-P(8)	175.48(3)	N(12)-N(11)-Fe(2)	138.9(2)
N(11)-Fe(2)-P(6)	178.00(7)	N(15)-N(14)-Fe(2)	152.4(2)
N(14)-Fe(2)-P(7)	174.44(8)	N(13)-N(12)-N(11)	176.2(3)
N(11)-Fe(2)-N(14)	84.12(10)	N(16)-N(15)-N(14)	176.3(3)
P(6)-Fe(2)-P(7)	80.77(3)		

Table 2.4b – Selected bond lengths (Å) and angles (°) for complex 7·0.812H_2O (molecule 2).

2.7 Reaction of $[Fe(L^1)(H_2O)_2]SO_4$ (1) with sodium carbonate

The reaction of an aqueous solution of **1** with sodium carbonate afforded a red solution of the neutral complex $[Fe(L^1)(\kappa^2\text{-}O_2CO)]$ (**8**), which is formed as a result of the replacement of the coordinated water molecules with a bidentate carbonate ligand (**Scheme 2.5**). The isolation of **8** was achieved by the addition of acetone to an aqueous solution.

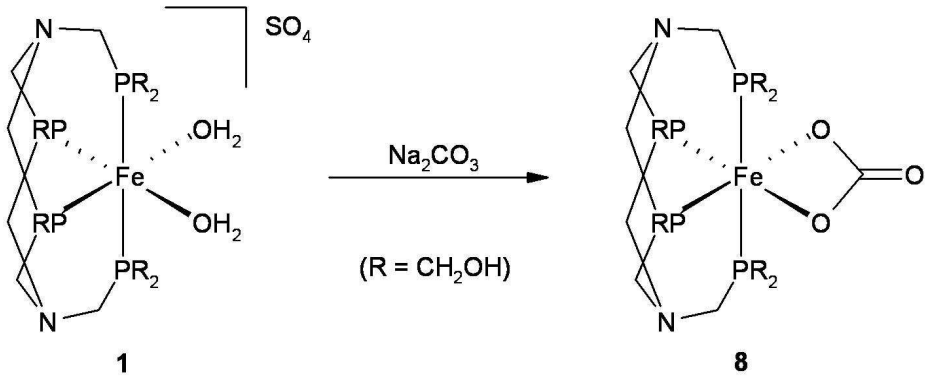

1 **8**

Scheme 2.5 – Reaction of 1 with sodium carbonate to give the κ^2-carbonato complex 8.

The $^{31}P\{^1H\}$ NMR spectrum of **8** in D_2O exhibited the anticipated pair of triplets at δ 23.5 and δ 9.4 ($^2J_{P\text{-}P}$ = 54 Hz). The IR spectrum of **8** showed a carbonate absorption band at 1681 cm^{-1}.

The reaction of a red aqueous solution of **8** with hydrochloric acid gave a purple solution, accompanied by the evolution of carbon dioxide. The $^{31}P\{^{1}H\}$ NMR spectrum showed the formation of a broad peak and a broad triplet at *ca*. δ 22 and 0.4 respectively, as observed in the reaction of **1** with sodium chloride in aqueous solution. This evolution of the gas suggests that the carbonate ligand had reacted with the acid to give a molecule each of CO_2 and H_2O, as well as two chloride ligands. However, the familiar broad $^{31}P\{^{1}H\}$ NMR resonance pattern suggests that the exchange between the H_2O solvent molecules is occurring, and attempts to isolate the dichloride resulted in the formation of the $^{31}P\{^{1}H\}$ NMR resonances associated with **1**.

2.8 X-ray structure of $[Fe(L^1)(\kappa^2\text{-}O_2CO)]\cdot 1.7H_2O$ ($8\cdot 1.7H_2O$)

Crystals of $\mathbf{8}\cdot 1.7H_2O$ suitable for X-ray analysis were grown from the slow diffusion of acetone into an aqueous solution of the iron complex. The diffraction revealed the structure to be of the hydrate $\mathbf{8}\cdot 1.7H_2O$, and the structure contains two independent molecules of **8** in the asymmetric unit. Both H_2O molecules have been substituted with the bidentate carbonate ligand (**Figure 2.17**), as suggested by NMR spectroscopy. The octahedral structure of **8** is much more distorted than the structures of **3**, **5**, **6** and **7** due to the bidentate carbonate ligand, which constrains the structure giving a O(1)-Fe(1)-O(2) angle of 63.8(2)° (63.9(2)° for O(10)-Fe(2)-O(11) in molecule 2), which is far less than the standard 90° angle expected for a normal octahedral structure. The equatorial crystallographic bite angle is 81.38(10)° (80.49(9) for molecule 2), which is similar to the structures of **3**, **5**, **6** and **7**. Other bond lengths and angles are similar to the previously crystallographically-characterised complexes in this chapter (**Tables 2.5a** and **2.5b**). The structure is organised into a three-dimensional network, with the hydroxymethyl and uncoordinated carbonate oxygen atoms acting as hydrogen bond acceptors. The included water molecules in the structure are also involved in the hydrogen bonding.

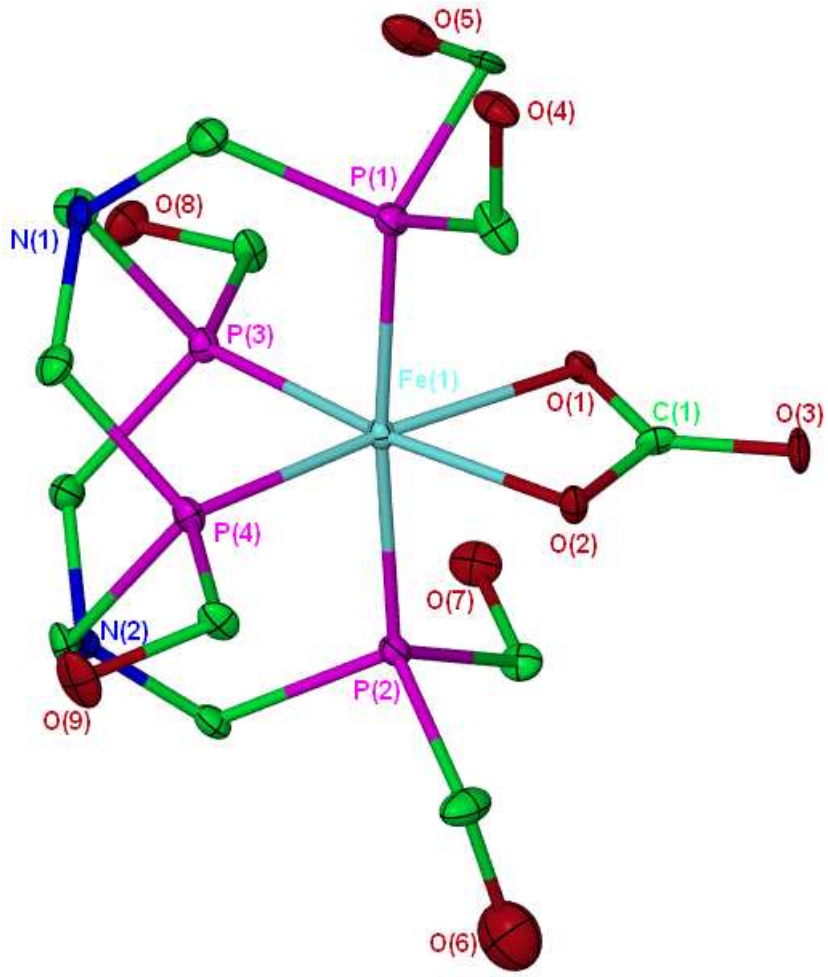

Figure 2.17 - Molecular structure of $[Fe(L^1)(\kappa^2\text{-}O_2CO)]\cdot 1.7H_2O$ ($8\cdot 1.7H_2O$) showing molecule 1 of two independent molecules in the asymmetric unit. Thermal ellipsoids are at the 30% probability level. The included water molecules and hydrogen atoms have been omitted for clarity.

Bond Lengths (molecule 1)

Fe(1)-P(1)	2.223(3)	Fe(1)-O(2)	2.073(5)
Fe(1)-P(2)	2.232(3)	O(1)-C(1)	1.307(9)
Fe(1)-P(3)	2.175(3)	O(2)-C(1)	1.286(10)
Fe(1)-P(4)	2.162(2)	O(3)-C(1)	1.271(9)
Fe(1)-O(1)	2.044(5)		

Bond Angles (molecule 1)

P(1)-Fe(1)-P(2)	174.30(9)	P(3)-Fe(1)-P(4)	81.38(10)
P(4)-Fe(1)-O(1)	171.50(19)	O(1)-Fe(1)-O(2)	63.8(2)
P(3)-Fe(1)-O(2)	170.85(18)	O(3)-C(1)-O(2)	123.9(8)
P(4)-Fe(1)-O(2)	107.76(17)	O(3)-C(1)-O(1)	121.8(8)
P(3)-Fe(1)-O(1)	107.05(18)	O(2)-C(1)-O(1)	114.2(7)

Table 2.5a – Selected bond lengths (Å) and angles (°) for complex $8\cdot 1.7H_2O$ (molecule 1) (standard deviation in brackets).

Bond Lengths (molecule 2)

Fe(2)-P(5)	2.216(2)	Fe(2)-O(11)	2.057(5)
Fe(2)-P(6)	2.243(3)	O(10)-C(14)	1.301(10)
Fe(2)-P(7)	2.164(2)	O(11)-C(14)	1.288(11)
Fe(2)-P(8)	2.186(3)	O(12)-C(14)	1.269(9)
Fe(2)-O(10)	2.032(5)		

Bond Angles (molecule 2)

P(5)-Fe(2)-P(6)	173.96(9)	P(6)-Fe(2)-P(7)	80.49(9)
P(7)-Fe(2)-O(10)	170.6(2)	O(10)-Fe(2)-O(11)	63.9(2)
P(8)-Fe(2)-O(11)	172.79(18)	O(10)-C(14)-O(12)	121.3(9)
P(7)-Fe(2)-O(11)	106.72(18)	O(11)-C(14)-O(12)	125.3(9)
P(8)-Fe(2)-O(10)	108.9(2)	O(10)-C(14)-O(11)	113.4(7)

Table 2.5b – Selected bond lengths (Å) and angles (°) for complex $8 \cdot 1.7H_2O$ (molecule 2).

2.9 Reactions of $[Fe(L^1)(H_2O)_2]SO_4$ (1) with CO

Stirring an aqueous solution of **1** saturated with CO for 24 hours resulted in a yellow solution. $^{31}P\{^1H\}$ NMR spectroscopy of the solution showed two new triplets to lower frequency than for **1**, at δ -14.9 and δ -39.4 ($^2J_{P\text{-}P}$ = 35 Hz), consistant with the formation of the iron(II) dicarbonyl complex $[Fe(L^1)(CO)_2]SO_4$ **9**. The lower value for the $^2J_{P\text{-}P}$ coupling constant going from **1** to **9** is expected due to the high *trans* influence of the π-acceptor carbonyl ligands, which weakens the bonds between the equatorial phosphine groups and the iron centre. The identity of **9** is supported by the IR spectrum, which displays two carbonyl stretches at 2059 and 2022 cm^{-1}.

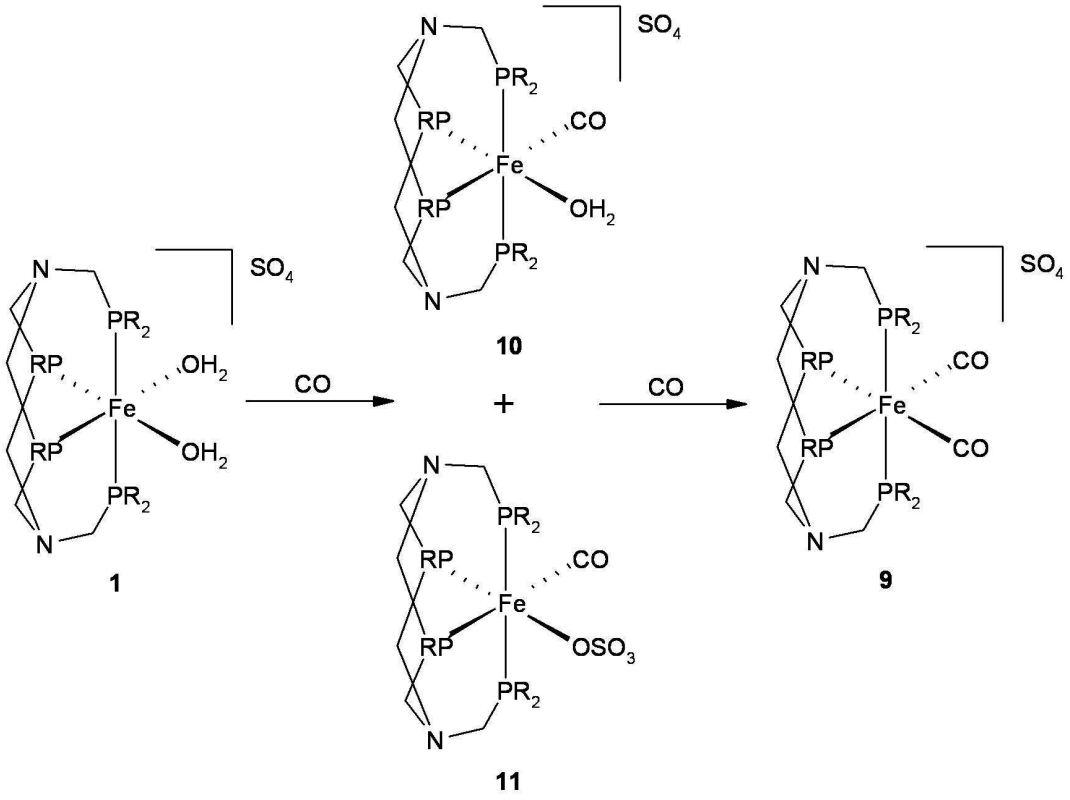

Scheme 2.6 – Reaction of 1 with CO to give the dicarbonyl complex 9, *via* the intermediate mono-carbonyl complexes 10 and 11.

When **1** is exposed to an atmosphere of CO for a shorter period of time, the intermediate mono-carbonyl complexes **10** and **11** (**Scheme 2.6**) can be observed by $^{31}P\{^{1}H\}$ NMR spectroscopy, in addition to resonances for **1** and **9**. Complexes **10** and **11** both display three resonances, consisting of two sets of doublets of triplets and one doublet of doublets (**Figure 2.18**). Upon further exposure to CO, the intermediates **10** and **11** are fully converted to the dicarbonyl **9**.

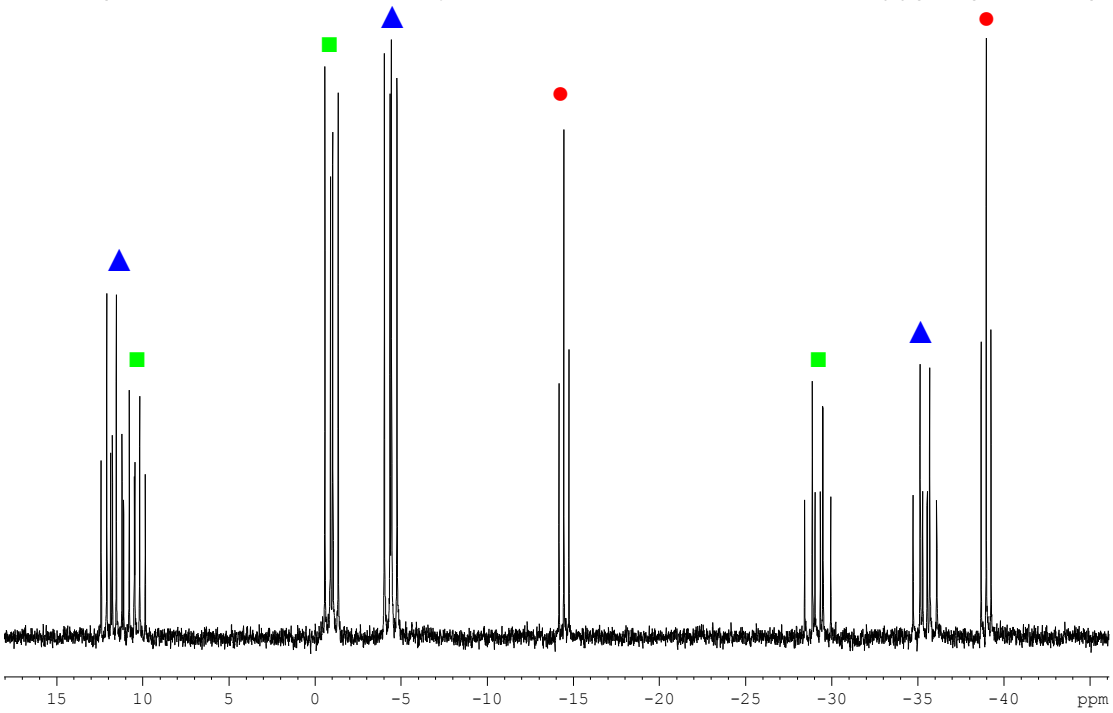

Figure 2.18 – $^{31}P\{^{1}H\}$ NMR spectrum of the reaction of $[Fe(L^1)(H_2O)_2]SO_4$ (1) with CO in D_2O at 122 MHz. Symbols ▲ and ■ signify complexes 10 and 11, ● signifies complex 9.

The relationship between these resonances was confirmed by ^{31}P-^{31}P COSY NMR spectroscopy. The A_2MX resonance patterns are consistent with both intermediates **10** and **11** having chemically inequivalent equatorial phosphine groups as a result of two different ligands occupying the *cis* sites on the iron (*i.e.* they have the general formula $[Fe(L^1)XY]^{n+}$). As **1** possesses C_2 symmetry and a mirror plane, it is not immediately obvious why there should be two separate mono(carbonyl) intermediates, as substitution of either of the two H_2O ligands should result in the aqua carbonyl complex $[Fe(L^1)(CO)(H_2O)]SO_4$ (**10**). This is an obvious intermediate in the stepwise replacement of both aqua ligands on **1** to form **9**. The second intermediate has been identified as the mono(carbonyl) mono(sulfato) complex $[Fe(L^1)(CO)(\kappa^1\text{-}OSO_3)]$ (**11**) on the basis of mass-spectral evidence. The positive ion electrospray mass spectrum of the mixture of **10** and **11** showed peaks at *m/z* = 625.0 and 603.0, which can be assigned as $[M+Na]^+$ and $[M+H]^+$, where M is $[Fe(L^1)(CO)(\kappa^1\text{-}OSO_3)]$ (**11**). When the reaction of **1** with CO is carried out in the presence of excess sulfate, poor conversion to **9** is observed and instead the proportion of the intermediates **10** and **11** is maximised. This adds additional evidence to the existence of the proposed $[Fe(L^1)(CO)(\kappa^1\text{-}OSO_3)]$ moiety (**11**). This is further backed up by the observation of the analogous sulfato carbonyl complex *trans*-$[Fe(L)(CO)(\kappa^1\text{-}OSO_3)]$, where L = bis(hydroxypropylphosphino)ethane (DHPrPE (**81b**) in Chapter 1, section 1.7.2) as a result of the reaction of *cis*-$[Fe(L)_2(SO_4)]$ with CO.[26] Although **10** and **11** can be identified as $[Fe(L^1)(CO)(H_2O)]SO_4$ and $[Fe(L^1)(CO)(\kappa^1\text{-}OSO_3)]$ respectively, it is not possible to unambiguously assign **10** and **11** to one set of resonances each, as they

only differ in ^{31}P chemical shift and $^{2}J_{P\text{-}P}$ coupling constant (*i.e.* **10** or **11**: δ 10.5 (dt, $^{2}J_{P\text{-}P}$ = 74, $^{2}J_{P\text{-}P}$ = 39 Hz), -0.93 (dd, $^{2}J_{P\text{-}P}$ = 39, $^{2}J_{P\text{-}P}$ = 56 Hz), -29.2 (dt, $^{2}J_{P\text{-}P}$ = 74, $^{2}J_{P\text{-}P}$ = 56 Hz); **10** or **11**: δ 11.8 (dt, $^{2}J_{P\text{-}P}$ = 68, $^{2}J_{P\text{-}P}$ = 40 Hz), -4.4 (dd, $^{2}J_{P\text{-}P}$ = 40, $^{2}J_{P\text{-}P}$ = 50 Hz), -35.5 (dt, $^{2}J_{P\text{-}P}$ = 68, $^{2}J_{P\text{-}P}$ = 50 Hz).

2.10 X-ray structure of $[Fe(L^1)(CO)_2]SO_4 \cdot H_2O$ ($9 \cdot H_2O$)

Yellow crystals suitable for X-ray analysis were grown by evaporation of an aqueous solution. The structural analysis showed the complex to be the hydrate $\mathbf{9} \cdot H_2O$. As expected, both aqua groups have been substituted with neutral carbonyl ligands to give the dicationic dicarbonyl complex (**Figure 2.19**). The Fe-P bonds *trans* to the CO ligands are longer than in the other complexes, due to the high *trans* influence of CO. As a result the crystallographic bite angle of the two equatorial phosphorus atoms (79.42(3)°) is smaller than that in the related dichloride complex **3** (80.190(15)°). In other crystallographically characterised complexes of L^1 the Fe-P bond lengths to the axial phosphorus atoms are significantly longer than those to the equatorial phosphines. The difference is much smaller in **9**, also due to the high *trans* influence of CO (**Table 2.6**).

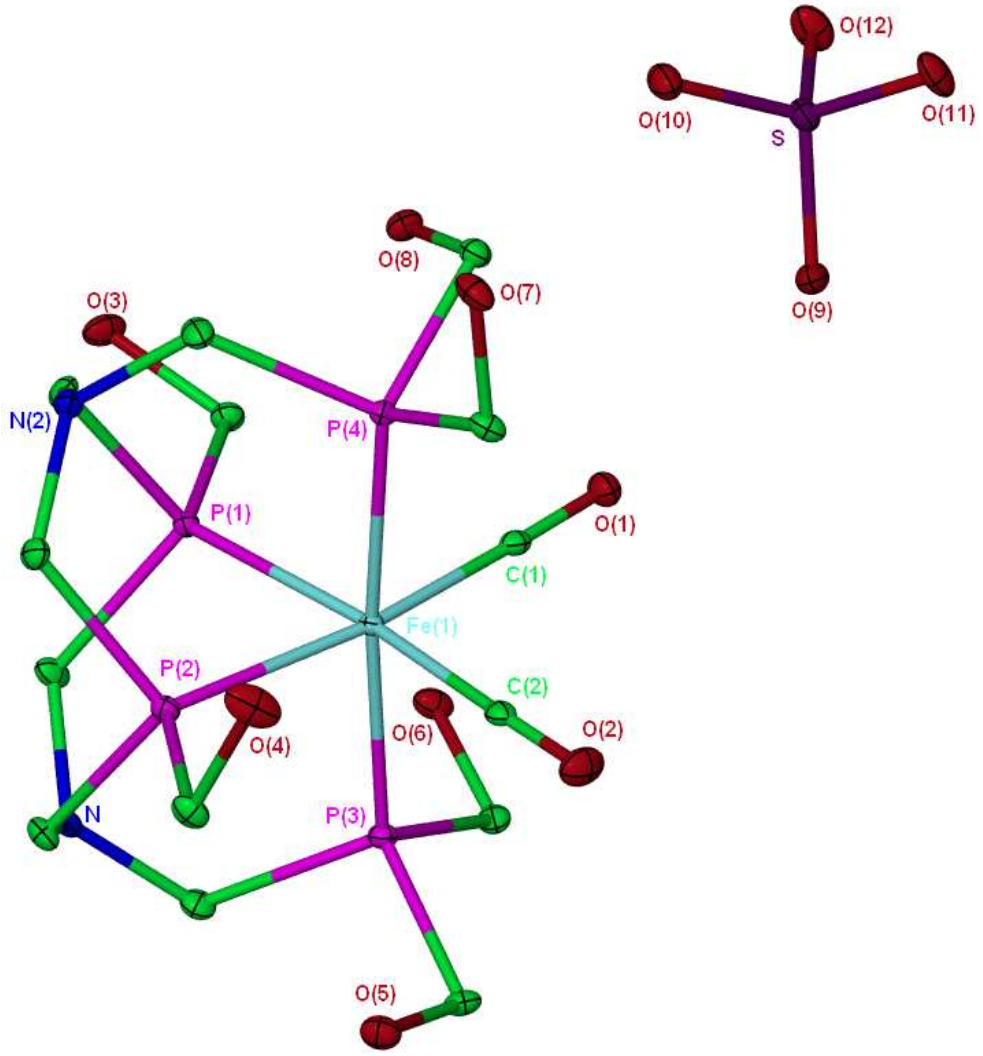

Figure 2.19 - Molecular structure of $[Fe(L^1)(CO)_2]SO_4 \cdot H_2O$ ($9 \cdot H_2O$). Thermal ellipsoids are shown at the 30% probability level. The included water molecule and hydrogen atoms have been omitted for clarity.

Bond Lengths

Fe(1)-P(1)	2.2771(7)	Fe(1)-C(1)	1.804(2)
Fe(1)-P(2)	2.2660(7)	Fe(1)-C(2)	1.824(3)
Fe(1)-P(3)	2.2628(7)	C(1)-O(1)	1.129(3)
Fe(1)-P(4)	2.2653(6)	C(2)-O(2)	1.120(3)

Bond Angles

P(3)-Fe(1)-P(4)	174.81(3)	C(1)-Fe(1)-C(2)	95.74(11)
P(2)-Fe(1)-C(1)	171.32(8)	Fe(1)-C(1)-O(1)	178.6(2)
P(1)-Fe(1)-C(2)	172.34(8)	Fe(1)-C(2)-O(2)	178.8(2)
P(1)-Fe(1)-P(2)	79.42(3)		

Table 2.6 – Selected bond lengths (Å) and angles (°) for complex $9 \cdot H_2O$.

2.11 Reaction of $[Fe(L^1)Cl_2]$ (3) with CO

Reaction of an acetone solution of $[Fe(L^1)Cl_2]$ (**3**) with CO in the presence of 1 equivalent of sodium tetraphenylborate gave an orange precipitate containing the mono(cationic) carbonyl complex $[Fe(L^1)(CO)Cl]^+$. The $^{31}P\{^1H\}$ NMR spectrum in D_2O shows the usual pattern for a hetero-substituted L^1 complex, *i.e.* two doublets of triplets (δ 4.6 and -30.1), and a doublet of doublets (δ -6.2) (**Figure 2.20**). Despite the presence of the tetraphenylborate, the complex crystallised as the chloride salt $[Fe(L^1)(CO)Cl]Cl$ **12**, as confirmed by microanalysis. The IR spectrum (KBr disc) showed the CO stretching frequency for **12** at 1987 cm^{-1}.

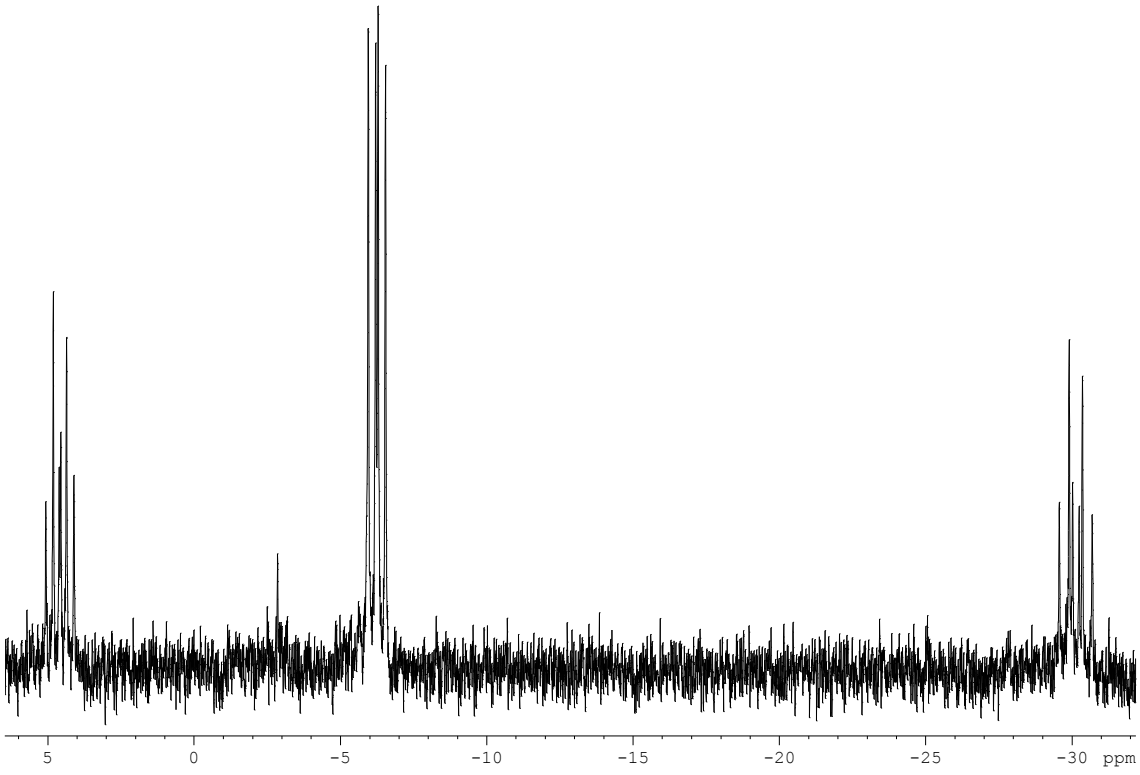

Figure 2.20 - $^{31}P\{^1H\}$ NMR spectrum of $[Fe(L^1)(CO)Cl]Cl$ (12) in D_2O at 162 MHz.

In contrast with the reaction of **1** with CO, the reaction of **3** with CO only affords one mono(carbonyl) complex due to the absence of the sulfate anion. The dicarbonyl complex $[Fe(L^1)(CO)_2]Cl_2$ was not formed because of the precipitation of **12** after the first substitution of chloride for CO, which is due to the insolubility of the ionic complex in acetone.

After 24 h, the $^{31}P\{^1H\}$ NMR spectrum of the D_2O solution of **12** showed the formation of some of the $[Fe(L^1)(CO)(D_2O)]^{2+}$ cation due to the substitution of the chloride ligand with D_2O, as well as the formation of some $[Fe(L^1)(D_2O)_2]SO_4$ (**1**) as a result of the substitution of both coordinated CO and Cl^- ligands.

2.12 Attempts to remove and isolate ligand L^1 from the metal

The tetradentate macrocyclic phosphine ligand L^1 is a very interesting ligand because of its ability to impart water-solubility and to form highly stable iron(II) complexes. Ligand L^1 has never been isolated as a free ligand and would be very difficult to synthesise without the metal template. It would be desirable to isolate the ligand so that its coordination chemistry can be explored with other metals, though it is not known whether or not the free ligand would be stable in solution. One method of removing the ligand from the iron(II) centre is by introducing a ligand with a higher binding constant than L^1 that will preferentially coordinate to the iron(II) centre. Ethylenediaminetetraacetate ($EDTA^{4-}$) is a hexadentate ligand that is expected to form a more stable complex with the iron than L^1.

Two equivalents of Na_4EDTA were added to an aqueous solution of **1** to give a deep red solution. $^{31}P\{^1H\}$ NMR spectroscopy (D_2O) showed peaks at δ 21.3 (broad) and 4.3 (t). The appearance of two small triplets at δ 24.1 and 10.0 was also observed. After 24 h, the two triplets at δ 24.1 and 10.0 had grown to be the major product, accompanied by the reduction in intensity of the peaks at δ 21.3 and 4.3. This is described in the kinetic NMR experiment in **Section 2.2**. This is very similar to the $^{31}P\{^1H\}$ NMR spectrum of the reaction with hydroxide, suggesting that $EDTA^{4-}$ in this case is deprotonating the water ligands to give the neutral di-hydroxy species **2a**. When a large excess of Na_4EDTA was added, the solution turned brown and, similar to the reactions with base, led to an insoluble brown precipitate believed to be iron(III) hydroxide. Orange/brown crystals suitable for X-ray diffraction were isolated from vapour diffusion of iso-propanol into an aqueous solution of complex **1** with two equivalents of Na_4EDTA after about six weeks.

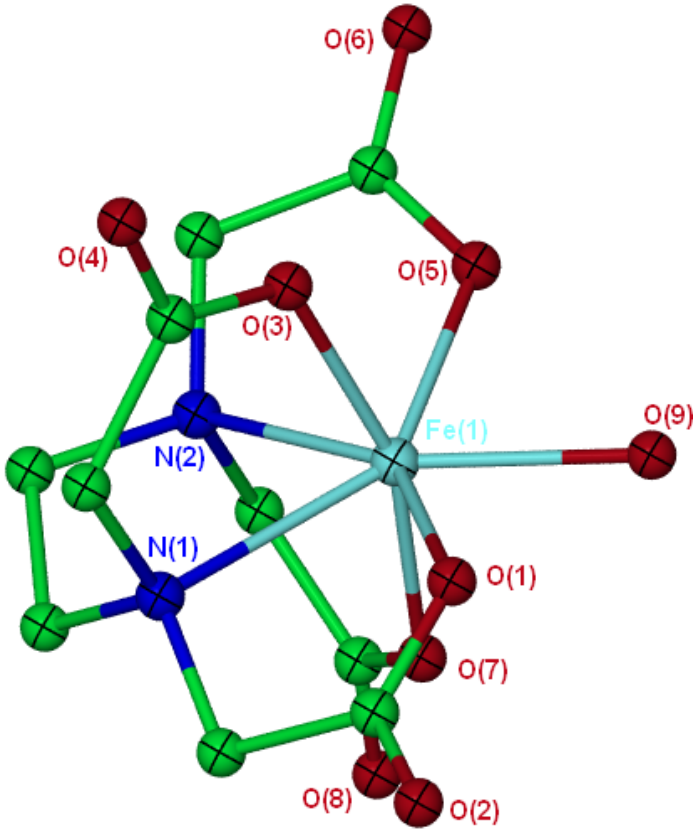

Figure 2.21 – X-ray molecular structure of Na[Fe(EDTA)(H_2O)] (sodium cation not shown).

The X-ray crystal structure showed the product to be the seven-coordinate iron(III) mono-aqua EDTA complex Na[Fe(EDTA)(H_2O)] (**Figure 2.21**). The $^{31}P\{^1H\}$ NMR spectrum of the remaining solution proved inconclusive as the signal/noise ratio was poor. It is possible that the ligand may have been oxidised and disassembled. A solution of **1** with two equivalents of Na_4EDTA that had been left for six weeks under an atmosphere of nitrogen did not give a similar brown solution, suggesting no oxidation of the Fe(II) to Fe(III) had occurred, and therefore the formation of Na[Fe(EDTA)(H_2O)] did not occur.

Ultimately, the isolation of the tetradentate macrocyclic phosphine ligand L^1 has proven difficult due to its ability to strongly bind to the Fe(II) centre. This is partly due to the chelating effect of the ligand, which helps to stabilise the complex. Removing the ligand from the metal centre has been shown to be possible despite the inherent stability offered by the coordination of the tetradentate ligand. The removal is achieved by using a potentially hexadentate ligand ($EDTA^{4-}$) to displace the phosphine ligand and form an iron complex of EDTA. It is not known whether L^1 is stable once decomplexed from the iron, and no spectroscopic evidence supported that the ligand had remained intact in solution.

2.13 Nuclear Resonance Vibrational Spectroscopic studies of 1 and 8 as models for the active site Iron-Sulfur Cluster-Free Hydrogenase (Hmd)

The importance of vibrational spectroscopy as a method for determining the molecular structures and functionalities of molecules is well established. In biochemistry, however, more advanced techniques are needed due to the complexity of biomolecules such as enzymes. In particular, site-selective techniques are needed to probe active sites of biomolecules to gain information about their structure. Established techniques such as resonance Raman,[27] difference infrared,[28, 29] and femtosecond coherence spectroscopy[30] offer a certain degree of site selectivity, but the information which they provide is limited. This is because the selection rules of infrared and Raman spectroscopies do not allow the observation of many important vibrational modes. For example, in-plane vibrational Fe modes for haem derivatives are effectively forbidden in IR and Raman spectroscopies, but could be expected to provide important information about bond strengths. Some other haem vibrations have (just simply) not been identified despite being allowed by selection rules.

Nuclear Resonance Vibrational Spectroscopy (NRVS) is a recent synchrotron-based spectroscopic technique combining nuclear excitation and vibrational motion.[31] NRVS (also known as Nuclear Resonant Inelastic X-ray Scattering – NRIXS) is selective for the vibrations of Mössbauer active nuclei such as ^{57}Fe, ^{83}Kr, ^{119}Sn and ^{157}Eu. The isotope of most interest is ^{57}Fe due to its importance at the centre of haems and other important biomolecules, and this has provided most of the results to date. Despite this dependence on Mössbauer active nuclei, NRVS gives the complete set of vibrational modes of the probe nucleus, including those forbidden by selection rules in IR and Raman spectroscopies. The technique is also highly selective due to its dependence on Mössbauer active nuclei, meaning that only vibrational modes involving the active nucleus are observed, and there is no interference from the vibrations involving only non-active nuclei, for example in ligands. Additional information in NRVS spectra can be obtained from the peak intensities, which are related to both the magnitude and direction of the vibrations, giving the technique an extra dimension. In the case of ^{57}Fe, for example, all iron-ligand modes are observed, including the in-plane Fe vibrations in haems and the iron-imidazole stretch in porphyrins, both of which are not observed by Raman spectroscopy.[31] Despite existing for a relatively short period of time, NRVS is showing potential to be an important technique for the characterisation of biomolecules, especially those containing iron-based active sites.

In collaboration with Prof. Stephen Cramer at the University of California, Davis and the Lawrence Berkeley National Laboratory in the USA, NRVS studies were carried out to investigate the possibility of using complex **1** as a model for the active site of the iron-containing enzyme H_2-forming methylene-tetrahydromethanopterin dehydrogenase (Hmd). The X-ray molecular structure of Hmd has not yet been solved and therefore current knowledge of its active site structure is obtained from the interpretation of IR,[32] Mössbauer,[33] and X-ray absorption spectra.[34] These techniques have revealed important information about the iron in Hmd, and it is now known that the iron is low-spin, and is believed to be complexed by two CO, one S, and one or two O/N based ligands (**Figure 2.22**).[35] It is still not known, however, whether the low-spin iron in Hmd is Fe(II) or Fe(0). As it is believed that the iron is five coordinate, this may suggest it is Fe(0), as low-spin Fe(II) is usually six-coordinate. The proposed vacant site is believed to be the H_2 activation site, and is modelled *trans* to the CO ligand, as it is believed that the function of the CO is to increase the acidity of the H_2 ligand trans to it.[36] This is still highly ambiguous, however, as X-ray absorption spectroscopy cannot differentiate between penta- and hexa-coordinated geometries.

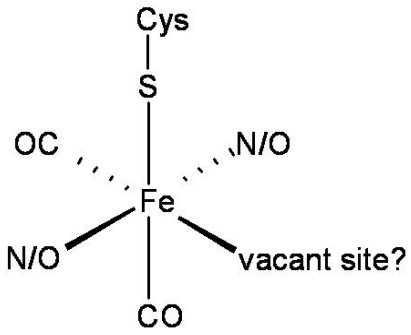

Figure 2.22 – Model of the proposed structure of the active site of H_2-forming methylene-tetrahydromethanopterin dehydrogenase (Hmd).

In order to find out more about the Fe-based active site of Hmd, highly selective techniques such as NRVS are required. In order to interpret results, simple models consisting of discrete iron complexes with similar ligands and geometries are needed for comparison of their NRVS spectra. As one possibility is that the active site of Hmd contains an low-spin Fe(II) with two carbonyl and two N or O based ligands (such as H_2O), complexes **1** and **9** are ideal candidates for such models.

As NRVS needs a Mössbauer active nucleus, ^{57}Fe analogues of **1** and **9** were synthesised. This was achieved by first making $^{57}FeSO_4$ from the reaction of ^{57}Fe metal powder with concentrated sulfuric acid. The $^{57}FeSO_4$ was then used in the reaction with THPS and ammonium sulfate to give ^{57}Fe labelled **1**, $[^{57}Fe(L^1)(H_2O)_2]SO_4$.

The ^{57}Fe analogue of **9**, $[^{57}Fe(L^1)(CO)_2]SO_4$, was prepared by the exposure of an aqueous solution of $[^{57}Fe(L^1)(H_2O)_2]SO_4$ to carbon monoxide, as in the synthesis of **9** from **1**. The $^{31}P\{^1H\}$ NMR spectra of ^{57}Fe labelled **1** and **9** showed the extra splitting associated with the coupling of the spin ½ ^{57}Fe nucleus with the ^{31}P nuclei to give two sets of doublets of triplets as expected.

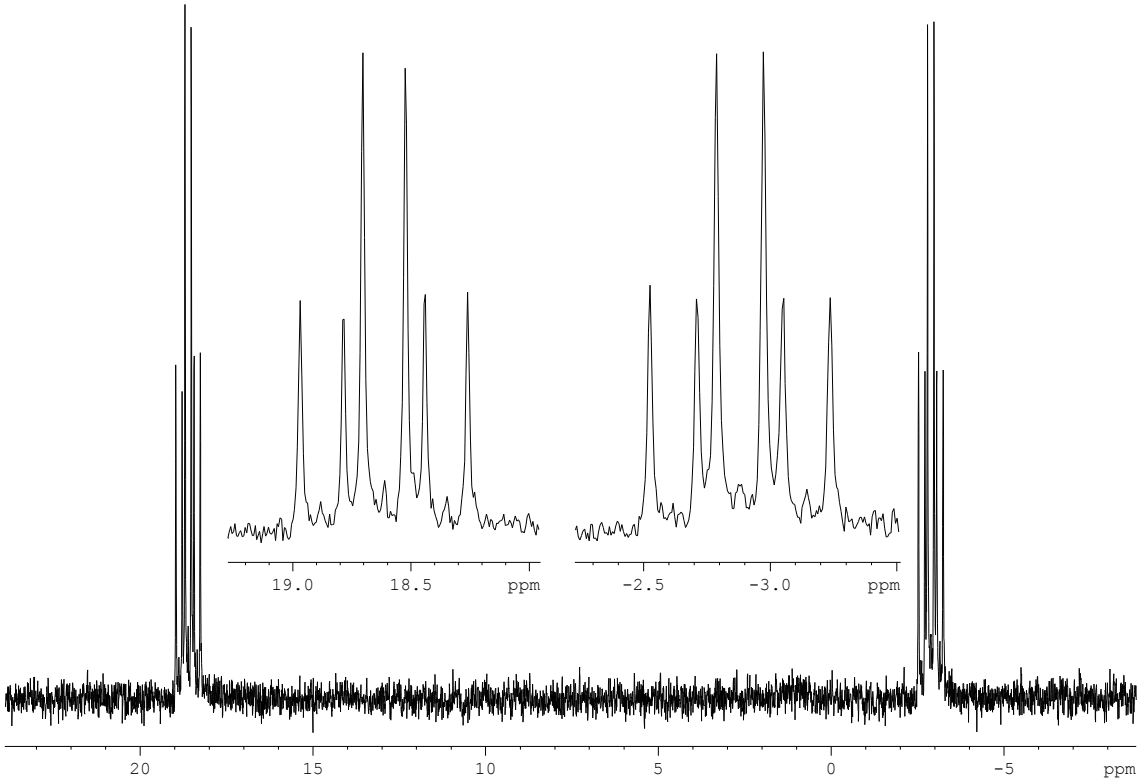

Figure 2.23 – $^{31}P\{^1H\}$ NMR spectrum of $[^{57}Fe(L^1)(H_2O)_2]SO_4$ in D_2O at 202 MHz.

Figure 2.23 shows the $^{31}P\{^1H\}$ NMR spectrum of $[^{57}Fe(L^1)(H_2O)_2]SO_4$ in D_2O. The extra splitting due to the coupling with the ^{57}Fe nucleus can clearly be seen, giving a $^1J_{Fe\text{-}P}$ coupling of 37 Hz to both the equatorial and axial phosphine environments. The $^{31}P\{^1H\}$ NMR spectrum of the dicarbonyl complex $[^{57}Fe(L^1)(CO)_2]SO_4$ (**Figure 2.24**) is similar in appearance to that of the diaqua complex, though in this case the $^1J_{Fe\text{-}P}$ coupling differs slightly for the axial and equatorial phosphines. The $^1J_{Fe\text{-}P}$ coupling constant for the coupling of the equatorial phosphines to the iron is 26 Hz, while the axial phosphine coupling constant is 28 Hz. In both cases, residual triplets belonging to the non-^{57}Fe labelled complexes can also be observed due to the ^{57}Fe metal powder used in the synthesis only being approximately 95% ^{57}Fe. Studies of $^1J_{Fe\text{-}P}$ coupling constants of iron phosphine complexes are relatively rare in the literature, and the values reported here are relatively low compared to others reported for iron-phosphine complexes. For example, a study on the $^1J_{Fe\text{-}P}$ coupling constants of a range of Fe(II) porphyrin complexes of the formula $[^{57}Fe(TPP)(PMe_3)(L)]$ (TPP = tetraphenylporphyrin)

ranged between 35 and 59 Hz depending on the ligand *trans* to the phosphine.[37, 38] The $^{1}J_{Fe\text{-}P}$ coupling increases from L = CO (36 Hz) < PMe_3 (45 Hz) < *N*-MeIm (59 Hz, *N*-MeIm = *N*-methylimidazole), suggesting that increasing the π-acceptor capability of the ligand *trans* to the phosphorus nucleus decreases the $^{1}J_{Fe\text{-}P}$ coupling constant. This correlates to the ^{57}Fe analogues of **1** and **9**, with the dicarbonyl complex having the lower $^{1}J_{Fe\text{-}P}$ value. The additional phosphine donors in **1** and **9** both *cis* and *trans* to the other donors have better π-acceptor capabilities than the N donor porphyrins, hence the lower overall $^{1}J_{Fe\text{-}P}$ values reported for the ^{57}Fe analogues of **1** and **9**.

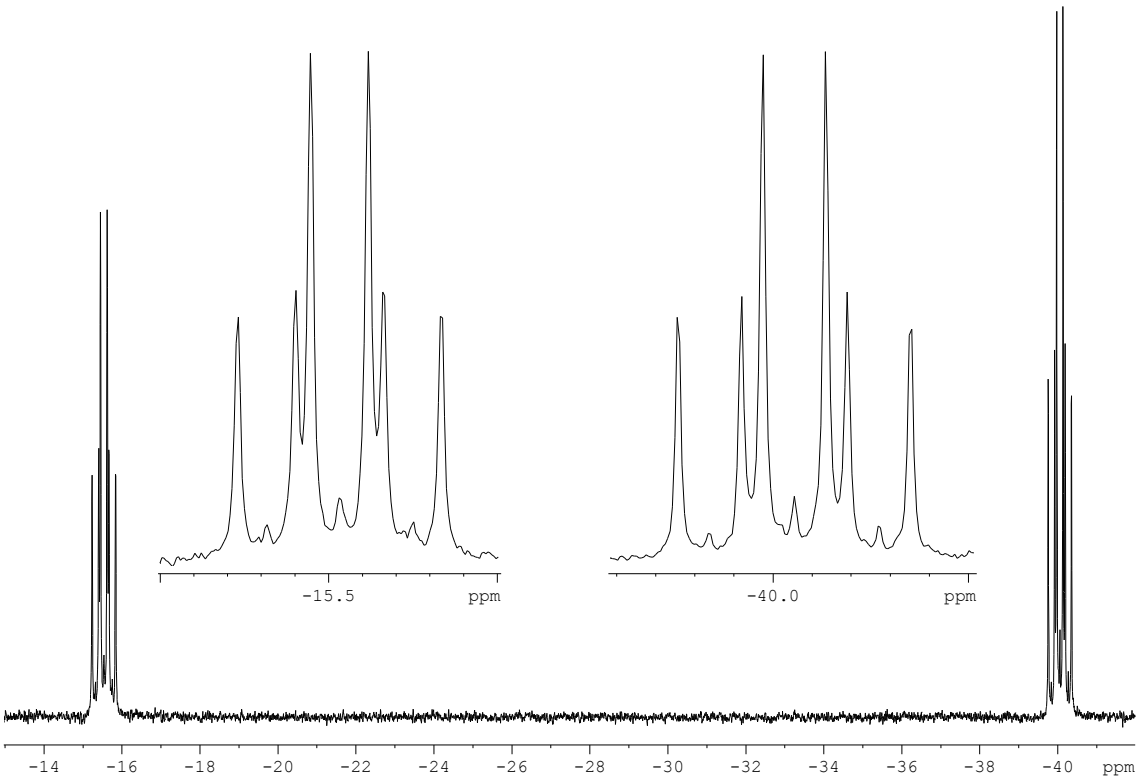

Figure 2.24 – $^{31}P\{^{1}H\}$ NMR spectrum of $[^{57}Fe(L^{1})(CO)_2]SO_4$ in D_2O at 162 MHz.

NRVS spectra of solid samples of ^{57}Fe analogues of **1** and **9** were recorded in collaboration with Prof. Cramer and coworkers. **Figure 2.25** shows the NRVS spectrum of $[^{57}Fe(L^{1})(H_2O)_2]SO_4$ (red) compared to other iron-phosphine complexes (blue and black). As NRVS is a relatively new technique, the exact position of iron-aqua vibrational modes is not known. In the NRVS spectra of $[^{57}Fe(edt)(CO)_2(dppv)]$ (blue) and $[^{57}Fe(edt)(CO)_2(PMe_3)_2]$ (black) (where edt = $^{-}S(CH_2)_2S^{-}$, dppv = *cis*-$Ph_2HC{=}CHPPh_2$) (measured in collaboration with Prof. Rauchfuss and coworkers), the peaks between 450 and 650 cm^{-1} are mainly contributions from the Fe-CO stretching and bending modes, which are clearly not visible in the spectrum of $[^{57}Fe(L^{1})(H_2O)_2]SO_4$. Preliminary DFT simulations of the NRVS spectra of Hmd carried out by Prof. Cramer and coworkers indicated that the proposed Fe-OH_2 peaks should occur around 380 cm^{-1}.

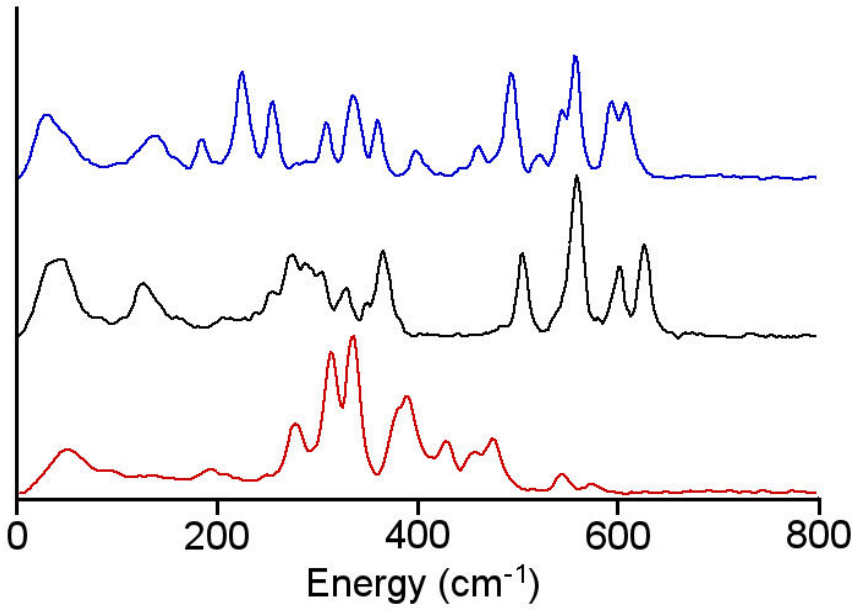

Figure 2.25 – NRVS spectra of [^{57}Fe(L^{1})(H$_2$O)$_2$]SO$_4$ (red) in comparison with spectra of [^{57}Fe(edt)(CO)$_2$(PMe$_3$)$_2$] (black) and [^{57}Fe(edt)(CO)$_2$(dppv)] (blue).

The NRVS spectrum of [^{57}Fe(L^{1})(CO)$_2$]SO$_4$ appears very different to the spectrum of [^{57}Fe(L^{1})(H$_2$O)$_2$]SO$_4$ (**Figure 2.26**). The peaks between 450 and 620 cm^{-1} are believed to be a result of Fe-CO stretching and bending motions, which are clearly absent in the NRVS spectrum of [^{57}Fe(L^{1})(H$_2$O)$_2$]SO$_4$. The other Fe carbonyl complexes in **Figure 2.25** also exhibit a number of peaks in this region, as would be expected.

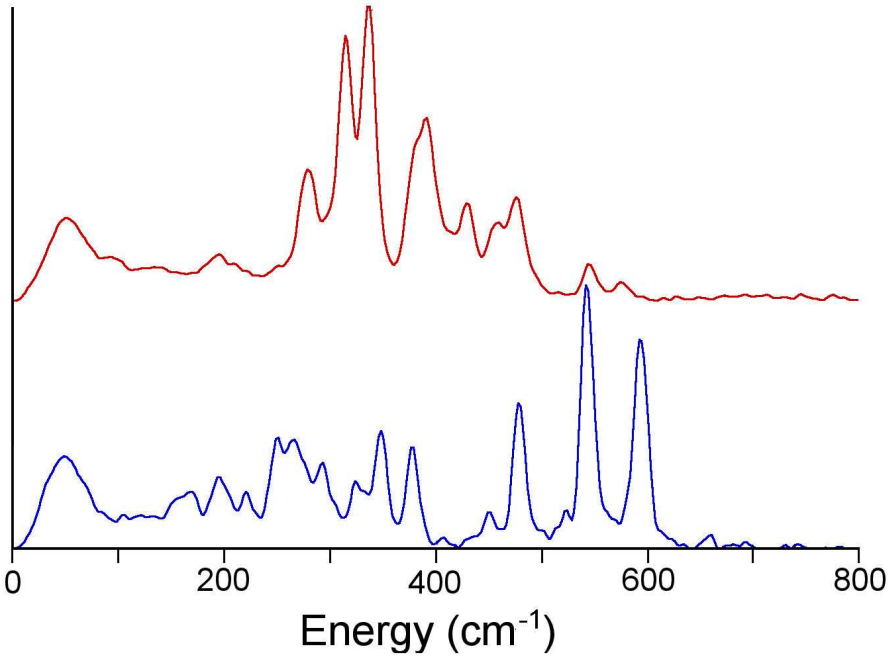

Figure 2.26 - NRVS spectra of [^{57}Fe(L^{1})(CO)$_2$]SO$_4$ (blue) in comparison with [^{57}Fe(L^{1})(H$_2$O)$_2$]SO$_4$ (red).

Further simulations carried out by Prof. Cramer and coworkers suggested that the largest peaks at 312 and 336 cm^{-1} in the NRVS spectrum of ^{57}Fe labelled **1** are the symmetric and asymmetric Fe-OH_2 stretching vibrations. To test this theory, the $^{18}OH_2$ labelled version of the complex was synthesised, to determine whether the peaks at 312 and 336 cm^{-1} were shifted upon exchange of the $^{16}OH_2$ for the $^{18}OH_2$ ligands. In order to prepare the $^{18}OH_2$ labelled product, $[^{57}Fe(L^1)(H_2O)_2]SO_4$ was recrystallised from >95% $^{18}OH_2$ to give $[^{57}Fe(L^1)(^{18}OH_2)_2]SO_4$. The exchange of the $^{16}OH_2$ for the $^{18}OH_2$ ligands could not easily be confirmed by traditional characterisation methods. NMR spectroscopy would not be able to distinguish the difference as both ^{16}O and ^{18}O have nuclear spins of zero. Mass spectrometry should theoretically determine if the substitution had taken place as long as the $^{18}OH_2$ sample was run in $^{18}OH_2$ to prevent exchange post-synthesis. However, this does not work as the electrospray mass spectrum of $[Fe(L^1)(H_2O)_2]SO_4$ **1** shows the main peak at *m/z* = 574.99, corresponding to the molecular ion $[[Fe(L^1)(SO_4)] + H]^+$, where the sulfate anion has coordinated to the metal by displacing the coordinated aqua ligands. This prevents the technique from being useful in determining whether the substitution had taken place.

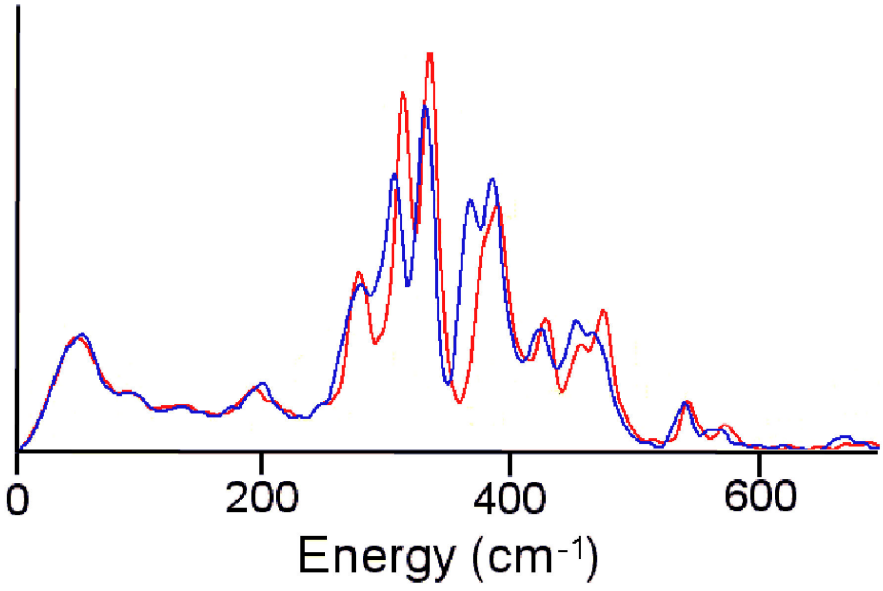

Figure 2.27 – NRVS spectra of $[^{57}Fe(L^1)(H_2O)_2]SO_4$ (red) in comparison with the $^{18}OH_2$ labelled version $[^{57}Fe(L^1)(^{18}OH_2)_2]SO_4$ (blue).

The NRVS spectrum of $[^{57}Fe(L^1)(^{18}OH_2)_2]SO_4$ compared to the non-$^{18}OH_2$ labelled version (**Figure 2.27**) unexpectedly shows that all the peaks between 300 and 600 cm^{-1} have been shifted as a result of the substitution. The reason for the shift of all the peaks in this region is hard to determine. It could be that the OH groups on the ligand have been exchanged with ^{18}OH groups as a result of the recrystallisation. Ultimately it

is difficult to determine with absolute certainty that the features at 312 and 336 cm^{-1} are those related to the Fe-OH_2 vibrational modes.

2.14 Functionalisation of the hydroxymethyl groups on 1 to give the acylated sulfato complex [Fe(L^2)(κ^2-O_2SO_2)] (13)

In order to explore the reactivity of the hydroxymethyl groups on **1**, reactions were carried out in order to convert them into different functionalities. Functionalised derivatives of complex **1** could also potentially exhibit different solubilities from **1**, which could allow the comparison of the different complexes in a range of solvents.

Complex **1** reacted with acetic anhydride upon heating to 100°C to give [Fe(L^2)(κ^2-O_2SO_2)] (**13**), in which all six hydroxymethyl groups have been acylated **(Scheme 2.7)**.

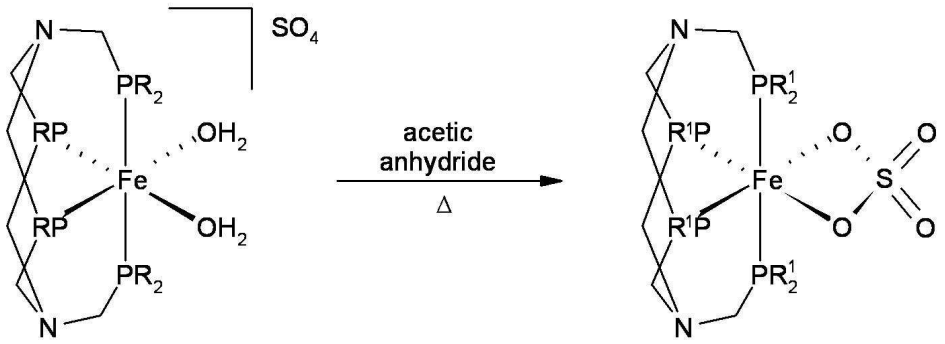

1
(R = CH_2OH)

13
(R^1 = $CH_2OC(O)Me$)

Scheme 2.7 – Reaction of 1 with acetic anhydride affords the acylated sulfato complex [Fe(L^2)(κ^2-O_2SO_2)] (13).

Complex **13** was isolated by reducing the volume of acetic anhydride solvent under reduced pressure followed by precipitation of the crude product with Et_2O. Washing with further diethyl ether and recrystallising from CH_2Cl_2/Et_2O yielded the purified product **13**. As expected, complex **13** is more soluble in organic solvents (such as acetone, chloroform, and dichloromethane) than its parent complex **1** (which is insoluble in these solvents).

The $^{31}P\{^1H\}$ NMR spectrum of **13** in $CDCl_3$ showed the expected pair of triplet resonances at δ 15.3 and 0.9 ($^2J_{P\text{-}P}$ = 50.5 Hz). The ^1H NMR spectrum showed the appearance of two singlets at δ 2.2 and 2.1 with a 2:1 integral ratio corresponding to the four methyl groups on the axial phosphine pendant arms and two methyl groups on the equatorial phosphines, as can be seen in the diagram of L^2 (**Figure 2.28**). Similar

to the homo-substituted complexes of the L^1 ligand (**1**, **2**, **3**-**9**), the methylene proton resonances in the ^1H NMR spectrum occur in four separate environments in an 8:8:4:4 ratio. These consist of eight CH_2 protons on the four axial pendant $CH_2OC(O)Me$ arms (♦), four on the two equatorial pendant arms (●), four on the two CH_2 groups linking between the axial phosphorus atoms and the nitrogen atoms (■), and eight on the four CH_2 groups in the eight-membered ring (▲). As in complexes **1**, **2**, **3**-**9** the methylene protons in the eight-membered ring (▲) have chemically inequivalent *exo*- and *endo*-protons giving an AB system at δ 4.87 ($^2J_{H-H}$ = 12.3 Hz, Δδ = 34.68 Hz). The two pendant equatorial $C\underline{H}_2OC(O)Me$ methylene groups (●) give rise to broad a singlet at δ 4.74, suggesting both CH_2 protons are equivalent due to their ability to rotate freely about the P-C bond. However, the four axial $C\underline{H}_2OC(O)Me$ methylene groups (♦) give a broad AB system centred at δ 3.38 (Δδ = 42.18 Hz), though the peaks were too broad to measure the $^2J_{H-H}$ coupling constant. It is therefore likely that these axial pendant arms cannot rotate about the P-C bond due to steric effects, causing both methylene protons to be chemically inequivalent. The remaining two methylene groups linking the nitrogen atoms of the eight-membered ring to the axial phosphines (■) give a broad singlet at δ 4.74.

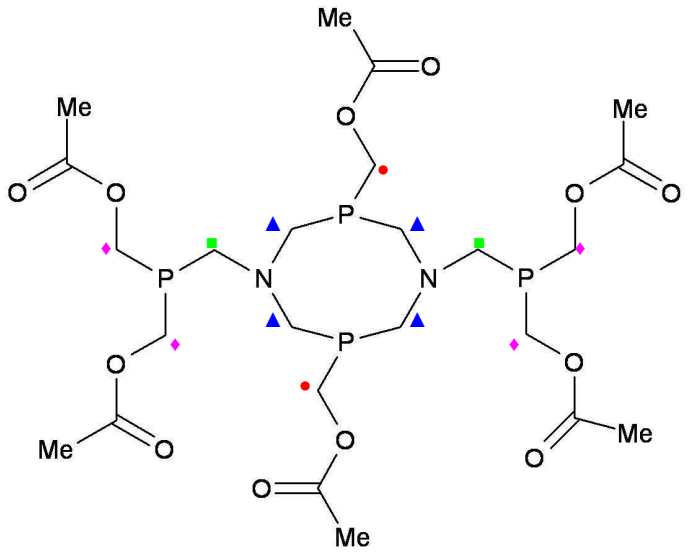

Figure 2.28 – Diagram of the acylated ligand L^2.

Perhaps surprisingly, **13** is also more soluble in water than **1**. One potential explanation is that the large degree of hydrogen bonding from the hydroxyl groups in complex **1** in the solid state is reduced upon conversion to methyl ester groups, therefore increasing the solubility of **13** in aqueous solution. However, the $^{31}P\{^1H\}$ NMR spectrum of **13** in D_2O showed that the main resonances in the spectrum (*ca.* 70% of the total material by integration) were two very broad triplet resonances at δ 17.3 and 0.8. The broadness indicates that the coordinated sulfate ligand is most likely exchanging with solvent D_2O molecules, affording $[Fe(L^2)(D_2O)_2]SO_4$ in solution. The

remaining peaks in the $^{31}P\{^{1}H\}$ NMR spectrum consisted of a number of triplets and multiplets which could not be easily indentified, suggesting that other reactions are occurring upon the solution of **13** in water. Attempts to isolate the di-aqua complex $[Fe(L^2)(H_2O)_2]SO_4$ from aqueous solution proved unsuccessful.

2.15 X-ray structure of $[Fe(L^2)(\kappa^2\text{-}O_2SO_2)]\cdot 1.3(CH_3)_2CO$ ($13\cdot 1.3(CH_3)_2CO$)

Red crystals of $[Fe(L^2)(\kappa^2\text{-}O_2SO_2)]\cdot 1.3(CH_3)_2CO$ (**13**$\cdot 1.3(CH_3)_2CO$) were grown upon layering an acetone solution with hexane. The X-ray structure (**Figure 2.29**) shows that all six hydroxyl groups have been functionalised to give methyl ester functionalities. The ligand structure itself otherwise remains intact and coordinates to the iron in a similar manner to the L^1 ligand in complexes **1** to **12**. Additionally, the sufate anion has coordinated to the iron centre, displacing the two water molecules to give an overall neutral complex. The presence of the acyl groups in place of the hydroxyl groups has little effect on the coordination sphere of the complex, with the bond angles and bond lengths remaining largely similar (**Table 2.7**). The absence of the hydroxymethyl groups in **13** means that there are no strong hydrogen bond donors, and as a result, the structure contains no strong intermolecular interactions. Instead, the supramolecular structure is dominated by C-H···O hydrogen bonds where the ester carbonyl moieties act as the hydrogen bond acceptors.

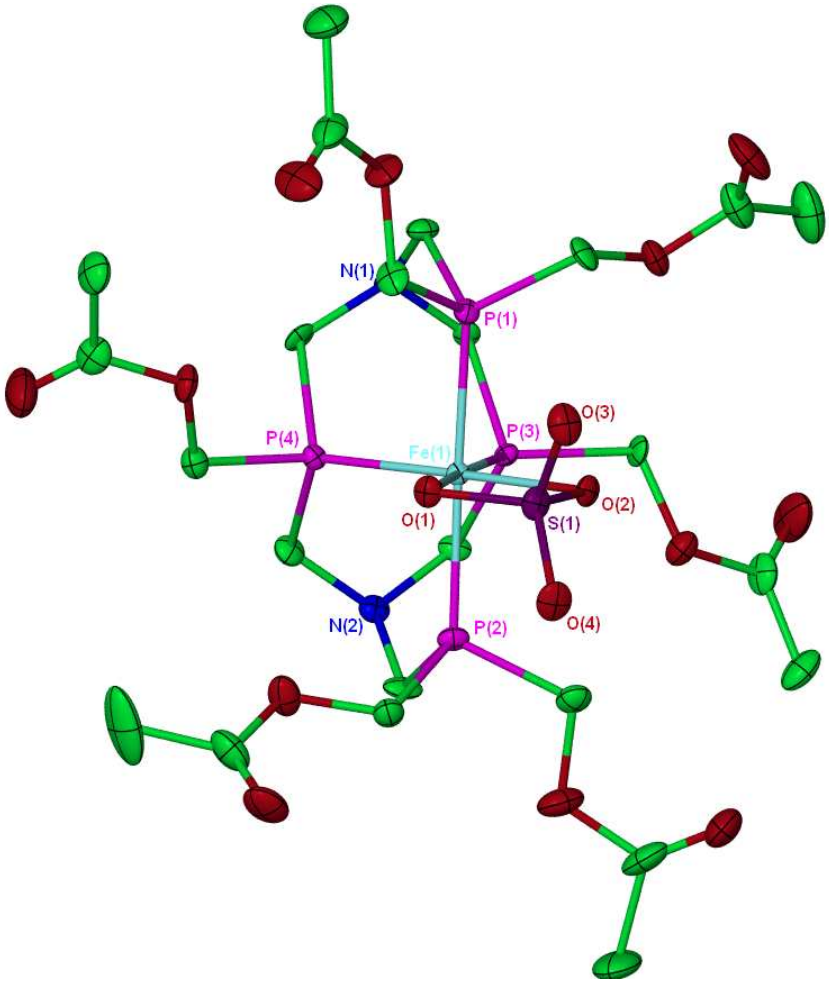

Figure 2.29 - Molecular structure of $[Fe(L^2)(\kappa^2\text{-}O_2SO_2)]\cdot 1.3(CH_3)_2CO$ ($13\cdot 1.3(CH_3)_2CO$). Thermal ellipsoids are at the 30% probability level. The included acetone molecule and hydrogen atoms have been omitted for clarity.

Bond Lengths

Fe(1)-P(1)	2.2256(16)	Fe(1)-O(2)	2.046(4)
Fe(1)-P(2)	2.2362(16)	S(1)-O(1)	1.513(5)
Fe(1)-P(3)	2.1803(17)	S(1)-O(2)	1.523(5)
Fe(1)-P(4)	2.1776(17)	S(1)-O(3)	1.463(5)
Fe(1)-O(1)	2.047(4)	S(1)-O(4)	1.451(5)

Bond Angles

P(1)-Fe(1)-P(2)	174.54(6)	O(3)-S(1)-O(1)	110.2(3)
O(1)-Fe(1)-P(3)	174.07(15)	O(4)-S(1)-O(1)	111.1(3)
O(2)-Fe(1)-P(4)	175.33(14)	O(3)-S(1)-O(2)	111.4(3)
O(2)-Fe(1)-O(1)	69.74(15)	O(4)-S(1)-O(2)	111.5(3)
P(3)-Fe(1)-P(4)	80.32(5)	O(4)-S(1)-O(3)	111.3(3)
O(1)-S(1)-O(2)	100.87(19)		

Table 2.7 – Selected bond lengths (Å) and angles (°) for complex $13\cdot 1.3(CH_3)_2CO$.

2.16 Reaction of $[Fe(L^1)(H_2O)_2]SO_4$ (1) with glycine

Following on from the reaction of **1** with acetic anhydride to afford the acylated complex **13**, further chemistry to functionalise the hydroxyl groups was explored. It has previously been reported that PCH_2OH groups can be converted into PCH_2NHR groups *via* a Mannich-type condensation reaction, and that this is a good method of introducing water-soluble carboxylate groups (**Scheme 2.10**).[39-42]

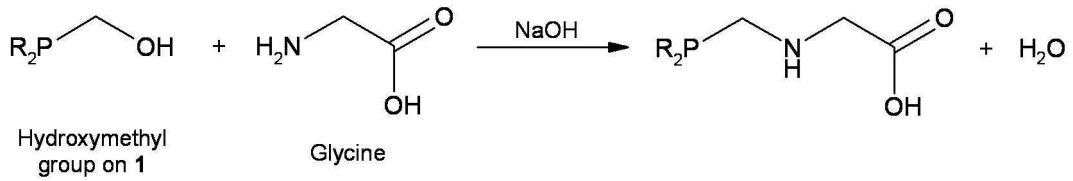

Scheme 2.8 – Proposed functionalisation of the hydroxyl groups on 1 in order to introduce carboxylate functionalities.

When an aqueous solution of **1** was heated at reflux with an excess of glycine, however, the above reaction to functionalise the CH_2OH groups did not occur. Instead, the deprotonated glycine coordinated to the iron metal as an N,O-bidentate ligand, resulting in the formation of the cationic complex $[Fe(L^1)(H_2NCH_2CO_2\text{-}\kappa^2\textit{N,O})]^+$ (**14**) (**Scheme 2.9**). The anion of the complex has not been unambiguously characterised, though it is possible that the sulfate anion has been protonated in solution to give the HSO_4^+ cation. The microanalysis fits this conclusion, though it is also theoretically possible that there is simply a ratio of two complex cations to one SO_4^{2-} anion.

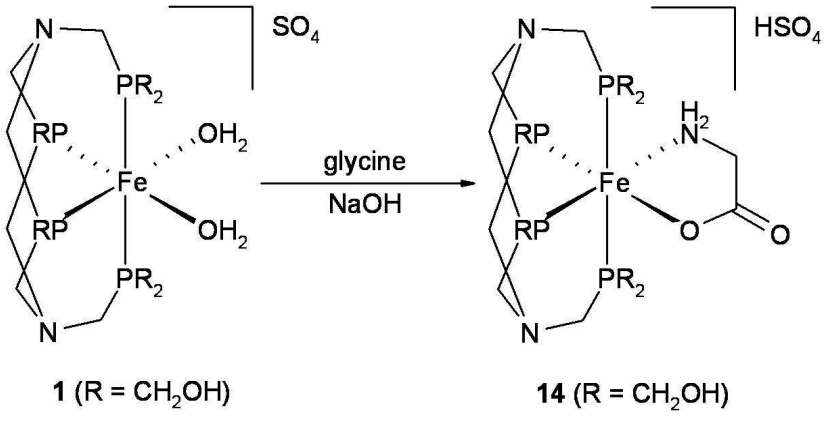

Scheme 2.9 – Reaction of 1 with glycine to give the N,O-coordinated glycinato complex 14.

The $^{31}P\{^1H\}$ NMR spectrum of **14** in D_2O showed a doublet of doublets at δ 3.5 ($^2J_{P\text{-}P}$ = 77, 51 Hz) and two sets of doublets of triplets at δ 19.7 ($^2J_{P\text{-}P}$ = 76, 51 Hz) and δ 7.2

($^2J_{P\text{-}P}$ = 76, 77 Hz). These resonances are of the A_2MX pattern similar to those observed for all of the asymmetrically substituted variants of **1**, such as **10**, **11**, and **12**. This is consistent with the proposed cationic structure of **14**. It is likely that the hydroxyl groups cannot be functionalised by this method because the phosphines are coordinated to the metal. The reason why uncomplexed hydroxymethylphosphines can be functionalised is due to the availability of the phosphine lone pair and the presence of catalytic amounts of formaldehyde (**Scheme 2.10**). These are both believed to be fundamental requirements for the Mannich-type reaction of hydroxymethylphosphines with primary amines.

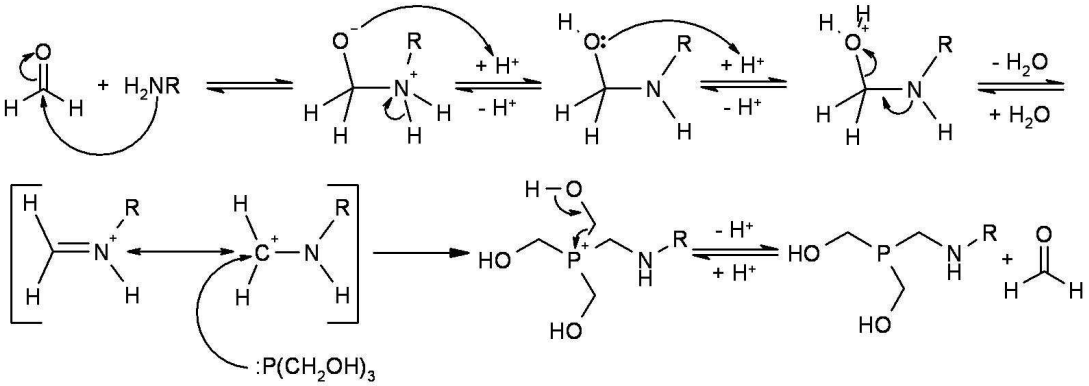

Scheme 2.10 – Mannich-type condensation reaction of a hydroxylmethylphosphine with a primary amine and formaldehyde.

The above mechanism shows the role of formaldehyde and the lone pair of the phosphorus in the reaction of a hydroxymethylphosphine with a primary amine. The formaldehyde is needed for the initial nucleophilic attack of the amine, to eventually form the carbenium cation *via* loss of H_2O. The lone pair of the phosphine attacks the positively charged carbon atom of the carbenium ion to give the substituted phosphonium cation. The addition of base to the phosphonium cation leads to the substituted phosphine and the elimination of a molecule of formaldehyde, hence the formaldehyde acts as a catalyst. This is in contrast to the functionalisation of **1** with acetic anhydride, which is a direct reaction of the hydroxyl groups with the anhydride to form the ester.

2.17 Synthesis of the dichloride complex $[Fe(L^2)Cl_2]$ (15) from $[Fe(L^2)(\kappa^2\text{-}O_2SO_2)]$ (13)

In order to investigate the coordination chemistry of **13** and compare it with that of the parent complex **1**, reactions of **13** were carried out with a variety of neutral and anionic ligands. Complex **13** differs from **1** not only in that it has a less polar acylated ligand backbone, but also because it possesses a coordinated chelating sulfate ligand giving a neutral complex. The chemistry of **13** can therefore be investigated in organic solvents. The coordinated sulfate anion on **13** can be substituted by reaction with [PPN]Cl (PPN = bis(triphenylphosphoranylidene)ammonium) in dichloromethane to give a purple solution of the dichloride species $[Fe(L^2)Cl_2]$ (**15**) (**Scheme 2.11**).

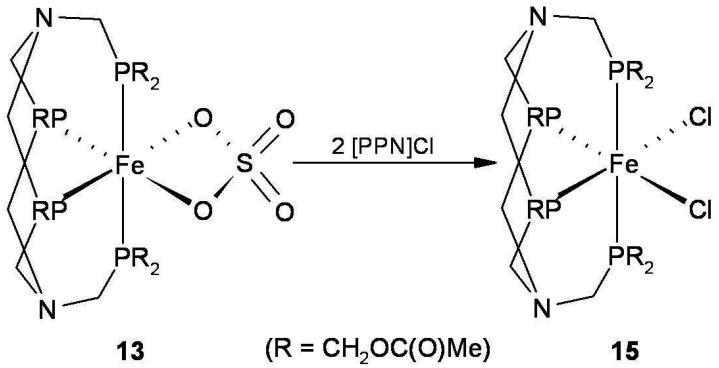

Scheme 2.11 – Reaction of 13 with [PPN]Cl to give the dichloro complex $[Fe(L^2)Cl_2]$ (15).

The $^{31}P\{^1H\}$ NMR spectrum of **15** showed the expected pair of triplets, shifted to δ 16.5 and δ -1.6 ($^2J_{P\text{-}P}$ = 59 Hz), suggesting the formation of the di-substituted product. In contrast to the reaction of **1** with chloride, there is no equilibrium between **13** and **15**, and **15** can be isolated by the addition of diethyl ether to the dichloromethane solution.

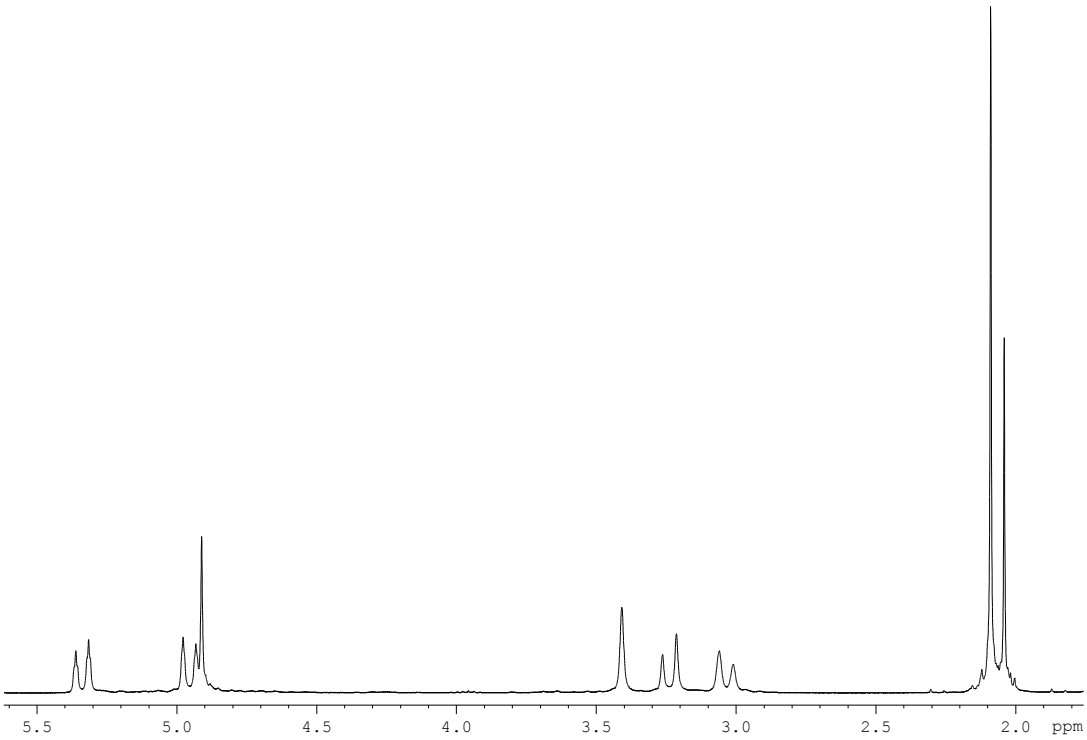

Figure 2.30 – ^{1}H NMR spectrum of [Fe(L^2)Cl_2] (15) in $CDCl_3$ at 300 MHz.

The ^{1}H NMR spectrum of **15** (**Figure 2.30**) shows a very similar spectrum to that of complex **13**, though the resonances are better resolved. The two singlets at *ca.* δ 2.1 corresponding to the two CH_3 environments of the methyl ester groups can clearly be seen. The methyene protons again occur in four different environments, with the CH_2 protons in the eight-membered ring and on the axial pendant C$\underline{H}_2$OC(O)Me groups giving AB systems at δ 5.18 ($^{2}J_{HH}$ =13.6 Hz, $\Delta\delta$ = 149.81 Hz) and δ 3.18 ($^{2}J_{HH}$ =14.9 Hz, $\Delta\ \delta$ = 86.15 Hz), respectively. The CH_2 groups linking the nitrogen atoms on the eight-membered ring to the axial phosphines appear as a singlet at δ 4.95, whereas the equatorial C$\underline{H}_2$OC(O)Me groups give a singlet at δ 3.46.

2.18 X-ray structure of [Fe(L^2)Cl_2] (15)

Crystals of [Fe(L^2)Cl_2] (**15**) were grown from the slow diffusion of hexane into a purple acetone solution. The X-ray structural analysis shows that the coordinated chelating sulfate anion has been replaced with two chloride ligands (**Figure 2.31**), as predicted by NMR spectroscopy. The Fe-Cl bond lengths in **15** are shorter (2.371(2) and 2.351(5)Å) than those in the corresponding L^1 complex **3** (2.4006(4) and 2.4001(4) Å) (**Table 2.8**). This could be due to the chloride anions in complex **3** acting as hydrogen bonding acceptors.

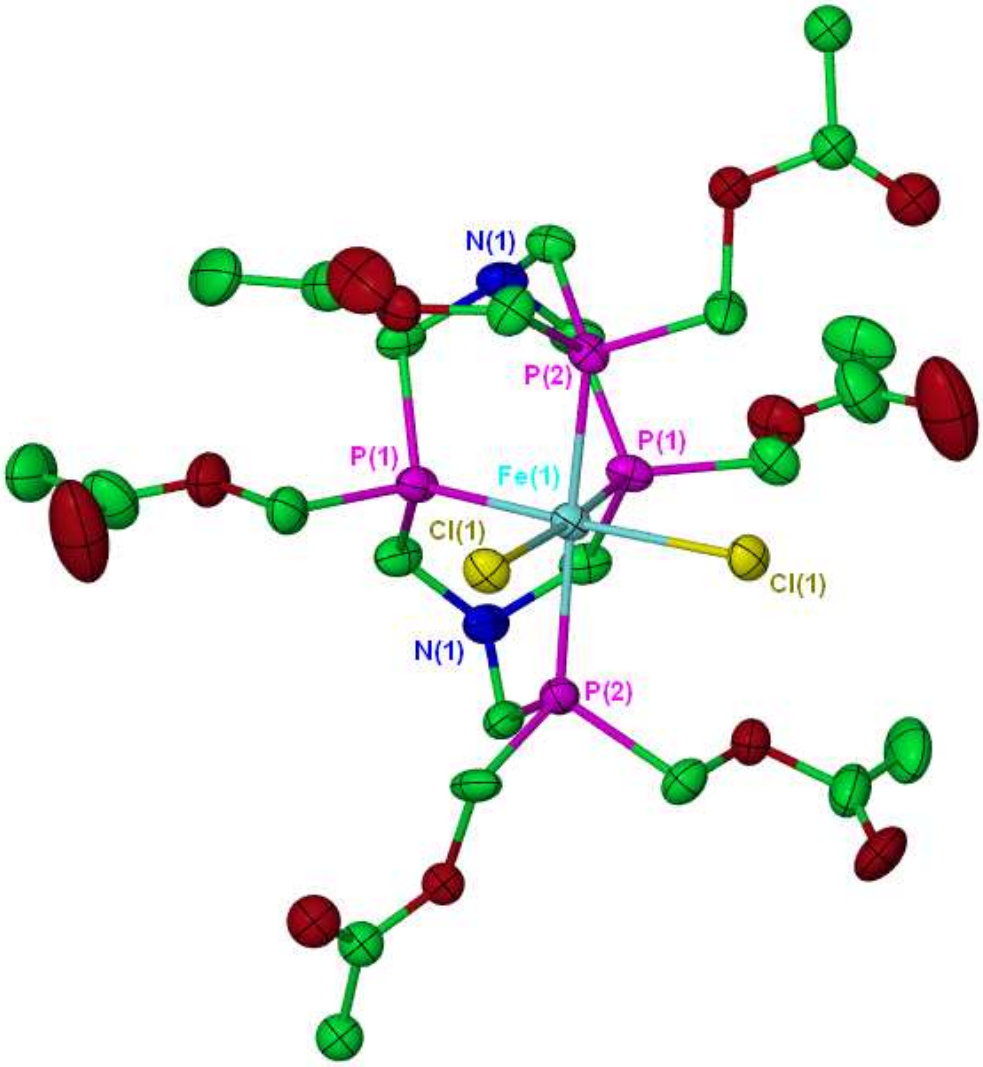

Figure 2.31 - Molecular structure of [Fe(L^2)Cl_2] (15) showing molecule 1 of two independent half-molecules in the asymmetric unit. Thermal ellipsoids are at the 30% probability level. Hydrogen atoms have been omitted for clarity.

Bond Lengths

Fe(1)-P(1)	2.164(2)	Fe(2)-P(3)	2.219(2)
Fe(1)-P(2)	2.2305(18)	Fe(2)-P(5)	2.161(2)
Fe(1)-Cl(1)	2.371(2)	Fe(2)-Cl(2)	2.351(5)

Bond Angles

P(2)-Fe(1)-P(2)'	173.97(14)	P(3)-Fe(2)-P(3)'	174.25(16)
P(1)-Fe(1)-Cl(1)'	173.89(10)	P(5)-Fe(2)-Cl(2)'	174.75(10)
Cl(1)-Fe(1)-Cl(1)'	92.65(12)	Cl(2)-Fe(2)-Cl(2)'	91.17(13)
P(1)-Fe(1)-P(1)'	80.44(13)	P(5)-Fe(2)-P(5)'	80.67(13)

Table 2.8 – Selected bond lengths (Å) and angles (°) for complex 15 (molecules 1 and 2).

2.19 Reaction of [Fe(L^2)(κ^2-O_2SO_2)] (13) with CO

Despite the broad resonances observed in the $^{31}P\{^1H\}$ NMR spectrum of [Fe(L^2)(κ^2-O_2SO_2)] **13** in D_2O, the reaction of **13** with CO in aqueous solution was carried out. The red aqueous solution took on a yellow colouration (similar to the reaction of **1** with CO) after stirring under an atmosphere of CO for two hours. Surprisingly, the $^{31}P\{^1H\}$ NMR spectrum in D_2O (**Figure 2.32**) showed a relatively clean spectrum with three sharp resonances coupling in an AMX_2 spin system; two doublets of triplets at δ 1.4 ($^2J_{P\text{-}P}$ = 37.7 Hz, $^2J_{P\text{-}P}$ = 71.3 Hz) and -31.6 ($^2J_{P\text{-}P}$ = 53.0 Hz, $^2J_{P\text{-}P}$ = 71.3 Hz) and a doublet of doublets at δ -3.5 ($^2J_{P\text{-}P}$ = 53.0 Hz, $^2J_{P\text{-}P}$ = 37.7 Hz). These resonances are reminiscent of the $^{31}P\{^1H\}$ NMR spectra of the mono-carbonyl complexes [Fe(L^1)(H_2O)(CO)]SO_4 (**10**) and [Fe(L^1)(CO)(κ^1-OSO_3)] (**11**) formed in the reaction of complex **1** with CO in aqueous solution. It is therefore likely that the complex formed in the reaction is another mono-carbonyl complex, either [Fe(L^2)(H_2O)(CO)]SO_4 (**16**) or [Fe(L^2)(CO)(κ^1-OSO_3)] (**17**). In agreement with this, the IR spectrum of the complex showed only one carbonyl stretching peak at 2001 cm^{-1}.

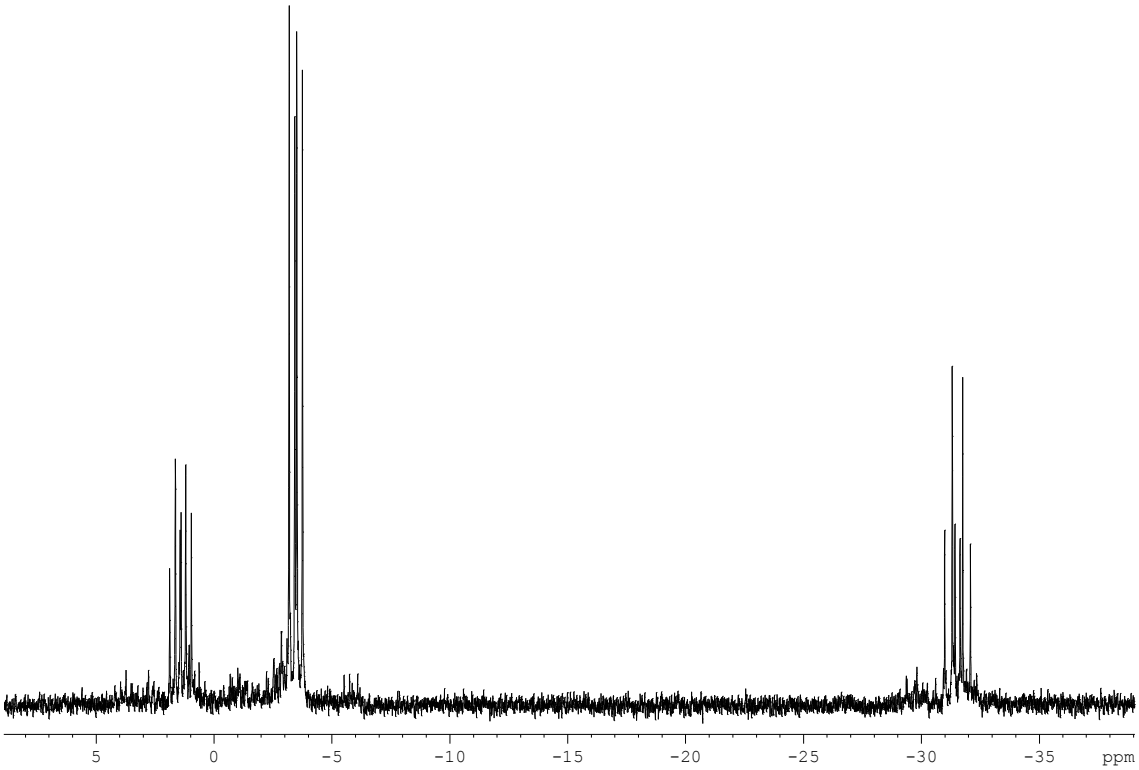

Figure 2.32 – $^{31}P\{^1H\}$ NMR spectrum of the reaction of [Fe(L^2)(κ^2-O_2SO_2)] (13) with CO in D_2O at 162 MHz.

When the solution was stirred under an atmosphere of CO for a further four days, another two doublets of triplets at δ 3.4 ($^2J_{P\text{-}P}$ = 39.4 Hz, $^2J_{P\text{-}P}$ = 72.8 Hz) and -29.6 ($^2J_{P\text{-}P}$ = 53.5 Hz, $^2J_{P\text{-}P}$ = 72.8 Hz) and a doublet of doublets at δ -2.3 ($^2J_{P\text{-}P}$ = 39.4 Hz, $^2J_{P\text{-}P}$ =

53.5 Hz) appeared in the $^{31}P\{^{1}H\}$ NMR spectrum, with the second set of resonances accounting for *ca*. 25% of the total material. The appearance of the second set of resonances suggests the conversion of one of the mono-carbonyl complexes (**16** or **17**) to the other, though it is difficult to determine which way round this reaction occurs. It is more likely, however, that the carbonyl sulfate complex **17** is initially formed, with the abundant solvent water molecules eventually replacing the coordinated sulfate ligand to give the carbonyl aqua complex **16**. Despite the prolonged exposure of the reaction to CO, no triplets relating to the di-carbonyl species $[Fe(L^2)(CO_2)]SO_4$ were observed.

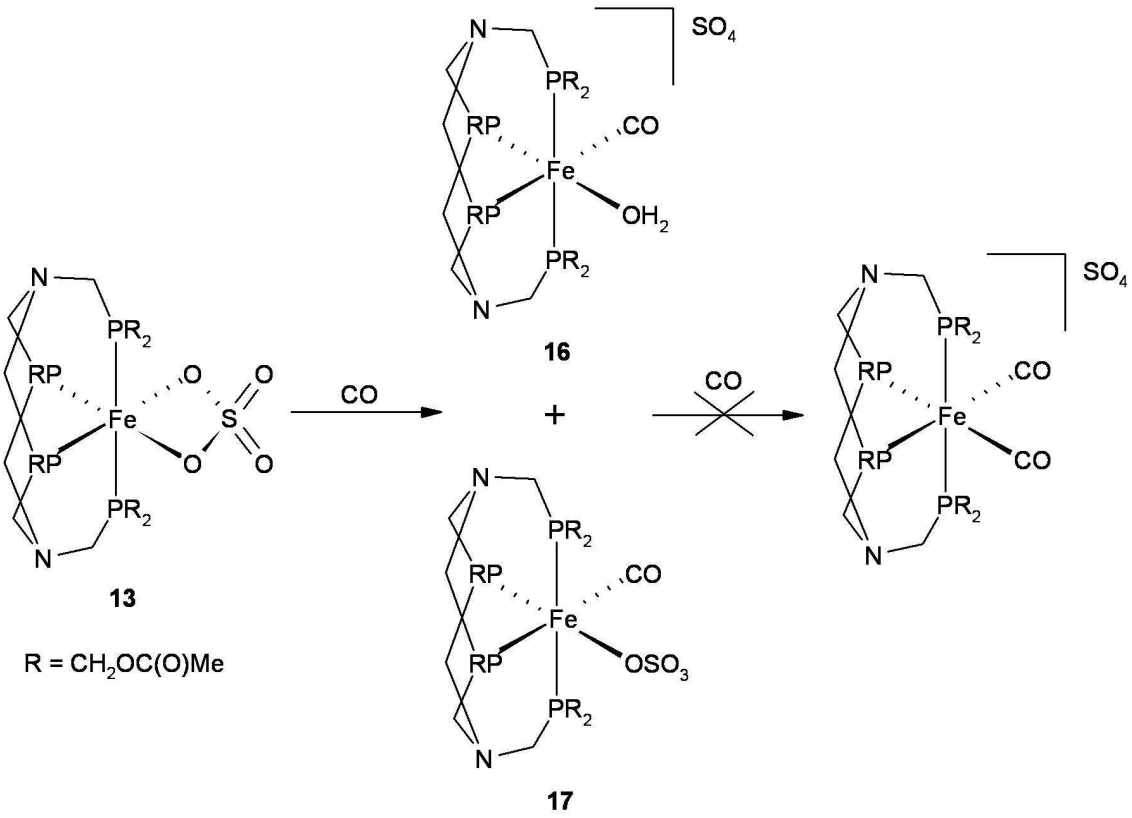

Scheme 2.12 – Reaction of $[Fe(L^2)(\kappa^2\text{-}O_2SO_2)]$ (13) with CO in H_2O.

The reaction was then repeated in acetonitrile in order to investigate the effect of solvent in the reaction. Firstly, the $^{31}P\{^{1}H\}$ NMR spectrum of **13** was recorded in CD_3CN in order to better understand the structural identity of **13** in acetonitrile solution. The $^{31}P\{^{1}H\}$ NMR spectrum indicated that the main species present (*ca.* 85% of the material by integration) was the mono-acetonitrile complex $[Fe(L^2)(CD_3CN)(\kappa^1\text{-}OSO_3)]$, represented by the familiar AMX_2 coupling pattern (two doublets of triplets at δ 8.0 and 5.2 and a doublet of doublets at δ -0.7). The remaining 15% of the material consisted of two triplet resonances representing the starting material $[Fe(L^2)(\kappa^2\text{-}O_2SO_2)]$ **13**.

Stirring the orange acetonitrile solution for twelve hours under an atmosphere of CO gave a yellow solution. The $^{31}P\{^{1}H\}$ NMR spectrum (CD_3CN) showed only one set of AMX_2 resonances, with the two doublets of triplet resonances occurring at δ -0.4 ($^{2}J_{P\text{-}P}$ = 37.9 Hz, $^{2}J_{P\text{-}P}$ = 66.8 Hz) and -30.0 ($^{2}J_{P\text{-}P}$ = 52.7 Hz, $^{2}J_{P\text{-}P}$ = 66.8 Hz) and the doublet of doublets at δ -3.9 ($^{2}J_{P\text{-}P}$ = 52.7 Hz, $^{2}J_{P\text{-}P}$ = 37.9 Hz). This indicates that only one mono-carbonyl complex has formed in the reaction, either $[Fe(L^2)(CO)(CD_3CN)]SO_4$ (**18**) or $[Fe(L^2)(CO)(\kappa^1\text{-}OSO_3)]$ (**17**). As the $^{2}J_{P\text{-}P}$ coupling constants of this set of resonances are different from those of **16** and **17**, it is therefore likely that the complex formed in the reaction is $[Fe(L^2)(CO)(CD_3CN)]SO_4$ (**18**). The *cis* $^{2}J_{P\text{-}P}$ coupling constants are especially notably different, with those of **16** and **17** being 71.3 and 72.8 Hz, while the *cis* $^{2}J_{P\text{-}P}$ coupling constant of **18** is 66.8 Hz. This is also likely considering that the initial $^{31}P\{^{1}H\}$ NMR spectrum of **13** in CD_3CN showed that the majority of the material was $[Fe(L^2)(CD_3CN)(\kappa^1\text{-}OSO_3)]$, with the monodentate sulfate ligand far more likely to be displaced by the carbonyl ligand than the coordinated solvent acetonitrile molecule. Stirring the reaction solution for a further three days under an atmosphere of CO led to no further change in the $^{31}P\{^{1}H\}$ NMR spectrum and none of the di-carbonyl complex was formed.

2.20 Reaction of $[Fe(L^2)Cl_2]$ (15) with CO

The chloride ligands in complex **15** can be readily substituted with a variety of other groups to give mono- and di-substituted $Fe(L^2)$ species. The dichloride complex **15** also proved to be a better starting material than the coordinated sulfate complex **13**, with fewer complications due to the ability of the sulfate ligand to act as a bidentate or monodentate ligand as well as a counter ion. The reaction of a dichloromethane solution of **15** with CO gave the asymmetrically substituted complex $[Fe(L^2)(CO)Cl]Cl$ **19a** (**Scheme 2.13**).

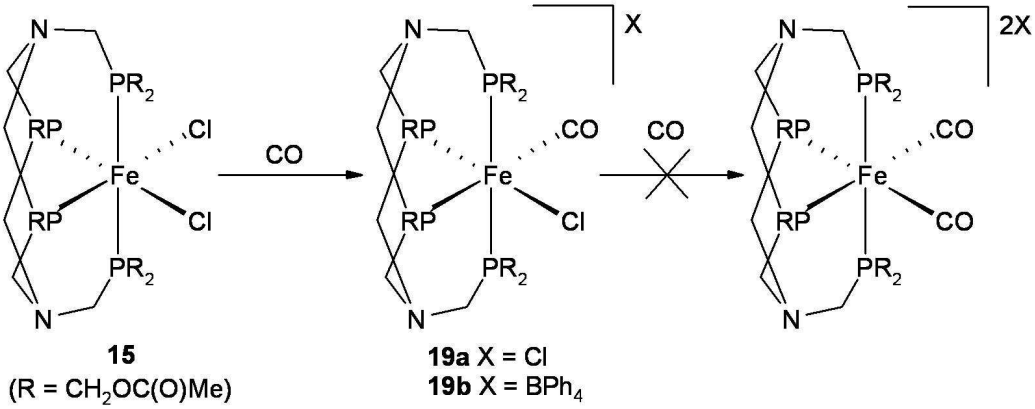

15
(R = $CH_2OC(O)Me$)

19a X = Cl
19b X = BPh_4

Scheme 2.13 – Reaction of $[Fe(L^2)Cl_2]$ (15) with CO.

The $^{31}P\{^{1}H\}$ NMR spectrum of **19a** (**Figure 2.33**) shows the expected A_2MX coupling pattern with a doublet of triplets at δ -6.4 ($^{2}J_{P\text{-}P}$ = 66, 40 Hz), a doublet of doublets at δ -11.8 ($^{2}J_{P\text{-}P}$ = 55, 40 Hz), and a doublet of triplets at δ -35.7 ($^{2}J_{P\text{-}P}$ = 66, 55 Hz). Exposure to further CO did not result in the formation of the dicarbonyl $[Fe(L^2)(CO)_2]^{2+}$ cation. Attempts to isolate **19a** as a solid resulted in the reformation and crystallisation of **15** *via* the loss of the coordinated CO molecule. However, when the reaction was carried out in the presence of sodium tetraphenylborate in acetone, sodium chloride was precipitated and removed as a white solid, leaving the tetraphenylborate salt $[Fe(L^2)(CO)Cl]BPh_4$ **19b** in solution.

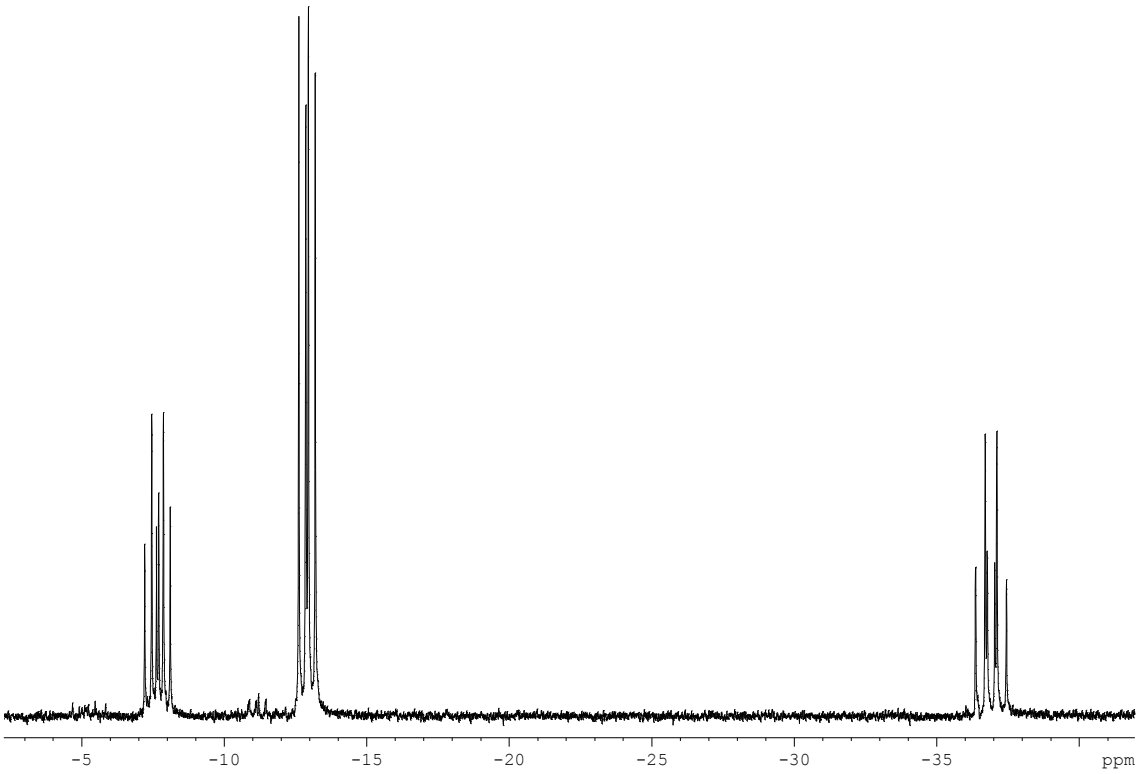

Figure 2.33 - $^{31}P\{^{1}H\}$ NMR spectrum of $[Fe(L^2)(CO)Cl]BPh_4$ (19b) in $CDCl_3$ at 162 MHz.

The $^{31}P\{^{1}H\}$ NMR spectrum of **19b** is identical to that of **19a**, confirming the presence of the same $[Fe(L^2)(CO)Cl]^{+}$ cation. The addition of diethyl ether to a dichloromethane solution led to the precipitation of **19b** as a yellow solid.

2.21 Reaction of $[Fe(L^2)Cl_2]$ (15) with pseudo-halides

The dichloride complex **15** reacted with KNCS or NaN_3 to form the disubstituted thiocyanato or azido complexes **20** or **21**, respectively (**Scheme 2.14**).

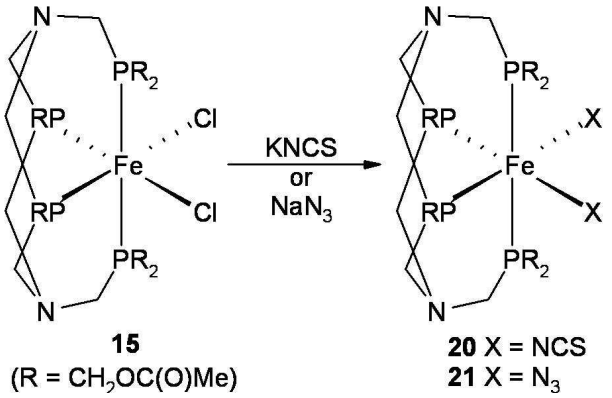

15 (R = $CH_2OC(O)Me$) **20** X = NCS **21** X = N_3

Scheme 2.14 – Reaction of 15 with thiocyanate and azide.

The reaction of **15** with two equivalents of potassium thiocyanate was carried out in a water/acetone mixture, affording an orange solution of $[Fe(L^2)(NCS)_2]$ (**20**). Slow evaporation of the acetone of the water/acetone mixture resulted in the formation of orange crystals of **20**. In contrast to the other L^2 complexes, **20** is sparsely soluble in most common solvents, but dissolves readily in DMSO. Surprisingly, the $^{31}P\{^1H\}$ NMR spectrum of **20** in d_6-DMSO showed a singlet resonance (at δ 4.1), instead of the expected pair of triplets associated with the A_2MX coupling pattern (**Figure 2.34**).

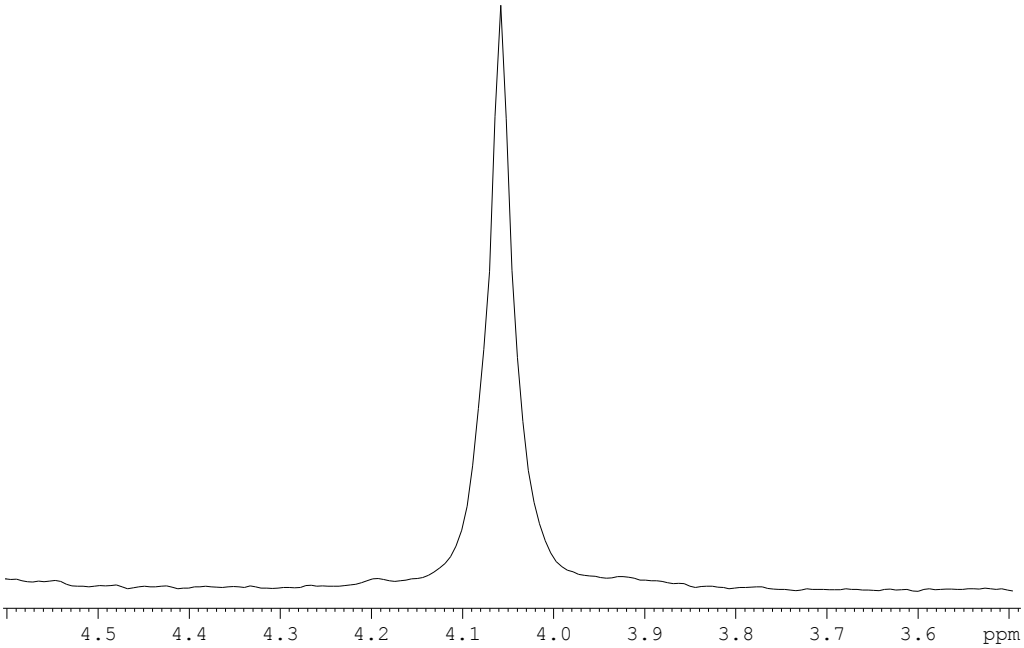

Figure 2.34 – $^{31}P\{^1H\}$ NMR spectrum of complex 20 in d_6-DMSO at 122 MHz.

However, the ^1H and $^{13}C\{^1H\}$ NMR spectra of **20** are consistent with all other complexes containing the L^2 ligand, suggesting it is intact and coordinated to the metal in the same manner. The appearance of **20** as a singlet in the $^{31}P\{^1H\}$ NMR spectrum is believed to be due to the coincidental occurrence of both phosphine resonances at the same chemical shift. The simulated $^{31}P\{^1H\}$ NMR spectrum of **20** with both

phosphine environments simulated at the same chemical shift also shows a singlet. The IR spectrum (KBr disc) revealed a single NCS stretching band at 2108 cm^{-1}. This is in contrast to $[Fe(L^1)(NCS)_2]$ (**6**), the IR spectrum of which shows both symmetric and asymmetric stretches (at 2098 and 2109 cm^{-1}). This suggests that the symmetric and asymmetric NCS stretches in **20** are very similar in energy.

Complex **15** also reacted with sodium azide in a water/acetone mixture in a similar manner to potassium thiocyanate to give a red solution of the bis(azido) complex $[Fe(L^2)(N_3)_2]$ **21**. The $^{31}P\{^1H\}$ NMR spectrum of **21** showed two second-order resonances at δ 10.0 and δ 8.6 (**Figure 2.35**). This is again due to the two phosphorus resonances occurring at similar chemical shifts and is field dependant. The simulated $^{31}P\{^1H\}$ NMR spectrum **21** matches the experimental data, affording a $^2J_{P\text{-}P}$ value of 57 Hz.

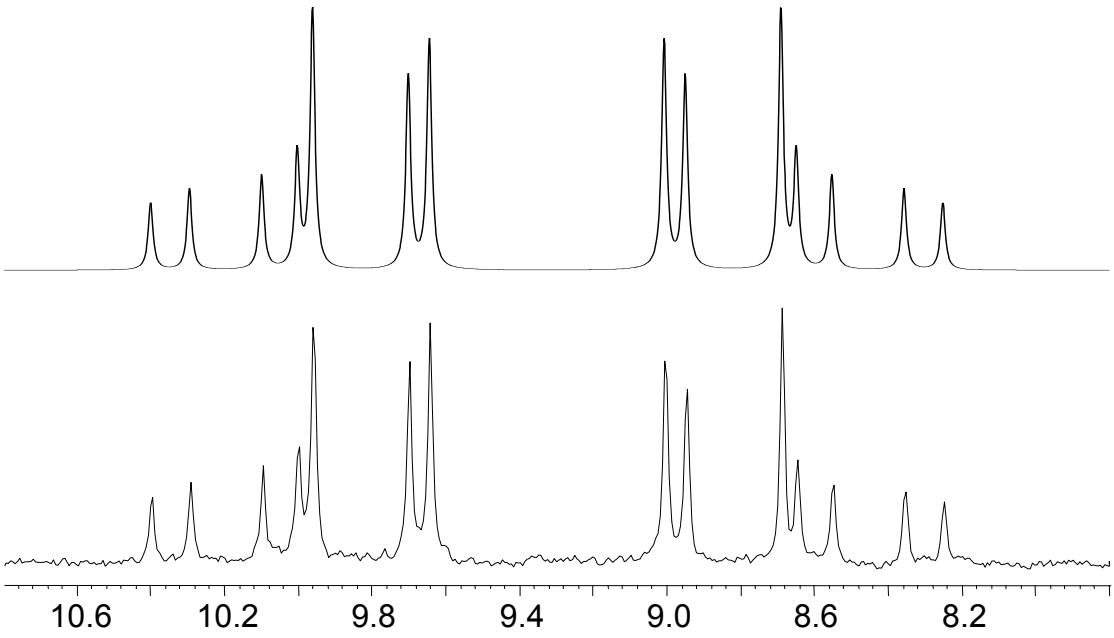

Figure 2.35 – Simulated (upper) and experimental (lower) $^{31}P\{^1H\}$ NMR spectra of $[Fe(L^2)(N_3)_2]$ (21) in d_6-acetone at 162 MHz.

2.22 X-ray structure of $[Fe(L^2)(N_3)_2]\cdot0.5H_2O$ ($21\cdot0.5H_2O$)

Orange crystals of $[Fe(L^2)(N_3)_2]\cdot0.5H_2O$ ($\mathbf{21}\cdot0.5H_2O$) suitable for X-ray analysis were isolated by slow evaporation of a water/acetone solution. The structure shows the two chloride ligands have been substituted with azide anions, without any alteration to the L^2 ligand (**Figure 2.36**). The asymmetric unit contains one half of an iron complex molecule. The Fe-N bond lengths in **21** are similar to those found in the related L^1 complex $[Fe(L^1)(N_3)_2]$ (**7**), suggesting that the electronic properties of both **21** and **7** are

comparable (**Table 2.9**). The Fe-P bond lengths in the structure of **21** are fairly similar to that of complex **7**. However, the difference between axial and equatorial bond lengths is less in the structure of **21** (2.2279(5) Å (axial) and 2.1951(6) Å (equatorial)) compared to the structure of **7** (2.2313(7), 2.2453(7) Å (both axial) and 2.1846(7), 2.1753(7) Å (both equatorial) for molecule 1; 2.2611(7), 2.2324(7) Å (both axial) and 2.1783(7), 2.1847(7) Å (both equatorial) for molecule 2). The closer similarities of the axial and equatorial Fe-P bond lengths in the structure of **21** compared to that of **7** may be related to the closer similarities in the chemical shift difference of the axial and equatorial environments in the $^{31}P\{^{1}H\}$ NMR spectrum. Therefore, it is possible that the difference in ^{31}P chemical shift of the axial and equatorial triplet resonances in solution may be directly proportional to the difference between the axial and equatorial Fe-P bond lengths in the solid state X-ray structure.

The crystallographic Fe-N-N bond angle of complex **21** (144.07(16)°) is similar to the Fe-N-N bond angles of molecule 1 of the structure of complex **7** (144.32(18) and 145.30(18)°). However, the Fe-N-N bond angles of molecule 2 of **7** are more varied, with one angle smaller (13.9(2)°) and one larger (152.4(2)°). As with the structure of complex **7**, the Fe-N-N bond angle in the structure of **21** is in between the bond angles that would expected for either *sp* or sp^2 hybridisation of the terminal nitrogen atoms of the azide ligands (120 and 180° respectively). As the Fe-N-N angle is closer to 120°, the hybridisation of the azide terminal nitrogen is most likely closer to sp^2 than *sp*, as would be expected for an azide ligand.

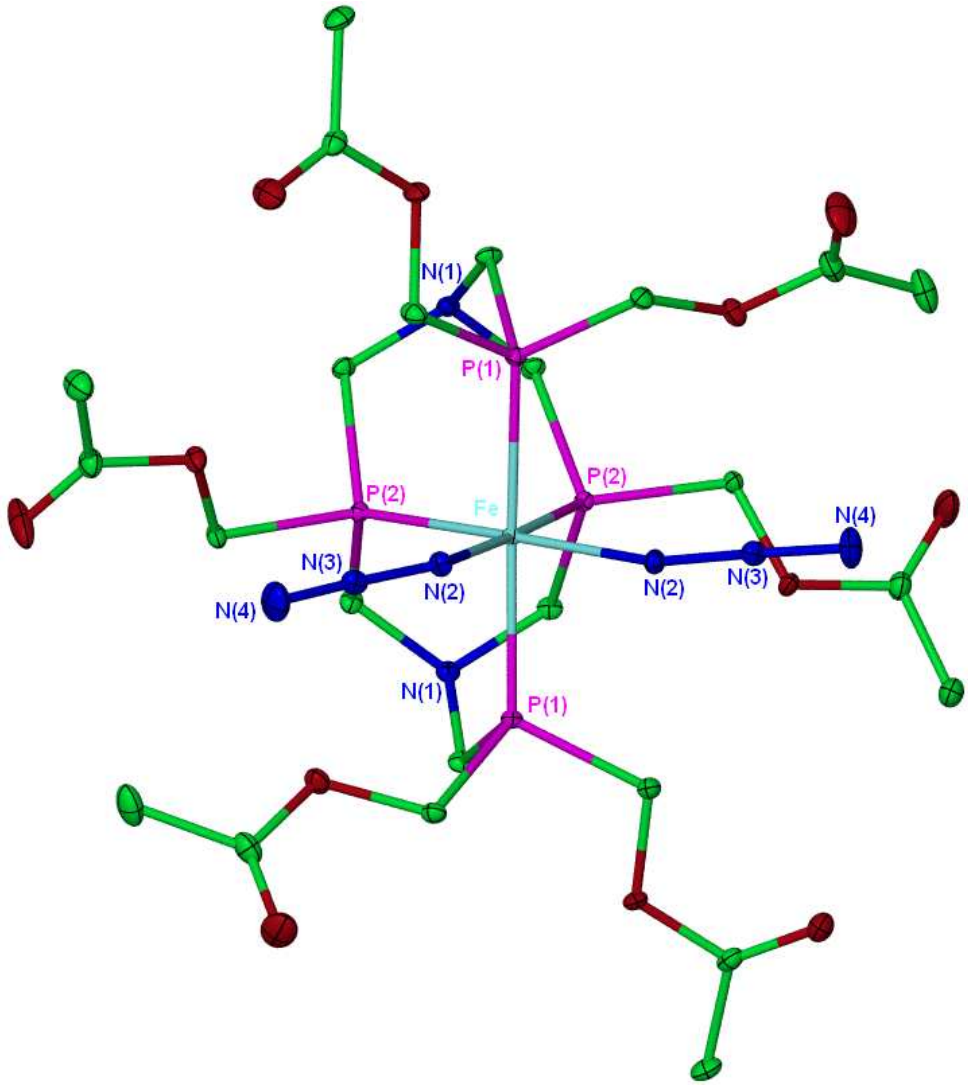

Figure 2.36 - Molecular structure of $[Fe(L^2)(N_3)_2]\cdot 0.5H_2O$ ($21\cdot 0.5H_2O$). Thermal ellipsoids are at the 30% probability level. Included water molecule and hydrogen atoms have been omitted for clarity.

Bond Lengths

Fe(1)-P(1)	2.2279(5)	N(2)-N(3)	1.190(3)
Fe(1)-P(2)	2.1951(6)	N(3)-N(4)	1.163(3)
Fe(1)-N(2)	2.092(19)		

Bond Angles

P(1)-Fe(1)-P(1)'	175.12(4)	N(3)-N(2)-Fe(1)	144.07(16)
N(2)-Fe(1)-P(2)	178.08(7)	N(4)-N(3)-N(2)	173.8(2)
N(2)-Fe(1)-N(2)'	82.24(11)	P(2)-Fe(1)-P(2)'	79.43(3)

Table 2.9 – Selected bond lengths (Å) and angles (°) for complex 21.

2.23 Reaction of $[Fe(L^2)Cl_2]$ (15) with sodium carbonate

The reaction of $[Fe(L^2)Cl_2]$ (**15**) with excess potassium carbonate in an acetone/water solution did not proceed at room temperature. Reacting the solution for two hours at reflux gave a red brown solution, which had seemingly decomposed. The $^{31}P\{^1H\}$ NMR spectrum (d_6-acetone) of the solution showed a wide range of broad resonances and singlets, confirming the decomposition.

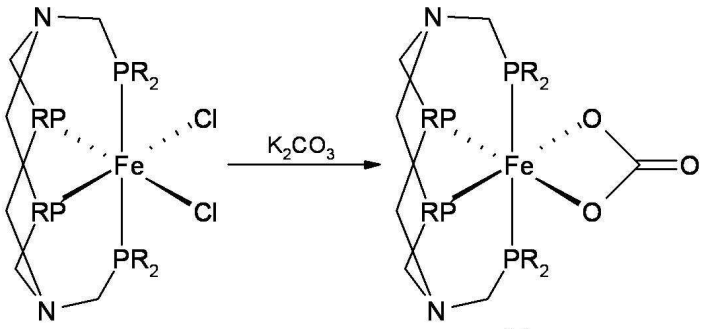

15
(R = $CH_2OC(O)Me$)

22

Scheme 2.15 – Reaction of $[Fe(L^2)Cl_2]$ (15) with potassium carbonate.

When the reaction was repeated in DMSO, the solution took on a red colouration after stirring for ten hours at room temperature. The $^{31}P\{^1H\}$ NMR spectrum (d_6-DMSO) showed the main product gives two triplet resonances at δ 15.9 and 7.5 ($^2J_{P\text{-}P}$ = 55 Hz) comprising *ca.* 60% of the material by integration. This is most likely the coordinated carbonate complex $[Fe(L^2)(\kappa^2\text{-}O_2CO)]$ (**22**) (**Scheme 2.15**). The spectrum included a number of singlet resonances and other broad peaks, suggesting some decomposition of the complex. This decomposition is most likely base-induced, caused by the high pH as a result of the addition of basic carbonate anions. Attempts to purify and isolate $[Fe(L^2)(\kappa^2\text{-}O_2CO)]$ (**22**) proved unsuccessful.

2.24 Electrochemical Studies

The use of electrochemical measurements in inorganic chemistry to help determine the ability of metal complexes to undergo electron-transfer processes has now become as routine a method of characterisation as NMR, vibrational spectroscopies and elemental analysis.[43] Electrochemistry can provide important information on a transition metal complex, including:

- whether the complex is redox active or not.
- the electrode potentials at which the redox processes take place.
- determining whether the redox processes lead to stable species.

The first target therefore in inorganic electrochemistry is to study the effects of electron addition and removal processes on the transition metal complex being studied. As metal-ligand bonds are primarily covalent in character, it is possible that the addition or removal of electrons within the molecule can lead to the cleavage of bonds or the formation of new ones. This essentially means that the complex being studied does not necessarily remain the same during the electron-transfer process, potentially leading to structural changes or even the formation of entirely new species.[43] The structural changes are controlled by the frontier orbitals of the complex. For example, in an oxidation process when an electron is removed from the highest occupied molecular orbital (HOMO), structural changes that can occur are dependant on the degree of bonding character of the HOMO, *i.e.* the more bonding character the HOMO possesses, the greater the structural changes that can occur. This also applies to the reduction process, the structural changes depending on the degree of anti-bonding character of the lowest unoccupied molecular orbital (LUMO) to which the electron is added. If the orbitals involved in the electron-transfer process are non-bonding then the changes to the complex are expected to be minimal.

Cyclic Voltammetry (CV) is the most common electrochemical technique employed to study electron-transfer processes and can yield both kinetic and thermodynamic information. CV works by applying a potential across electrodes immersed in a solution containing the species being studied, and varying that potential with time. A plot of current vs. potential is then recorded to give the relevant current-potential curves. These curves reveal both the potential at which such redox processes occur, as well as the size of the currents generated, these being related to the concentration of the species being studied. Finally, the shape of the curve allows the determination of whether the process is straightforward, or whether it involves potential complications

such as adsorption processes. Cyclic Voltammetric studies of the Fe(II) complexes of L^1 and L^2 were undertaken to find out more about their redox properties and to determine whether the related oxidised Fe(III) analogues would be stable and potentially isolable.

2.24.1 Electrochemistry of L^1 complexes

A 1 mM aqueous solution of $[Fe(L^1)(H_2O)_2]SO_4$ **1** was prepared, using 0.1 M potassium chloride as the electrolyte, which gives the dichloride complex **3** in solution. Cyclic voltammograms were recorded using a 1 mm platinum electrode using an initial scan rate of 100 mVs^{-1}. The initial scan showed an irreversible oxidation peak at *ca.* 0.3 - 0.4 V vs. SCE (**Figure 2.36**). In the second scan and other subsequent scans this peak was not observed. Only upon polishing of the electrode was this peak observed again, followed by its disappearance in subsequent scans. This signifies that irreversible structural changes are occurring to the iron complex during or quickly after the oxidation process, instead of the simple reversible Nernstian redox process associated with the oxidation of the Fe(II) metal centre to Fe(III) and its subsequent reduction back to Fe(II). The fact that the electrode needs polishing in order to repeatedly observe this peak could be due to the decomposition products of the oxidation reaction coating the electrode and essentially blocking further electrochemical processes occurring at the electrode surface. Replacing the aqua groups with other ligands such as azido, cyano and carbonato groups did not serve to stabilise any oxidation products, though slight shifts in potential were observed. The same experiments were attempted using 0.1 M sodium sulfate solution as the electrolyte, though $[Fe(L^1)(H_2O)_2](SO_4)$ **1** is not soluble enough by itself to make a 1 mM solution at room temperature. Observed cyclic voltammograms for a saturated solution of **1** using the Na_2SO_4 electrolyte gave a much smaller oxidation peak as expected, but otherwise gave similar voltammograms.

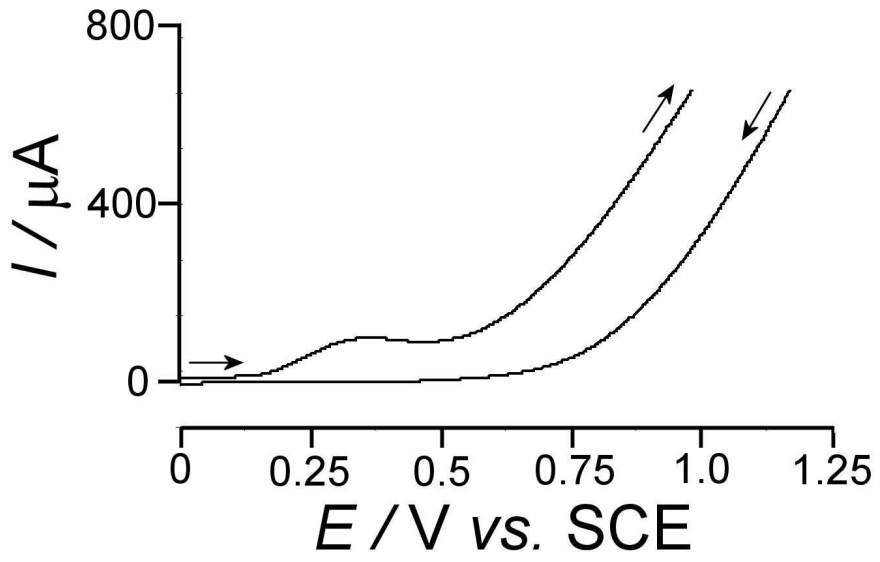

Figure 2.36 – First scan of the CV of a 1 mM aqueous solution of $[Fe(L^1)(H_2O)_2]SO_4$ (1), using a 1 mm Pt electrode at 100 mVs-1. 0.1 M KCl was used as the electrolyte.

Further experiments were carried out to determine the approximate timescale for the decomposition process. Theoretically, by increasing the scan rate of the voltammogram, the length of time available for the oxidised form to decompose will also be decreased. Therefore at high scan rates it can be determined whether the decomposition is effectively prevented due to insufficient time, giving a more reversible voltammogram. By repeating the above experiment at 1 Vs^{-1} (ten times the initial scan rate), the voltammogram shows signs of becoming more reversible. This suggests that if the oxidised Fe(III) complex is denied enough time to decompose then a reversible voltammogram may be possible. However, a completely reversible voltammogram was not observed even at such high scan rates.

2.24.2 Electrochemistry of L^2 complexes

The electrochemistry of the iron complexes containing the L^2 ligand was explored in order to compare and contrast to the largely irreversible voltammograms observed in the cyclic voltammograms of the related L^1 complexes. The L^2 ligand is more lipophilic than L^1 due to the presence of the less polar methyl ester groups, making it readily soluble in organic solvents such as 1,2-dichloroethane and acetonitrile. With the exception of $[Fe(L^2)(\kappa^2\text{-}O_2SO_2)]$ (**13**), the L^2 complexes are largely insoluble in water, so the similar study of the L^2 complexes could not be carried out in aqueous solution. Complex **13** was not studied in H_2O as the $^{31}P\{^1H\}$ NMR spectrum in D_2O showed that multiple complexes were formed, as well as the main product showing broad peaks suggesting that the coordinated sulfate ligand was exchanging with solvent H_2O molecules.

Cyclic voltammetry of the dichloro complex $[Fe(L^2)Cl_2]$ was initially carried out in 1,2-dichloroethane. A 1 mM 1,2-dichloroethane solution of $[Fe(L^2)Cl_2]$ (**15**) was made up containing 0.1M tetrabutylammonium hexafluorophosphate as an electrolyte, on a 1 mm platinum electrode using an initial scan rate of 50 mVs^{-1} ((i) in **figure 2.37**). Cyclic voltammograms were repeated at 100, 200, and 500 mVs^{-1} ((ii), (iii), and (iv) in **figure 2.37** respectively).

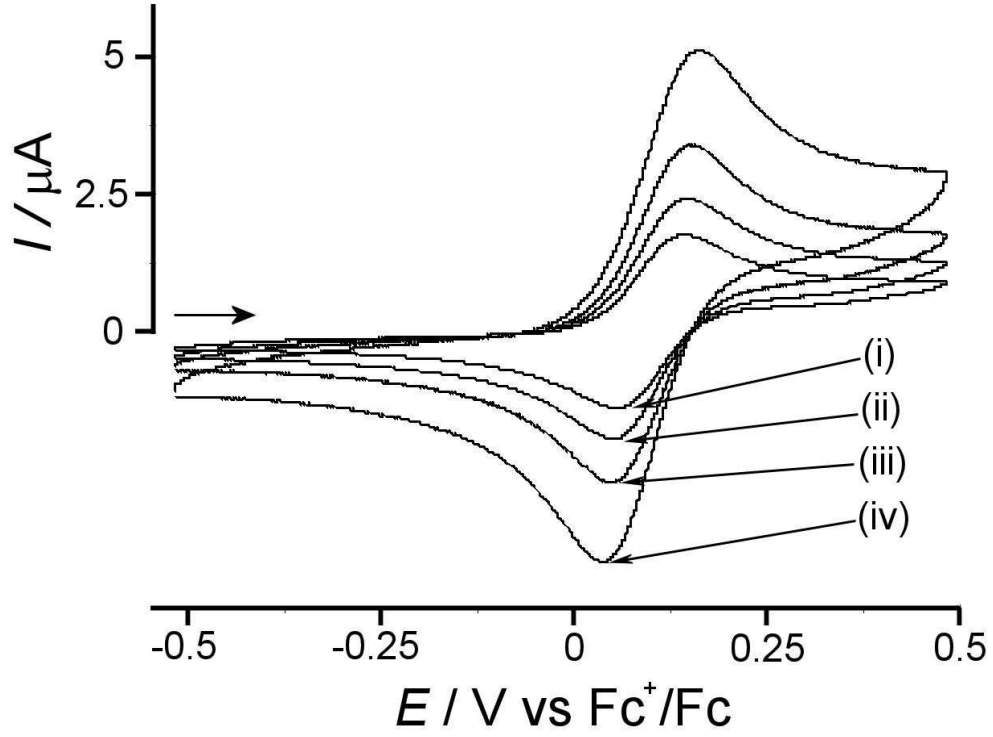

Figure 2.37 – Cyclic voltammograms of $[Fe(L^2)Cl_2]$ (15) in 1,2-dichloroethane, using a 1 mm Pt electrode at 50, 100, 200, and 500 mVs^{-1} ((i), (ii), (iii), and (iv) respectively). 0.1 M Bu_4NPF_6 was used as the electrolyte.

Interestingly, the above voltammogram shows a fully reversible Nernstian Fe(II)/Fe(III) redox process at *ca*. 0.1 V vs. Fc^+/Fc with no apparent decomposition of the complex. This is in direct contrast to the cyclic voltammogram of $[Fe(L^1)(H_2O)_2](SO_4)$ **1** and related complexes, though it is not immediately clear whether this is due to the difference in functionality of the esterified ligand L^2, or the difference of solvent between aqueous solution and dichloroethane. **Figure 2.37** also shows the dependence of the voltammograms on the scan rate, with the faster scan rates giving proportionally larger peak areas, and therefore peak currents. The cyclic voltammograms appear fully reversible at all four scan rates, suggesting that the reversibility of the Fe(II)/Fe(III) redox system in $[Fe(L^2)Cl_2]$ (**15**) in dichloroethane is not dependant on scan rate, unlike with the L^1 complexes. The same experiment was

repeated in acetonitrile to determine the effect of using a more polar, more coordinating solvent (**Figure 2.38**, vide infra).

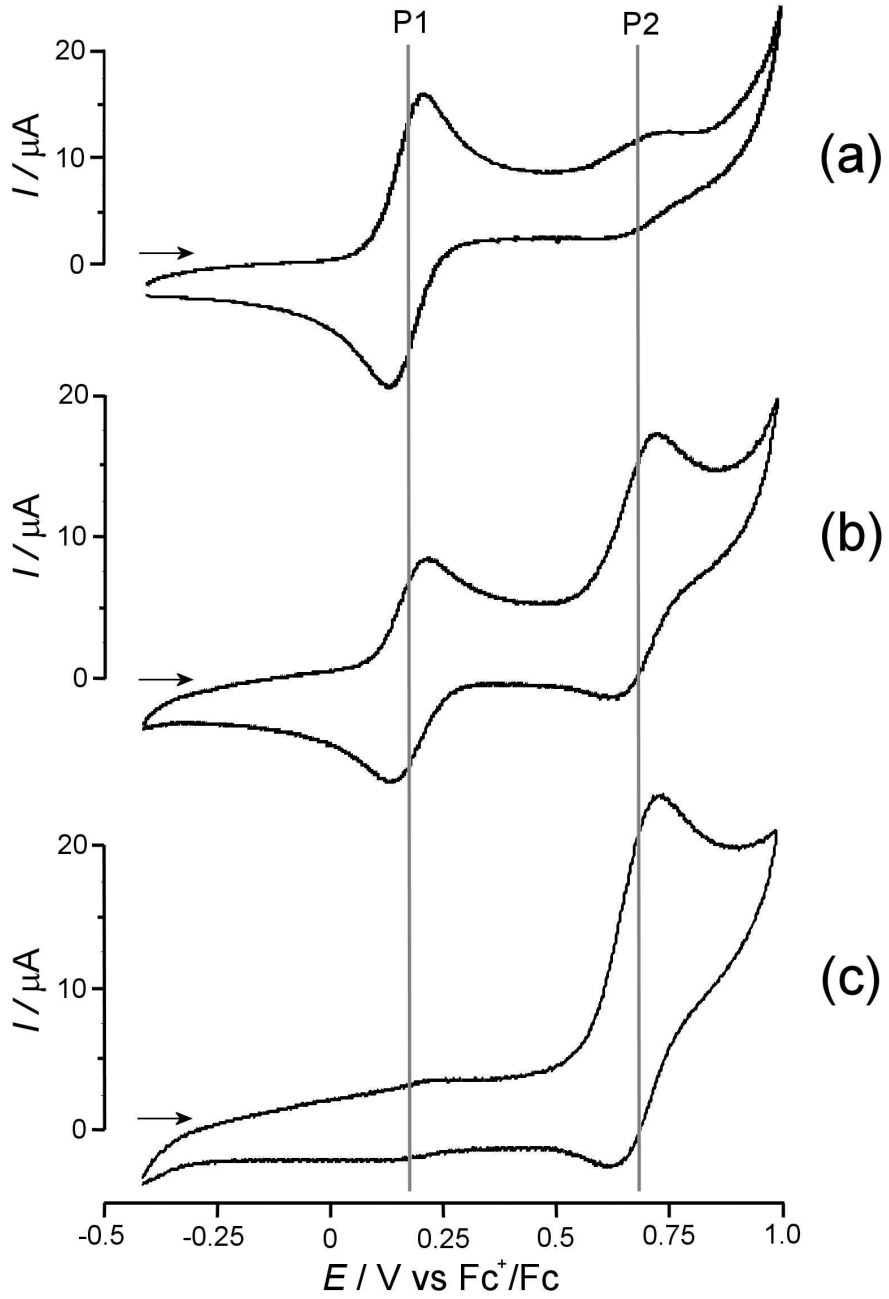

Figure 2.38 – Cyclic voltammograms of $[Fe(L^2)Cl_2]$ (15) in acetonitrile, using a 3 mm diamond electrode at 100 mVs-1 after 1, 10, and 60 minutes ((a), (b), and (c), respectively). 0.1 M Bu_4NPF_6 was used as the electrolyte.

When the experiment was conducted after one minute, two redox processes were observed ((a) in **Figure 2.38**). The oxidation/reduction peaks at 0.1 V vs. Fc^+/Fc seem fully reversible and correlate with the Fe(II)/Fe(III) redox process of the dichloro complex $[Fe(L^2)Cl_2]$ (**15**) as seen in the voltammograms carried out in 1,2-

dichloroethane. However, a second redox process is apparent at *ca*. 0.7 V vs. Fc^+/Fc, the identity of which is less immediately obvious.

After a total of ten minutes, the colour of the acetonitrile solution had changed from purple to a more purple/orange colour. CV of the solution at this point showed that the second redox process had grown in intensity with respect to the peak at *ca.* 0.1 V vs. Fc^+/Fc ((b) in **Figure 2.38**). It is therefore reasonable to suggest that the second redox process results from the cationic mono-chloro mono-acetonitrile complex $[Fe(L^2)(MeCN)Cl]^+$, which forms as a result of the replacement of one of the chloride anions coordinated to the iron centre by an acetonitrile ligand. Additionally, the redox process at *ca*. 0.7 V vs. Fc^+/Fc does not appear completely reversible, with the oxidation peak seeming slightly larger than the complementary reduction peak, suggesting that the complex is structurally altered upon reduction from Fe(III) back to Fe(II).

Recording the cyclic voltammogram after 1 hr showed that most of the $[Fe(L^2)Cl_2]$ (**15**) complex had reacted to form $[Fe(L^2)(MeCN)Cl]^+$, at which point the solution had taken on an orange colouration. The irreversibility of the $[Fe(L^2)(MeCN)Cl]^+$ Fe(II)/Fe(III) redox process was even more apparent from this voltammogram. The asymmetry of this second peak could also be due to the oxidation of traces of water present in the acetonitrile solvent catalysed by either $[Fe(L^2)Cl_2]$ (**15**) or $[Fe(L^2)(MeCN)Cl]^+$, as the oxidation of water occurs at a similar potential.

$^{31}P\{^1H\}$ NMR studies of $[Fe(L^2)Cl_2]$ (**15**) were carried out in CD_3CN in order to confirm the formation of $[Fe(L^2)(CD_3CN)Cl]^+$. The study showed conversion over time of the two triplet resonances associated with **15** to two second order doublets of triplets at δ 4.1 and 3.1 and a doublet of doublets at δ -6.0 respectively, the expected coupling pattern for an asymmetric complex such as $[Fe(L^2)(CD_3CN)Cl]^+$. Despite leaving the solution for 48 hrs, no formation of the di-acetonitrile complex was observed.

Overall the electrochemical studies have provided an interesting insight into the stability and reactivity of the iron(II) complexes studied. The contrast in electrochemical behaviour between the L^1 and L^2 complexes is particularly interesting, with the L^1 complexes exhibiting largely irreversible behaviour solution at most standard scan rates in aqueous solution, whilst the equivalent L^2 complexes showing reversible Nernstian Fe(II)/(III) redox processes in non-coordinating organic solvents such as dichloroethane. In a more coordinating organic solvent such as MeCN, the L^2 complexes also exhibit reversible Fe(II)/(III) redox behaviour, though the substitution of

a chloride ligand for an acetonitrile molecule also occurs, which can be monitored with CV over time.

No cyclic voltammetry studies of similar iron hydroxymethylphosphine complexes appear in the literature to date, so it is difficult to compare the results with related complexes. It is also therefore difficult to draw conclusions as to why the L^1 complexes give irreversible voltammograms, more specifically why the electrode blocking occurs after the oxidation of the L^1 complexes. As this does not happen with the related L^2 complexes, it is reasonable to suggest that the derivatisation of the CH_2OH groups into methyl ester groups prevents the decomposition of the complex upon oxidation. This decomposition could be because the hydroxymethylphosphine groups have an affinity for the electrode surface, thus coating it and causing the electrode blocking, or it could simply be a matter of stability. However, these two sets of results cannot be directly compared to one another as the conditions (*i.e.* solvent, electrolyte) in which they are studied are not identical.

2.25 Conclusion

A comparison of the coordination chemistry of the complexes of both the L^1 and L^2 ligands shows many similarities, with some notable differences. Firstly, due to the differences in polarity of the ligands, the majority of the coordination chemistry of the L^1 complexes was carried out in aqueous solution, whereas most of the coordination chemistry of the L^2 complexes took place in organic solvents such as dichloromethane and acetone.

Substituting the aqua groups on complex **1** with chloride and bromide ligands to form the dihalide complexes required the use of an organic solvent (acetone) to prevent the ligand exchange with solvent H_2O molecules that occurs in aqueous solution. The acylated equivalent of complex **1**, $[Fe(L^2)(\kappa^2\text{-}O_2SO_2)]$ (**13**), also reacted with a chloride salt to form the dichloride complexes in dichloromethane, though *via* the substitution of the coordinated chelating sulfate ligand instead of two H_2O ligands. It can therefore be concluded that both L^1 and L^2 complexes behave fairly similarly when reacting with halides in organic solvent, despite the differences in the ligands.

In contrast to the reactions of complex **1** with halides, the reactions of **1** with pseudo-halides in aqueous solution did not give reversible equilibria with the solvent molecules as indicated by sharp triplet resonances in the $^{31}P\{^1H\}$ NMR spectra. This is partially due to the insolubility of the products relative to the starting materials (with the notable

exception of $[Fe(L^1)(NCS)_2]$ (**6**)), which is the reverse of the reaction of **1** with halides. The reactions of complexes **1** and **15** with potassium thiocyanate in aqueous solution (**1**) and an acetone/water solution (**15**) proceeded similarly and both led to the precipitation of di-thiocyanate complexes $[Fe(L^1)(NCS)_2]$ (**6**) and $[Fe(L^2)(NCS)_2]$ (**20**) respectively. Similarly, complexes **1** and **15** also reacted with sodium azide in H_2O (**1**) and acetone/water (**15**) to both form the diazide complexes $[Fe(L^1)(N_3)_2]$ (**7**) and $[Fe(L^2)(N_3)_2]$ (**21**) respectively, though **21** precipitated from solution whereas **7** was very soluble. The formation of complex **7** also required an excess of sodium azide to drive the reaction to completion, partially due to the fact that mono-azide intermediate complexes were formed on the way to **7**. The observance of the mono-azide intermediates in this reaction suggests that it is more favourable for an azide ligand to coordinate to another molecule of complex **1**, rather than to coordinate as a second azide ligand. This suggests the substitution of the second aqua ligand on **1** is the rate determining step. As mono-thiocyanato complexes are never observed as intermediate complexes in the reactions of **1** and **15** with potassium thiocyanate, the rate determing step in these reactions is the first substitution of an aqua or chloride ligand for a thiocyanate anion. This also applies to the reaction of **15** with sodium azide.

The reaction of complex **1** with sodium carbonate in aqueous solution led to the formation of the chelating carbonate complex $[Fe(L^1)(\kappa^2\text{-}O_2CO)]$ (**8**). No equilibrium with the solvent was observed, despite the solubility of **8** in aqueous solution. This is partially due to the carbonate ligand, which formed a highly thermodynamically stable complex due to the chelate effect. In contrast to this, the similar reaction of $[Fe(L^2)Cl_2]$ (**15**) with potassium carbonate in acetone/water led to complete decomposition of the starting material. However, when the reaction was repeated in DMSO, the appearance of two new triplet resonances suggested the formation of the carbonate complex $[Fe(L^2)(\kappa^2\text{-}O_2CO)]$ (**22**) had occurred. Complex **22** could not be isolated or purified, however, due to the decomposition of *ca.* 40% of the material.

The reaction of complex **1** with CO offers interesting contrasts when comparing to the similar reaction of the L^2 complex **13**. Complex **1** reacted with CO in aqueous solution to afford the di-carbonyl complex $[Fe(L^1)(CO)_2]SO_4$ (**9**). When the reaction was stopped before completion, two mono-carbonyl intermediates were observed which could be identified as $[Fe(L^1)(CO)(H_2O)]SO_4$ (**10**) and $[Fe(L^1)(CO)(\kappa^1\text{-}OSO_3)]$ (**11**). In contrast, the reaction of **13** with CO in aqueous solution gave only one mono-carbonyl complex, most likely the carbonyl sulfate complex $[Fe(L^1)(CO)(\kappa^1\text{-}OSO_3)]$ (**17**). Further exposure of **17** to CO did not lead the di-carbonyl complex. It is not clear why the di-

carbonyl complex formed in aqueous solution in the case of the L^1 complex, whereas with the similar L^2 complex the second substitution did not occur. When $[Fe(L^1)(CO)(\kappa^1\text{-}OSO_3)]$ (**17**) was left in aqueous solution, the slow conversion to $[Fe(L^1)(CO)(H_2O)]SO_4$ (**17**) occurred *via* substitution of the coordinated sulfate ligand for an aqua ligand. In comparison, **13** dissolved in acetonitrile (mainly $[Fe(L^1)(MeCN)(\kappa^1\text{-}OSO_3)]$ in solution by $^{31}P\{^1H\}$ NMR spectroscopy) reacted to rapidly give $[Fe(L^1)(CO)(MeCN)]SO_4$ (**18**) *via* the substitution of the coordinated sulfate ligand with a highly-coordinated acetonitrile solvent ligand.

While the coordination chemistry of both $[Fe(L^1)Cl_2]$ (**3**) and $[Fe(L^2)Cl_2]$ (**15**) with CO in acetone gave similar mono-carbonyl mono-chloride complexes $[Fe(L^1)(CO)Cl]Cl$ (**12**) and $[Fe(L^2)(CO)Cl]Cl$ (**19a**) respectively, the main difference in these reactions lies in the relative solubilities of the starting materials and products. Complex **3** was sparsely soluble in acetone, and formed the even less soluble product **12**. This therefore precipitated, automatically preventing reversion back to **3**. In contrast, complex **19a** formed in the reaction of **15** with CO is soluble and stays in solution. This allows the back reaction to **15** to occur when the atmosphere of CO is removed. Only when the coordinating chloride anion was removed was the $Fe(L^2)(CO)Cl]^+$ cation stable in solution and could be isolated as the tetraphenylborate salt **19b**.

In contrast to the reaction of **1** with acetic anhydride, attempts to functionalise the CH_2OH groups on **1** with the amino acid glycine to afford carbamate moieties led to the formation of the N,O-coordinated glycine complex **14** *via* substitution of the aqua groups. However, the hydroxymethyl groups of **14** remained unfunctionalised. This is presumably because the functionalisation of a hydroxymethyl phosphine with an amine (*i.e.* the Mannich reaction) requires the availability of the phosphorus lone pair, which is unavailable when complexed to the iron centre.

The Nuclear Resonance Vibrational Spectroscopy (NRVS) of ^{57}Fe versions of complexes $[Fe(L^1)(H_2O)_2]SO_4$ **1** and $[Fe(L^1)(CO)_2]SO_4$ **9** showed interesting results. Peaks relating to the Fe-H_2O and Fe-CO modes were tentatively assigned after comparison with other aqua and carbonyl complexes. The H_2O groups on $[^{57}Fe(L^1)(H_2O)_2]SO_4$ were then exchanged with $^{18}OH_2$ in an attempt to confirm the identity of the Fe-aqua vibrational modes by looking for a shift in frequency of the relevant peaks.

Electrochemical studies of both the L^1 and L^2 series of complexes provided insight into their redox behaviour. Complexes of the L^1 ligand proved to give largely irreversible

cyclic voltammograms in aqueous solution, likely as a result of electrode blocking due to decomposition of the complexes upon oxidation of the Fe(II) to Fe(III). In contrast, the L^2 complexes showed completely reversible cyclic voltammograms in 1,2-dichloroethane, showing that the equivalent Fe(III) complexes are stable in solution. Cyclic voltammetry of the L^2 complexes in MeCN showed that a chloride ligand is replaced with an acetonitrile ligand over time. As a result of these electrochemical studies, the isolation of the 17 electron Fe(III) L^2 complexes would appear to be feasible. This could be achieved by either chemical or bulk electrochemical methods. Investigations could then be carried out to determine whether these complexes show any catalytic activity or the ability to reversibly bind small molecules such as dinitrogen.

2.26 References

1. J. Chatt, G. J. Leigh and R. M. Slade, *J. Chem. Soc., Dalton Trans.*, 1973, 2023.
2. K. N. Harrison, P. A. T. Hoye, A. G. Orpen, P. G. Pringle and M. B. Smith, *J. Chem. Soc., Chem. Commun.*, 1989, 1096.
3. J. W. Ellis, K. N. Harrison, P. A. T. Hoye, A. G. Orpen, P. G. Pringle and M. B. Smith, *Inorg. Chem.*, 1992, **31**, 3026.
4. E. Costa, M. Murray, P. G. Pringle and M. B. Smith, *Inorg. Chim. Acta.*, 1993, **213**, 25.
5. P. A. T. Hoye, P. G. Pringle, M. B. Smith and K. Worboys, *J. Chem. Soc., Dalton Trans.*, 1993, 269.
6. S. Komiya, H. Awata, S. Ishimatsu and A. Fukuoka, *Inorg. Chim. Acta.*, 1994, **217**, 201.
7. D. E. Berning, K. V. Katti, C. L. Barnes and W. A. Volkert, *Chem. Ber.*, 1997, **130**, 907.
8. D. E. Berning, K. V. Katti, L. J. Barbour and W. A. Volkert, *Inorg. Chem.*, 1998, **37**, 344.
9. L. Higham, A. K. Powell, M. K. Whittlesey, S. Wocadlo and P. T. Wood, *Chem. Commun.*, 1998, 1107.
10. B. Drießen-Hölscher and J. Heinen, *J. Organomet. Chem.*, 1998, **570**, 141.
11. A. Salvani, P. Frediani, M. Bianchi, F. Piacenti, L. Pistolesi and L. Rosi, *J. Organomet. Chem.*, 1999, **582**, 218.
12. A. Fukuoka, W. Kosugi, F. Morishita, M. Hirano, L. McCaffrey, W. Henderson and S. Komiya, *Chem. Commun.*, 1999, 489.
13. Y. Kayaki, T. Suzuki and T. Ikariya, *Chem. Lett.*, 2001, 1016.

14. D. S. Bharathi, M. A. Sridhar, J. S. Prasad and A. G. Samuelson, *Inorg. Chem. Commun.*, 2001, **4**, 490.
15. L. J. Higham, M. K. Whittlesey and P. T. Wood, *Dalton Trans.*, 2004, 4202.
16. V. Cadierno, P. Crochet, S. E. García-Garrido and J. Gimeno, *Dalton Trans.*, 2004, 3635.
17. J. C. Jeffery, B. Odell, N. Stevens and R. E. Talbot, *Chem. Commun.*, 2000, 101.
18. A. A. Karasik, R. N. Naumov, R. Sommer, O. G. Sinyashin and E. Hey-Hawkins, *Polyhedron*, 2002, **21**, 2251.
19. M. Antberg and L. Dahlenburg, *Inorg. Chim. Acta.*, 1985, **104**, 51.
20. F. A. Cotton, G. Wilkinson, C. A. Murillo and M. Bochmann, *"Advanced Inorganic Chemistry"*, Wiley-Interscience, New York, 1999.
21. M. Bacci, S. Midollini, P. Stoppioni and L. Sacconi, *Inorg. Chem.*, 1973, **12**, 1801.
22. A. B. P. Lever, B. S. Ramaswamy, S. H. Simonsen and L. K. Thompson, *Can. J. Chem.*, 1970, **48**, 3076.
23. L. D. Field, B. A. Messerle and R. J. Smernik, *Inorg. Chem.*, 1997, **36**, 5984.
24. F. H. Allen and O. Kennard, *Automat. News.*, 1993, **8**, 31.
25. D. A. Fletcher, R. F. McMeeking and D. Parkin, *J. Chem. Comput. Sci.*, 1996, **36**, 746.
26. W. K. Miller, J. D. Gilbertson, C. Leiva-Paredes, P. R. Bernatis, T. J. R. Weakley, D. K. Lyon and D. R. Tyler, *Inorg. Chem.*, 2002, **41**, 5453.
27. T. G. Spiro, Ed., *"Biological Applications of Raman Spectroscopy"*, Wiley-Interscience, New York, 1988.
28. A. Dong and W. S. Caughey, *Meth. Enzymol.*, 1994, **232**, 139.
29. A. Barth and C. Zscherp, *Q. Rev. Biophys.*, 2002, **35**, 369.
30. L. Zhu, J. T. Sage and P. M. Champion, *Science*, 1994, **266**, 629.
31. W. R. Scheidt, S. M. Durbin and J. T. Sage, *J. Inorg. Biochem.*, 2005, **99**, 60.
32. E. J. Lyon, S. Shima, R. Boecher, R. K. Thauer, F. W. Grevels, E. Bill, W. Roseboom and S. P. J. Albracht, *J. Am. Chem. Soc.*, 2004, **126**, 14239.
33. S. Shima, E. J. Lyon, R. K. Thauer, B. Mienert and E. Bill, *J. Am. Chem. Soc.*, 2005, **127**, 10430.
34. M. Korbas, W. Meyer-Klaucke, S. Vogt, E. Bill, E. J. Lyon, R. K. Thauer and S. Shima, *J. Biol. Chem.*, 2006, **281**, 30804.
35. S. Shima and R. K. Thauer, *Chem. Rec.*, 2007, **7**, 37.
36. J. Huhmann-Vincent, B. L. Scott and G. J. Kubas, *Inorg. Chim. Acta.*, 1999, **294**, 240.

37. L. M. Mink, J. R. Polam, K. A. Christensen, M. A. Bruck and F. A. Walker, *J. Am. Chem. Soc.*, 1995, **117**, 9329.
38. L. M. Mink, K. A. Christensen and F. A. Walker, *J. Am. Chem. Soc.*, 1992, **114**, 6930.
39. A. W. Frank and D. J. Daigle, *Textile Res. J.*, 1982, **52**, 751.
40. W. Henderson, G. M. Olsen and L. S. Bonnington, *J. Chem. Soc., Chem. Commun.*, 1994, 1863.
41. D. E. Berning, K. V. Katti, C. L. Barnes and W. A. Volkert, *J. Am. Chem. Soc.*, 1999, **121**, 1658.
42. A. A. Karasik, R. N. Naumov, O. G. Sinyashin, G. P. Belov, H. V. Novikova, P. Lönnecke and E. Hey-Hawkins, *Dalton Trans.*, 2003, 2209.
43. P. Zanello, *"Inorganic Electrochemistry"*, The Royal Society of Chemistry, Cambridge, 2003.

Chapter 3 – Self-assembly and coordination chemistry of a new iron(II) phosphine complex

3.1 Introduction: Further modification of the self-assembly reaction

In Chapter 2, reactions were undertaken to derivatise the hydroxymethyl groups on ligand L^1 in complex **1** in order to create similar ligands with different properties, such as solubility. This gave interesting results, with the reaction of **1** with acetic anhydride successfully functionalising the hydroxymethyl groups to give methyl ester moieties, while the amino acid glycine coordinated to the iron centre instead of giving the intended carbamate group.

Another method of creating a derivatised version of ligand L^1 would be to use a different phosphine in the self-assembly reaction, instead of directly reacting the hydroxymethyl groups on complex **1** with a reagent. For example, if one of the hydroxymethyl groups on the phosphine used in the self-assembly had been replaced with a phenyl group, the reaction could give the same tetradentate 1,5-diaza-3,7-diphosphacyclooctane motif, only with each phosphine possessing one phenyl group (**Figure 3.1**).

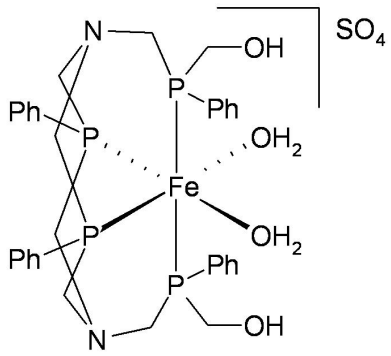

Figure 3.1 – Potential structure of the product from the self-assembly reaction of $PhP(CH_2OH)_2$.

The formation of the above complex would depend on whether the same or similar motifs to ligands L^1 and L^2 are formed, or whether an entirely new ligand structure is assembled on the metal. A good starting point is to carry out the self-assembly reaction using a phosphonium salt based on the phosphine $PhP(CH_2OH)_2$, in order to determine if a similar reaction proceeds at all, and then attempt to characterise any products formed. Using a phosphonium salt based on a di-substituted hydroxymethylphosphine such as $Ph_2P(CH_2OH)$ in the self-assembly reaction is also a

possibility, although this would have to give a different ligand motif to L^1 and L^2. This is because the neutral phosphine $Ph_2P(CH_2OH)$ only possesses one CH_2OH group and so it can only undergo one condensation reaction to form a single P-CH_2-N linkage. Therefore, the most complex ligand that could possibly form with $Ph_2P(CH_2OH)$ is the tridentate phosphine ligand $N(CH_2PPh_2)_3$.

3.2 Synthesis of 1 using THMP and formaldehyde

Reactions were carried out to investigate the possibility of using a phosphine directly in the self-assembly reaction itself, rather than using the related phosphonium salt. This was attempted to avoid the additional reaction step needed to convert a phosphine into a phosphonium salt, only to then convert it back again by the addition of base. Therefore, the self-assembly reaction to form complex **1** was carried out adding tris(hydroxymethyl)phosphine (THMP) dropwise in the presence of formaldehyde, rather than using the phosphonium salt THPS. THMP was synthesised following a literature procedure,[1] involving the reaction of dry tetrakis(hydroxymethyl)phosphonium chloride (THPC) with triethylamine and subsequent removal of the triethylammonium chloride, formaldehyde, and excess triethylamine *via* distillation.

When the self-assembly reaction to synthesise complex **1** (**Scheme 2.1** in chapter 2) was carried out using THMP in the presence of formaldehyde instead of THPS (keeping the conditions and stoichiometry constant), a red solution was formed identical in appearance to when THPS was used. A red crystalline solid was formed after *ca*. 5 days at 5° C, which showed the characteristic triplet resonances at δ 20.1 and -1.5 in the $^{31}P\{^1H\}$ NMR spectrum in D_2O. This showed that complex **1** had successfully been formed using THMP and formaldehyde instead of THPS.

3.3 Synthesis of $[Fe(L^3)_2(\kappa^2\text{-}O_2SO_2)]$ (23)

The self-assembly reaction was then attempted using $PhP(CH_2OH)$ instead of THPS. An aqueous solution of the phosphine was slowly added to an aqueous solution of iron(III) sulfate and ammonium sulfate. No reaction was apparent after the addition of a few drops of phosphine, so formaldehyde solution was added to determine whether its presence was necessary in order to 'catalyse' the reaction, as it is a key component of the mechanism of the Mannich reaction (see Chapter 2, section 2.16). The pale green solution immediately turned a purple colour, quickly giving rise to a purple precipitate. Subsequent addition of the remaining aqueous $PhP(CH_2OH)_2$ solution resulted in the precipitation of further material. The pH of the reaction solution was

monitored and kept below pH 5 by slowly adding the phosphine, which gives the phosphine time to react and for the pH to fall. This was done in order to prevent base-induced decomposition of any products, which are likely to be sensitive to high pH. The purple material was found to be soluble in polar organic solvents such as chloroform, dichloromethane and acetone, but insoluble in less polar solvents like THF and benzene. Subsequent syntheses were carried out in the presence of formaldehyde from the start.

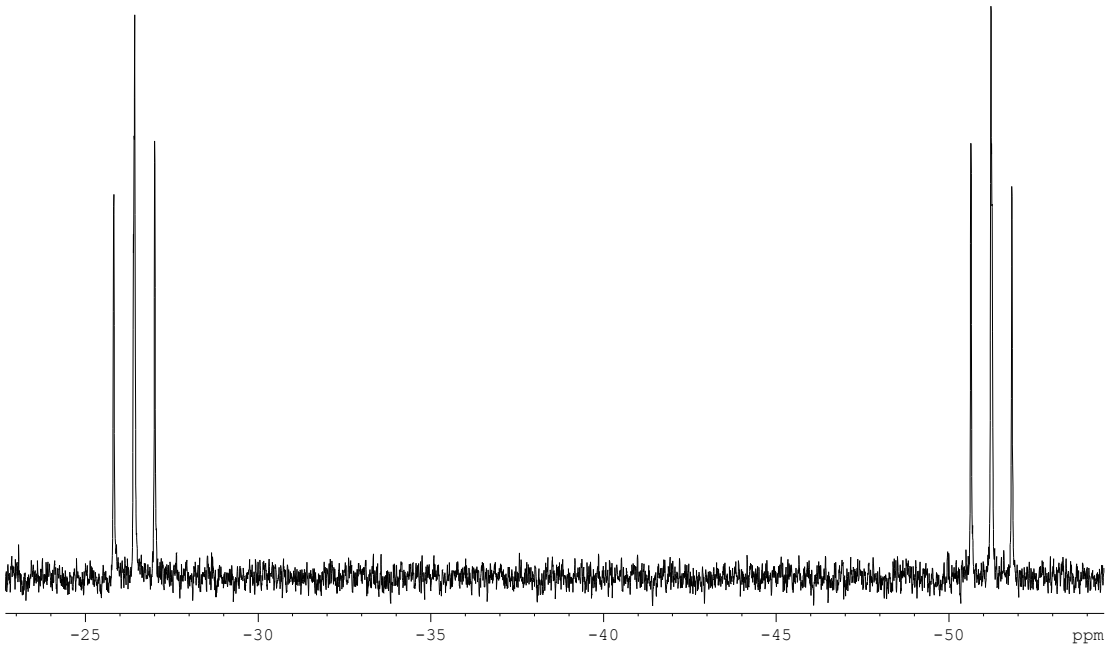

Figure 3.2 – $^{31}P\{^{1}H\}$ NMR spectrum of the product from the $PhP(CH_2OH)_2$ self-assembly reaction in $CDCl_3$ at 122 MHz.

$^{31}P\{^{1}H\}$ NMR spectroscopy of the purple material **23** in $CDCl_3$ (**Figure 3.2**) showed two triplet resonances at δ -26.4 and -52.2, suggesting that the material could be analogous to that of $[Fe(L^1)(H_2O)_2]SO_4$, only with phenyl groups in place of some of the hydroxymethyl groups. Small single crystals of **23** suitable for X-ray analysis were grown from the evaporation of a dichloromethane solution. The crystallographic analysis shows that the complex does not have the expected structure as shown in **Figure 3.1**, but instead contains two bidentate phosphine ligands (L^3) coordinated in a *cis* manner to the iron centre (**Scheme 3.1**). The sulfate anion is coordinated in a bidentate manner to the metal. The overall structure from the X-ray data fits with the two triplet resonances observed in the $^{31}P\{^{1}H\}$ NMR spectrum of **23** in $CDCl_3$. This does not necessarily mean that the crude material isolated from the reaction is the same as that recrystallised from dichloromethane, though this is likely to be the case. Electrospray mass spectrometry of complex **23** shows a major peak at m/z = 803.1, which corresponds to the molecular ion plus sodium $[M+Na]^+$.

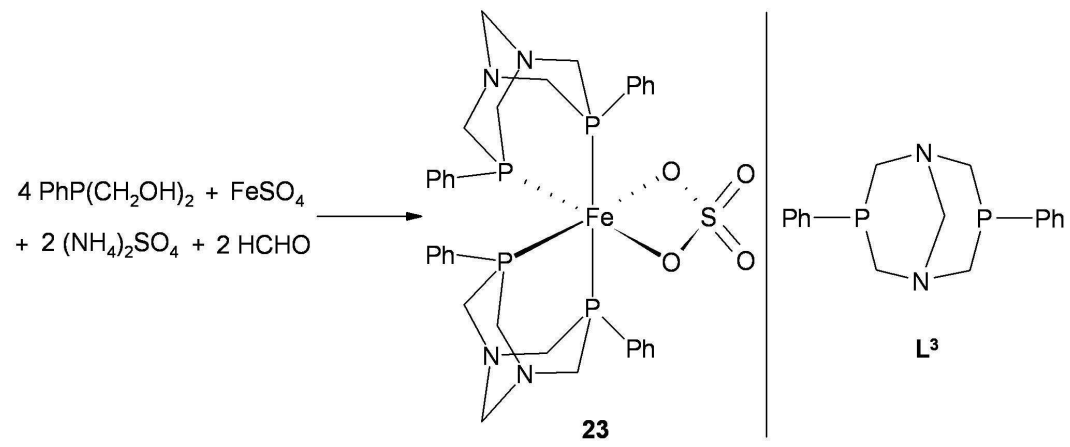

Scheme 3.1 – Self-assembly synthesis of $[Fe(L^3)_2(\kappa^2\text{-}O_2SO_2)]$ (23) (left) and its self-assembled ligand L^3.

Following the X-ray structural analysis, the ratio of phosphine to iron sulfate to ammonium sulfate to formaldehyde was adjusted to 4:1:2:2 respectively in order to match the stoichiometry of the product and give an optimal yield (**Scheme 3.1**). Though the formaldehyde is essentially catalytic (with respect to the Mannich reaction as shown on page 93), the methylene group between the nitrogen atoms on each ligand is a result of the condensation of a molecule of formaldehyde, and is therefore also a reagent.

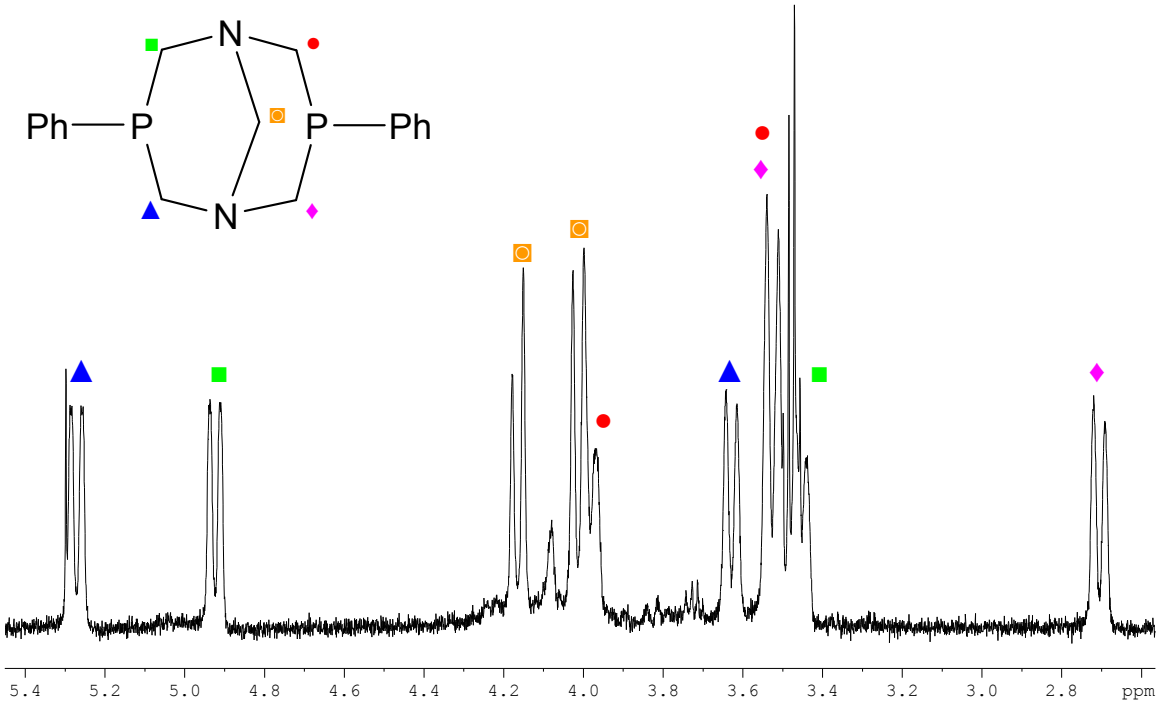

Figure 3.4 – ^{1}H NMR spectrum of $[Fe(L^3)_2(\kappa^2\text{-}O_2SO_2)]$ (23) at 500 MHz in $CDCl_3$. The different chemical environments of the ligand methylene groups shown arise from its coordination to the metal and *cis* octahedral geometry of the complex.

The ^{1}H NMR spectrum of complex **23** (**Figure 3.4**) showed five different AB signals arising from the five different methylene proton environments, four from the P-CH_2-N groups (▲, ■, ●, ♦) and one from the N-CH_2-N moiety (◙). This means that all ten methylene protons on the L^3 ligand backbone are magnetically inequivalent in the ^{1}H NMR spectrum. The N-CH_2-N methylene protons give rise to the AB system centred at *ca*. δ 4.1 (◙). The four sets of P-CH_2-N methylene resonances (▲, ■, ●, ♦) cannot be individually assigned to a particular P-CH_2-N group, which are only magnetically inequivalent due to the *cis* geometry of the complex.

3.4 X-ray structure of $[Fe(L^3)_2(\kappa^2\text{-}O_2SO_2)]\cdot 2H_2O$ ($23\cdot 2H_2O$)

Purple crystals of **23**·$2H_2O$ were grown by slow evaporation of a dichloromethane solution. The asymmetric unit of the structure contains one half molecule of the complex and a molecule of H_2O, with the other half being generated by symmetry. The structure shows the octahedral iron(II) complex with two of the bidentate L^3 phosphine ligands arranged in a *cis* configuration, with the remaining two coordination sites occupied by a coordinated bidentate sulfate ligand, giving an overall neutral molecule (**Figure 3.5**). The L^3 ligand contains two fused six-membered PN_2C_3 rings, with both rings sharing the two nitrogen atoms and the N-CH_2-N methylene group. A phenyl group is the third substituent on both of the phosphine donors.

The two fused six-membered PN_2C_3 rings that make up the backbone of each L^3 ligand both possess chair conformations. This enables the lone pairs of the phosphines to point at (almost) 90° to each other, which allows the donation of electron density to the empty orbitals on the metal. The ligand can also be thought of as an eight-membered $P_2N_2C_4$ ring (*i.e.* a 1,5-diaza-3,7-diphosphacyclooctane) with a methylene bridge between the two nitrogen atoms. This bridging CH_2 moiety is formed from the condensation of a formaldehyde molecule with the remaining N-H group on each side of the eight-membered ring, losing one molecule of water for each ligand. This means that the formaldehyde plays two roles in the self-assembly of the L^3 ligand; acting as a catalyst in the Mannich reaction involved in the self-assembly process, as well as a reagent that is an essential part of the final ligand structure.

The crystallographic bite angle of L^3 in this structure is 83.41(6)°. This angle is significantly larger than the average equatorial crystallographic bite angle (*i.e.* of the phosphines in the eight membered $P_2N_2C_4$ ring) of the L^1 and L^2 complexes in chapter 2 (80.51(9.5) and 80.06(7)°, respectively). However, this cannot be directly compared

as the bite angle of the L^3 ligand is not in the equatorial plane. The bite angle of L^3 is fairly similar to average values of other similar diphosphine ligands in the literature, such as dppe (82.55(3.65)°) and dpp-benzene (81.95(3.25)°), as shown in Chapter 1, Figure 1.5.[2] The crystallographic bite angle of the coordinated sulfate molecule is 68.4(2)°, which is marginally smaller than the crystallographic bite angle of the coordinated sulfate molecule in $[Fe(L^2)(\kappa^2\text{-}O_2SO_2)]$ (complex **13** in chapter 2), which is 69.74(15)°. Due to these constrained bite angles the octahedral geometry of the complex is distorted, giving a wide range of *cis* equatorial bond angles between 69.74 and 99.55°, which are far from the ideal 90° angles in a perfect octahedron.

The analogous L^2 sulfate complex **13** has similar Fe-P bond lengths to **23**, with 2.1840(18) Å (equatorial) and 2.2829(16) Å (axial) for **23** compared to 2.1803(17) and 2.1776(17) Å (equatorial) and 2.2256(16) and 2.2362(16) Å (axial) for **13**. As with the complexes of L^1 and L^2 in chapter 2, the axial Fe-P bonds of **23** are noticeably longer than their equatorial equivalents due to the greater *trans* influence of the *trans* phosphine donor compared to the oxygen donor of the sulfate ligand *trans* to the equatorial phosphines. This effect is even more pronounced in **23**, with *ca*. 0.1 Å difference between the axial and equatorial Fe-P bond lengths. The Fe-O bond lengths of **13** and **23** are also similar, with 2.061(4) Å for **23** compared to 2.047(4) and 2.046(4) Å for complex **13**.

The phenyl groups on the ligand do not face one another and there is no intramolecular π-π stacking in each ligand, neither does there appear to be any intermolecular π-π interactions between individual discrete molecules. The two phenyl groups on each ligand are oriented almost perpendicular to one another (*i.e.* by rotation about the P-C bond attaching the aromatic ring to the phosphine), and each ligand is positioned on the metal in a way which minimises the inter-ligand steric interactions between the aromatic rings.

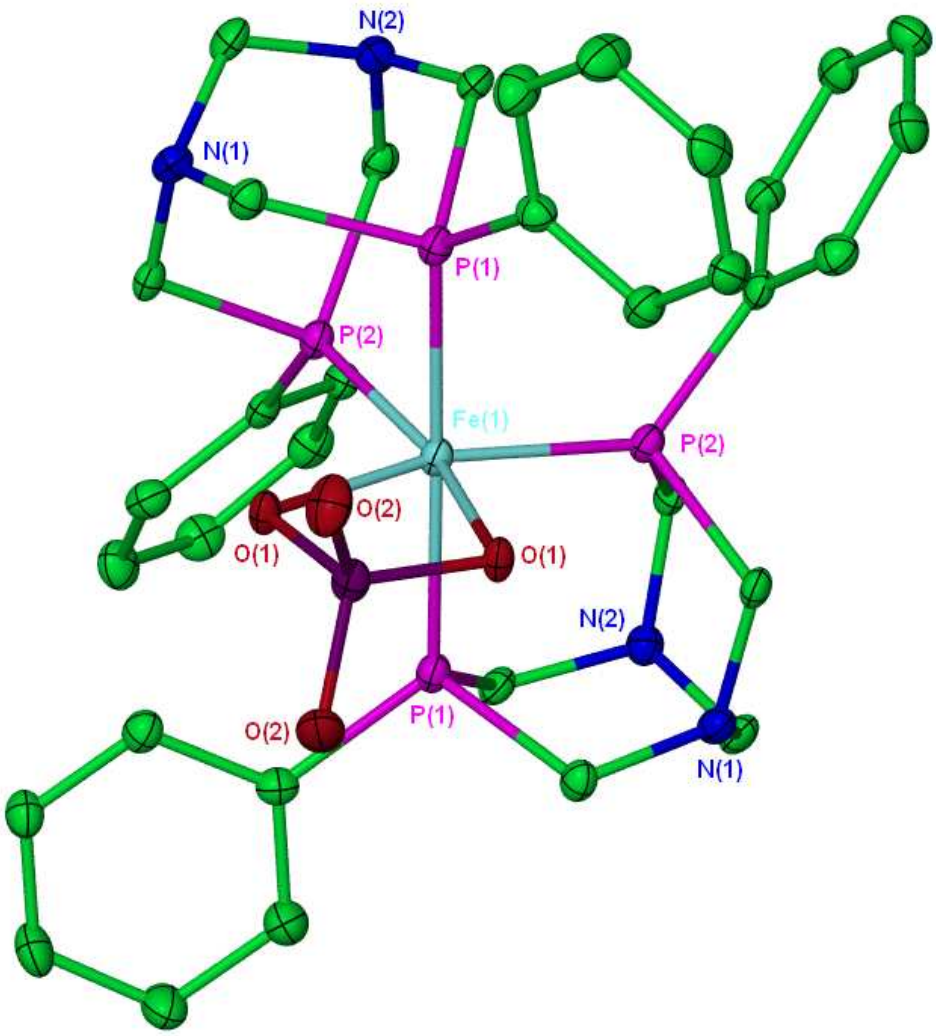

Figure 3.5 – Molecular structure of *cis*-[Fe(L^3)$_2$(κ^2-O_2SO_2)]·2H_2O (23·2H_2O). The asymmetric unit contains ½ a molecule of complex 1 with one full water molecule. Thermal ellipsoids are at the 30% probability level. Included water molecules and hydrogen atoms have been omitted for clarity.

Bond Lengths

Fe(1)-P(1)	2.2829(16)	S(1)-O(1)	1.502(4)
Fe(1)-P(2)	2.1840(18)	S(1)-O(2)	1.452(4)
Fe(1)-O(1)	2.061(4)		

Bond Angles

P(1)-Fe(1)-P(2)	83.41(6)	P(1)-Fe(1)-P(1)'	177.00(11)
O(1)-Fe(1)-P(2)	96.20(11)	O(1)-S(1)-O(1)'	101.0(3)
O(1)-Fe(1)-O(1)'	68.4(2)	O(1)-S(1)-O(2)	109.8(2)
P(2)-Fe(1)-P(2)'	99.55(10)	O(2)-S(1)-O(2)'	112.5(4)

Table 3.1 – Selected bond lengths (Å) and angles (°) for complex 23·2H_2O (standard deviation in brackets).

3.5 Synthesis of *cis*-[Fe(L^3)$_2$Cl$_2$] (24a)

Initial attempts to displace the coordinated sulfate ligand in **23** were unsuccessful. In direct contrast to the iron(II) complexes of L^2, when PPNCl was added to a dichloromethane solution of **23** no reaction occurred. [Fe(L^3)$_2$(κ^2-O_2SO_2)] (**23**) does not appear to be the best precursor for the investigation of further coordination chemistry. In order to synthesise a bis-L^3 dichloride complex, iron(III) chloride and ammonium chloride (rather than the equivalent sulfate salts) were reacted with PhP(CH_2OH)$_2$ and formaldehyde as in **Scheme 3.1** in section 3.2. Using the same stoichiometry, the reaction gave a similar purple precipitate as in the formation of complex **23**.

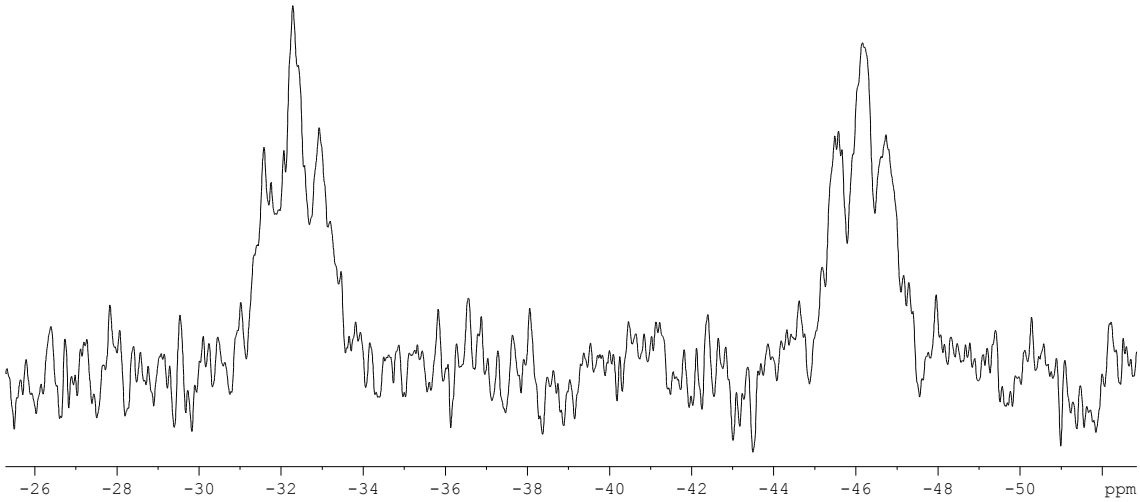

Figure 3.6 – $^{31}P\{^1H\}$ NMR spectrum of the dichloride complex *cis*-[Fe(L^3)$_2$Cl$_2$] (24a) in $CDCl_3$ at 122 MHz.

The $^{31}P\{^1H\}$ NMR spectrum of the purple solid in $CDCl_3$ (**Figure 3.6**) showed two triplet resonances (at *ca*. δ -32 and -46) as would be expected, suggesting the dichloride complex *cis*-[Fe(L^3)$_2$Cl$_2$] (**24a**) had been successfully formed. However, the resonances were broad suggesting the complex is fluxional or unstable. This fluxionality could be the result of the ability of the complex to isomerise between the *cis* and *trans* isomers of the complex, as it is not seen in the case of the chelating sulfate complex **23**, which cannot switch between the *cis* and *trans* isomers. Complex **24a** partially dissolves in aqueous solution to give a purple solution. When the $^{31}P\{^1H\}$ NMR spectrum was recorded in D_2O two sharper resonances were observed at δ -17.8 and -38.2 (**Figure 3.7**), although these were now doublets of doublets rather than triplets.

As complex **24a** is partially soluble in aqueous solution at neutral pH but does not possess any highly soluble functional groups, it is likely that the chloride ligands are being displaced with solvent H_2O molecules to give the dicationic diaqua complex

cis-[Fe(L^3)$_2$(H_2O)$_2$]Cl_2, which should be far more polar and therefore soluble in water. Complex **24a** is increasingly soluble with decreasing pH, possibly due to protonation of the nitrogen groups. If an excess of sodium chloride is added to the aqueous solution of *cis*-[Fe(L^3)$_2$(H_2O)$_2$]Cl_2, the dichloride complex *cis*-[Fe(L^3)$_2$$Cl_2$] (**24a**) precipitates from solution. In comparison, the similar bidentate sulfate complex **23** is completely insoluble in aqueous solution. This is presumably due to the fact that the chelating bidentate sulfate ligand cannot be as easily displaced as the monodentate chloride ligands on **24a** to give a cationic water-soluble complex.

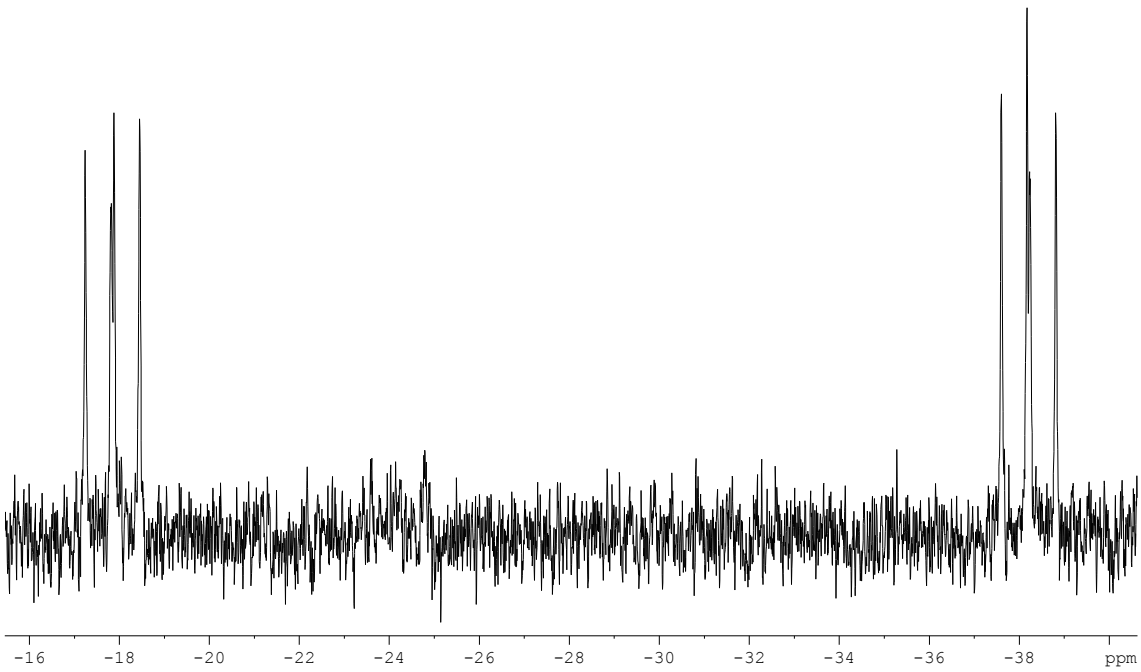

Figure 3.7 – $^{31}P\{^1H\}$ NMR spectrum of *cis*-[Fe(L^3)$_2$(H_2O)$_2$]Cl_2 in D_2O at 122 MHz.

A closer inspection of the resonances reveals that they have a small splitting of *ca*. 7 Hz, making the peaks appear like doublets of doublets. This suggests that both equatorial phosphines are magnetically inequivalent and that each axial phosphine couples to each equatorial phosphine with a slightly different coupling constant.

Attempts to grow crystals of the purple material from most organic solvents or from aqueous solution proved unsuccessful. However, it was observed that despite the complex being largely insoluble in diethyl ether, washings of the purple solid gave a very dilute pale yellow ether solution. Slow evaporation of the ether solution gave yellow crystals suitable for X-ray crystallography. The resulting structure showed that complex was the *trans* isomer of the dichloride complex *trans*-[Fe(L^3)$_2$$Cl_2$] (**24b**), with two identical L^3 bidentate phosphine ligands as in complex **23**. Due to the very low solubility of **24b** in diethyl ether, a good $^{31}P\{^1H\}$ NMR spectrum proved very difficult to obtain. When dissolved in other more polar organic solvents such as dichloromethane,

chloroform or acetone, the yellow crystals of **24b** dissolved to give a purple solution. $^{31}P\{^{1}H\}$ NMR spectroscopic analysis of this solution showed the familiar broad triplet resonances at *ca*. δ -32 and -46, suggesting that the fluxional *cis* dichloride complex **24a** had been reformed. Dissolving the *trans* complex **24b** in D_2O also gave a purple solution, the $^{31}P\{^{1}H\}$ NMR spectrum of which displayed two doublet of doublet resonances at δ -17.8 and -38.2. This suggests that the diaqua complex *cis*-$[Fe(L^3)_2(H_2O)_2]Cl_2$ had formed, identical to when the *cis* isomer **24a** was dissolved in aqueous solution.

3.6 X-ray structure of *trans*-$[Fe(L^3)_2Cl_2]$ (24b)

The X-ray analysis of the yellow crystals of **24b** grown from the evaporation of an Et_2O solution confirmed the *trans* geometry of the complex (**Figure 3.8**). The complex in the structure is unsolvated, and the asymmetric unit contains a total of 1.5 molecules of **24b**, comprising of one full molecule and one half molecule residing on a mirror plane.

The three independent crystallographic bite angles for the L^3 ligand in the structure are 82.01(2) and 81.67(2)° for the full molecule, and 80.840(17)° for the half molecule. These are all notably lower than in *cis*-$[Fe(L^3)_2(\kappa^2\text{-}O_2SO_2)]$ (**1**) (83.41(6)°), and are in general closer in value to the crystallographic bite angles for the L^1 and L^2 complexes in chapter 2. Similar to complex **1** as well as many complexes in chapter 2, the geometry of **24b** is quite distorted from a regular octahedron, with the *cis* equatorial P-Fe-P bond angles ranging between 80.840(17) and 99.160(17)° for the half molecule (molecule 1) and between 81.67(2) and 99.98(2)° for the full molecule (molecule 2). This is most notable in the full molecule in the structure, with the two L^3 ligands being staggered in relation to one another, both being tilted in opposite directions away from the equatorial plane. The phenyl rings on each L^3 ligand in this molecule are also tilted away from the axial plane in opposite directions from each other. In contrast, the L^3 ligands on the half molecule almost completely eclipse one another in the equatorial plane, with the phenyl groups lying perpendicular to the equatorial plane, giving a more regular octahedral geometry. In both molecules, the phenyl groups face one another and are between 3.30 and 3.64 Å in the symmetrical half molecule, though the less symmetrical full molecule has phenyl groups which do not directly face each other so the distance is harder to judge, though the distance between rings is approximately 3.4 Å in this case. All these distances are typical values for face to face π-π stacking interactions between two aromatic rings.[3]

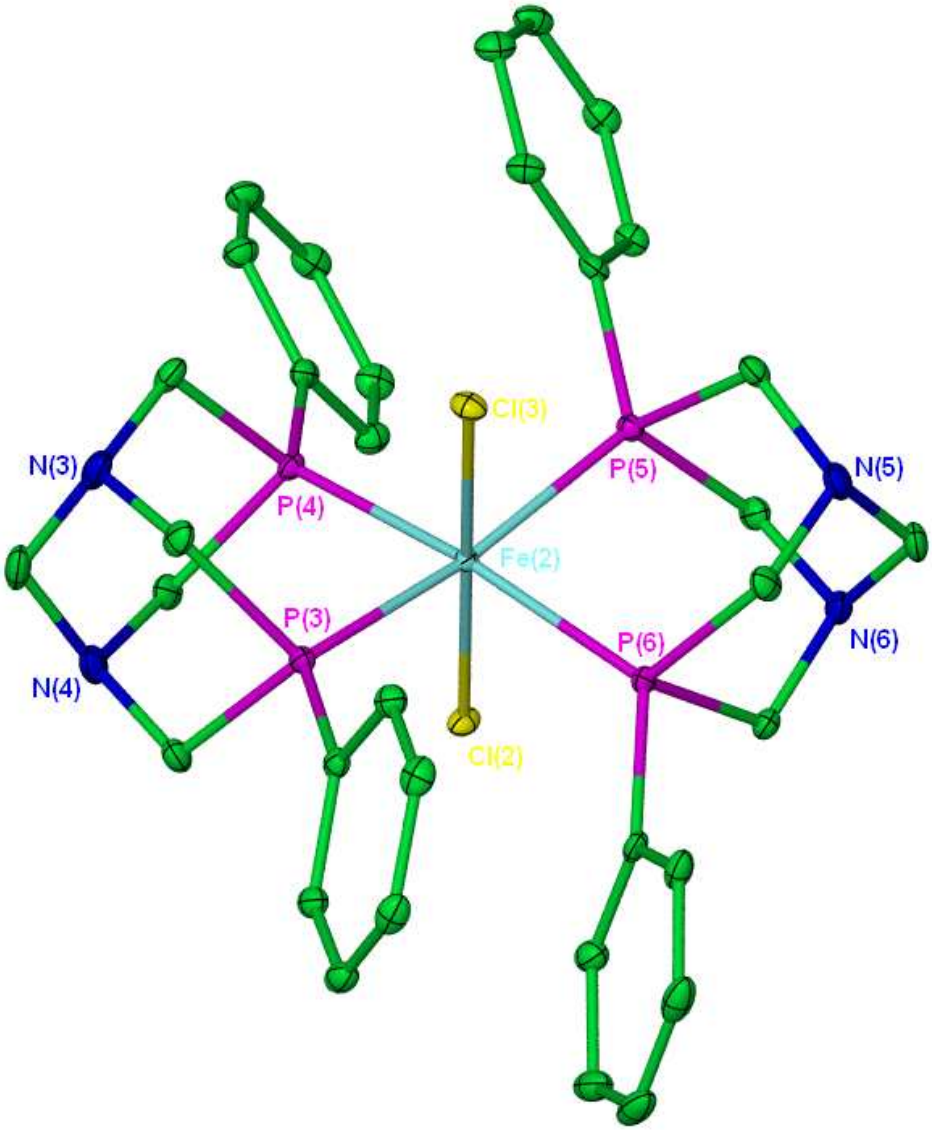

Figure 3.8 – Molecular structure of *trans*-[Fe(L^3)$_2$$Cl_2$] (24b). The asymmetric unit contains 1.5 molecules of complex 20b, consisting of one full and one half molecule (molecule 2 (full molecule) is shown). Thermal ellipsoids are at the 30% probability level. Hydrogen atoms have been omitted for clarity.

Bond Lengths (molecule 1)

Fe(1)-Cl(1)	2.3598(5)	Fe(1)-P(2)	2.2954(5)
Fe(1)-P(1)	2.2674(5)		

Bond Angles (molecule 1)

Cl(1)-Fe(1)-Cl(1)'	180.00(2)	P(2)-Fe(1)-P(2)'	180.000(17)
P(1)-Fe(1)-P(2)	80.840(17)	P(1)-Fe(1)-P(2)'	99.160(17)
P(1)-Fe(1)-P(1)'	180.000(17)	P(2)-Fe(1)-P(1)'	99.160(17)

Table 3.2 – Selected bond lengths (Å) and angles (°) for complex 24b (standard deviation in brackets).

Bond Lengths (molecule 2)

Fe(2)-Cl(2)	2.3675(5)	Fe(2)-P(4)	2.2476(5)
Fe(2)-Cl(3)	2.3610(5)	Fe(2)-P(5)	2.2615(5)
Fe(2)-P(3)	2.2469(5)	Fe(2)-P(6)	2.2506(5)

Bond Angles (molecule 2)

Cl(2)-Fe(2)-Cl(3)	177.47(2)	P(5)-Fe(2)-P(6)	81.67(2)
P(3)-Fe(2)-P(5)	168.17(2)	P(3)-Fe(2)-P(6)	99.98(2)
P(4)-Fe(2)-P(6)	169.12(2)	P(4)-Fe(2)-P(5)	98.60(2)
P(3)-Fe(2)-P(4)	82.01(2)		

Table 3.3 – Selected bond lengths (Å) and angles (°) for complex 24b (standard deviation in brackets).

The six different equatorial Fe-P bond lengths in the structure of **24b** 2.2674(5), 2.2954(5), 2.2469(5), 2.2476(5), 2.2615(5) and 2.2506(5) Å (arising from the 1.5 independent molecules in the asymmetric unit) are closer in value to the axial rather than the equatorial Fe-P bond lengths in the structure of **23**. This is because all six Fe-P bonds are *trans* to another phosphine as a result of the complex possessing *trans* geometry, and is again a result of the phosphine having a greater *trans* influence than the oxygen of the sulfate ligand on **23**. However, the Fe-P bond lengths of the similar complex *trans*-$[Fe(dmpe)_2Cl_2]$ (dmpe = 1,2-bis(dimethylphosphino)ethane) are 2.241(1) and 2.230(1) Å,[4] which are shorter than those reported for **24b**. The shorter Fe-P bond lengths in *trans*-$[Fe(dmpe)_2Cl_2]$ can be explained partially by the lower steric requirement for the smaller dimethylphosphine groups compared to the larger aromatic groups on L^3 in **24a**, and partially because of the increased σ-donor ability of the dmpe ligand compared to L^3. The Fe-Cl bonds lengths of **24b** (2.3596(5), 2.3675(5), and 2.3610(5) Å), however, are similar in value to the Fe-Cl bond lengths of $[Fe(L^2)Cl_2]$ (**15**) (2.371(2) and 2.351(5) Å). This is despite the fact that the chloride ligands in **24b** are *trans* to each other whereas they are *trans* to a phosphine donor in **15**. The Fe-Cl bond length in *trans*-$[Fe(dmpe)_2Cl_2]$ is 2.352(1) Å,[4] which is largely similar to those of **24a**.

3.7 Coordination chemistry of *cis*-$[Fe(L^3)_2Cl_2]$ (24a) with pseudo-halides

In order to compare and contrast the coordination chemistry of the L^3 complexes with that of the related L^1 and L^2 complexes, $[Fe(L^3)_2Cl_2]$ was reacted with a range of neutral and anionic ligands.

3.7.1 Reaction of *cis*-[Fe(L^3)$_2$Cl$_2$] (24a) with potassium thiocyanate

Yellow crystals of *trans*-[Fe(L^3)$_2$Cl$_2$] (**24b**) were dissolved in ethanol to give a purple solution of **24a**. An aqueous solution of potassium thiocyanate was added to the purple acetone solution, which afforded an orange suspension. Leaving the aqueous ethanol solution to slowly evaporate allowed the favourable evaporation of the ethanol, slowly increasing the water/acetone ratio. This caused more of the neutral bis(thiocyanato) complex **25a** to precipitate out of solution (**Scheme 3.2**), resulting in a 78% yield of the bis(thiocyanato) complex (**25a**).

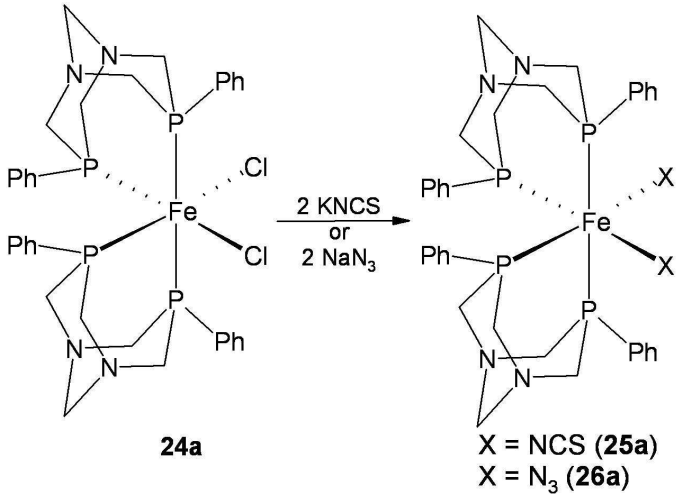

Scheme 3.2 – Synthesis of *cis*-[Fe(L^3)$_2$(NCS)$_2$] (25a) and *cis*-[Fe(L^3)$_2$(N_3)$_2$] (26a).

$^{31}P\{^1H\}$ NMR spectroscopy of orange **25a** in $CDCl_3$ after *ca*. 20 minutes showed two second order resonances at δ -31.0 and -38.6, as well as a singlet at δ -42.2 in a 4:1 ratio respectively (**Figure 3.9**).

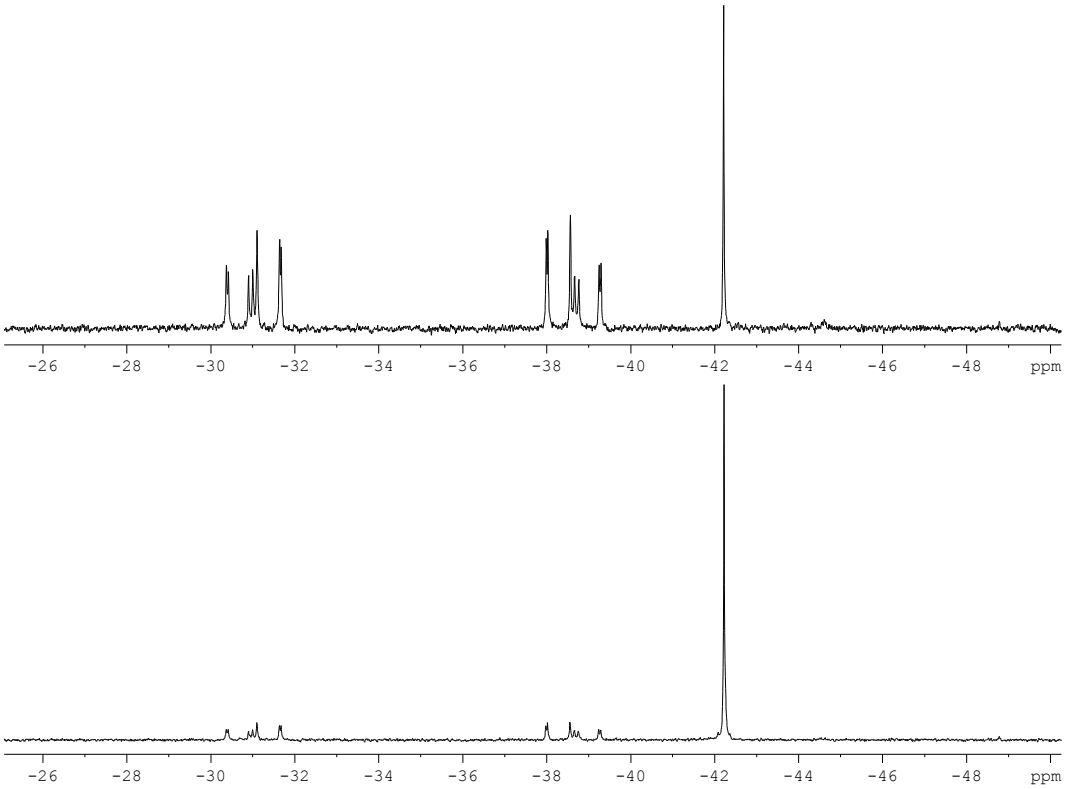

Figure 3.9 – $^{31}P\{^{1}H\}$ NMR spectroscopy of *cis*- and *trans*-$[Fe(L^3)_2(NCS)_2]$ (25a) and (25b) in $CDCl_3$ at 122 MHz after *ca*. 20 minutes (top) and *ca*. 48 hours (bottom).

The resonance pattern corresponds to the *cis*-$[Fe(L^3)_2(NCS)_2]$ complex (**25a**), whereas the singlet represents the related *trans* isomer *trans*-$[Fe(L^3)_2(NCS)_2]$ (**25b**). Over time the ratio of *cis* to *trans* isomers in $CDCl_3$ solution decreased, as shown by the $^{31}P\{^{1}H\}$ NMR spectrum recorded after 48 hr. (**Figure 3.9**), showing that the *cis*:*trans* ratio had changed from 4:1 to 2:3. Orange crystals suitable for X-ray crystallography also grew over time, and which proved to be of the *trans* isomer **25b**.

^{1}H NMR spectroscopic analysis of the mixture of *cis* and *trans* isomers showed a complex spectrum. As in the ^{1}H NMR spectrum of *cis*-$[Fe(L^3)_2(\kappa^2\text{-}O_2SO_2)]$ (**23**), *cis*-$[Fe(L^3)_2(NCS)_2]$ (**25a**) gave rise to five separate AB resonances arising from the four P-CH_2-N methylene groups and the one N-CH_2-N group. The *trans* isomer **25b**, displayed one AB system and a singlet as a result of the increased symmetry of the *trans* isomer, in which all four P-CH_2-N methylene groups are magnetically equivalent. The two protons on each P-CH_2-N methylene group are, however, magnetically inequivalent, as one is essentially axial and the other is equatorial in the PN_2 six-membered rings of the L^3 ligand. The N-CH_2-N methylene group gave rise to a singlet as both protons on this methylene group are magnetically equivalent.

3.7.2 X-ray structure of *trans*-[Fe(L^3)$_2$(NCS)$_2$] (25b)

The X-ray analysis of the orange crystals isolated from the $CDCl_3$ solution of **25b** showed the structure to be of the *trans* isomer of the bis(isothiocyanato) complex *trans*-[Fe(L^3)$_2$(NCS)$_2$] (**25b**) (**Figure 3.10**), with the structure being unsolvated. The asymmetric unit of the structure contains one half molecule of **25b**. The coordinated thiocyanate ligands bind to the iron centre *via* the nitrogen atoms, which is consistent with the L^1 isothiocyanato complex [Fe(L^1)(NCS)$_2$] (**6** in Chapter 2).

The Fe-N bond length in **25b** is 1.9387(14) Å, which is noticeably shorter than the Fe-N bond lengths in complex **6** (1.960(3) and 1.952(3) Å). This is because the thiocyanate ligands in **6** are *trans* to phosphine donors, which have a greater *trans* influence than the nitrogen of the other thiocyanate ligand in complex **25b**. The greater *trans* influence of the phosphine groups compared to nitrogen causes the Fe-N bond in **6** to become longer and therefore weaker. As a result, it would therefore be expected that the Fe-P bonds in the equatorial plane in complex **25b** to be longer than those of **6** in Chapter 2 as they are now positioned *trans* to other phosphine donors from another L^3 ligand. This is indeed the case, with the equatorial Fe-P bond lengths in **6** being 2.1840(10) and 2.1907(11) Å, compared to 2.2453(4) and 2.2592(4) Å for complex **25b**. This phenomenon is also observed for similar *cis* and *trans* iron(II) thiocyanato tetraphosphine complexes in the literature. The Fe-N bond lengths of *trans*-[Fe(*rac*-prP$_4$)(NCS)$_2$] (*rac*-prP$_4$ = 1,1,4,8,11,11-hexaphenyl-1,4,8,11-tetraphosphaundecane) are 1.932(2) and 1.933(2) Å compared to 1.973(2) and 1.964(2) Å for *cis*-α-[Fe(*rac*-prP$_4$)(NCS)$_2$].[5]

The conformation of **25b** is similar to that of the full molecule in the X-ray structure of *trans*-[Fe(L^3)$_2$Cl$_2$] **24b**, *i.e.* the two L^3 ligands on the metal are staggered with respect to each other and are both tilted in opposite directions away from the equatorial plane. The phenyl groups are also twisted from the axial plane and face the equivalent phenyl group on the opposite ligand, suggesting that π-π interactions of *ca*. 3.3 Å are also occurring in this structure.

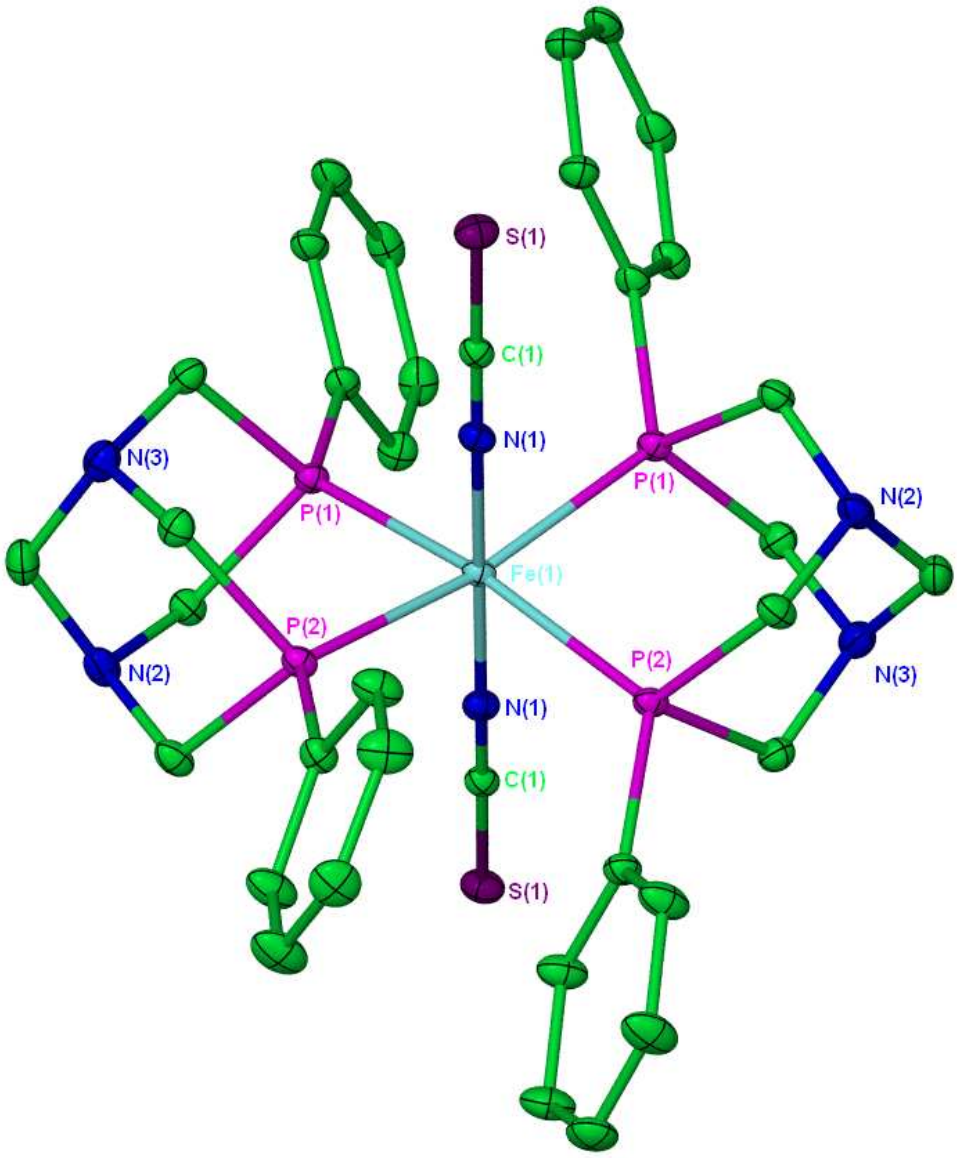

Figure 3.10 – Molecular structure of *trans*-[Fe(L^3)$_2$(NCS)$_2$] (25b). The asymmetric unit contains a ½ molecule of complex 25b. Thermal ellipsoids are at the 30% probability level. Hydrogen atoms have been omitted for clarity.

Bond Lengths

Fe(1)-P(1)	2.2453(4)	N(1)-C(1)	1.165(2)
Fe(1)-P(2)	2.2592(4)	S(1)-C(1)	1.6339(16)
Fe(1)-N(1)	1.9387(14)		

Bond Angles

N(1)-Fe(1)-N(1)'	179.20(8)	P(1)-Fe(1)-P(1)'	98.24(2)
P(1)-Fe(1)-P(2)'	166.572(15)	P(2)-Fe(1)-P(2)'	99.97(2)
P(2)-Fe(1)-P(1)'	166.572(15)	Fe(1)-N(1)-C(1)	177.58(12)
P(1)-Fe(1)-P(2)	82.469(15)	N(1)-C(1)-S(1)	179.50(16)

Table 3.4 – Selected bond lengths (Å) and angles (°) for complex 25b (standard deviation in brackets).

3.7.3 Reaction of *cis*-[Fe(L^3)$_2$Cl$_2$] (24a) with sodium azide

The reaction of **24a** with sodium azide was carried out in a similar manner to the reaction of **24a** with potassium thiocyanate. An aqueous solution of sodium azide was added to an ethanol solution of *cis*-[Fe(L^3)$_2$Cl$_2$] (**24a**), resulting in a purple/red suspension presumably of *cis*-[Fe(L^3)$_2$(N_3)$_2$] (**26a**). As before, the ethanol was allowed to evaporate, resulting in the formation of a purple/red precipitate.

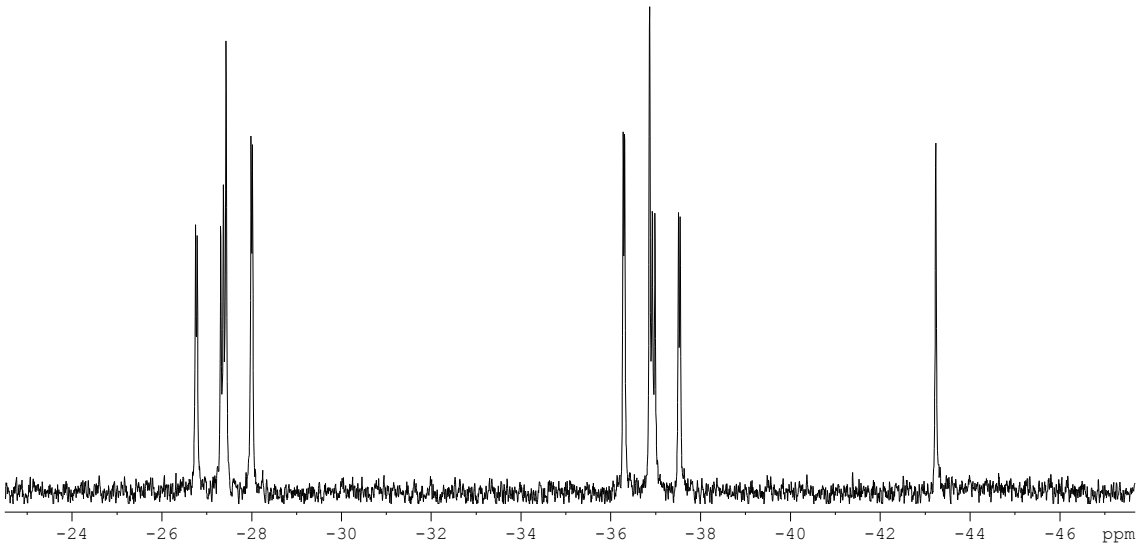

Figure 3.11 – $^{31}P\{^1H\}$ NMR spectrum of *cis*- and *trans*-[Fe(L^3)$_2$(N_3)$_2$] (26a, 26b) in $CDCl_3$ at 122 MHz after *ca.* 20 minutes. The spectrum was identical after 48 hours.

$^{31}P\{^1H\}$ NMR spectroscopy of the purple/red solid in $CDCl_3$ after *ca*. 20 minutes showed two second order resonances at δ -27.4 and -36.9, as well as a singlet at δ -43.2 in an 11:1 ratio (**Figure 3.11**). As with the thiocyanate reaction, the reaction was monitored over time, although the $^{31}P\{^1H\}$ NMR spectrum was unchanged after 48 hours, showing that the isomerisation process is not as favourable for the bis(azido) complexes (**26a** and **26b**). As a result, the crystallisation of neither the *cis* or *trans* isomers could be achieved. The formation of both *cis* and *trans* isomers of **26** is in contrast to the synthesis of the similar bis(azido) complex *trans*-[Fe(dmpe)$_2$(N_3)$_2$] (dmpe = bis(dimethylphosphino)ethane), which showed no evidence for the formation of the *cis* isomer and only the *trans* isomer was observed in the $^{31}P\{^1H\}$ NMR spectrum.[6]

The ^1H NMR spectrum of the mixture of **26a** and **26b** showed a similar series of resonances to that of the bis(thiocyanato) complexes **25a** and **25b**. Therefore, one AB system and a singlet were observed for the *trans* isomer **25b**, and five AB resonances for the *cis* isomer **25a**. IR spectroscopy of the mixture showed a peak at 2043 cm^{-1}, which is likely to be of the *cis* isomer **25a** due to the 11:1 *cis*:*trans* ratio. The *cis* isomer

would be expected to show both symmetric and antisymmetric stretches, though one peak was also observed for $[Fe(L^1)(N_3)_2]$ (**7**) in Chapter 2 (section 2.5) and by Field *et al.* in related *cis* bis(azido) iron(II) phosphine complexes.[7]

3.8 Coordination chemistry of *cis*-$[Fe(L^3)_2Cl_2]$ (24a) with carbonate

The reaction of an ethanol solution of *cis*-$[Fe(L^3)_2Cl_2]$ (**24a**) with an aqueous solution of sodium carbonate gave a pink suspension of $[Fe(L^3)_2(\kappa^2\text{-}O_2CO)]$ (**27**) (**Scheme 3.3**).

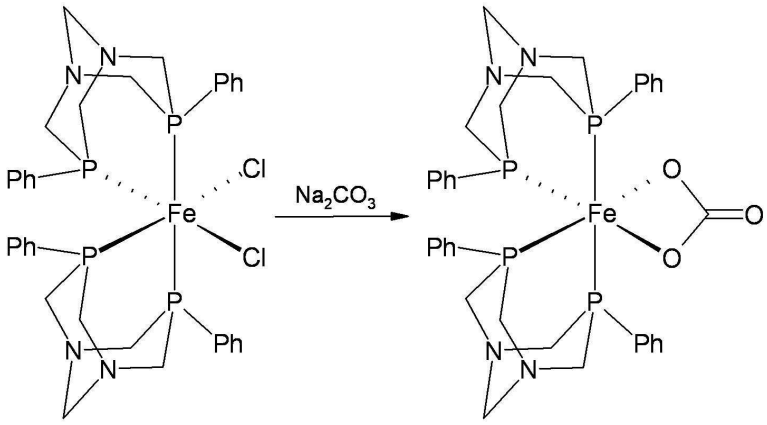

Scheme 3.3 – Reaction of *cis*-$[Fe(L^3)_2Cl_2]$ (24a) with sodium carbonate to give the carbonato complex $[Fe(L^3)_2(\kappa^2\text{-}O_2CO)]$ (27).

The $^{31}P\{^1H\}$ NMR spectrum of the pink precipitate in $CDCl_3$ showed two triplet resonances at δ -20.2 and -41.4 with $^2J_{P\text{-}P}$ = 72.0 Hz (**Figure 3.12**).

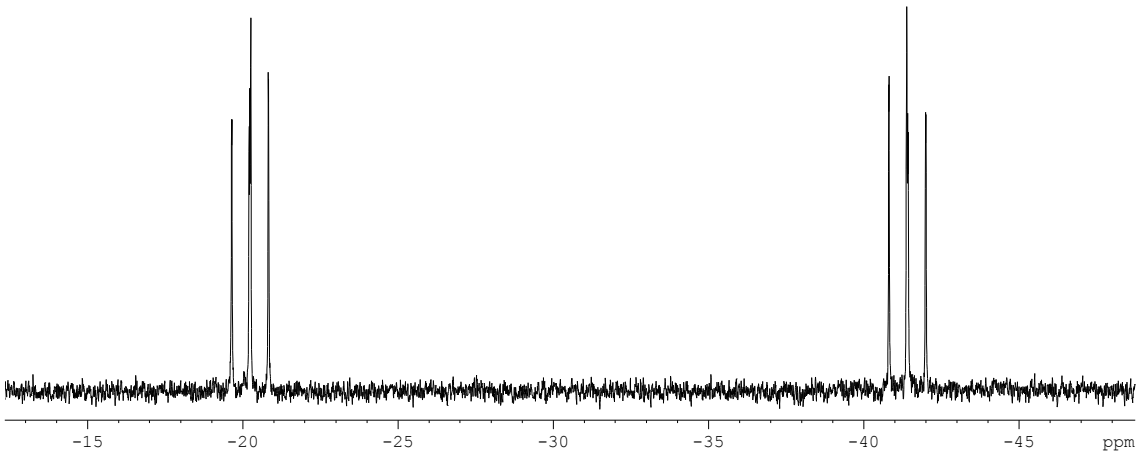

Figure 3.12 – $^{31}P\{^1H\}$ NMR spectrum of *cis*-$[Fe(L^3)_2(\kappa^2\text{-}O_2CO)]$ (27) in $CDCl_3$ at 122 MHz.

The ^{1}H NMR spectrum of **27** showed the expected pattern for a bis L^3 complex possessing *cis* geometry, *i.e.* four AB resonances for the P-CH_2-N methylene protons and one AB system for the N-CH_2-N methylene protons (**Figure 3.13**).

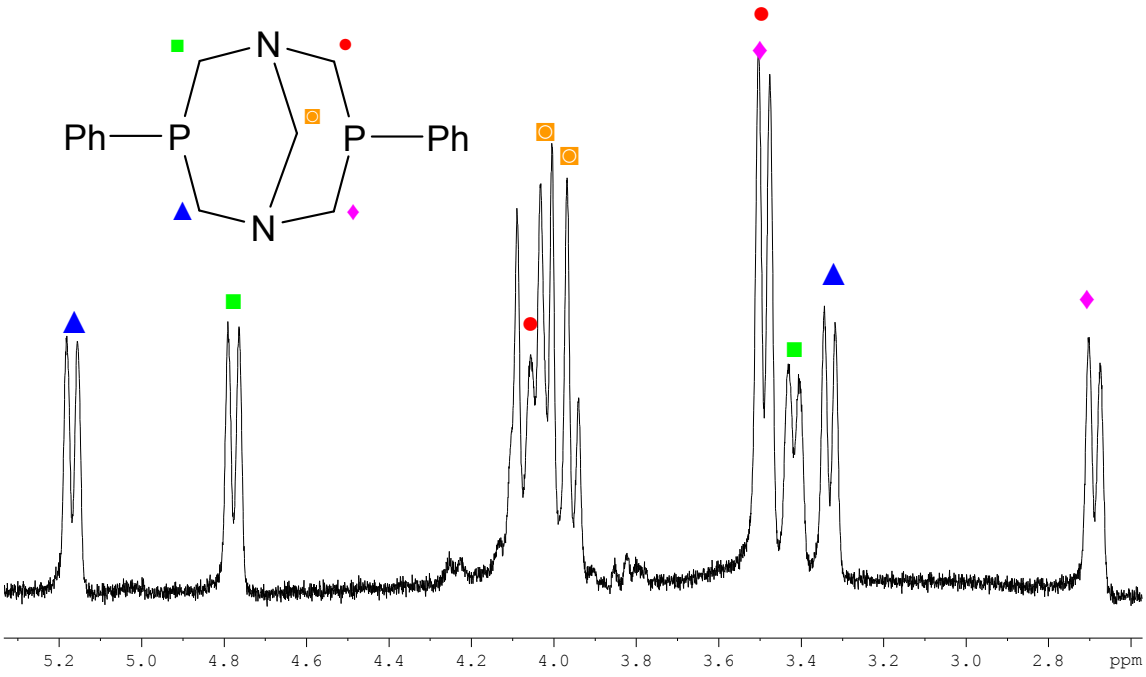

Figure 3.13 – Selected ^{1}H NMR spectrum of *cis*-[Fe(L^3)$_2$(κ^2-O_2CO)] (27) in $CDCl_3$ at 500 MHz. The different chemical environments of the ligand methylene groups shown arise from its coordination to the metal and *cis* octahedral geometry of the complex.

The N-CH_2-N protons give rise to the second order AB system centred at δ 3.9 (▣), with the four remaining P-CH_2-N methylene proton groups giving four sets of AB systems between δ 5.2 and 2.6 (some of which overlap) (▲, ■, ●, ♦). The connectivity of these resonances was confirmed by ^{1}H COSY NMR spectroscopy. As with **23**, the four P-CH_2-N methylene groups (▲, ■, ●, ♦) cannot be individually assigned to a particular P-CH_2-N group, which are only magnetically inequivalent due to the *cis* geometry of the complex.

3.9 X-ray structure of [Fe(L^3)$_2$(CO_3)]·7H_2O (27·7H_2O)

Purple crystals of **27** were grown from the slow evaporation of the aqueous reaction filtrate over *ca*. eight weeks, and are of the heptahydrate (**27**·7H_2O). The structure confirms that the two chloride ligands have been replaced with a bidentate carbonate molecule, giving a *cis* octahedral geometry as expected (**Figure 3.14**). The chelating carbonate ligand has a small bite angle (65.01(9)°), which results in a structure that is far from a regular octahedral geometry. The *cis* equatorial bond angles range between 65.01(9) and 100.98(3)°. The crystallographic bite angles of the L^3 ligand in the

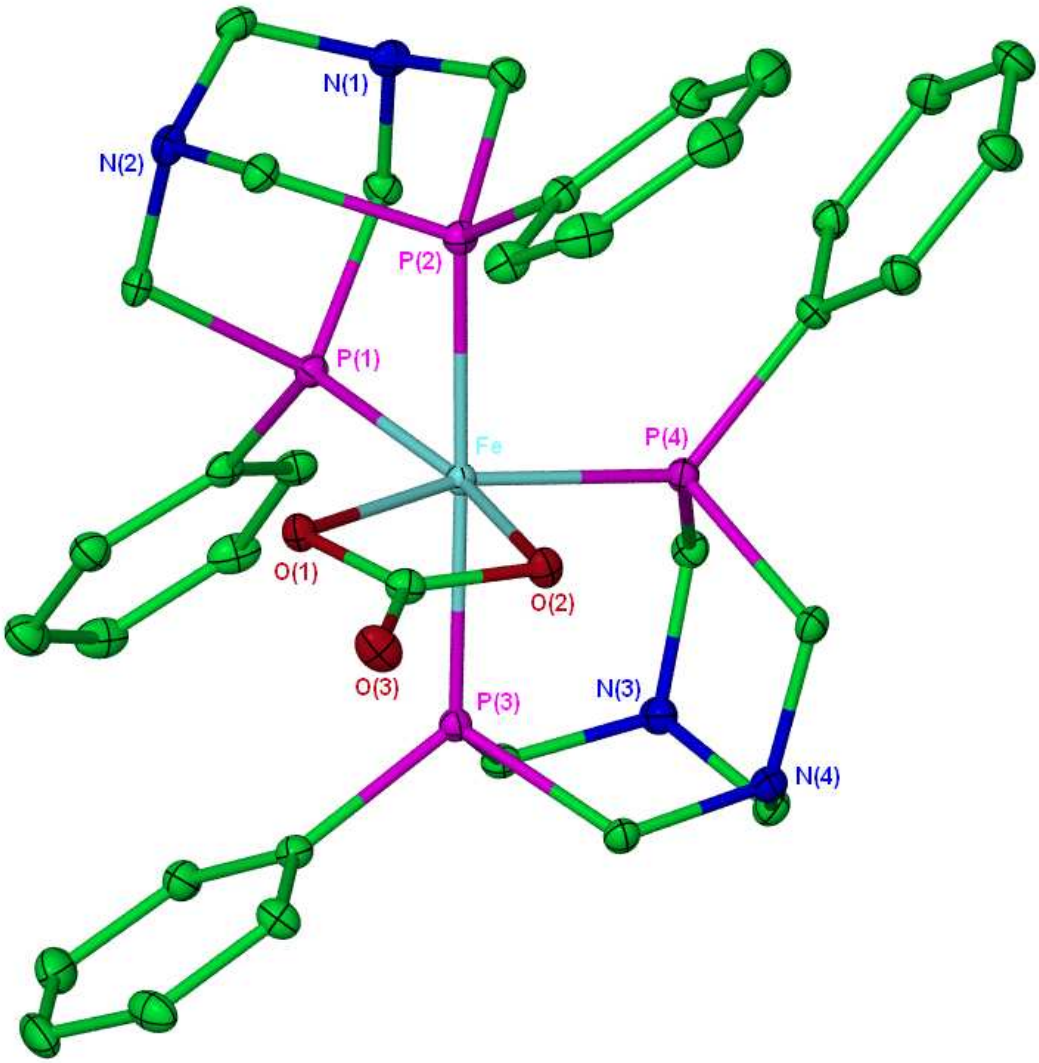

Figure 3.14 – Molecular structure of $[Fe(L^3)_2(\kappa^2\text{-}O_2CO)]\cdot 7H_2O$ ($27\cdot 7H_2O$). Thermal ellipsoids are at the 30% probability level. Hydrogen atoms and included water molecules have been omitted for clarity.

Bond Lengths

Fe(1)-P(1)	2.2046(9)	Fe(1)-O(2)	2.016(2)
Fe(1)-P(2)	2.2631(10)	O(1)-C(20)	1.317(4)
Fe(1)-P(3)	2.2573(10)	O(2)-C(20)	1.315(4)
Fe(1)-P(4)	2.1910(9)	O(3)-C(20)	1.246(4)
Fe(1)-O(1)	2.029(2)		

Bond Angles

P(1)-Fe(1)-P(2)	82.61(3)	P(1)-Fe(1)-O(1)	99.29(7)
P(3)-Fe(1)-P(4)	82.89(3)	P(4)-Fe(1)-O(2)	95.08(7)
O(1)-Fe(1)-O(2)	65.01(9)	O(1)-C(20)-O(2)	111.4(3)
P(1)-Fe(1)-P(4)	100.98(3)		

Table 3.5 – Selected bond lengths (Å) and angles (°) for complex $27\cdot 7H_2O$ (standard deviation in brackets).

structure are 82.61(3) and 82.89(3)°, which are similar to those in complexes **23**, **24b**, and **25b**, though somewhat less than that in the coordinated sulfate complex **23**. In comparison with the X-ray structure of [Fe(L^1)(κ^2-O_2CO)] (complex **8** in Chapter 2), the Fe-O iron-carbonate bonds are similar (2.029(2) and 2.016(2) Å for **27** compared to 2.044(5) and 2.073(5) Å for complex **8**). The O-Fe-O bond angle in complex **27** (65.01(9) Å) is larger than that of **8** (63.8(2) Å).

3.10 Reaction of *cis*-[Fe(L^3)$_2$Cl$_2$] (24a) with CO

The reaction of an aqueous solution of *cis*-[Fe(L^3)$_2$Cl$_2$] (**24a**) with CO resulted in a colour change from a purple to a yellow solution over *ca*. 1 hr, suggesting that one or both of the coordinated chlorides may have been displaced by a carbonyl ligand to give a complex such as **28a** (**Scheme 3.4**) or a dicarbonyl such as [Fe(L^3)$_2$(CO)$_2$]Cl$_2$.

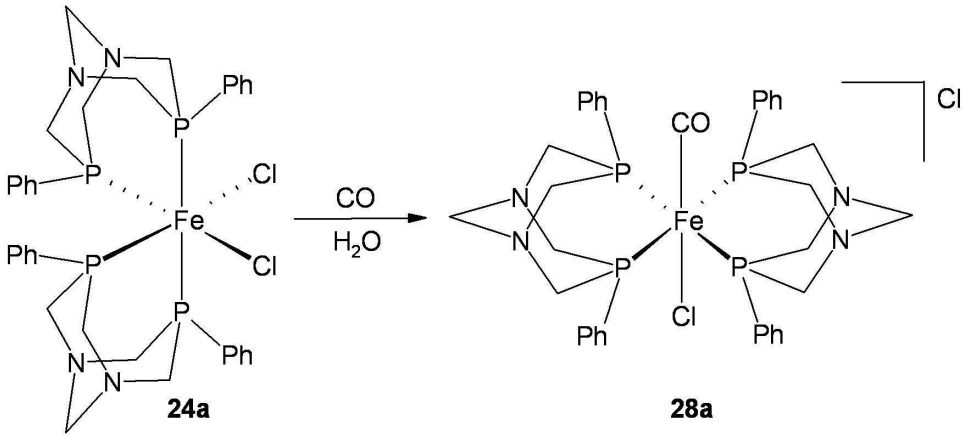

Scheme 3.4 – Possible product from the reaction of *cis*-[Fe(L^3)$_2$Cl$_2$] (24a) with CO in aqueous solution.

The $^{31}P\{^1H\}$ NMR spectrum of the yellow solution in D_2O showed a singlet resonance at δ -51.1 (**Figure 3.15**), consistent with formation of a *trans* L^3 complex. However, this does not determine whether the *trans* complex is mono- or di-substituted, meaning that the identity of the complex could be one of three likely structures, (i) [Fe(L^3)$_2$(CO)$_2$]$^{2+}$, (ii) [Fe(L^3)$_2$(CO)(H_2O)]$^{2+}$, or (iii) [Fe(L^3)$_2$(CO)(Cl)]$^+$.

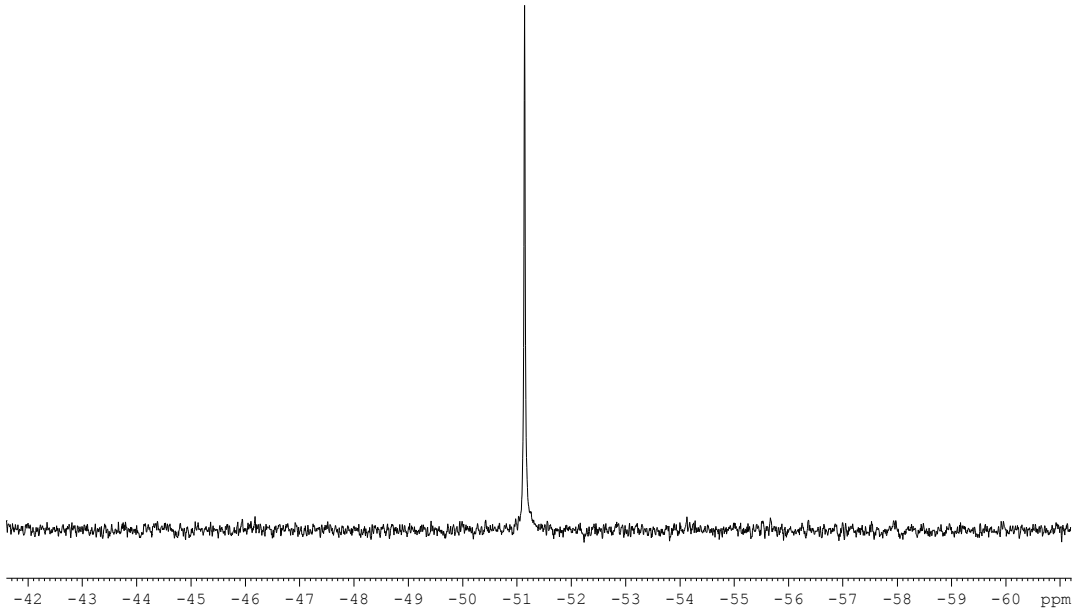

Figure 3.15 - $^{31}P\{^{1}H\}$ NMR spectrum following reaction of 24a with CO in D_2O at 122 MHz.

^{1}H NMR spectroscopy showed two sets of AB doublets at δ 5.1, 4.6 and 4.0, 3.7, as well as a singlet at δ 4.1 (**Figure 3.16**). This indicates that the complex is mono-substituted *i.e.* product (ii) or (iii), since the ^{1}H NMR spectrum of (i) would give one pair of doublets and one singlet in a 2:2:1 ratio because the four P-C$\underline{H_2}$-N proton groups on each L^3 ligand would be equivalent.

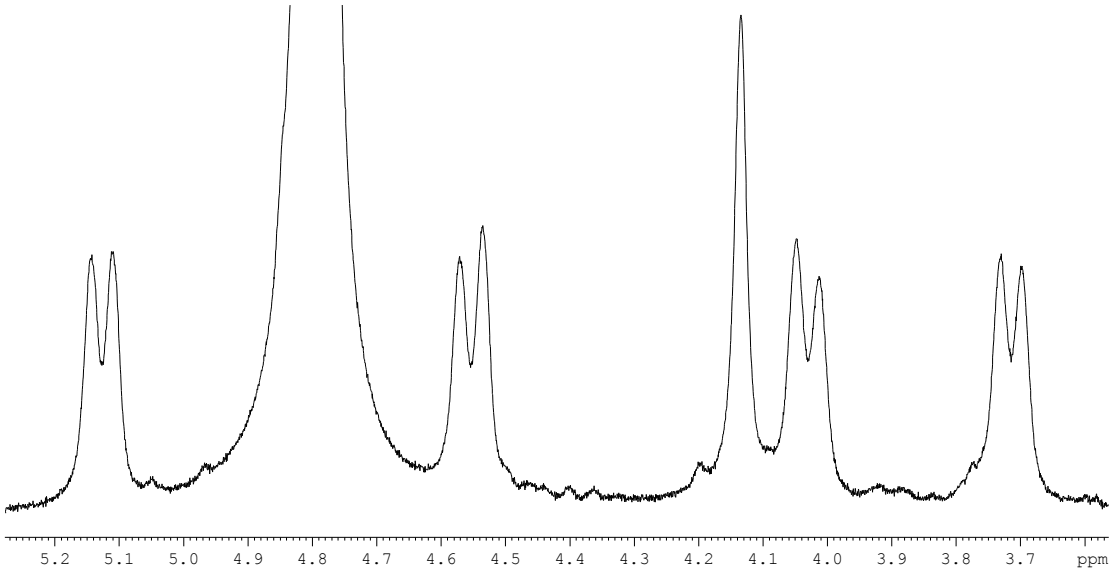

Figure 3.16 – ^{1}H NMR spectrum following reaction of 24a with CO in D_2O at 500 MHz.

When the reaction was repeated with ^{13}CO the same yellow solution was produced, but now the $^{31}P\{^{1}H\}$ NMR spectrum showed a doublet at δ -51.1 with $^{2}J_{P\text{-}C}$ = 25.8 Hz. The doublet indicates that only one ^{13}CO ligand is bound to the iron metal. The $^{13}C\{^{1}H\}$ NMR spectrum is consistent with this, showing a quintet ^{13}CO resonance at δ 214.7.

IR spectroscopy showed a single ^{12}CO stretching frequency at 1939 cm^{-1}, which would be expected for a mono-carbonyl complex. The IR spectrum of the corresponding ^{13}CO complex showed the equivalent ^{13}CO stretching frequency at 1895 cm^{-1}. This value is very close to the calculated ^{13}CO value for the complex, which is 1896 cm^{-1}. Mass spectrometry of the complex showed the major peak to be at m/z = 747.1, which equates to the chloride carbonyl complex cation $[Fe(L^3)_2(CO)Cl]^+$. As a result of the NMR, IR, and mass spectral evidence the complex has been identified as the *trans*-$[Fe(L^3)_2(CO)(Cl)]$ Cl (**28a**)

When the *trans*-$[Fe(L^3)_2Cl_2]$ complex (**24b**) was reacted with CO in diethyl ether solution (**Scheme 3.5**), a pale orange precipitate was formed suggesting the formation of a different product to that found in aqueous solution.

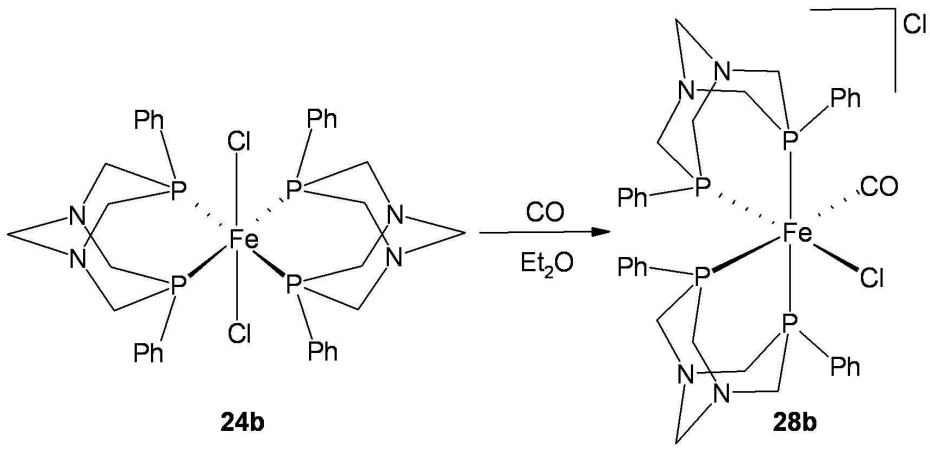

24b **28b**

Scheme 3.5 – Reaction of *trans*-$[Fe(L^3)_2Cl_2]$ (24b) with CO in diethyl ether solution.

The $^{31}P\{^1H\}$ NMR spectrum of the orange solid showed four main resonances at δ -39.4, -55.3, -59.4, and -69.0, which are all doublets of doublets of doublets (**Figure 3.17**). The resonance at δ -69.0 appears simplified due to two of the $^2J_{P\text{-}P}$ values being very similar. This coupling pattern means that all four phosphine groups on the complex are inequivalent, indicating that the product is *cis*-$[Fe(L^3)_2(CO)Cl]Cl$ (**28b**).

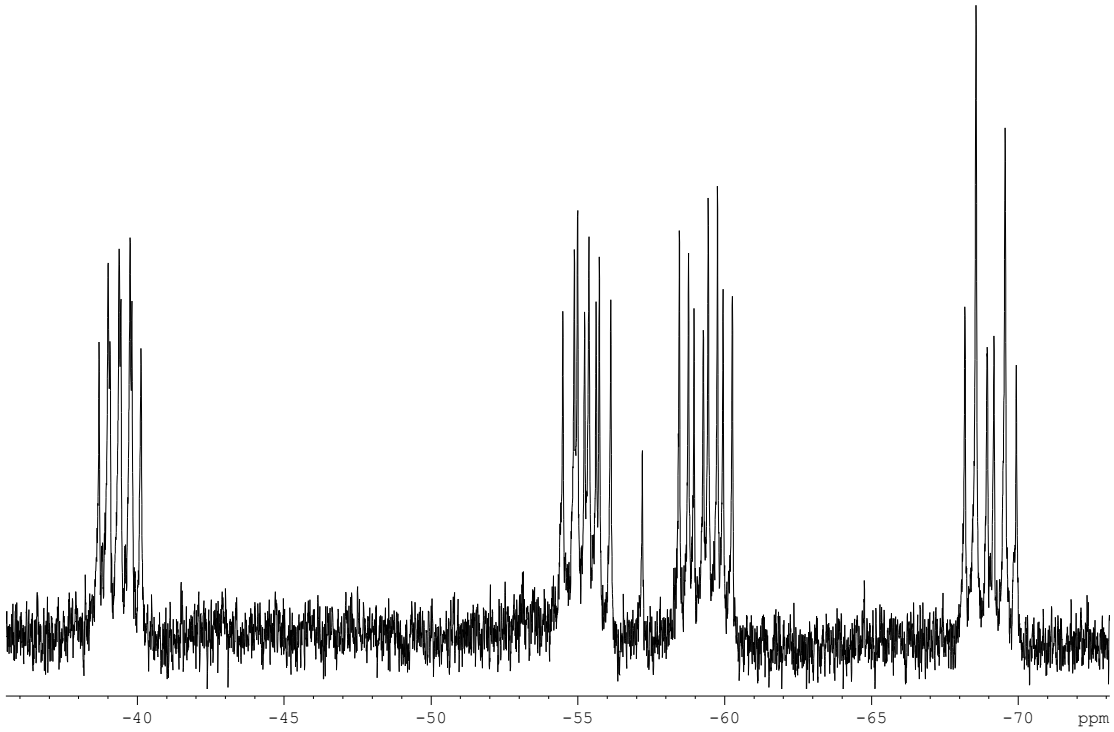

Figure 3.17 - $^{31}P\{^{1}H\}$ NMR spectrum of *cis*-$[Fe(L^3)_2(CO)Cl]Cl$ (28b) in $CDCl_3$ at 122 MHz.

When **28b** was redissolved in D_2O a yellow solution is immediately observed, the $^{31}P\{^{1}H\}$ NMR spectrum of which showed a singlet resonance at δ -51.1. This is the same resonance as observed for complex **28a**, meaning that *cis*-$[Fe(L^3)_2(CO)Cl]Cl$ (**28b**) undergoes an isomerisation in water to give *trans*-$[Fe(L^3)_2(CO)Cl]Cl$ (**28a**). Another example of the synthesis of both *cis* and *trans* carbonyl chloride complexes under different conditions is provided by Bellerby *et al*.[8] When *trans*-$[Fe(dmpe)_2Cl_2]$ was reacted with CO in an acetone solution, the corresponding *cis* carbonyl chloride *cis*-$[Fe(dmpe)_2(CO)Cl]^+$ was formed, which was isolated as the tetraphenylborate salt upon addition of $NaBPh_4$. In contrast, when *trans*-$[Fe(dmpe)_2Cl_2]$ was reacted with CO in an acetone solution at reflux, the majority of the material isomerised to give *trans*-$[Fe(dmpe)_2(CO)Cl]^+$ as the major product, though some *cis*-$[Fe(dmpe)_2(CO)Cl]^+$ was also formed. When depe was used as the ligand, *trans*-$[Fe(depe)_2Cl_2]$ reacted with CO in methanol to give *trans*-$[Fe(depe)_2(CO)Cl]BPh_4$ in the presence of $NaBPh_4$, and no *cis* isomer was formed.

3.11 Reaction of *cis*-$[Fe(L^3)_2Cl_2]$ (24a) with sodium borohydride

Two equivalents of sodium borohydride were added to a suspension of *cis*-$[Fe(L^3)_2Cl_2]$ (**24a**) in ethanol under a nitrogen atmosphere (**Scheme 3.6**). The purple solution quickly changed colour to orange, followed by formation of an orange precipitate over *ca*. 1 hr. The reaction mixture was stirred at room temperature for a further 1 hr to

allow the reaction of any undissolved starting material with the borohydride. The resulting crude material was recrystallised from degassed benzene to give *trans*-[Fe(L^3)$_2$(H)Cl] (**29**) as a dark orange microcrystalline solid.

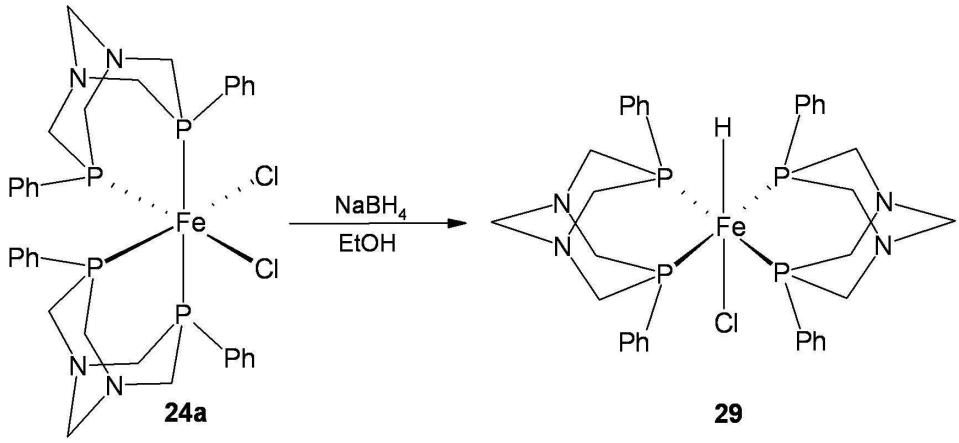

Scheme 3.6 – Reaction of *cis*-[Fe(L^3)$_2$Cl$_2$] (24a) with $NaBH_4$ to give *trans*-[Fe(L^3)$_2$(H)Cl] (29).

The $^{31}P\{^1H\}$ NMR spectrum of **29** in C_6D_6 showed a singlet at δ -27.5 consistent with a *trans* complex. When the same ^{31}P NMR experiment was run without proton decoupling, the singlet split into a doublet with a $^2J_{P\text{-}H}$ coupling constant of 49.0 Hz (**Figure 3.18**). This suggests the phosphorus resonance is coupling to one hydride nucleus, as two hydride nuclei would give rise to a triplet resonance pattern.

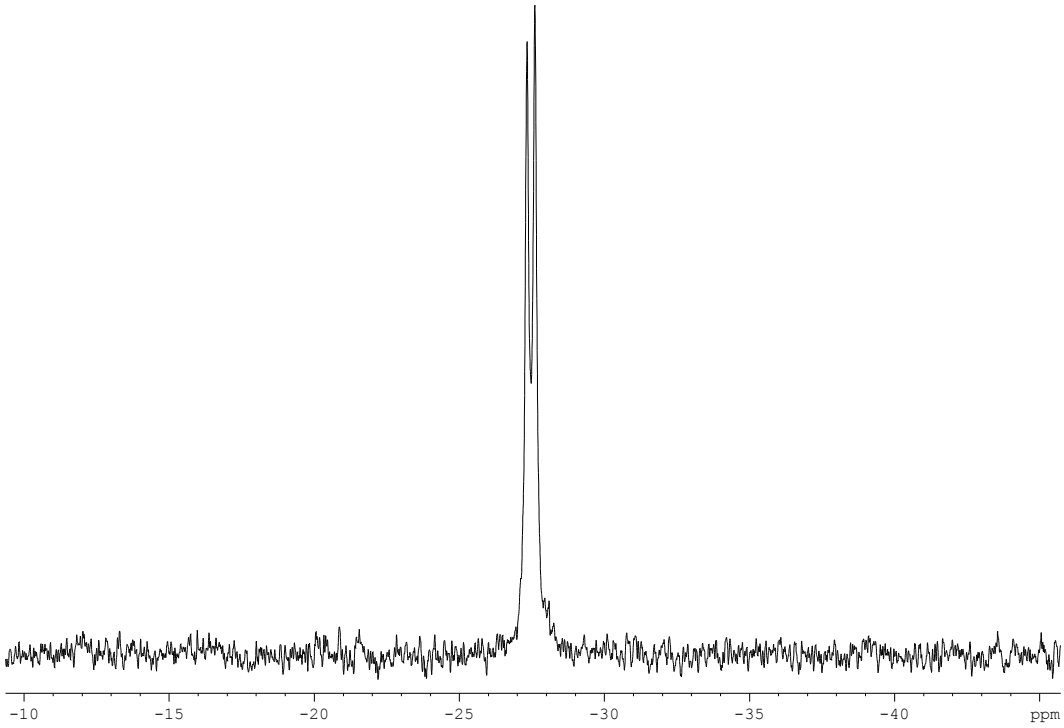

Figure 3.18 - ^{31}P NMR spectrum of *trans*-[Fe(L^3)$_2$(H)Cl] (29) in C_6D_6 at 162 MHz. Long range proton decoupling is disabled.

The ^{1}H NMR spectrum of the solid showed a quintet at δ -28.45 due to the coupling of the hydride with the four equivalent phosphorus nuclei, confirming the presence of the hydride in the complex (**Figure 3.19**). The $^{2}J_{P\text{-}H}$ coupling constant matches that of the $^{31}P\{^{1}H\}$ NMR experiment.

These observations are similar to those of Tyler and coworkers for the similar *trans*-[Fe(DMeOPrPE)$_2$(H)Cl] complex (DMeOPrPE = 1,2-bis(bis-(methoxypropyl)phosphino)ethane), the (uncoupled) ^{31}P NMR spectrum of which showed a doublet at δ 83.5 with a $^{2}J_{P\text{-}H}$ coupling constant of 45 Hz, indicative of *cis* P-H coupling. The ^{1}H NMR spectrum showed a quintet at δ -31.8.[9] Holah and coworkers also found similar observations in the complex *trans*-[Fe(dppm)$_2$(H)Cl] (dppm = bis(diphenylphosphino)methane), the $^{31}P\{^{1}H\}$ NMR spectrum of which showed a singlet at δ 24.2. The ^{1}H NMR spectrum showed a quintet at δ -21.2 with $^{2}J_{P\text{-}H}$ = 44 Hz.[10]

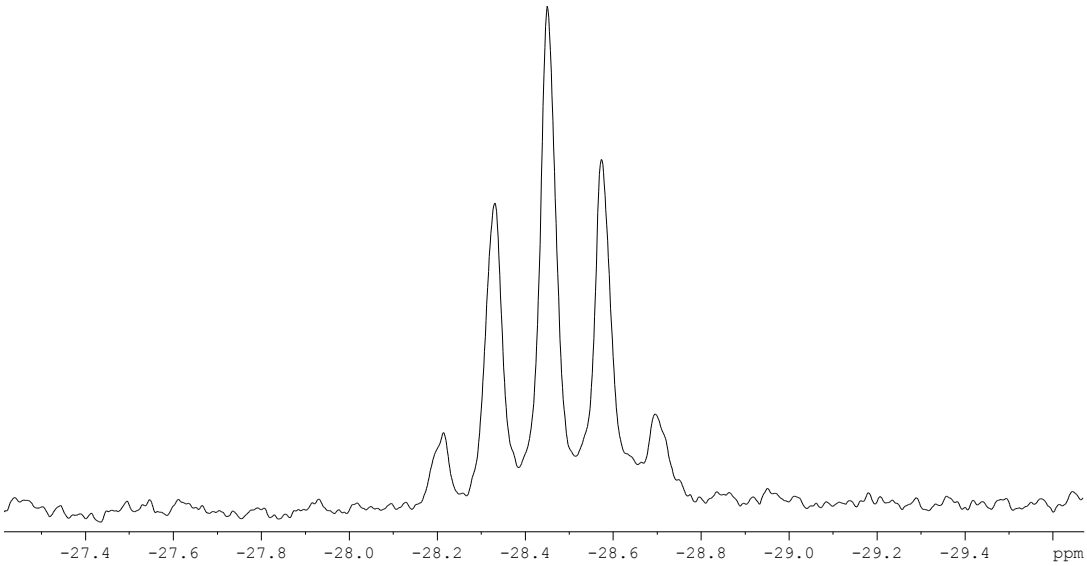

Figure 3.19 – Hydride region of the ^{1}H NMR spectrum of *trans*-[Fe(L^{3})$_2$(H)Cl] (29) in C_6D_6 at 400 MHz.

Mass spectrometry of the product was carried out in order to fully characterise it and determine which ligand occupies the site *trans* from the hydride. The ES-MS of **29** was first carried out in acetonitrile and gave the major peak at *m*/*z* = 685.16, which fits the molecular weight of the five coordinate complex [Fe(L^{3})$_2$(H)]$^{+}$. This unfortunately does not give light to the identity of the other ligand, which has been removed during the ionisation process. The mass spectrum was re-recorded in dichloromethane under an inert atmosphere and now afforded the major peak at *m*/*z* = 720.13, corresponding to *trans*-[Fe(L^{3})$_2$(H)Cl]$^{+}$.

The reaction of **24a** with six equivalents of $NaBH_4$ in EtOH in an attempt to synthesise the dihydride complex was also attempted. The $^{31}P\{^1H\}$ NMR spectrum of the reaction solution showed three broad resonances at *ca.* δ -4, -6 and -29 in a 1:3:1 ratio, respectively. Attempts to isolate any complexes from the reaction solution proved unsuccessful.

3.12 X-ray structure of *trans*-[Fe(L^3)$_2$(H)Cl]·1.5C_6H_6 (29·1.5C_6H_6)

The orange microcrystalline solid of **29** formed from benzene solution upon leaving it at room temperature for a few days. The crystals did not decompose in air even after exposure for 24 hours, though the ethanolic solution of unpurified **29** turned brown and decomposed upon exposure to air after a few minutes. The X-ray analysis showed the expected octahedral iron complex with two bidentate L^3 ligands arranged in a *trans* configuration. One of the axial sites is occupied by a chloride ligand, while the opposite *trans* axial site does not have significant electron density. This lack of electron density is expected for a hydride ligand, which possesses no electrons other than the electron pair used in bonding to the iron centre. In collaboration with the NMR and mass spectral data, it can therefore be concluded that the complex is indeed the hydride chloride complex *trans*-[Fe(L^3)$_2$(H)Cl] (**29**) (**Figure 3.20**).

The asymmetric unit of the structure contains two independent half molecules of complex **29**. The complex crystallises with one half molecule of benzene with full occupancy, as well as one whole molecule of benzene exhibiting 1:1 disorder. The compound is therefore **29**·1.5C_6H_6. The hydride ligands in the structure cannot be located by their electron density, therefore the hydride nuclei H(1) and H(2) have been modelled equidistant from Fe(1) and Fe(2) respectively, at approximately 1.46 Å.

The two Fe-Cl bond lengths in the structure are 2.461(2) and 2.454(2) Å for the Fe(1)-Cl(1) and Fe(1)-Cl(2) bonds, respectively. Only two other X-ray crystal structures of similar complexes of the formula *trans*-[Fe(L)$_2$(H)Cl] (where L = any bidentate phosphine ligand) have been reported in the literature to date, of *trans*-[Fe(dppe)$_2$(H)Cl] (dppe = bis(diphenylphosphino)ethane)[11] and *trans*-[Fe(depe)$_2$(H)Cl] (depe = bis(diethylphosphino)ethane).[12] Both structures have similar Fe-Cl bond lengths to **29**, which are 2.404(2) Å for *trans*-[Fe(dppe)$_2$(H)Cl] and 2.4044(12) Å for *trans*-[Fe(depe)$_2$(H)Cl].

The three crystallographically independent Fe-Cl bond lengths for the *trans* dichloride complex *trans*-[Fe(L^3)$_2$$Cl_2$] (**24b**) are 2.3598(5) Å for the half molecule, as well as

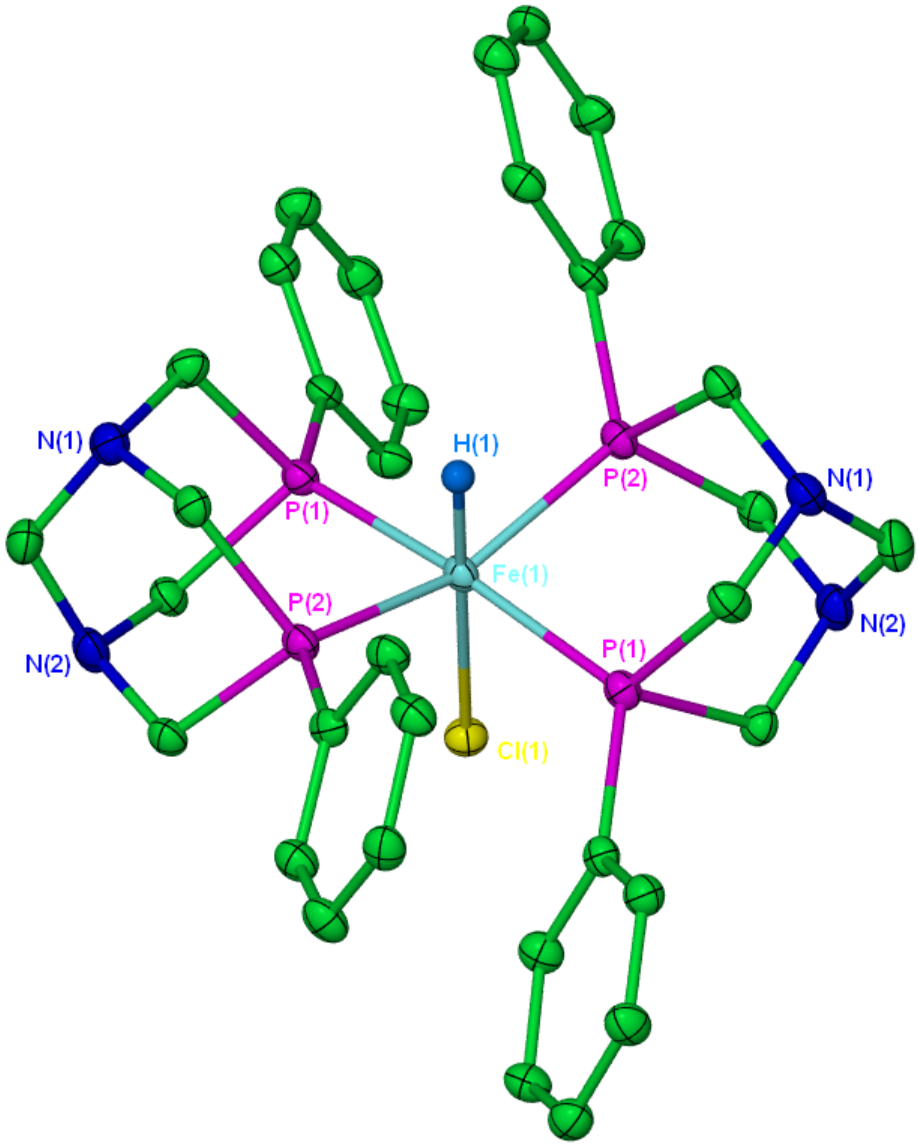

Figure 3.20 – Molecular structure of *trans*-[Fe(L^3)$_2$(H)Cl]·1.5C_6H_6 (29·1.5C_6H_6). The asymmetric unit contains two independent ½ molecules of complex 29, showing molecule 1 of 2. Thermal ellipsoids are at the 30% probability level. Hydrogen atoms (except H(1)) and benzene solvent molecules have been omitted for clarity.

Bond Lengths (molecule 1)

Fe(1)-P(1)	2.2050(14)	Fe(1)-Cl(1)	2.461(2)
Fe(1)-P(2)	2.1595(13)		

Bond Angles (molecule 1)

P(1)-Fe(1)-P(1)'	172.16(9)	P(1)-Fe(1)-P(2)'	98.20(5)
P(2)-Fe(1)-P(2)'	153.72(9)	P(2)-Fe(1)-P(1)'	98.20(5)
P(1)-Fe(1)-P(2)	83.59(5)		

Table 3.6 – Selected bond lengths (Å) and angles (°) for complex 29·1.5C_6H_6 (standard deviation in brackets).

Bond Lengths (molecule 2)

Fe(2)-P(3)	2.1708(14)	Fe(2)-Cl(2)	2.454(2)
Fe(2)-P(4)	2.2075(15)		

Bond Angles (molecule 2)

P(3)-Fe(2)-P(3)'	154.44(10)	P(3)-Fe(2)-P(4)'	98.22(5)
P(4)-Fe(2)-P(4)'	173.99(9)	P(4)-Fe(2)-P(3)'	98.21(5)
P(3)-Fe(2)-P(4)	83.13(5)		

Table 3.7 – Selected bond lengths (Å) and angles (°) for complex 29·1.5C_6H_6 (standard deviation in brackets).

2.3675(5) and 2.3610(5) Å for the full molecule. It can therefore be observed that the Fe-Cl bonds for the *trans* hydride complex **29** are longer than those of **24b**. This is because of the *trans* influence of the hydride ligands *trans* to the chloride, which effectively lengthens and therefore weakens the *trans* Fe-Cl bond. The conformations of both of the independent half molecules in the structure are similar to the full molecule of complex **24b**, *i.e.* the two L^3 ligands are staggered with respect to each other. π-π stacking interactions of *ca*. 3.4 Å also occur between the phenyl groups of both L^3 ligands.

3.13 Attempts to coordinate dinitrogen

Many researchers have strived to synthesise complexes containing bound dinitrogen as a ligand for a variety of applications, including nitrogen fixation and reversible dinitrogen binding for the scrubbing of natural gas streams. Giannoccaro *et al*. reported the abstraction of the chloride ligand on the iron(II) phosphine complex *trans*-$[Fe(dppe)_2(H)Cl]$, by reacting the complex with sodium tetraphenylborate in benzene to give the five coordinate iron(II) hydride complex $[Fe(H)(dppe)_2]BPh_4$.[13] Upon dissolving in THF under an atmosphere of dinitrogen, the dinitrogen complex *trans*-$[Fe(dppe)_2(H)(N_2)]BPh_4$ was formed. Leigh,[14] and more recently, Tyler and coworkers[15] have synthesised *trans* dinitrogen chloride complexes of the formula *trans*-$[Fe(N_2)Cl(P_2)_2]$ BPh_4 (where P_2 is a bidentate phosphine) by abstraction of a chloride ligand from the related dichloride.

Initial attempts to synthesise the dinitrogen hydride complex $[Fe(L^3)_2(H)(N_2)]^+$ from **29** involved reaction with sodium tetraphenylborate under an atmosphere of dinitrogen in benzene at room temperature. The reaction was carried out for *ca*. 24 hours but, after this time no change had occurred to the orange solution and no precipitate had formed.

The $^{31}P\{^{1}H\}$ NMR spectrum of the solution showed no change to the singlet resonance at δ -27.5. The reaction of *cis*-[Fe(L^3)$_2$Cl$_2$] (**24a**) with sodium tetraphenylborate under dinitrogen was also attempted, although again no reaction with N_2 occurred as indicated by $^{31}P\{^{1}H\}$ NMR spectroscopy. Further work in this area needs to be carried out in order to successfully coordinate dinitrogen.

3.14 Electrochemistry of L^3 complexes

Cyclic voltammetry studies were carried out on a range of L^3 complexes in order to determine more about their redox properties, as well as to establish whether the related Fe(III) complexes were stable and potentially isolable. The comparison of electrochemical data of the L^3 complexes to those of the L^1 and L^2 ligands from Chapter 2 should also yield important information.

A 1 mM 1,2-dichloroethane solution of [Fe(L^3)$_2$(κ^2-O_2SO_2)] (**23**) was prepared, using 0.1 M tetrabutylammonium hexafluorophosphate as the electrolyte. Cyclic voltammograms were recorded using a 1 mm platinum electrode and an initial scan rate of 20 mVs^{-1}. The voltammogram showed an irreversible peak at *ca.* 0 V vs Fc^+/Fc, which suggests that the complex is disassembling upon oxidation. The voltammograms were then repeated at 50, 100, and 200 mVs^{-1} to determine the effect of varying the scan rate on the voltammogram (**Figure 3.21**). As the scan rate of the voltammogram is increased, the Fe(II)/Fe(III) redox peak becomes more reversible. The voltammogram at 200 mVs^{-1} shows a redox system, which is far more reversible than at 20 mVs^{-1}, though it is not a fully reversible Nernstian redox process. This phenomenon shows some similarities to the cyclic voltammetry of the complexes of L^1 in Chapter 2, *i.e.* shows a more reversible redox process at higher scan rates due to the decrease in the time available for the oxidised species to decompose. The main difference between the voltammograms of [Fe(L^3)$_2$(κ^2-O_2SO_2)] (**23**) and those of the L^1 complexes is that for **23** there is no need to polish the electrode in between scans in order to observe the redox process. This means that the decomposed complex which results from oxidation does not stick to the electrode and cause electrode blocking. The very small redox process at *ca.* -0.4 V vs Fc^+/Fc could not be identified, though is believed to be a result of either a small impurity or a new species as a result of some decomposition of complex **23**. The complex was insoluble in acetonitrile, thus preventing the cyclic voltammetry being investigated in this solvent.

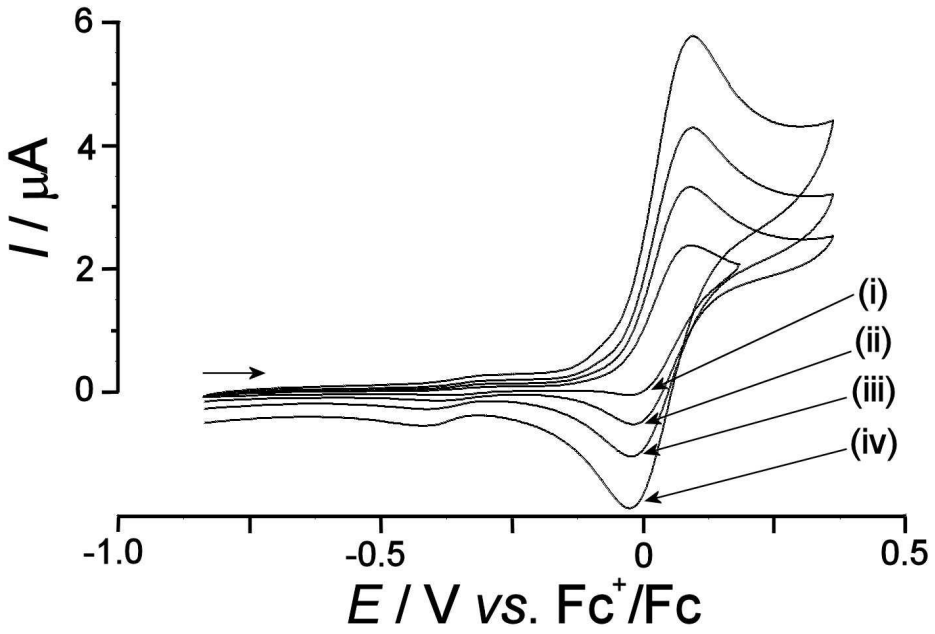

Figure 3.21 - Cyclic voltammograms of $[Fe(L^3)_2(\kappa^2\text{-}O_2SO_2)]$ (23) in 1,2-dichloroethane, using a 1 mm Pt electrode at 20, 50, 100, and 200 mVs^{-1} ((i), (ii), (iii), and (iv) respectively). 0.1 M Bu_4NPF_6 was used as the electrolyte.

The dichloride complex *cis*-$[Fe(L^3)_2Cl_2]$ (**24a**) was also studied using cyclic voltammetry. A 1 mM 1,2-dichloroethane solution of *cis*-$[Fe(L^3)_2Cl_2]$ (**24a**) was made up, using 0.1 M tetrabutylammonium hexafluorophosphate as the electrolyte. The cyclic voltammograms were recorded using a 1 mm platinum electrode. The cyclic voltammogram was first recorded at 200 mVs^{-1}, which showed two main reversible processes, with the major process P1 at *ca.* -0.35 V vs. Fc^+/Fc and the minor process P2 at -0.05 V vs. Fc^+/Fc (**Figure 3.22**).

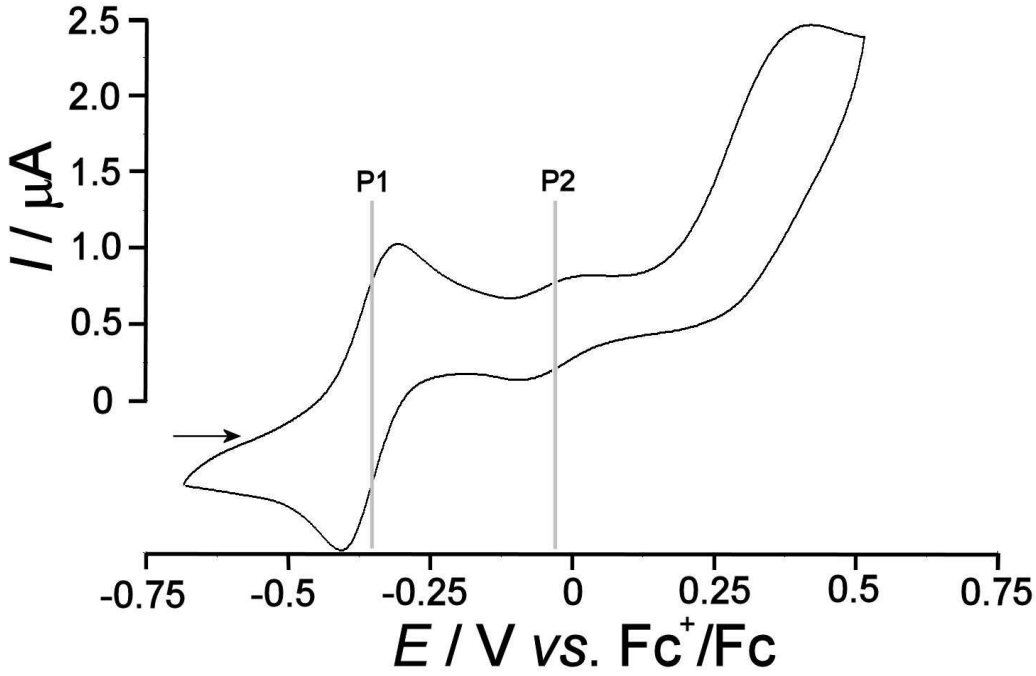

Figure 3.22 - Cyclic voltammogram of *cis*-[Fe(L^3)$_2$Cl$_2$] (24a) in 1,2-dichloroethane, using a 1 mm Pt electrode at 200 mVs^{-1}. 0.1 M Bu_4NPF_6 was used as the electrolyte.

When the voltammogram of **24a** was run at lower scan rates, reversible redox processes were still observed, meaning that the reversibility of the processes are not dependant on scan rate. Unlike the sulfate complex [Fe(L^3)$_2$(κ^2-O_2SO_2)] (**23**), the dichloride complex [Fe(L_3)$_2$Cl$_2$] can potentially switch between the *cis* isomer **24a** and the *trans* isomer **24b**. As the purple *cis* isomer **24a** was used in the experiment and the 1,2-dichloroethane solution was purple, it seems highly likely that the main Fe(II)/Fe(III) redox process P1 at *ca.* -0.35 V vs. Fc^+/Fc is of the *cis* isomer **24a**. As the Fe(II)/Fe(III) redox process for [Fe(L^3)$_2$(κ^2-O_2SO_2)] (**23**) occurs at a more negative potential (*ca*. -0.35 V) than for *cis*-[Fe(L^3)$_2$Cl$_2$] (**24a**), it can be concluded that the dichloride complex **24a** is therefore easier to oxidise than **23**.

The assignment of the complex represented by the main redox process P1 at *ca.* -0.35 V vs. Fc^+/Fc as *cis*-[Fe(L^3)$_2$Cl$_2$] (**24a**) can be backed up by the $^{31}P\{^1H\}$ NMR spectrum of **24a** in section 3.4, which showed that **24a** gives two broad triplet resonances in DCM/$CDCl_3$ at δ -31.6 and -41.3 (**Figure 3.6**) arising from the *cis* isomer. It therefore seems logical that the smaller redox process at *ca.* 0.05 V vs. Fc^+/Fc could be due to the *trans* isomer **24b**. Cyclic voltammetry of the trans complex **24b** in 1,2-dichloroethane would be ideal for comparison. However, the complex reverted back to the *cis* isomer **24a** in 1,2-dichloroethane, as indicated by the deep purple colouration of the solution when the yellow crystals of (**24b**) were dissolved. Therefore, it is the solvent that dictates whether the complex is the *cis* or *trans* isomer, and

clomplex **24** forms the *cis* isomer **24a** in almost all common organic solvents apart from diethyl ether.

Cyclic voltammetry studies of *cis*-[Fe(L^3)$_2$Cl$_2$] (**24a**) were also carried out in acetonitrile using the same conditions. A 1 mM acetonitrile solution of *cis*-[Fe(L^3)$_2$Cl$_2$] (**24a**) was made up using 0.1 M tetrabutylammonium hexafluorophosphate as the electrolyte. The cyclic voltammograms were recorded using a 1 mm platinum electrode with the initial scan rate at 100 mVs^{-1}. The cyclic voltammogram now showed only one reversible redox process at *ca*. -0.35 V vs. Fc+/Fc relating to the *cis* isomer **24a** (**Figure 3.23**).

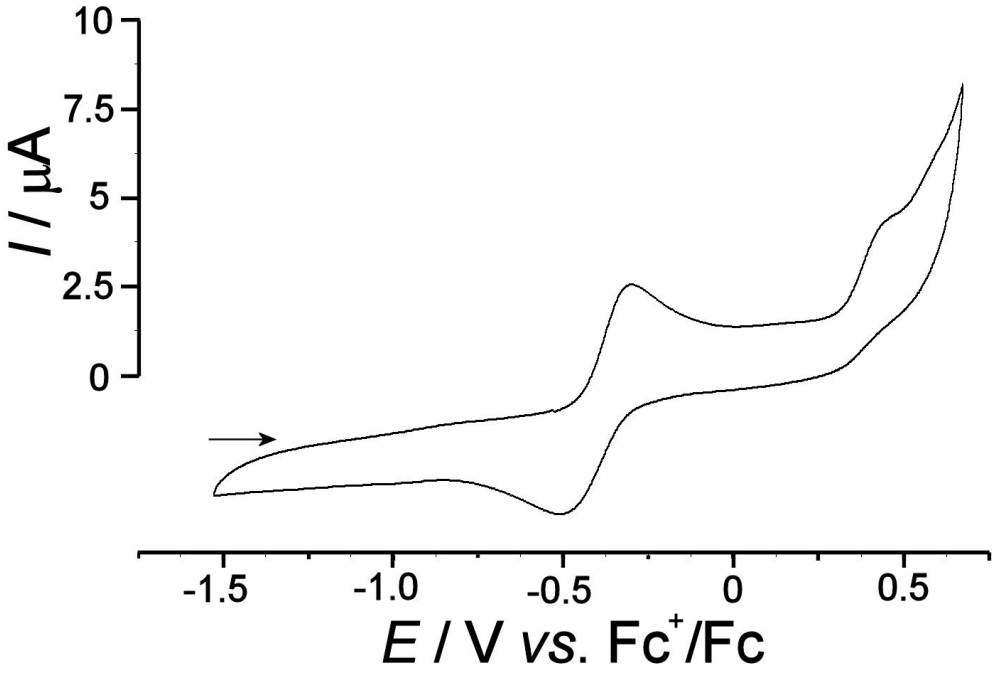

Figure 3.23 - Cyclic voltammogram of *cis*-[Fe(L^3)$_2$Cl$_2$] (24a) in acetonitrile, using a 1 mm Pt electrode at 100 mVs^{-1}. 0.1 M Bu$_4$NPF$_6$ was used as the electrolyte.

No redox system at *ca.* -0.1 V vs. Fc$^+$/Fc was observed in the voltammogram, *i.e.* there appeared to be no appearance of the *trans* isomer **24b**. Therefore, this indicates that the complex stays as the *cis* isomer **24a** when in acetonitrile solution. As acetonitrile is more polar than dichloroethane, it would be expected that the increased polarity of the acetonitrile solvent would lead to an increased amount of the more polar *cis* isomer **24a**. In contrast with the cyclic voltammetry of [Fe(L^2)Cl$_2$] (**15**) in acetonitrile, no ligand substitution was observed. $^{31}P\{^1H\}$ NMR spectroscopy of **24a** in CD_3CN showed the familiar broad triplets associated with **24a**, also suggesting no substitution had occurred.

Cyclic voltammetry studies of the *trans* hydride chloride complex *trans*-[Fe(L^3)$_2$(H)Cl] (**29**) were also carried in order to investigate the stability of the related Fe(III) complex. A 1 mM 1,2-dichloroethane solution of *trans*-[Fe(L^3)$_2$(H)Cl] (**29**) was made up using 0.1 M tetrabutylammonium hexafluorophosphate as the electrolyte. The cyclic voltammograms were recorded using a 1 mm platinum electrode with the initial scan at 10 mVs^{-1}. The voltammogram showed a number of redox processes, with the main process occurring at *ca*. -0.85 V vs. Fc^+/Fc, which is the Fe(II)/Fe(III) redox process for the *trans* hydride chloride complex **29**. The experiment was repeated at 20, 50, 100, and 200 mVs^{-1} (**Figure 3.24**), which showed that the peak was seemingly reversible at all scan rates measured. Therefore the oxidised Fe(III) version of complex **29** is stable even at low scan rates, making it a rare example of a stable 17 electron metal(III) hydride complex formed from the oxidation of the corresponding neutral 18-electron species.[16] Another example is the 17 electron radical cation iron hydride [Fe(Cp*)(dppe)H]PF_6 (dppe = 1,2-bis-(diphenylphosphino)ethane).[17]

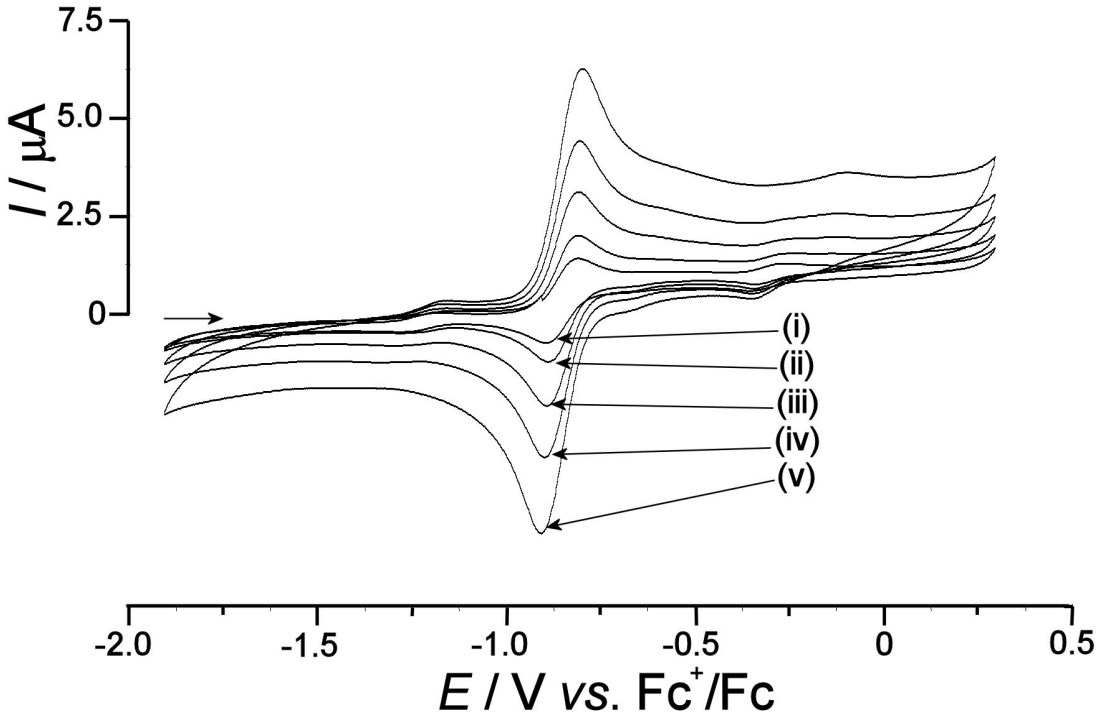

Figure 3.24 - Cyclic voltammograms of [Fe(L^3)$_2$(H)Cl] (29) in 1,2-dichloroethane, using a 1 mm Pt electrode at 10, 20, 50, 100, and 200 mVs^{-1} ((i), (ii), (iii), (iv), and (v) respectively). 0.1 M Bu_4NPF_6 was used as the electrolyte.

After leaving the 1,2-dichloroethane solution for 30 mins still under argon, the cyclic voltammogram was again recorded. The colour of the solution changed over time from a bright orange colour to a darker orange/purple solution. The voltammogram (at 100 mVs^{-1}) showed that the other redox processes had grown with respect to the peak at

ca. -0.85 V vs. Fc^+/Fc (P2), with two processes at *ca*. -1.25 (P1) and -0.35 V (P3) vs. Fc^+/Fc particularly notable (**Figure 3.25**). Both processes appear reversible, but are difficult to unambiguously characterise.

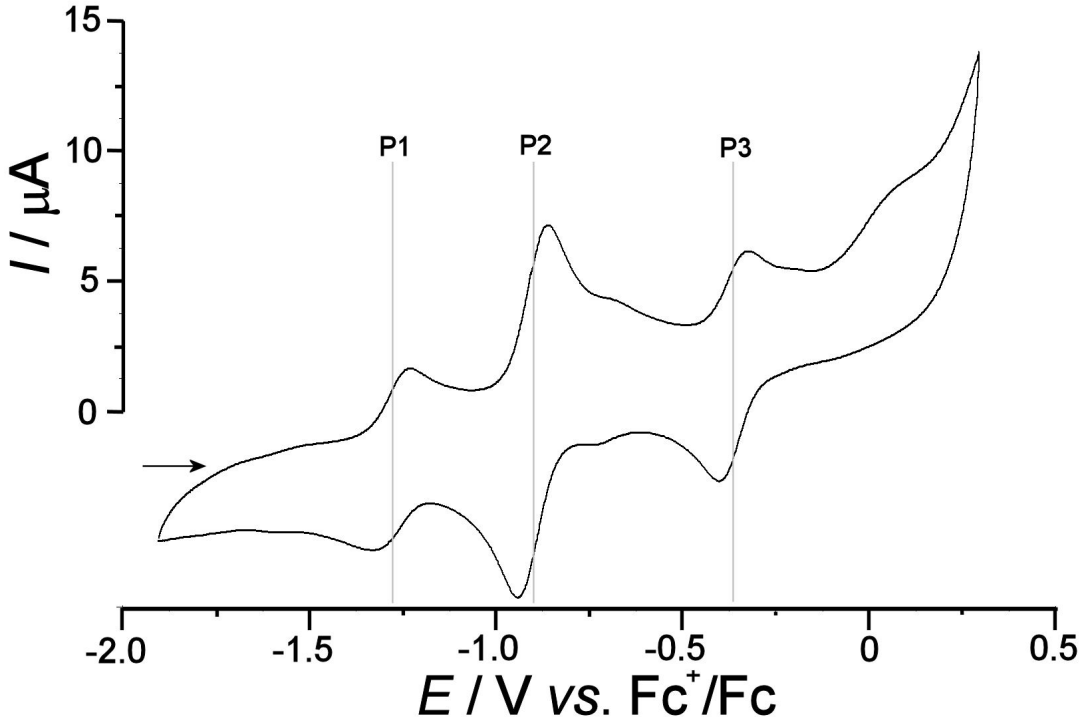

Figure 3.25 - Cyclic voltammogram of $[Fe(L^3)_2(H)Cl]$ (29) in 1,2-dichloroethane, using a 1 mm Pt electrode at 100 mVs^{-1} after ca. 30 mins in solution. 0.1 M Bu_4NPF_6 was used as the electrolyte.

As complex **29** is the *trans*-isomer, it can potentially isomerise to give the equivalent *cis* isomer. The similar *trans* dichloride complex *trans*-$[Fe(L^3)_2Cl_2]$ (**24b**) when dissolved in similar chlorinated solvents (dichloromethane and chloroform) gives the *cis* isomer **24a**. It is therefore likely that complex **29** could undergo a similar *cis*/*trans* isomerisation in 1,2-dichloroethane.

The redox processes in the cyclic voltammograms of the dichloride complexes **24a** (*cis*) and **24b** (*trans*) in 1,2-dichloroethane solution occurred at *ca.* 0.3 V apart from one another, with the *cis* complex **24a** occurring at the more negative potential (-0.35 *vs*. -0.05 V). This is also the case for the processes at -1.25 (P1) and -0.95 V *vs*. Fc^+/Fc (P2), suggesting that the peak at -1.25 could be the *cis* isomer *cis*-$[Fe(L^3)_2(H)Cl]$. Interestingly, the process at -0.35 V *vs*. Fc^+/Fc (P3) occurs at the same potential as the *cis*-$[Fe(L^3)_2Cl_2]$ complex (**24a**) in dichloromethane, suggesting the identity of the process could be the *cis*-dichloride complex. The observed colour change of the solution from orange to a darker orange/purple colour also supports this idea.

Additionally, the more negative potential of the hydride complex **29** compared to the dichloride complex **24a** shows that complex **29** is far easier to oxidise than **24a**, which would be expected for a hydride complex. In general, all the Fe(II) L^3 complexes oxidise at lower potentials than for the Fe(II) L^2 complexes ($[Fe(L^2)Cl_2]$ (**15**) oxidises at *ca*. 0.1 and 0.2 V vs Fc^+/Fc in dichloroethane and acetonitrile respectively), meaning that the L^3 complexes are easier to oxidise. One potential explanation is the chelate effect, with complexes of a tetradentate ligand (such as L^2) expected to be more energetically stable than two similar bidentate ligands (such as L^3).

One possible explanation is that complex **29** undergoes isomerisation to give the *cis* isomer, which then undergoes a metathesis reaction with a molecule of HCl generated by the chlorinated solvent to give the *cis*-dichloride complex **24a** and a molecule of dihydrogen. Another possibility is that the metathesis occurs directly with the solvent itself. A similar reaction occurs when the molybdenum hydride complex *cis*-$[HMo(CO)_2(L)(C_5H_5)]$ (L = $P(C_6H_5)_3$, $P(OC_6H_5)_3$, or $P(OCH_3)_3$) reacts with carbon tetrachloride to give the chloride complex *cis*-$[ClMo(CO)_2(L)(C_5H_5)]$.[18] As the rate of formation of the two processes at *ca*. -1.25 (P1) and -0.35 V vs. Fc^+/Fc (P3) seems to be equivalent, it could be concluded that the rate of isomerisation from *trans*-$[Fe(L^3)_2(H)Cl]$ (**29**) to *cis* is approximately equivalent to the rate of substitution of the hydride ligand for the chloride. This of course assumes that the reaction does proceed in this order and the *cis* isomer is not formed independently from the *cis*-$[Fe(L^3)_2Cl_2]$ complex (**24a**).

When the cyclic voltammograms of the L^1, L^2, and L^3 complexes are compared, the most noticeable difference is the fact that the L^1 complexes do not give reversible voltammograms. This is most likely a result of the instability of the L^1 Fe(III) analogues that are produced in the oxidation process. This instability could be a result of the affinity of the hydroxymethyl groups for the working electrode, as the similar L^2 and L^3 complexes (which do not possess hydroxymethyl groups) generally give reversible CVs. The L^3 complexes generally exhibited redox activity at lower potential (between *ca.* 0.5 and 1.0 V) than their L^1 and L^2 counterparts, signifying that the Fe(II) L^3 complexes are easier to oxidise and therefore their Fe(III) analogues would be more difficult to reduce. Due to their stability as 17-electron Fe(III) complexes, further work to isolate the Fe(III) variants of L^2 and L^3 either by chemical or bulk electrochemical methods should provide interesting results.

3.15 Further modification of the self-assembly reaction

Other possibilities exist for the modification of the self-assembly reaction to form new products, such as using a different metal salt, using a substitutued amine/ammonium salt instead of ammonium sulphate, using a substituted aldehyde instead of formaldehyde, and even using a different counter ion other than sulfate. One possibility is to attempt the self-assembly reaction using a different metal salt, in order to determine whether the same or similar ligand motif would be formed, or even an entirely new ligand structure.

The self-assembly reaction to form complex **1** has two important factors that have allowed **1** to be isolated and characterised. The first is that complex **1** crystallises from solution, which allows its isolation and separation from any other complexes that are formed. The second factor is that **1** is diamagnetic as a result of its d^6 low-spin octahedral structure, which allows it to be easily characterised by NMR spectroscopy without the broad NMR spectra associated with paramagnetic complexes. If a complex formed in an analogous self-assembly reaction does not preferentially crystallise from solution or is paramagnetic (or both), then its isolation and identification would be harder. Therefore it would be useful to attempt similar reactions with diamagnetic metal salts such as zinc(II) sulfate (d^{10}).

The self-assembly reaction was attempted with $Zn(II)SO_4$ as the templating metal salt along with the same stoichiometries of THPS and ammonium sulfate as was used to form **1**. This was attempted in order to determine whether the reaction would give a zinc(II) analogue of complex **1**, or even any product at all. The addition of sodium hydroxide to the colourless solution over time did not lead to any change in colour of the solution, which would be expected for a d^{10} complex assuming no oxidation had occurred (unlikely for zinc(II)). Following completion of the reaction the solution was left at 5° C for *ca.* one week, but no material crystallised from the solution. The $^{31}P\{^1H\}$ NMR spectrum of the reaction mixture both before and after the week showed a large number of singlet resonances suggesting the presence of a variety of phosphine-containing species. There was no indication that any complexes similar to complex **1** had formed, and as no complexes had crystallised from solution, the isolation, separation and identification of the different species would be very difficult.

Other metals were attempted in the self-assembly reaction, including copper(II), nickel(II), and cobalt(II) sulfates. In all cases a colour change occurred, but no material

crystallised from solution despite leaving the solutions at 5° C for *ca.* one week. The $^{31}P\{^{1}H\}$ NMR spectra of the solutions all showed broad resonances due the metals all being paramagnetic, and therefore no useful structural information could be obtained from them. Due to these reactions yielding no useful results it was decided to not investigate this area further.

To determine whether the self-assembly reaction would occur with the addition of a substituted amine instead of an ammonium salt, the reaction was attempted with glycine. As with replacing the phosphine/phosphonium salt in the reaction with a substituted variant, changing the amine/ammonium salt could lead to a number of possible outcomes. An analogous ligand to L^1 could form maintaining the eight-membered ring system, an entirely different new ligand could form, or even no reaction at all. One possible structure is that if two glycine molecules condense with two phosphine moieties, the familiar eight-membered ring could form with the pendant gycine molecules coordinating to the axial coordination sites (**Figure 3.26**). Assuming the carboxylic acid groups would deprotonated upon the addition of base and water molecules take up the remaining two equatorial coordination sites, the complex would be of neutral charge.

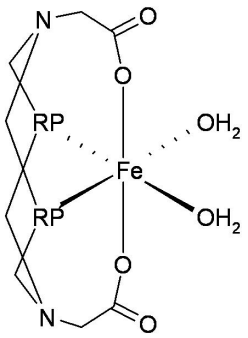

Figure 3.26 – Proposed structure of the potential product from the self-assembly reaction using glycine instead of ammonium sulfate.

When the reaction was attempted, addition of sodium hydroxide to the aqueous solution of $FeSO_4$, THPS, and glycine gave a red colouration to the solution, suggesting the formation of some iron(II) complex or complexes had occurred. The reaction was stopped at *ca.* pH 6 in order to prevent any decomposition that occurs at higher pH with the other complexes. $^{31}P\{^{1}H\}$ NMR spectroscopy of the solution showed a large amount of unreacted THPS present, as well as number of broad peaks between δ 50 and δ -200. The red solution was left at 5° C for *ca*. one week, though no solid crystallised from solution. Further NaOH was added to the solution in an attempt to

produce more of the product/products, though this did not lead to the crystallisation of any material from solution. Without isolating any complex from solution, it is very difficult to determine the nature of any products formed in solution. Also, glycine is zwitterionic, which could also have a large effect on the outcome of the reaction.

3.16 Self-assembly reactions in the absence of metals

The self-assembly reactions to synthesise both complexes **1** and **23** were attempted without the presence of a metal template to determine the outcome of the reaction. The reaction between THPS, ammonium sufate, and sodium hydroxide was carried out without the presence of the iron(II) sulfate as a metal template. Following the addition of the sodium hydroxide, no obvious visual change of the colourless solution occurred. The $^{31}P\{^{1}H\}$ NMR spectrum of the solution in D_2O showed a large number of singlet peaks between δ 50 and -150, suggesting that many species were present in solution. The solution was left at 5° C for *ca*. one week to see if any of these compounds would crystallise. No solid material precipitated from solution despite extended time at 5° C and the addition of further NaOH.

The self-assembly reaction using bis(hydroxymethyl)phenylphosphine to form complex **23** was also carried out in the absence of the iron(II) sulfate. Following addition of the bis(hydroxymethyl)phenylphosphine to an aqueous solution of ammonium sulfate and formaldehyde, a white precipitate formed. The $^{31}P\{^{1}H\}$ NMR spectrum of the white solid in $CDCl_3$ showed a number of singlet resonances, indicating either that many species had precipitated from solution, or maybe one compound had initially formed but reacted with the $CDCl_3$ solvent to give multiple species that could not be easily identified.

In order to attempt to synthesise the L^3 ligand without the use of the iron(II) template, the reaction between $PhP(CH_2OH)_2$, formaldehyde and ammonia was attempted using ethanol as the solvent instead of water. As ammonium sulfate is not soluble in ethanol, ammonia was used as an alternative. It was hoped that using an organic solvent such as ethanol for the reaction may give only one product, as the solvent H_2O molecules maybe interfering in the reaction in the previous case in aqueous solution. The bis(hydroxymethyl)phenylphosphine was added dropwise to an ethanolic solution of ammonia and formaldehyde, which did not result in the formation of a precipitate as in the similar reaction in aqueous solution. The reaction was then brought to reflux, which resulted in the precipitation of a white solid after *ca*. five minutes. The reflux was continued for a further two hours until no further solid precipitated. The $^{31}P\{^{1}H\}$ NMR

spectrum of the white solid in $CDCl_3$ showed one singlet resonance at δ -46.7 (**Figure 3.27**).

Importantly, the precipitate (**30**) is of only one phosphorus containing species, as observed by $^{31}P\{^1H\}$ NMR spectroscopy. However, its structure could not be easily assigned. This could potentially be of the desired free L^3 ligand, as the two phosphine donors on the ligand should be chemically and magnetically equivalent, though more characterisation is needed to unambiguously identify the structure of this species. The chemical shift of the $PhP(CH_2OH)_2$ starting material is δ -20.0, meaning a shift of $\Delta\delta$ -26.6 has occurred upon reaction. The ^1H NMR spectrum showed broad peaks which could not easily be interpreted.

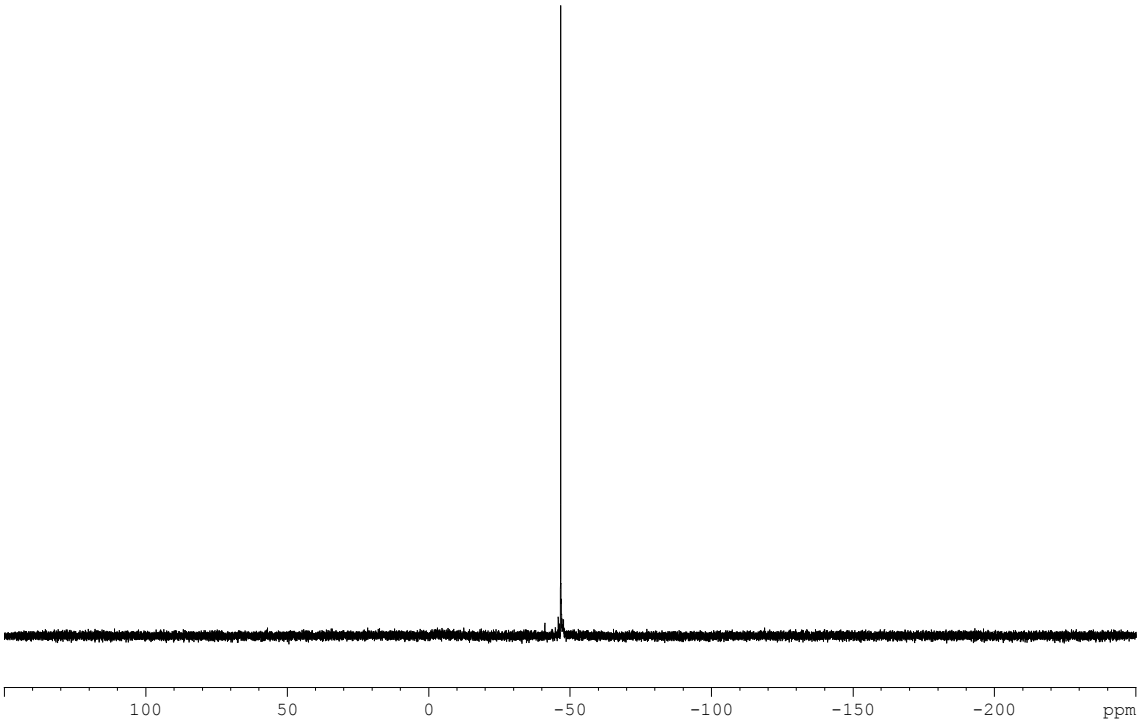

Figure 3.27 – $^{31}P\{^1H\}$ NMR spectrum of the precipitate (30) from the reaction of $PhP(CH_2OH)_2$, NH_3, and H_2CO carried out in ethanol. Spectrum recorded in $CDCl_3$ at 122 MHz.

The reaction to form **30** was repeated using different stoichiometries of ammonia and the phosphine, but the same white solid precipitated in all cases, with only the yield of material affected. One possible alternative structure of this compound arises from the condensation of a third molecule of $PhP(CH_2OH)_2$ with the remaining two NH groups instead of a molecule of formaldehyde to give a tri-phosphine structure. The microanalysis of the solid matched the proposed tri-phosphine structure (Expected

(found) for $C_{24}H_{27}N_2P_3 \cdot H_20$: C 63.4(64.0), H 6.43(6.20), N 6.16(6.04) %), though this is not enough evidence to fully support this conclusion.

Electrospray mass spectrometry of **30** was carried out in order to fully identify its structure. The spectrum shows a large number of peaks, including a prominent peak at *m*/*z* = 272.1. **30** was then reacted with sulfur in order to help determine its structure. The $^{31}P\{^1H\}$ NMR spectrum of the material after stirring with excess sulfur after four days in $CDCl_3$ showed the singlet resonance had shifted to δ 33.8. The electrospray mass spectrum of the phosphine sulphide was recorded, which showed only two main peaks at *m*/*z* = 304.2 and 585.5. If the mass of sodium (23) is subtracted from these values we get 281.2 and 462.5. As one value is double the other, it is likely that these peaks are $[M+Na]^+$ (304.2) and $[2M+Na]^+$ (585.5), meaning the molecular ion [M] of the phosphine sulfide is 281.2. When the mass of sulfur (*ca*. 32) is subtracted from the peak at *m*/*z* = 304.2, we get a peak at approximately *m*/*z* = 272.1, which is what we see in the mass spectrum of **30** before the addition of sulfur (i.e. $[M+Na]^+$ of the phosphine). Therefore the molecular ion [M] of the phosphine itself without the sodium ion is *m*/*z* = 272.1 – 23.0 = 249.1.

30 was also reacted with one equivalent of sulfur in an attempt to determine the number of phosphine donors of the compound. The $^{31}P\{^1H\}$ NMR spectrum after the reaction showed two broad phosphine resonances in a 1:1 ratio at *ca*. δ 35 and -43, suggesting that the ligand is a bidentate phosphine, though this would rule out the possibility of the tri-phosphine structure. Despite the efforts to fully characterise the ligand made in the reaction, full structural characterisation remained elusive. Further work needs to be done in order to identify the structure of **30**.

3.17 Conclusions and further work

The investigation of the self-assembly reaction by altering the starting materials (such as the phosphine/phosphonium salt or amine/ammonium salt) gave some interesting results. Using bis(hydroxymethyl)phenylphosphine in the presence of formaldehyde instead of using THPS gave the complex $[Fe(L^3)_2(\kappa^2\text{-}O_2SO_2)]$ **23**, containing the new bidentate phosphine ligand L^3. Ligand L^3 consists of two fused PN_2 six-membered rings with a phenyl group as the third substituent on each phosphine. A sulfate ligand coordinates to the Fe centre in a bidentate manner and occupies the remaining equatorial sites. The equivalent dichloride complex *cis*-$[Fe(L^3)_2Cl_2]$ (**24a**) can be synthesised by using iron(II) chloride and ammonium chloride instead of the sulfate salts.

Further reactions involving changes to the other starting materials in the self-assembly reaction proved less successful. Attempts to replace the ammonium salts with other amines or ammonium salts did not lead to the isolation of any analogous phosphine complexes. Replacement of the sulfate counter ions for chlorides, or even using other metals in the self-assembly reaction to form **1** did not lead to the isolation of any complexes. However, replacing the sulfate salts with chloride salts in the reaction to form **23** gave the related *cis*-dichloride complex **24a**.

A comparison of the coordination chemistry of the L^3 complexes shows some similarities to the coordination chemistry of the L^1 and L^2 complexes as all three series of complexes have four phosphine donors coordinated to a low-spin iron(II) centre. However, there are also differences due to the nature of the bidentate L^3 ligand versus the tetradentate L^1 and L^2 ligands, such as the potential for *cis*/*trans* isomerisation. The solubility of the L^3 complexes are in general similar to those of the L^2 complexes, *i.e.* largely soluble in fairly polar organic solvents such as acetone, dichloromethane, and chloroform. The *trans*-dichloride L^3 complex **24b** could be prepared by extraction with diethyl ether, despite the low solubility of the complex in that solvent. However, the *cis* complex **24a** reformed upon dissolving in all tested organic solvents except Et_2O. Both **24a** and **24b** dissolve in H_2O to give the same species, most likely the diaqua complex *cis*-$[Fe(L^3)_2(H_2O)_2]Cl_2$. The sulfate complex **23**, however, was completely insoluble in water. This is also in direct contrast with the L^2 complexes, with the sulfate complex **13** being more soluble in H_2O than the dichloride complex **15**.

The chloride ligands on complexes **24a** and **24b** can be readily substituted with other ionic and neutral ligands. However, the sulfate ligand on the similar sulfate complex **23** is not readily substituted, which is most likely due to the extra stability that the chelate effect affords. As a result, complex **24a** proved to be a useful precursor for the synthesis of other L^3 complexes. Again, there are contrasts between the L^2 and L^3 systems, as the coordinated sulfate ligand on the L^2 complex **13** can be readily substituted, whereas the sulfate ligand on **23** cannot. The reason for the greater reactivity of complex **13** compared to **23** is not entirely clear.

The reactions of **24a** with thiocyanate and azide salts in an water/acetone mixture led to the precipitation of the bis-thiocyanato and bis-azido complexes respectively. In both cases the $^{31}P\{^1H\}$ NMR spectra showed a mixture of both *cis* and *trans* isomers, though in the case of the bis-thiocyanato complexes, the *cis*/*trans* ratio decreases over time as a result of the crystallisation of the *trans* isomer **25b**. This is in contrast to the

L^1 and L^2 bis-thiocyanato and bis-azido complexes, which cannot undergo isomerisation due to the tetradentate phosphine ligand.

The reactions of the L^3 dichloride complexes **24a** and **24b** with CO are similar to those of the L^1 and L^2 dichloride complexes **3** and **15**, in that they all form mono-carbonyl mono-chloride complexes. Interestingly, the *trans* dichloride **24b** gives the *cis* mono-carbonyl mono-chloride complex **28b** upon reaction with CO in diethyl ether, whereas the *cis* dichloride **24a** gives the *trans* mono-carbonyl mono-chloride complex **28a** upon reaction with CO in aqueous solution (*via* the *cis* di-aquo complex). Again, the L^1 and L^2 dichloride complexes **3** and **15** cannot undergo isomerisation, and only the *cis* complexes [Fe(L^1)(CO)Cl]Cl (**12**) and [Fe(L^2)(CO)Cl]Cl (**19**) are formed. Reactions of **24a** with carbonate produced the chelating carbonate complex **27**, in contrast to the analogous L^2 reaction, in which the complex was unstable to the basic carbonate anion and decomposed.

The *trans* hydride chloride complex *trans*-[Fe(L^3)$_2$(H)Cl] (**29**) was synthesised by the reaction of **24a** with sodium borohydride. Further investigations into the reactivity of **29** need to be carried out in order to find out more about its coordination chemistry, such as the reactivity towards dinitrogen.

Attempts to synthesise the free bidentate L^3 ligand proved unsuccessful. Further investigation therefore needs to be carried out in this area, as well as efforts to remove the ligand intact from the metal. If the L^3 ligand could be synthesised or isolated, its coordination chemistry could be investigated with a wide range of metals.

The electrochemistry of the L^3 compounds measured gave some interesting results. Like the L^2 complexes, cyclic voltammetry of the L^3 complexes in general gave reversible voltammograms, unlike the L^1 complexes. Cyclic voltammetry of the *cis*-dichloride complex **24a** in dichloroethane showed two reversible redox processes which presumably arise from the *cis* and *trans* isomers, with the *cis* isomer being far more abundant. When the CV is repeated in acetonitrile, the redox process due to the *trans* isomer is not observed, presumably due to the more polar nature of acetonitrile compared to dichloroethane. No substitution of a chloride ligand of **24a** with an acetonitrile ligand in acetonitrile was observed electrochemically or by $^{31}P\{^1H\}$ NMR spectroscopy, though this was not studied extensively. Similar to the L^1 diaqua complex with the sulfate counter ion (**1**), the voltammograms of the L^3 sulfate complex **23** were irreversible at lower scan rates and more reversible at higher scan rates, though the irreversibility of the L^1 complexes was far greater. CVs of the hydride

complex *trans*-[Fe(L^3)$_2$(H)Cl] (**29**) gave reversible voltammograms at all scan rates measured, suggesting the related Fe(III) complex is relatively stable, though this undergoes further isomerisation and substitution reactions with the dichloroethane solvent. The Fe(III) version of complex **29** is therefore a rare example of a 17 electron iron hydride complex. Further attempts to isolate this complex and explore its reactivity could lead to some interesting results.

3.18 References

1. L. Higham, PhD Thesis, University of East Anglia, 2000.
2. P. Dierkes and P. W. N. M. v. Leeuwen, *J. Chem. Soc., Dalton Trans.*, 1999, 1519.
3. H. W. Roesky and M. Andruh, *Coord. Chem. Rev.*, 2003, **236**, 91.
4. M. Di Vaira, S. Midollini and L. Sacconi, *Inorg. Chem.*, 1981, **20**, 3430.
5. C. M. Habeck, C. Hoberg, G. Peters, C. Näther and F. Tuczek, *Organometallics*, 2004, **23**, 3252.
6. L. D. Field, A. V. George, S. R. Pike, I. E. Buys and T. W. Hambley, *Polyhedron*, 1995, **14**, 3133.
7. L. D. Field, B. A. Messerle and R. J. Smernik, *Inorg. Chem.*, 1997, **36**, 5984.
8. J. M. Bellerby, M. J. Mays and P. L. Sears, *J. Chem. Soc., Dalton Trans.*, 1976, 1232.
9. J. D. Gilbertson, N. K. Szymczak, J. L. Crossland, W. K. Miller, D. K. Lyon, B. M. Foxman, J. Davis and D. R. Tyler, *Inorg. Chem.*, 2007, **46**, 1205.
10. Y. Gao, D. G. Holah, A. N. Hughes, G. J. Spivak, M. D. Havighurst, V. R. Magnuson and V. Polyakov, *Polyhedron*, 1997, **16**, 2797.
11. J.-G. Lee, G.-S. Jung and S.-W. Lee, *Bull. Korean. Chem. Soc.*, 1998, **19**, 267.
12. B. Wiesler, F. Tuczek, C. Näther and W. Bensch, *Acta Crystallogr., Sect. C: Cryst. Struct. Commun.* , 1998, **C54**, 44.
13. P. Giannoccaro and A. Sacco, *Inorg. Synth.*, 1977, **17**, 69.
14. A. Hills, D. L. Hughes, M. Jimenez-Tenorio and G. J. Leigh, *J. Organomet. Chem.*, 1990, **391**, C41.
15. W. K. Miller, J. D. Gilbertson, C. Leiva-Paredes, P. R. Bernatis, T. J. R. Weakley, D. K. Lyon and D. R. Tyler, *Inorg. Chem.*, 2002, **41**, 5453.
16. P. Hamon, J.-R. Hamon and C. Lapinte, *J. Chem. Soc., Chem. Commun.*, 1992, 1602.
17. P. Hamon, L. Toupet, J.-R. Hamon and C. Lapinte, *Organometallics*, 1992, **11**, 1429.
18. A. Bainbridge, P. J. Craig and M. Green, *J. Chem. Soc. A.*, 1968, 2715.

Chapter 4 – Experimental section

4.1 General Experimental

Reactions were typically carried out in air, though manipulations on a Schlenk line under dinitrogen were used as indicated. All chemical reagents were obtained from Aldrich and used without further purification unless otherwise stated. $[Fe(L^1)(H_2O)_2]SO_4$ (**1**) was prepared according to the literature procedure.[1] NMR spectra were recorded at 298 K on Bruker Avance 300, 400, and 500 MHz NMR spectrometers, and referenced to residual protio solvent signals for ^1H NMR spectra, δ 2.05 (acetone-*d*$_6$), 4.80 (D_2O), 7.24 ($CDCl_3$), 2.50 (DMSO-*d*$_6$), 7.15 (C_6D_6) and to solvent resonances for $^{13}C\{^1H\}$ NMR: δ 29.9 (acetone-*d*$_6$), 49.5 (D_2O + 1% MeOH), 77.2 ($CDCl_3$), 39.5 (DMSO-*d*$_6$).[2] $^{31}P\{^1H\}$ NMR chemical shifts were referenced externally to 85% H_3PO_4 (δ 0.0). The low frequency $^{31}P\{^1H\}$ NMR spectrum (81 MHz) of complex **6** was carried out by Dr. Alan Boyd at Heriot-Watt University. The $^{31}P\{^1H\}$ NMR simulations for complexes **6**, **20**, and **21** were carried out by Dr. John Lowe. Microanalyses were carried out by Mr Alan Carver (Chemistry Department, University of Bath). IR spectra were recorded as KBr discs on a Nicolet Protégé 460 FTIR spectrometer. Electrospray mass spectrometry was carried out by the EPSRC National Service at the University of Swansea for complex **7**, and at the University of Bath Mass Spectrometry Service on a Bruker MicrOTOF or MicrOTOF-Q spectrometer for all other complexes reported.

Phenylphosphine (98%) was purchased from Strem Chemicals, Inc, USA. THPS (50% aqueous solution) and THPC (80% aqueous solution) were kindly provided by Rhodia Ltd. ^{57}Fe metal powder and $^{18}OH_2$ were kindly provided by Prof. Stephen Cramer and coworkers at the University of California, Davis and Lawrence Berkeley National Laboratories, California, USA. NRVS spectra were also carried out by Prof. Stephen Cramer and coworkers.

4.2 Syntheses of chapter 2 compounds

Synthesis of $[Fe(L^1)Cl_2]$ (3)

$[Fe(L^1)(H_2O)_2]SO_4$ (**1**) (50 mg, 0.0733 mmol) and NaCl (86 mg, 1.47 mmol, 20 Eq) were heated to reflux in acetone (50 mL) for four hours, generating a purple suspension. After cooling, the solution was filtered to remove the excess NaCl and Na_2SO_4 side-

products. Purple needle-like crystals were grown by leaving the acetone solution to evaporate at room temperature. Yield = 20 mg (49%).

^{1}H NMR (400 MHz, acetone-d_6): δ 5.14 (AB, 8H, $\Delta\nu$ = 62 Hz, $^{2}J_{H\text{-}H}$ = 13.7 Hz), 4.88 (s, 4H), 3.75 (s, 4H), 3.41 (AB, 8H, $\Delta\nu$ = 23 Hz, $^{2}J_{H\text{-}H}$ =15.2 Hz).

^{31}P{^{1}H} NMR (122 MHz, acetone-d_6): δ 14.8 (t, $^{2}J_{P\text{-}P}$ = 56 Hz), -7.9 (t, $^{2}J_{P\text{-}P}$ = 56 Hz).

Anal. Calc. For $C_{12}H_{30}N_2O_6FeP_4Cl_2{\cdot}0.5H_2O$: C, 25.8; H, 5.60; N, 5.02%. Found: C, 25.9; H, 5.72; N, 5.26%.

Synthesis of [Fe(L^{1})Br$_2$] (5)

Same as the synthesis of **3** only using KBr instead of NaCl.

^{1}H NMR (300 MHz, acetone-d_6): δ 4.54 (AB, 8H, $\Delta\nu$ = 27 Hz, $^{2}J_{H\text{-}H}$ =13.2 Hz), 4.32 (s, 4H), 3.62 (s, 4H), 3.25 (AB, 8H, $\Delta\nu$ = 23 Hz, $^{2}J_{H\text{-}H}$ = 15.5 Hz).

^{31}P{^{1}H} NMR (122 MHz, acetone-d_6): δ 15.6 (t, $^{2}J_{P\text{-}P}$ = 56 Hz), -12.2 (t, $^{2}J_{P\text{-}P}$ = 56 Hz)

Anal. Calc. For $C_{12}H_{30}N_2O_6FeP_4Br_2$: C, 22.6; H, 4.74; N, 4.39%. Found: C, 22.5; H, 4.89; N, 3.98%.

Synthesis of [Fe(L^{1})(NCS)$_2$] (6)

[Fe(L^{1})(H$_2$O)$_2$]SO$_4$ (**1**) (30 mg, 0.044 mmol) and potassium thiocyanate (18 mg, 0.185 mmol) were heated to reflux in acetone (15 mL) for ca. 18 hours, slowly dissolving the [Fe(L^{1})(H$_2$O)$_2$]SO$_4$ to give an yellow/orange solution with an orange precipitate. The solvent was removed under reduced pressure. The orange solid was washed with Et$_2$O (10 mL) and collected by filtration, then washed with cold H$_2$O (2 mL) and further Et$_2$O (5 mL). Orange crystals of **6** were isolated upon leaving an acetone solution of the product to evaporate slowly. Yield = 23 mg (81%).

^{1}H NMR (400 MHz, acetone-d_6): δ 4.45 (AB, 8H, $\Delta\nu$ = 21 Hz, $^{2}J_{H\text{-}H}$ =13.6 Hz), 4.33 (s, 4H), 3.83 (s, 4H), 3.37 (m, 8H, $\Delta\nu$ = 86 Hz, $^{2}J_{H\text{-}H}$ = 14.9 Hz).

^{13}C{^{1}H} NMR (100 MHz, acetone-d_6): δ 140.7 (s, N<u>C</u>S), 60.1 (m), 58.9 (m), 50.0 (m), 44.9 (m).

$^{31}P\{^{1}H\}$ NMR (122 MHz, acetone-d_6): δ 12.6 (second order, $^{2}J_{P\text{-}P}$ = 51 Hz), 4.6 (second order, $^{2}J_{P\text{-}P}$ = 51 Hz).

Anal. Calc. For $C_{14}H_{30}N_4O_6FeP_4S_2 \cdot 3H_2O$: C, 25.9; H, 5.60; N, 8.64%. Found: C, 26.1; H, 5.23; N, 8.71%.

IR (cm^{-1}): 2109 (ν_{NCS}), 2098 (ν_{NCS}).

Synthesis of $[Fe(L^1)(N_3)_2]$ (7)

Sodium azide (60 mg, 0.92 mmol) was added to a solution of $[Fe(L^1)(H_2O)_2]SO_4$ (**1**) (100 mg, 0.15 mmol) in H_2O (10 mL) under an atmosphere of N_2 and the solution stirred for 1h at ambient temperature. A red solid of $[Fe(L^1)(N_3)_2]$ (**7**) was isolated upon the addition of acetone (5 mL). Repeated attempts to record an elemental analysis gave consistently high %N values due to the difficulty in removing excess sodium azide leftover from the reaction.

^{1}H NMR (400 MHz, D_2O): δ 4.54 (s, 8H), 4.36 (s, 4H), 3.72 (s, 4H), 3.19 (AB, 8H, $\Delta\nu$ = 16 Hz, $^{2}J_{H\text{-}H}$ =16.0 Hz).

$^{13}C\{^{1}H\}$ NMR (76 MHz, D_2O): δ 58.9 (s), 58.0 (m), 50.7 (m), 46.4 (m).

$^{31}P\{^{1}H\}$ NMR (122 MHz, D_2O): δ 16.9 (t, $^{2}J_{P\text{-}P}$ = 54 Hz), 12.4 (t, $^{2}J_{P\text{-}P}$ = 54 Hz).

IR (cm^{-1}): 2056 (ν_{N3}).

Electrospray MS: *m*/*z* 580.0 $[M+Na]^+$.

Synthesis of $[Fe(L^1)(\kappa^2\text{-}O_2CO)]$ (8)

Sodium carbonate decahydrate (47 mg, 0.164 mmol) was added to a solution of $[Fe(L^1)(H_2O)_2]SO_4$ (**1**) (100 mg, 0.147 mmol) in H_2O (20 mL), giving a red solution of $[Fe(L^1)(\kappa^2\text{-}O_2CO)]$ (**8**) almost immediately. A red microcrystalline solid of **8** was isolated from solution by the addition of acetone. Yield = 80 mg (94%).

^{1}H NMR (400 MHz, D_2O): δ 4.41 (s, 4H), 4.40 (AB, 8H, $\Delta\nu$ = 21 Hz, $^{2}J_{H\text{-}H}$ =13.7 Hz), 3.70 (s, 4H), 3.14 (AB, 8H, $\Delta\nu$ = 24 Hz, $^{2}J_{H\text{-}H}$ =16.0 Hz).

$^{13}C\{^1H\}$ NMR (100 MHz, D_2O): δ 164.6 (s, carbonate), 59.7 (m), 56.3 (m), 50.9 (m), 46.3 (m).

$^{31}P\{^1H\}$ NMR (122 MHz, D_2O): δ 23.5 (t, $^2J_{P\text{-}P}$ = 54 Hz), 9.4 (t, $^2J_{P\text{-}P}$ = 54 Hz).

Anal. Calc. For $C_{13}H_{30}N_2O_9FeP_4 \cdot 2.5H_2O$: C, 26.8; H, 6.05; N, 4.80%. Found: C, 26.4; H, 5.65; N, 4.58%.

IR (cm^{-1}): 1681 (ν_{CO}), 1620 (ν_{CO}).

Synthesis of $[Fe(L^1)(CO)_2](SO_4)$ (9)

A solution of $[Fe(L^1)(H_2O)_2]SO_4$ (**1**) (30 mg, 0.044 mmol) in H_2O (30 mL) was purged with CO for 30 mins and stirred for a further 3 hours under an atmosphere of CO, resulting in a yellow solution of **9**. The solution was reduced to dryness, giving a yellow microcrystalline solid, which was washed with acetone. Yellow crystals suitable for X-ray crystallography were grown from an aqueous solution of **9** under an atmosphere of CO at 5°C. Yield = 27 mg (93%).

^1H NMR (400 MHz, D_2O): δ 4.73 (s, 4H,), 4.53 (s, 8H), 3.71 (s, 4H), 3.67 (AB, 8H, $\Delta\nu$ = 71 Hz, $^2J_{H\text{-}H}$ =15.0 Hz).

$^{13}C\{^1H\}$ NMR (101 MHz, D_2O): δ 204.2 (m, CO), 59.9 (m), 58.7 (m), 49.3 (m), 46.5 (m).

$^{31}P\{^1H\}$ NMR (122 MHz, D_2O): δ -14.9 (t, $^2J_{P\text{-}P}$ = 35 Hz), -39.4 (t, $^2J_{P\text{-}P}$ = 35 Hz).

Anal. Calc. For $C_{14}H_{30}N_2O_{12}FeP_4S \cdot 2H_2O$: C, 25.2; H, 5.14; N, 4.20%. Found: C, 25.4; H, 5.08; N, 4.11%.

IR (cm^{-1}): 2059 (ν_{CO}), 2022 (ν_{CO}).

Synthesis of $[Fe(L^1)(CO)Cl](Cl)$ (12)

$[Fe(L^1)Cl_2]$ (**3**) (7 mg, 0.013 mmol) was dissolved in acetone (20 mL) with heating. The purple solution was purged with carbon monoxide for 10 mins and stirred for 15 minutes, affording an orange precipitate. The solid **12** was collected by filtration and washed with acetone (10 mL). Yield = 7 mg (97%).

^{1}H NMR (400 MHz, D2O): δ 4.74 (s, 2H), 4.56 (AB, 4H, $\Delta\nu$ = 20 Hz, $^{2}J_{H-H}$ = 13.1 Hz), 4.42 (AB, 4H, $\Delta\nu$ = 28 Hz, $^{2}J_{H-H}$ = 13.5 Hz), 4.31 (s, 2H), 3.74 (AB, 4H, $\Delta\nu$ = 27 Hz, $^{2}J_{H-H}$ = 15.3 Hz), 3.61 (AB, 4H, $\Delta\nu$ = 120 Hz, $^{2}J_{H-H}$ =16.3 Hz), 3.26 (AB, 4H, $\Delta\nu$ = 105 Hz, $^{2}J_{H-H}$ =15.2 Hz).

^{31}P{^{1}H} NMR (122 MHz, D_2O): δ 5.3 (dt, $^{2}J_{P-P}$ = 74 Hz, $^{2}J_{P-P}$ = 41 Hz), -5.5 (dd, $^{2}J_{P-P}$ = 54 Hz, $^{2}J_{P-P}$ = 41 Hz), -29.4 (dt, $^{2}J_{P-P}$ = 74 Hz, $^{2}J_{P-P}$ = 54 Hz).

Anal. Calc. For $C_{13}H_{30}N_2O_7FeP_4Cl_2$: C, 27.1; H, 5.24; N, 4.85%. Found: C, 26.9; H, 5.25; N, 4.52%.

IR (cm^{-1}): 1987 (ν_{CO}).

Synthesis of $^{57}FeSO_4.7H_2O$

^{57}Fe metal powder (320 mg, 5.61 mmol) was stirred in conc. H_2SO_4 solution (8 mL of 4.5 M) for 2 hrs under an atmosphere of dinitrogen. The solution took on a pale green colouration with a pale green precipitate with stirring, and *ca*. half of the solvent was removed after the evolution of hydrogen gas had finished. The suspension was left at 5°C for *ca*. 24 hrs, after which time more of the pale green solid had formed. Solid was filtered, washed with cold H_2O (2 mL) and dried in a desiccator. Yield = 888 mg (57%).

Synthesis of $[^{57}Fe(L^1)(H_2O)_2]SO_4$

The synthesis was carried out exactly the same as for **1**, only $^{57}FeSO_4.7H_2O$ was used. Yield = 350 mg (16%).

Synthesis of $[^{57}Fe(L^1)(CO)_2]SO_4$

The synthesis was carried out exactly the same as for **9**, only $[^{57}FeL^1(H_2O)_2]SO_4$ was used instead of **1**. Yield = 70 mg (67 %).

Synthesis of $[Fe(L^2)(\kappa^2\text{-}O_2SO_2)]$ (13)

$[Fe(L^1)(H_2O)_2]SO_4$ (**1**) (100 mg, 0.147 mmol) was heated in acetic anhydride (30 mL) at 120°C under an atmosphere of N_2 for 2 hrs, slowly dissolving the complex over time to give a red solution. The solution was reduced in volume to *ca*. 1-2 mL under vacuum,

and a red solid was precipitated on addition of diethyl ether (30 mL) and the solution decanted. The crude red solid of **13** was washed thoroughly with diethyl ether (20 mL) and recrystallised from CH_2Cl_2/Et_2O. Yield = 83 mg (69%).

^{1}H NMR (400 MHz, $CDCl_3$): δ 4.87 (AB, 8H, $\Delta\nu$ = 35 Hz, $^2J_{H-H}$ = 12.3 Hz), 4.74 (s, 4H), 3.89 (s, 4H), 3.57 (br, 4H), 3.22 (br, 4H), 2.18 (s, 6H, equatorial OCH_3), 2.17 (s, 12H axial OCH_3).

$^{13}C\{^1H\}$ NMR (100 MHz, $CDCl_3$): δ 170.5 (s, equatorial ester C=O), 170.4 (s, axial ester C=O), 58.6 (m), 57.0 (m), 51.1 (m), 46.8 (m), 20.6 (s, axial methyl), 20.5, (s, equatorial methyl).

$^{31}P\{^1H\}$ NMR (122 MHz, $CDCl_3$): δ 15.3 (t, $^2J_{P-P}$ = 51 Hz), 0.9 (t, $^2J_{P-P}$ = 51 Hz).

Anal. Calc. For $C_{24}H_{42}N_2O_{16}FeP_4S$: C, 34.9; H, 5.13; N, 3.39%. Found: C, 34.7; H, 5.17; N, 3.16%.

IR (cm^{-1}): 1744 ($\nu_{C=O}$), 1219 (ν_{C-O}).

Synthesis of $[Fe(L^1)(H_2NCH_2CO_2\text{-}\kappa^2\textit{N,O})]HSO_4$ (14)

$[Fe(L^1)(H_2O)_2]SO_4$ (**1**) (100 mg, 0.147 mmol) was stirred in H_2O (20 mL) for 10 mins, dissolving some of the solid. A solution of glycine (13.2 mg, 0.176 mmol) and NaOH (7.4 mg, 0.185 mmol) in H_2O (3 mL) was added dropwise over an hour under an atmosphere of N_2, keeping the pH below 7. The addition of the glycine/NaOH solution dissolved all the remaining **1**, resulting in an orange solution. An orange solid of **14** was isolated by the addition of acetone (20 mL) to the solution. The orange solid was dried under vacuum at 50° C to remove any water. The solid was then washed with acetone (10 mL), filtered and dried in a dessicator. Yield = 89 mg (89%).

^{1}H NMR (400 MHz, D_2O): δ 4.47 (s, 2H), 4.46 (br m, 4H), 4.23 (AB, 4H, $\Delta\nu$ = 53 Hz, $^2J_{H-H}$ =13.9 Hz), 4.22 (s, 2H), 3.53 (AB, 4H, $\Delta\nu$ = 206 Hz, $^2J_{H-H}$ =15.6 Hz), 3.32 (AB, 4H, $\Delta\nu$ = 31 Hz, $^2J_{H-H}$ =14.8 Hz), 3.0 (AB, 4H, $\Delta\nu$ = 60 Hz, $^2J_{H-H}$ =15.6 Hz).

$^{31}P\{^1H\}$ NMR (122 MHz, D_2O): δ 19.7 (d of t, $^2J_{P-P}$ = 76 Hz, $^2J_{P-P}$ = 51 Hz), 7.2 (d of t, $^2J_{P-P}$ = 76Hz, $^2J_{P-P}$ = 56 Hz), 3.5 (d of d, $^2J_{P-P}$ = 51 Hz, $^2J_{P-P}$ = 56 Hz).

Anal. Calc. For $C_{14}H_{35}N_3O_{12}FeP_4S{\cdot}2H_2O$: C, 24.5; H, 5.74; N, 6.13%. Found: C, 24.7; H, 5.40; N, 6.27%.

IR (cm^{-1}): 1629 (ν_{CO}).

Synthesis of $[Fe(L^2)Cl_2]$ (15)

Bis(triphenylphosphoranylidene)ammonium chloride (PPNCl) (308 mg, 0.537 mmol) was added to a red solution of $[Fe(L^2)(\kappa^2\text{-}O_2SO_2)]$ (**13**) (200 mg, 0.242 mmol) in CH_2Cl_2 (20 mL), resulting in a purple solution of $[Fe(L^2)Cl_2]$ (**15**). A purple solid of **15** was isolated by the addition of diethyl ether, which was isolated by filtration and washed with MeOH (20 mL) and Et_2O (10 mL). Yield = 103 mg (50%).

^1H NMR (400 MHz, $CDCl_3$): δ 5.18 (AB, 8H, $\Delta\nu$ = 150Hz, $^2J_{H\text{-}H}$ =13.6 Hz), 4.95 (s, 4H), 3.46 (s, 4H), 3.18 (AB, 8H, $\Delta\nu$ = 86 Hz, $^2J_{H\text{-}H}$ =14.9 Hz), 2.13 (s, 12H, axial OCH_3), 2.08 (s, 6H, equatorial OCH_3).

$^{13}C\{^1H\}$ NMR (100 MHz, $CDCl_3$): δ 170.7 (s, axial ester C=O), 170.3 (s, equatorial ester C=O), 61.2 (m), 59.2 (m), 52.7 (m), 47.4 (m), 20.8 (s, axial methyl), 20.4 (s, equatorial methyl).

$^{31}P\{^1H\}$ NMR (122 MHz, $CDCl_3$): δ 16.5 (t, $^2J_{P\text{-}P}$ = 59 Hz), -1.6 (t, $^2J_{P\text{-}P}$ = 59 Hz).

Anal. Calc. For $C_{24}H_{42}N_2O_{12}FeP_4Cl_2{\cdot}0.5CH_2Cl_2$: C, 34.9; H, 5.14; N, 3.32%. Found: C, 34.9; H, 5.15; N, 3.10%.

IR (cm^{-1}): 1743 ($\nu_{C=O}$), 1215 ($\nu_{C\text{-}O}$).

Synthesis of $[Fe(L^2)(CO)Cl]BPh_4$ (19)

Sodium tetraphenylborate (22 mg, 0.064 mmol) was added to a purple solution of $[Fe(L^2)Cl_2]$ (**15**) (50 mg, 0.059 mmol) in acetone (10 mL). The solution was stirred under an atmosphere of carbon monoxide at room temperature overnight, resulting in a yellow solution with a white suspension of sodium chloride. The NaCl was removed by filtration, the yellow solution of **19** was reduced to dryness and washed with diethyl ether. Yield = 49 mg (74%).

^{1}H NMR (400 MHz, acetone-d_6): δ 7.34 (m, 8H, Ar), 6.93 (m, 8H, Ar), 6.78 (m, 4H, Ar), 5.19 (s, 2H), 5.02 (AB, 4H, Δν = 17 Hz, $^{2}J_{H-H}$ =13.5 Hz), 4.97 (m, 4H, Δν = 58 Hz, $^{2}J_{H-H}$ =14.1 Hz), 4.74 (s, 2H), 4.06 (AB, 4H, Δν = 22 Hz, $^{2}J_{H-H}$ =16.0 Hz), 3.92 (AB, 4H, Δν = 146 Hz, $^{2}J_{H-H}$ =15.4 Hz), 3.62 (AB, 4H, Δν = 106 Hz, $^{2}J_{H-H}$ =15.4 Hz), 2.22 (s, 3H, equatorial OCH_3), 2.19 (s, 6H, axial OCH_3), 2.15 (s, 3H, equatorial OCH_3), 2.13 (s, 6H, axial OCH_3).

^{13}C{^{1}H} NMR (100 MHz, acetone-d_6): δ 170.9 (m, axial and equatorial ester C=O), 165.0 (q, Ar, $^{1}J_{C-B}$ = 49.5 Hz), 137.1 (s, Ar), 126.1 (q, Ar, $^{3}J_{C-B}$ = 2.4 Hz), 122.3 (s, Ar), 60.8 (m), 58.8 (m), 51.7 (m), 51.1 (m), 46.8 (m), 20.7 (s, axial OCH_3), 20.7 (s, axial OCH_3), 20.6 (s, equatorial OCH_3), 20.5 (s, equatorial OCH_3).

^{31}P{^{1}H} NMR (122 MHz, acetone-d_6): δ -6.4 (dt, $^{2}J_{P-P}$ = 66, 40 Hz), -11.8 (dd, $^{2}J_{P-P}$ = 40, 55 Hz), -35.7 (dt, 1P, $^{2}J_{P-P}$ = 54, 66 Hz).

Anal. Calc. For $C_{49}H_{62}N_2O_{13}FeP_4ClB$: C, 52.9; H, 5.61; N, 2.52%. Found: C, 52.6; H, 5.59; N, 2.49%.

IR (cm^{-1}): 1993 (ν_{CO}), 1751 ($\nu_{C=O}$), 1204 (ν_{C-O}).

Synthesis of [Fe(L^2)$(NCS)_2$] (20)

A solution of potassium thiocyanate (8 mg, 0.0823 mmol) in H_2O (1 mL) was added to a purple solution of [Fe(L^2)Cl_2] (**15**) (30 mg, 0.0356 mmol) in acetone (2 mL), resulting in an orange solution of [Fe(L^2)$(NCS)_2$] (**20**). An orange microcrystalline solid of **20** was isolated by slow evaporation of the acetone from the acetone/water solution. Yield = 26 mg (85%).

^{1}H NMR (400 MHz, DMSO-d_6): δ 4.75 (AB, 8H, Δν = 44 Hz, $^{2}J_{H-H}$ =13.5 Hz), 4.55 (s, 4H), 3.68 (s, 4H), 3.32 (AB, 8H, Δν = 49 Hz, $^{2}J_{H-H}$ =15.2 Hz), 2.14 (s, 6H, equatorial OCH_3), 2.13 (s, 12H axial OCH_3).

^{13}C{^{1}H} NMR (100 MHz, DMSO-d_6): δ 170.4 (s, equatorial ester C=O), 170.3 (s, axial ester C=O), 59.0 (m), 50.0 (m, 4C), 45.7 (m), 20.6 (s, axial OCH_3), 20.5, (s, equatorial OCH_3).

^{31}P{^{1}H} NMR (122 MHz, DMSO-d_6): δ 4.1 (s).

Anal. Calc. For $C_{26}H_{42}N_4O_{12}FeP_4S_2 \cdot H_2O$: C, 36.12; H, 5.13; N, 6.48%. Found: C, 35.8; H, 4.98; N, 5.74%

IR (cm^{-1}): 2108 (ν_{NCS}), 1748 ($\nu_{C=O}$), 1213 (ν_{C-O}).

Synthesis of $[Fe(L^2)(N_3)_2]$ (21)

A solution of sodium azide (5 mg, 0.0769 mmol) in H_2O (1 mL) was added to a purple solution of $[Fe(L^2)Cl_2]$ (**15**) (30 mg, 0.0356 mmol) in acetone (2 mL), resulting in an red solution of $[Fe(L^2)(N_3)_2]$ (**21**). Red crystals of **21** were isolated by slow evaporation of the acetone from the acetone/water solution. Yield = 27 mg (91%).

^1H NMR (400 MHz, acetone-d_6): δ 5.00 (AB, 8H, $\Delta\nu$ = 44 Hz, $^2J_{H-H}$ =13.5 Hz), 4.82 (s, 4H), 3.82 (s, 4H), 3.41 (s, 8H), 2.17 (s, 12H, axial OCH_3), 2.10 (s, 6H, equatorial OCH_3).

$^{13}C\{^1H\}$ NMR (100 MHz, acetone-d_6): δ 171.2 (s, axial ester C=O), 171.0 (s, equatorial ester C=O), 60.2 (m), 59.8 (m), 52.7 (m), 47.9 (m), 20.9 (s, axial OCH_3), 20.6 (s, equatorial OCH_3).

$^{31}P\{^1H\}$ NMR (162 MHz, acetone-d_6): δ 10.0 (second order), 8.6 (second order).

Anal. Calc. For $C_{24}H_{42}N_8O_{12}FeP_4 \cdot H_2O$: C, 34.63; H, 5.33; N, 13.46%. Found: C, 34.7; H, 5.10; N, 13.3%.

IR (cm^{-1}): 2047 (ν_{N3}), 1735 ($\nu_{C=O}$), 1219 (ν_{C-O}).

4.3 Syntheses of chapter 3 compounds

Synthesis of $P(CH_2OH)_3$ (THMP)[3]

$[P(CH_2OH)_4]Cl$ (50.0g of 80% aqueous solution, 262 mmol) solution was evaporated to dryness on a rotary evaporator, and dried further with an azeotropic toluene distillation for 2 hrs. Dry triethylamine (100 mL) was added to the white solid of $[P(CH_2OH)_4]Cl$, and the reaction was stirred at 60°C for two hours. The resulting white precipitate of $[NEt_4]Cl$ was removed by filtration. The reaction solution was then vacuum distilled at atmospheric pressure, which removed the excess triethylamine and sublimed the formaldehyde out in the condenser. The resulting colourless oil of $P(CH_2OH)_3$ was left

to cool and crystallised into a white solid upon leaving at -20°C for *ca*. 7 days. Yield = 29.0 g (89%).

Synthesis of $PhP(CH_2OH)_2$

Phenylphosphine (10.0 g, 90.8 mmol) was added dropwise to a solution of formaldehyde (15.1 g of 37% solution, 186 mmol) in degassed ethanol (80 mL) under an atmosphere of dinitrogen. The reaction mixture was stirred for 5 hrs, after which the solvent was removed in vacuo, giving a colourless oil. The oil crystallised into a white solid of $PhP(CH_2OH)_2$ upon leaving at -20°C for *ca*. 48 hrs. Yield = 13.5 g (87%).

Synthesis of $[Fe(L^3)_2(\kappa^2\text{-}O_2SO_2)]$ (23)

Iron(II) sulphate heptahydrate (101 mg, 0.363 mmol), ammonium sulphate (97 mg, 0.734 mmol), and formaldehyde solution (66 mg of 37% solution, 0.813 mmol) were dissolved in H_2O (20 mL) under an atmosphere of N_2 to give a pale green solution. $PhP(CH_2OH)_2$ was separately dissolved in degassed H_2O (10 mL), which was then slowly added dropwise over *ca*. 30 mins to the iron-containing solution whist stirring, taking care to keep the pH below ca. 5.5. The addition of the aqueous phosphine solution gave rise to a purple colouration of the solution, which increased in intensity with further addition of the phosphine solution. As the solution became darker, a purple solid began to precipitate, which continued with the addition until there was a large amount of the purple precipitate. The reaction was left to stir for one hour further, the purple product then collected by filtration and washed with 2 mL cold H_2O. The purple solid **23** was then dried in a dessicator under reduced pressure overnight. Yield = 93 mg (33%).

^{1}H NMR (500 MHz, $CDCl_3$): δ 7.4-7.1 (m, 20H, Ar), 5.27 (d, 2H, P-CH_2-N AB1, $\Delta\nu$ = 821 Hz, $^2J_{H\text{-}H}$ = 13.9 Hz), 4.92 (d, 2H, P-CH_2-N AB2, $\Delta\nu$ = 736 Hz, $^2J_{H\text{-}H}$ = 12.9 Hz), 4.17 (d, 2H, N-CH_2-N AB, $\Delta\nu$ = 76 Hz, $^2J_{H\text{-}H}$ = 13.9 Hz), 4.01 (d, 2H, N-CH_2-N AB, $\Delta\nu$ = 76 Hz, $^2J_{H\text{-}H}$ = 13.9 Hz), 4.03 (d, 2H, P-CH_2-N AB3, $\Delta\nu$ = 228 Hz, $^2J_{H\text{-}H}$ = 13.9 Hz), 3.63 (d, 2H, P-CH_2-N AB1, $\Delta\nu$ = 821 Hz, $^2J_{H\text{-}H}$ = 13.9 Hz), 3.53 (d, 2H, P-CH_2-N AB4, $\Delta\nu$ = 411 Hz, $^2J_{H\text{-}H}$ = 13.9 Hz), 3.53 (d, 2H, P-CH_2-N AB3, $\Delta\nu$ = 228 Hz, $^2J_{H\text{-}H}$ = 13.9 Hz), 3.45 (d, 2H P-CH_2-N AB2, $\Delta\nu$ = 736 Hz, $^2J_{H\text{-}H}$ = 12.9 Hz), 2.71 (d, 2H, P-CH_2-N AB4, $\Delta\nu$ = 411 Hz, $^2J_{H\text{-}H}$ = 13.9 Hz).

^{31}P $\{^1$H$\}$ NMR (122 MHz, $CDCl_3$): δ -26.4 (t, $^2J_{P\text{-}P}$ = 72 Hz), -51.2 (t, $^2J_{P\text{-}P}$ = 72 Hz).

Anal. Calc. for $C_{34}H_{40}N_4O_4FeP_4S_1 \cdot H_2O$: C, 51.1; H, 5.30; N, 6.99%. Found: C, 50.7; H, 5.25; N, 6.28%

Electrospray MS: *m*/*z* = 803.1 $[M+Na]^+$.

Synthesis of *cis*-$[Fe(L^3)_2Cl_2]$ (24a) and *trans*-$[Fe(L^3)_2Cl_2]$ (24b)

The reaction was carried out as for the synthesis of **23**, except using iron(II) chloride tetrahydrate (335 mg, 1.69 mmol) and ammonium chloride (362 mg, 6.77 mmol) in the same stoichiometry, instead of the equivalent chloride salts. The purple product was then collected by filtration and washed with 2 mL cold H_2O. The purple solid of *cis*-$[Fe(L^3)_2Cl_2]$ (**24a**) was dried in a desiccator under reduced pressure overnight. Yield = 1.01g (79%).

$^{31}P\{^1H\}$ NMR (122 MHz, $CDCl_3$): -32.4 (br t), -46.5 (br t).

$^{31}P\{^1H\}$ NMR (122 MHz, D_2O - *cis*-$[Fe(L^3)_2(H_2O)_2]Cl_2$): δ -17.9 (t, $^2J_{P\text{-}P}$ = 74 Hz), -38.2 (t, $^2J_{P\text{-}P}$ = 74 Hz).

cis-$[Fe(L^3)_2Cl_2]$ was placed in a cellulose extraction thimble inserted into a Soxhlet extractor fitted with a condenser and round bottomed flask. Diethyl ether was placed in the RBF and the extraction was left for 24 hours. This gave a yellow solution of *trans*-$[Fe(L^3)_2Cl_2]$, which gave yellow crystals upon evaporation of the ether solution at room temperature. No NMR spectra of *trans*-$[Fe(L^3)_2Cl_2]$ (**24b**) were recorded as the complex isomerises to the *cis* isomer **24a** when dissolved in most organic solvents, and is not soluble enough in Et_2O to be able to get a concentrated enough sample for NMR analysis.

Anal. Calc. for $C_{34}H_{40}N_4FeP_4Cl_2$: C, 54.0; H, 5.34; N, 7.42%. Found: C, 53.4; H, 5.33; N, 7.23%

Electrospray MS: *m*/*z* = 684.2 $[M-2Cl]^+$.

Synthesis of *cis*-$[Fe(L^3)_2(NCS)_2]$ (25a) and *trans*-$[Fe(L^3)_2(NCS)_2]$ (25b)

cis-$[Fe(L^3)_2Cl_2]$ (**24a**) (50 mg, 0.66 mmol) was dissolved in ethanol (10 mL) giving a purple suspension. Excess potassium thiocyanate (129 mg, 1.33 mmol) was added to the reaction mixture, reacting any undissolved **24a** and giving an orange precipitate of

25a. The orange solid was collected and washed with cold H_2O (5 mL). Yield = 43 mg (78%). Single crystals of **25b** suitable for X-ray diffraction were grown from a $CDCl_3$ solution over *ca*. 48 hrs. $^{31}P\{^1H\}$ and ^1H NMR spectroscopy showed a mixture of **26a** and **26b** in an 4:1 ratio after 20 mins in solution, which changed to 2:3 ratio after 48 hrs.

^1H NMR (**25a**) (300 MHz, $CDCl_3$): δ 7.8-6.6 (m, 20H, Ar), 4.6 (d, 2H, P-CH_2-N AB1, $\Delta\nu$ = 391 Hz, $^2J_{H-H}$ = 13.9 Hz), 4.3 (d, 2H, P-CH_2-N AB2, $\Delta\nu$ = 387 Hz, $^2J_{H-H}$ = 13.4 Hz), 4.0 (d, 2H, P-CH_2-N AB3, $\Delta\nu$ = 161 Hz $^2J_{H-H}$ = 13.8 Hz), 3.9 (d, 2H, N-CH_2-N AB, $\Delta\nu$ = 24 Hz, $^2J_{H-H}$ = 13.9 Hz), 3.8 (d, 2H, N-CH_2-N AB, $\Delta\nu$ = 24 Hz, $^2J_{H-H}$ = 13.9 Hz), 3.5 (d, 2H, P-CH_2-N AB4, $\Delta\nu$ = 309 Hz, $^2J_{H-H}$ = 13.8 Hz), 3.5 (d, 2H, P-CH_2-N AB3, $\Delta\nu$ = 161 Hz, $^2J_{H-H}$ = 13.8 Hz), 3.3 (d, 2H, P-CH_2-N AB1, $\Delta\nu$ = 391 Hz, $^2J_{H-H}$ = 13.9 Hz), 3.0 (d, 2H P-CH_2-N AB2, $\Delta\nu$ = 387 Hz, $^2J_{H-H}$ = 13.4 Hz), 2.4 (d, 2H, P-CH_2-N AB4, $\Delta\nu$ = 309 Hz, $^2J_{H-H}$ = 13.8 Hz).

$^{31}P\{^1H\}$ NMR (**25a**) (122 MHz, $CDCl_3$): δ -31.0 (t, 2P, $^2J_{P-P}$ = 77 Hz), -38.6 (t, 2P, $^2J_{P-P}$ = 77 Hz).

^1H NMR (**25b**) (300 MHz, $CDCl_3$): δ 7.8-6.6 (m, 20H, Ar), 4.3 (d, 8H, P-CH_2-N AB, $\Delta\nu$ = 221 Hz, $^2J_{H-H}$ = 13.4 Hz), 4.0 (s, 4H, N-CH_2-N), 3.5 (d, 8H, P-CH_2-N AB, $\Delta\nu$ = 221 Hz, $^2J_{H-H}$ = 13.4 Hz).

$^{31}P\{^1H\}$ NMR (**25b**) (122 MHz, $CDCl_3$): δ -42.2 (s, 4P).

Anal. Calc. for $C_{36}H_{40}N_6FeP_4S_2 \cdot 4H_2O$: C, 49.6; H, 5.54; N, 9.63%. Found: C, 49.2; H, 4.74; N, 9.41%

IR (cm^{-1}): 2098 (ν_{NCS}).

Electrospray MS: *m*/*z* = 742.1 $[M\text{-}NCS]^+$.

Synthesis of *cis*-$[Fe(L^3)_2(N_3)_2]$ (26a) and *trans*-$[Fe(L^3)_2(N_3)_2]$ (26b)

cis-$[Fe(L^3)_2Cl_2]$ (**24a**) (50 mg, 0.066 mmol) was dissolved in ethanol (10 mL) giving a purple suspension. Excess sodium azide (86 mg, 1.32 mmol) was added to the reaction mixture, reacting any undissolved **24a** and giving a red suspension of **26a**. The red solid was collected and washed with cold H_2O (5 mL). As with complex **7**, repeated attempts to record an elemental analysis gave consistently high %N values

due to the difficulty in removing excess sodium azide leftover from the reaction. $^{31}P\{^1H\}$ and ^1H NMR spectroscopy showed a mixture of **26a** and **26b** in an 11:1 ratio, which did not change over time.

^1H NMR (**26a**) (300 MHz, $CDCl_3$): δ 7.5-7.1 (m, 20H, Ar), 4.7 (d, 2H, P-CH_2-N AB1, Δν = 30 Hz, $^2J_{H-H}$ = 13.6 Hz), 4.6 (d, 2H, P-CH_2-N AB2, Δν = 473 Hz, $^2J_{H-H}$ = 13.6 Hz), 3.9 (d, 2H, P-CH_2-N AB3, Δν = 155 Hz, $^2J_{H-H}$ = 13.6 Hz), 3.9 (d, 2H, N-CH_2-N AB, Δν = 25 Hz, $^2J_{H-H}$ = 13.6 Hz,), 3.9 (d, 2H, N-CH_2-N AB, Δν = 25 Hz, $^2J_{H-H}$ = 13.6 Hz,), 3.5 (d, 2H, P-CH_2-N AB4, Δν = 293 Hz, $^2J_{H-H}$ = 13.6 Hz), 3.4 (d, 2H, P-CH_2-N AB3, Δν = 155 Hz, $^2J_{H-H}$ = 13.6 Hz), 3.4 (d, 2H, P-CH_2-N AB1, Δν = 30 Hz, $^2J_{H-H}$ = 13.6 Hz), 3.0 (d, 2H, P-CH_2-N AB2, Δν = 473 Hz, $^2J_{H-H}$ = 13.6 Hz), 2.5 (d, 2H, P-CH_2-N AB4, Δν = 293 Hz, $^2J_{H-H}$ = 13.6 Hz).

$^{31}P\{^1H\}$ NMR (**26a**) (122 MHz, $CDCl_3$): δ -27.4 (t, $^2J_{P-P}$ = 75 Hz), -36.9 (t, $^2J_{P-P}$ = 75 Hz).

^1H NMR (**26b**) (300 MHz, $CDCl_3$): δ 7.5-7.1 (m, 20H, Ar), 4.3 (d, 8H, P-CH_2-N AB, Δν = 186 Hz, $^2J_{H-H}$ = 14.1 Hz), 4.2 (s, 4H, N-CH_2-N), 3.6 (d, 8H, P-CH_2-N AB, Δν = 186 Hz, $^2J_{H-H}$ = 14.1 Hz).

$^{31}P\{^1H\}$ NMR (**26b**) (122 MHz, $CDCl_3$): δ -43.2 (s).

IR (cm^{-1}): 2043 (ν_{N3} - mainly *trans* isomer).

Electrospray MS: *m*/*z* = 684.2 $[M-2N_3]^+$.

Synthesis of $[Fe(L^3)_2(\kappa^2\text{-}O_2CO)]$ (27)

cis-$[Fe(L^3)_2Cl_2]$ (**24a**) (107 mg, 0.142 mmol) was dissolved in ethanol (20 mL) giving a purple suspension. Excess sodium carbonate (170 mg, 1.60 mmol) was added, reacting any undissovled **24a** and giving a pink suspension. The resulting pink solid was recrystallised from chloroform. Yield = 61 mg (59%) Single crystals suitable for X-ray diffraction grew from the aqueous reaction filtrate over *ca*. 8 weeks.

^1H NMR (500 MHz, $CDCl_3$): δ 7.6-7.1 (m, 20H, Ar), 5.16 (d, 2H, P-CH_2-N AB1, Δν = 918 Hz, $^2J_{H-H}$ = 12.9 Hz,), 4.76 (d, 2H, P-CH_2-N AB2, Δν = 680 Hz, $^2J_{H-H}$ = 12.9 Hz,), 4.03 (d, 2H, P-CH_2-N AB3, Δν = 277 Hz, $^2J_{H-H}$ = 12.9 Hz,), 4.00 (d, 2H, N-CH_2-N AB, Δν = 33 Hz, $^2J_{H-H}$ = 14.5 Hz), 3.94 (d, 2H, N-CH_2-N AB, Δν = 33 Hz, $^2J_{H-H}$ = 13.9 Hz), 3.48 (d, 2H, P-CH_2-N AB4, Δν = 401 Hz, $^2J_{H-H}$ = 13.9 Hz), 3.48 (d, 2H, P-CH_2-N AB3, Δν = 277

Hz, $^{2}J_{H\text{-}H}$ = 12.9 Hz), 3.40 (d, 2H, P-CH_2-N AB2, Δν = 680 Hz, $^{2}J_{H\text{-}H}$ = 12.9 Hz), 3.32 (d, 2H P-CH_2-N AB1, Δν = 918 Hz, $^{2}J_{H\text{-}H}$ = 12.9 Hz), 2.68 (d, 2H, P-CH_2-N AB4, Δν = 401 Hz, $^{2}J_{H\text{-}H}$ = 13.9 Hz).

$^{13}C\{^{1}H\}$ NMR (125 MHz, $CDCl_3$): δ 163.7 (s, $O_2\underline{C}O$), 131-128 (m, Ar), 72.8 (s, N-$\underline{C}H_2$-N), 53.3 (m, P-$\underline{C}H_2$-N), 51.2 (m, P-$\underline{C}H_2$-N), 50.9 (s, P-$\underline{C}H_2$-N), 48.0 (s, P-$\underline{C}H_2$-N).

$^{31}P\ \{^{1}H\}$ NMR (122 MHz, $CDCl_3$): δ -20.2 (t, $^{2}J_{P\text{-}P}$ = 72 Hz), -41.4 (t, $^{2}J_{P\text{-}P}$ = 72 Hz).

Anal. Calc. for $C_{35}H_{40}N_4O_3FeP_4$: C, 56.5; H, 5.42; N, 7.53%. Found: C, 56.1; H, 5.29; N, 7.46.

IR (cm^{-1}): 1556 ($\nu_{C=O}$).

Electrospray MS: *m*/*z* = 701.2 $[M\text{-}CO_2]^{+}$.

Synthesis of *trans*-$[Fe(L^3)_2(CO)Cl]Cl$ (28a)

cis-$[Fe(L^3)_2Cl_2]$ (**24a**) (100 mg, 0.133 mmol) was dissolved in H_2O (20 mL) and purged with CO for *ca*. 20 mins. The reaction was stirred for *ca*. two hrs, resulting in a yellow solution. A yellow solid was precipitated from solution by the addition of acetone. The yellow solid of **28a** was washed with additional acetone (5 mL) and dried in a desiccator. Yield = 87 mg (83%).

^{1}H NMR (400 MHz, D_2O): δ 7.1-6.9 (m, 20H, Ar), 4.9 (d, 4H, P-CH_2-N AB1, Δν = 423 Hz, $^{2}J_{H\text{-}H}$ = 13.5 Hz), 4.4 (d, 4H, P-CH_2-N AB2, Δν = 156 Hz, $^{2}J_{H\text{-}H}$ = 14.5 Hz), 3.9 (s, 4H, N-CH_2-N), 3.8 (d, 4H, P-CH_2-N AB2, Δν = 156 Hz, $^{2}J_{H\text{-}H}$ = 14.5 Hz), 3.5 (d, 4H, P-CH_2-N AB1, Δν = 423 Hz, $^{2}J_{H\text{-}H}$ = 13.5 Hz).

$^{13}C\{^{1}H\}$ NMR (*trans*-$[Fe(L^3)_2(^{13}CO)Cl]Cl$, 126 MHz, D_2O): δ 214.7 (quintet, $^{13}\underline{C}O$), 132-129 (m, Ar), 72.2 (s, N-$\underline{C}H_2$-N), 52.3 (s, P-$\underline{C}H_2$-N), 49.1 (s, P-$\underline{C}H_2$-N).

$^{31}P\{^{1}H\}$ NMR (122 MHz, D_2O): δ -51.0 (s).

Anal. Calc. for $C_{35}H_{40}N_4O_1FeP_4Cl_2{\cdot}6H_2O$: C, 46.6; H, 5.81; N, 6.21%. Found: C, 46.3; H, 5.47; N, 6.06%.

IR (cm^{-1}): 1939 (ν_{12CO}), 1895 (ν_{13CO}).

Electrospray MS: *m*/*z* = 747.1 $[M]^+$.

Synthesis of *cis*-[Fe(L^3)$_2$(CO)Cl]Cl (28b)

trans-[Fe(L^3)$_2$$Cl_2$] (**24a**) (10 mg, 0.013 mmol) was dissolved in diethyl ether (20 mL) giving a pale yellow solution. CO was purged through the reaction mixture for *ca*. 20 mins and the reaction mixture was stirred for a further 4 hrs, after which time a pale pink precipitate began to form. The pink solid was filtered off after a further 7 days of stirring, washed with Et_2O (5 mL) and dried in air. Yield = 5 mg (48%).

$^{31}P\{^1H\}$ NMR (122 MHz, $CDCl_3$): δ -39.4 (ddd, $^2J_{P\text{-}P}$ = 91, 38, 45 Hz), -55.3 (ddd, $^2J_{P\text{-}P}$ = 91, 61, 48 Hz), -59.4 (ddd, $^2J_{P\text{-}P}$ = 38, 61, 120 Hz), -69.0 (ddd, $^2J_{P\text{-}P}$ = 45, 48, 120 Hz).

Anal. Calc. for $C_{35}H_{40}N_4O_1FeP_4Cl_2$: C, 53.6; H, 5.15; N, 7.15%. Found: C, 53.0; H, 5.54; N, 4.91%.

IR (cm^{-1}): 1974 (ν_{CO}).

Electrospray MS: *m*/*z* = 747.1 $[M]^+$.

Synthesis of *trans*-[Fe(L^3)$_2$(H)Cl] (29)

cis-[Fe(L^3)$_2$$Cl_2$] (**24a**) (200 mg, 0.265 mmol) and sodium borohydride (20 mg, 0.529 mmol) were placed in a Schlenk tube under dinitrogen, to which was added 10 mL of degassed ethanol, dissolving the starting materials to give an orange solution. Upon stirring for *ca*. 1hr, all the starting materials had reacted resulting in an orange suspension. The solution was filtered by cannula under dinitrogen and the solid washed with 5 mL of degassed ethanol and dried under vacuum. Yield = 128 mg (67%).

^1H NMR (400 MHz, C_6D_6): δ 7.0-6.8 (m, 20H, Ar), 5.5 (d, 4H, P-CH_2-N <u>A</u>B1, $\Delta\nu$ = 806 Hz, $^2J_{H\text{-}H}$ = 12.9 Hz), 3.9 (s, 4H, N-CH_2-N), 3.9 (d, 4H, P-CH_2-N <u>A</u>B2, $\Delta\nu$ = 107 Hz, $^2J_{H\text{-}H}$ = 13.3 Hz), 3.6 (d, 4H, P-CH_2-N A<u>B</u>2, $\Delta\nu$ = 107 Hz, $^2J_{H\text{-}H}$ = 13.3 Hz), 3.5 (d, 4H, P-CH_2-N A<u>B</u>1, $\Delta\nu$ = 806 Hz, $^2J_{H\text{-}H}$ = 12.9 Hz), -28.6 (quintet, hydride, $^2J_{P\text{-}C}$ = 49 Hz).

^{31}P NMR (162 MHz, C_6D_6): δ -27.5 (d, $^2J_{P\text{-}H}$ = 49 Hz).

Anal. Calc. for $C_{34}H_{41}N_4FeP_4Cl_1$: C, 56.6; H, 5.73; N, 7.77%. Found: C, 55.4; H, 5.36; N, 6.08%.

Electrospray MS: m/z = 720.1 $[M]^+$.

4.4 Electrochemistry

All reagents used for electrochemical analyses were of analytical or electrochemical grade purity. The supporting electrolyte used for the analyses of the L^1 complexes in aqueous solution was potassium chloride, whereas tetrabutylammonium hexafluorophosphate was used as the supporting electrolyte for measurements of the L^2 and L^3 complexes in acetonitrile and dichloroethane solutions. Solvents used (acetonitrile, dichloroethane, H_2O) were purged with argon to deoxygenate the solution prior to use. All experiments were conducted at 22 ± 2°C.

Voltammetric experiments were performed using an Ecochemie Autolab potentiostat. For the purpose of these experiments a three electrode cell setup was used, comprising of working, counter and reference electrodes. The working electrode used was a 3mm diameter platinum electrode unless otherwise stated. The counter electrode consisted of a spiral of platinum wire. All potentials were referenced to internal cobaltocenium hexafluorophosphate, which was referenced to ferrocene ($E_{1/2}$ = 0.00 V) but were measured using a platinum wire pseudo reference (a platinum wire which was immersed and equilibrated in the electrolyte containing solvent used for the experiment).

4.5 Crystallography

Data for complexes **3**, **5**, **6**, **7**, **8**, **13**, **21**, **24b**, and **27** were collected on a Nonius Kappa CCD diffractometer. Data for complexes **15** and **25b** were collected at Daresbury SRS Station 9.8 and **23** recorded at Daresbury SRS Station 16.2 SMX by Dr. Mary F. Mahon and Dr. John E. Warren. Data for complex **29** were recorded at Daresbury SRS Station 16.2 SMX Dr. Ross W. Harrington. Data for complex **9** was collected by Dr. Michael Ruf on a Bruker SMART 1000 CCD diffractometer at Bruker in Germany. All structures were solved by Dr. Mary F. Mahon or Dr. Gabriele Kociok-Köhn. The solution of all structures was carried out using SHELX-97 while refinements were completed using SHELXL-97.

4.6 References

1. J. C. Jeffery, B. Odell, N. Stevens and R. E. Talbot, *Chem. Commun.*, 2000, 101.
2. H. E. Gottlieb, V. Kotlyar and A. Nudelman, *J. Org. Chem.*, 1997, **62**, 7515.
3. L. Higham, PhD Thesis, University of East Anglia, 2000.

Appendix – Crystallographic Data

Table 1. Crystal data and structure refinement for $[Fe(L^1)Cl_2]$ (**3**).

Compound	$[Fe(L^1)Cl_2]$ (**3**)
Identification code	k06adb1
Empirical formula	$C_{12}\ H_{32}\ Cl_2\ Fe\ N_2\ O_7\ P_4$
Formula weight	567.03
Temperature	150(2) K
Wavelength	0.71073 Å
Crystal system	monoclinic
Space group	$P\ 2_1/n$
Unit cell dimensions	a = 8.00200(10) Å, α = 90°
	b = 17.3350(2) Å, β = 101.0040(10)°
	c = 15.6440(2) Å, γ = 90°
Volume	2130.15(5) $Å^3$
Z	4
Calculated density	1.768 Mg/m^3
Absorption coefficient	1.298 mm^{-1}
F(000)	1176
Crystal size	0.60 x 0.15 x 0.03 mm
Theta range for data collection	3.34 to 30.06°
Limiting indices	-11<=h<=11, -24<=k<=24, -22<=l<=22
Reflections collected / unique	40074 / 6235 [R(int) = 0.0475]
Completeness to theta = 30.06	99.7 %
Max. and min. transmission	0.9621 and 0.5098
Refinement method	Full-matrix least-squares on F^2
Data / restraints / parameters	6235 / 0 / 285
Goodness-of-fit on F^2	1.131
Final R indices [$I>2\sigma(I)$]	R_1 = 0.0310, wR_2 = 0.0614
R indices (all data)	R_1 = 0.0364, wR_2 = 0.0631
Largest diff. peak and hole	0.499 and -0.600 $eÅ^{-3}$

Table 2. Crystal data and structure refinement for $[Fe(L^1)Br_2]$ (**5**).

Compound	$[Fe(L^1)Br_2]$ (**5**)
Identification code	k06adb7
Empirical formula	$C_{12}\ H_{32}\ Br_2\ Fe\ N_2\ O_7\ P_4$
Formula weight	655.95
Temperature	150(2) K
Wavelength	0.71073 Å
Crystal system	monoclinic
Space group	$P\ 2_1/n$
Unit cell dimensions	a = 8.11200(10) Å, α = 90°
	b = 17.2920(2) Å, β = 101.75°
	c = 15.8760(2) Å, γ = 90°
Volume	2180.26(5) $Å^3$
Z	4
Calculated density	1.998 Mg/m^3
Absorption coefficient	4.688 mm^{-1}
F(000)	1320
Crystal size	0.40 x 0.10 x 0.08 mm
Theta range for data collection	3.52 to 30.02°
Limiting indices	-11<=h<=11, -24<=k<=24, -22<=l<=22
Reflections collected / unique	46023 / 6361 [R(int) = 0.0446]
Completeness to theta = 30.02	99.8 %
Max. and min. transmission	0.7055 and 0.2557
Refinement method	Full-matrix least-squares on F^2
Data / restraints / parameters	6361 / 0 / 280
Goodness-of-fit on F^2	1.122
Final R indices [$I>2\sigma(I)$]	R_1 = 0.0249, wR_2 = 0.0501
R indices (all data)	R_1 = 0.0291, wR_2 = 0.0513
Largest diff. peak and hole	0.556 and -0.590 $eÅ^{-3}$

Table 3. Crystal data and structure refinement for $[Fe(L^1)(NCS)_2]$ (**6**).

Compound	$[Fe(L^1)(NCS)_2]$ (**6**)
Identification code	k02dd01
Empirical formula	$C_{14}\ H_{34}\ Fe\ N_4\ O_8\ P_4\ S_2$
Formula weight	630.30
Temperature	150(2) K
Wavelength	0.71073 Å
Crystal system	monoclinic
Space group	$P\ 2_1/a$
Unit cell dimensions	a = 15.7040(5) Å, α = 90°
	b = 9.7750(3) Å, β = 110.309(2)°
	c = 17.6430(5) Å, γ = 90°
Volume	2539.95(13) $Å^3$
Z	4
Calculated density	1.648 Mg/m^3
Absorption coefficient	1.057 mm^{-1}
F(000)	1312
Crystal size	0.50 x 0.40 x 0.30 mm
Theta range for data collection	3.65 to 27.48°
Limiting indices	-20<=h<=20, -12<=k<=12, -22<=l<=22
Reflections collected / unique	33960 / 5799 [R(int) = 0.1231]
Completeness to theta = 27.48	99.5 %
Max. and min. transmission	0.81 and 0.76
Refinement method	Full-matrix least-squares on F^2
Data / restraints / parameters	5799 / 2 / 318
Goodness-of-fit on F^2	1.012
Final R indices [$I>2\sigma(I)$]	R_1 = 0.0465, wR_2 = 0.0889
R indices (all data)	R_1 = 0.0938, wR_2 = 0.1054
Largest diff. peak and hole	1.134 and -0.577 $eÅ^{-3}$

Table 4. Crystal data and structure refinement for $[Fe(L^1)(N_3)_2]$ (**7**).

Compound	$[Fe(L^1)(N_3)_2]$ (**7**)
Identification code	k05ak2
Empirical formula	$C_{12}\ H_{31.75}\ Fe\ N_8\ O_{6.88}\ P_4$
Formula weight	577.93
Temperature	150(2) K
Wavelength	0.71073 Å
Crystal system	monoclinic
Space group	C 2/c
Unit cell dimensions	a = 33.1620(4) Å, α = 90°
	b = 9.60700(10) Å, β = 93.6860(10)°
	c = 27.8860(4) Å, γ = 90°
Volume	8865.75(19) $Å^3$
Z	16
Calculated density	1.732 Mg/m^3
Absorption coefficient	1.023 mm^{-1}
F(000)	4812
Crystal size	0.30 x 0.25 x 0.03 mm
Theta range for data collection	2.94 to 27.47°
Limiting indices	-42<=h<=42, -12<=k<=12, -36<=l<=36
Reflections collected / unique	54628 / 9979 [R(int) = 0.0443]
Completeness to theta = 27.47	98.1 %
Max. and min. transmission	0.9700 and 0.7489
Refinement method	Full-matrix least-squares on F^2
Data / restraints / parameters	9979 / 9 / 656
Goodness-of-fit on F^2	1.076
Final R indices [I>2σ(I)]	R_1 = 0.0384, wR_2 = 0.0809
R indices (all data)	R_1 = 0.0497, wR_2 = 0.0849
Largest diff. peak and hole	0.756 and -0.650 $eÅ^{-3}$

Table 5. Crystal data and structure refinement for [Fe(L^1)(κ^2-O_2CO)] (**8**).

Compound	[Fe(L^1)(κ^2-O_2CO)] (**8**)
Identification code	k03dd02
Empirical formula	C_{13} $H_{33.40}$ Fe N_2 $O_{10.70}$ P_4
Formula weight	568.75
Temperature	150(2) K
Wavelength	0.71073 Å
Crystal system	monoclinic
Space group	P 2_1/c
Unit cell dimensions	a = 8.6900(1) Å, α = 90°
	b = 16.3080(2) Å, β = 91.948(1)°
	c = 32.2980(5) Å, γ = 90°
Volume	4574.51(10) $Å^3$
Z	8
Calculated density	1.652 Mg/m^3
Absorption coefficient	0.995 mm^{-1}
F(000)	2376
Crystal size	0.25 x 0.20 x 0.20 mm
Theta range for data collection	3.68 to 27.50°
Limiting indices	-8<=h<=10, -17<=k<=21, -40<=l<=39
Reflections collected / unique	15715 / 7791 [R(int) = 0.1020]
Completeness to theta = 27.50	74.2 %
Max. and min. transmission	0.84 and 0.77
Refinement method	Full-matrix least-squares on F^2
Data / restraints / parameters	7791 / 0 / 586
Goodness-of-fit on F^2	1.022
Final R indices [I>2σ(I)]	R_1 = 0.0793, wR_2 = 0.1532
R indices (all data)	R_1 = 0.1985, wR_2 = 0.1985
Largest diff. peak and hole	1.048 and -0.727 $eÅ^{-3}$

Table 6. Crystal data and structure refinement for $[Fe(L^1)(CO)_2]SO_4$ (**9**).

Compound	$[Fe(L^1)(CO)_2]SO_4$ (**9**)
Identification code	fepco
Empirical formula	$C_{4.67}\,H_{10.67}\,S_{10.33}\,Fe_{0.33}\,N_{0.67}\,O_{4.33}\,P_{1.33}$
Formula weight	216.07
Temperature	293(2) K
Wavelength	0.71073 Å
Crystal system	orthorhombic
Space group	Pbca
Unit cell dimensions	a = 16.3440(9) Å, α = 90°
	b = 14.2436(7) Å, β = 90°
	c = 20.7566(10) Å, γ = 90°
Volume	4832.1(4) $Å^3$
Z	8
Calculated density	1.791 Mg/m^3
Absorption coefficient	1.068 mm^{-1}
F(000)	2696
Crystal size	0.22 x 0.18 x 0.08 mm
Theta range for data collection	1.96 to 28.28°
Limiting indices	-20<=h<=21, -10<=k<=18, -27<=l<=27
Reflections collected / unique	33269 / 5982 [R(int) = 0.0731]
Completeness to theta = 28.28	100.0%
Max. and min. transmission	0.91 and 0.79
Refinement method	Full-matrix least-squares on F^2
Data / restraints / parameters	5982 / 0 / 414
Goodness-of-fit on F^2	0.978
Final R indices [I>2σ(I)]	R_1 = 0.0368, wR_2 = 0.0815
R indices (all data)	R_1 = 0.0569, wR_2 = 0.0882
Largest diff. peak and hole	0.657 and -0.686 $eÅ^{-3}$

Table 7. Crystal data and structure refinement for [Fe(L^2)(κ^2-O_2SO_2)] (**13**).

Compound	[Fe(L^2)(κ^2-O_2SO_2)] (**13**)
Identification code	ko5ak1
Empirical formula	$C_{27.90}$ $H_{49.80}$ Fe N_2 $O_{17.30}$ P_4 S
Formula weight	901.89
Temperature	150(2) K
Wavelength	0.71073 Å
Crystal system	monoclinic
Space group	P n
Unit cell dimensions	a = 9.4460(2) Å, α = 90°
	b = 16.4950(3) Å, β = 90.274(1)°
	c = 13.4620(3) Å, γ = 90°
Volume	2097.51(7) $Å^3$
Z	2
Calculated density	1.428 Mg/m^3
Absorption coefficient	0.631 mm^{-1}
F(000)	943
Crystal size	0.15 x 0.15 x 0.07 mm
Theta range for data collection	3.61 to 27.48°
Limiting indices	-12<=h<=12, -21<=k<=21, -17<=l<=17
Reflections collected / unique	39066 / 9522 [R(int) = 0.0563]
Completeness to theta = 27.48	99.7%
Max. and min. transmission	0.94 and 0.86
Refinement method	Full-matrix least-squares on F^2
Data / restraints / parameters	9522 / 46 / 517
Goodness-of-fit on F^2	1.096
Final R indices [I>2σ(I)]	R_1 = 0.0599, wR_2 = 0.1251
R indices (all data)	R_1 = 0.0686, wR_2 = 0.1281
Largest diff. peak and hole	0.610 and -0.566 $eÅ^{-3}$

Table 8. Crystal data and structure refinement for $[Fe(L^2)Cl_2]$ (**15**).

Compound	$[Fe(L^2)Cl_2]$ (**15**)
Identification code	bath147
Empirical formula	$C_{24}\ H_{42}\ Cl_2\ Fe\ N_2\ O_{12}\ P_4$
Formula weight	801.23
Temperature	150(2) K
Wavelength	0.6751 Å
Crystal system	tetragonal
Space group	$P\ 4_2bc$
Unit cell dimensions	a = 21.5338(7) Å, α = 90°
	b = 21.5338(7) Å, β = 90°
	c = 15.5334(8) Å, γ = 90°
Volume	7202.9(5) $Å^3$
Z	8
Calculated density	1.478 Mg/m^3
Absorption coefficient	0.802 mm^{-1}
F(000)	3328
Crystal size	0.03 x 0.02 x 0.02 mm
Theta range for data collection	3.47 to 23.65°
Limiting indices	-14<=h<=25, -25<=k<=17, -18<=l<=9
Reflections collected / unique	20213 / 4868 [R(int) = 0.0622]
Completeness to theta = 23.65	99.5%
Max. and min. transmission	0.9823 and 0.9715
Refinement method	Full-matrix least-squares on F^2
Data / restraints / parameters	4468 / 4 / 403
Goodness-of-fit on F^2	1.026
Final R indices [I>2σ(I)]	R_1 = 0.0550, wR_2 = 0.1408
R indices (all data)	R_1 = 0.0820, wR_2 = 0.1587
Largest diff. peak and hole	0.482 and -0.264 $eÅ^{-3}$

Table 9. Crystal data and structure refinement for $[Fe(L^2)(N_3)_2]$ (**21**)

Compound	$[Fe(L^2)(N_3)_2]$ (**21**)
Identification code	k06adb2
Empirical formula	$C_{24}\ H_{43}\ Fe\ N_8\ O_{12.50}\ P_4$
Formula weight	823.39
Temperature	150(2) K
Wavelength	0.71073 Å
Crystal system	orthorhombic
Space group	P 2 n n (no. 34)
Unit cell dimensions	a = 7.62600(10) Å, α = 90°
	b = 13.8310(2) Å, β = 90°
	c = 16.7350(3) Å, γ = 90°
Volume	1675.13(5) $Å^3$
Z	2
Calculated density	1.549 Mg/m^3
Absorption coefficient	0.679 mm^{-1}
F(000)	858
Crystal size	0.20 x 0.15 x 0.05 mm
Theta range for data collection	3.82 to 27.50°
Limiting indices	-9<=h<=9, -17<=k<=17, -21<=l<=21
Reflections collected / unique	31324 / 4021 [R(int) = 0.0625]
Completeness to theta = 27.50	99.5%
Max. and min. transmission	0.9668 and 0.8761
Refinement method	Full-matrix least-squares on F^2
Data / restraints / parameters	4021 / 1 / 231
Goodness-of-fit on F^2	1.049
Final R indices [I>2σ(I)]	R_1 = 0.0321, wR_2 = 0.0580
R indices (all data)	R_1 = 0.0369, wR_2 = 0.0591
Largest diff. peak and hole	0.323 and -0.545 $eÅ^{-3}$

Table 10. Crystal data and structure refinement for $[Fe(L^3)_2(\kappa^2\text{-}O_2SO_2)]$ (**23**)

Compound	$[Fe(L^3)_2(\kappa^2\text{-}O_2SO_2)]$ (**23**)
Identification code	bath229
Empirical formula	$C_{34}\ H_{44}\ Fe\ N_4\ O_6\ P_4\ S$
Formula weight	816.52
Temperature	150(2) K
Wavelength	0.69040 Å
Crystal system	monoclinic
Space group	C 2/c
Unit cell dimensions	a = 15.422(3) Å, α = 90°
	b = 9.5514(18) Å, β = 100.469(2)°
	c = 24.333(5) Å, γ = 90°
Volume	3524.5(11) $Å^3$
Z	4
Calculated density	1.539 Mg/m^3
Absorption coefficient	0.721 mm^{-1}
F(000)	1704
Crystal size	0.03 x 0.03 x 0.01 mm
Theta range for data collection	3.65 to 22.55°
Limiting indices	-16<=h<=17, -10<=k<=9, -21<=l<=26
Reflections collected / unique	7752 / 2513 [R(int) = 0.0981]
Completeness to theta = 22.55	99.6%
Max. and min. transmission	0.991 and 0.975
Refinement method	Full-matrix least-squares on F^2
Data / restraints / parameters	2513 / 2 / 235
Goodness-of-fit on F^2	0.976
Final R indices [I>2σ(I)]	R_1 = 0.0522, wR_2 = 0.1117
R indices (all data)	R_1 = 0.1064, wR_2 = 0.1314
Largest diff. peak and hole	0.362 and -0.370 $eÅ^{-3}$

Table 11. Crystal data and structure refinement for *trans*-[Fe(L^3)$_2$Cl$_2$] (**24b**)

Compound	*trans*-[Fe(L^3)$_2$Cl$_2$] (**24b**)
Identification code	k06adb9
Empirical formula	C_{68} H_{80} Cl_4 Fe_2 N_8 P_8
Formula weight	1510.66
Temperature	150(2) K
Wavelength	0.71073 Å
Crystal system	monoclinic
Space group	P 2_1/c
Unit cell dimensions	a = 21.9030(2) Å, α = 90°
	b = 10.38000(10) Å, β = 97.99°
	c = 22.1870(2) Å, γ = 90°
Volume	4995.32(8) Å^3
Z	3
Calculated density	1.507 Mg/m^3
Absorption coefficient	0.838 mm^{-1}
F(000)	2352
Crystal size	0.45 x 0.30 x 0.25 mm
Theta range for data collection	3.15 to 27.49°
Limiting indices	-27<=h<=28, -13<=k<=13, -28<=l<=28
Reflections collected / unique	63321 / 11443 [R(int) = 0.0500]
Completeness to theta = 27.49	99.7%
Max. and min. transmission	0.8178 and 0.7041
Refinement method	Full-matrix least-squares on F^2
Data / restraints / parameters	11443 / 0 / 610
Goodness-of-fit on F^2	1.046
Final R indices [I>2σ(I)]	R_1 = 0.0334, wR_2 = 0.0731
R indices (all data)	R_1 = 0.0519, wR_2 = 0.0806
Largest diff. peak and hole	0.575 and -0.525 eÅ^{-3}

Table 12. Crystal data and structure refinement for *trans*-[Fe(L^3)$_2$(NCS)$_2$] (**25b**)

Compound	*trans*-[Fe(L^3)$_2$(NCS)$_2$] (**25b**)
Identification code	bath324
Empirical formula	C_{36} H_{40} Fe N_6 P_4 S_2
Formula weight	800.59
Temperature	150(2) K
Wavelength	0.69070 Å
Crystal system	orthorhombic
Space group	P bcn
Unit cell dimensions	a = 15.0527(9) Å, α = 90°
	b = 14.9361(9) Å, β = 90°
	c = 16.0794(9) Å, γ = 90°
Volume	3615.1(4) Å^3
Z	4
Calculated density	1.471 Mg/m^3
Absorption coefficient	0.747 mm^{-1}
F(000)	1664
Crystal size	0.07 x 0.01 x 0.01 mm
Theta range for data collection	3.09 to 29.56°
Limiting indices	-21<=h<=21, -17<=k<=21, -21<=l<=22
Reflections collected / unique	28014 / 5481 [R(int) = 0.0564]
Completeness to theta = 27.49	99.3%
Max. and min. transmission	0.981 and 0.923
Refinement method	Full-matrix least-squares on F^2
Data / restraints / parameters	5481 / 0 / 222
Goodness-of-fit on F^2	1.014
Final R indices [I>2σ(I)]	R_1 = 0.0343, wR_2 = 0.0792
R indices (all data)	R_1 = 0.0525, wR_2 = 0.0868
Largest diff. peak and hole	0.468 and -0.402 eÅ^{-3}

Table 13. Crystal data and structure refinement for $[Fe(L^3)_2(\kappa^2\text{-}O_2CO)]$ (**27**)

Compound	$[Fe(L^3)_2(\kappa^2\text{-}O_2CO)]$ (**27**)
Identification code	k07adb2
Empirical formula	$C_{35}\ H_{54}\ Fe\ N_4\ O_{10}\ P_4$
Formula weight	870.55
Temperature	150(2) K
Wavelength	0.71073 Å
Crystal system	triclinic
Space group	P -1
Unit cell dimensions	a = 9.4170(2) Å, α = 87.9250(10)°
	b = 10.5490(2) Å, β = 79.2230(10)°
	c = 22.2750(6) Å, γ = 65.6000(10)°
Volume	1977.53(8) $Å^3$
Z	2
Calculated density	1.462 Mg/m^3
Absorption coefficient	0.604 mm^{-1}
F(000)	916
Crystal size	0.25 x 0.15 x 0.05 mm
Theta range for data collection	3.97 to 27.54°
Limiting indices	-12<=h<=12, -13<=k<=13, -28<=l<=28
Reflections collected / unique	23919 / 8778 [R(int) = 0.0669]
Completeness to theta = 27.49	96.3%
Max. and min. transmission	0.9704 and 0.8637
Refinement method	Full-matrix least-squares on F^2
Data / restraints / parameters	8778 / 4 / 543
Goodness-of-fit on F^2	1.111
Final R indices [I>2σ(I)]	R_1 = 0.0606, wR_2 = 0.1355
R indices (all data)	R_1 = 0.0823, wR_2 = 0.1464
Largest diff. peak and hole	0.860 and -0.699 $eÅ^{-3}$

Table 14. Crystal data and structure refinement for *trans*-[Fe(L^3)$_2$(H)Cl] (**29**)

Compound	*trans*-[Fe(L^3)$_2$(H)Cl] (**29**)
Identification code	ssg1322
Empirical formula	C_{43} H_{50} Cl Fe N_4 P_4
Formula weight	838.05
Temperature	150(2) K
Wavelength	0.68840 Å
Crystal system	monoclinic
Space group	C 2/c
Unit cell dimensions	a = 26.873(3) Å, α = 90°
	b = 14.5374(17) Å, β = 111.244(1)°
	c = 22.100(3) Å, γ = 90°
Volume	8047.0(17) Å^3
Z	8
Calculated density	1.383 Mg/m^3
Absorption coefficient	0.637 mm^{-1}
F(000)	3512
Crystal size	0.02 x 0.01 x 0.01 mm
Theta range for data collection	3.44 to 23.91°
Limiting indices	-31<=h<=31, -17<=k<=17, -26<=l<=26
Reflections collected / unique	27709 / 6833 [R(int) = 0.1122]
Completeness to theta = 27.49	99.6%
Max. and min. transmission	0.995 and 0.978
Refinement method	Full-matrix least-squares on F^2
Data / restraints / parameters	6833 / 1 / 516
Goodness-of-fit on F^2	0.958
Final R indices [I>2σ(I)]	R_1 = 0.0562, wR_2 = 0.1229
R indices (all data)	R_1 = 0.1217, wR_2 = 0.1530
Largest diff. peak and hole	0.690 and -0.312 eÅ^{-3}